NUREG/CR-3272
PNL-4669

LOCA Simulation in NRU Program

Data Report for the Fourth Materials Experiment (MT-4)

Prepared by C. L. Wilson, C. L. Mohr, G. M. Hesson, N. J. Wildung,
G. E. Russcher, B. J. Webb, M. D. Freshley

Pacific Northwest Laboratory
Operated by
Battelle Memorial Institute

Prepared for
U.S. Nuclear Regulatory
Commission

NOTICE

This report was prepared as an account of work sponsored by an agency of the United States Government. Neither the United States Government nor any agency thereof, or any of their employees, makes any warranty, expressed or implied, or assumes any legal liability of responsibility for any third party's use, or the results of such use, of any information, apparatus, product or process disclosed in this report, or represents that its use by such third party would not infringe privately owned rights.

Availability of Reference Materials Cited in NRC Publications

Most documents cited in NRC publications will be available from one of the following sources:

1. The NRC Public Document Room, 1717 H Street, N.W.
   Washington, DC 20555
2. The NRC/GPO Sales Program, U.S. Nuclear Regulatory Commission,
   Washington, DC 20555
3. The National Technical Information Service, Springfield, VA 22161

Although the listing that follows represents the majority of documents cited in NRC publications, it is not intended to be exhaustive.

Referenced documents available for inspection and copying for a fee from the NRC Public Document Room include NRC correspondence and internal NRC memoranda; NRC Office of Inspection and Enforcement bulletins, circulars, information notices, inspection and investigation notices; Licensee Event Reports; vendor reports and correspondence; Commission papers; and applicant and licensee documents and correspondence.

The following documents in the NUREG series are available for purchase from the NRC/GPO Sales Program: formal NRC staff and contractor reports, NRC-sponsored conference proceedings, and NRC booklets and brochures. Also available are Regulatory Guides, NRC regulations in the *Code of Federal Regulations,* and *Nuclear Regulatory Commission Issuances.*

Documents available from the National Technical Information Service include NUREG series reports and technical reports prepared by other federal agencies and reports prepared by the Atomic Energy Commission, forerunner agency to the Nuclear Regulatory Commission.

Documents available from public and special technical libraries include all open literature items, such as books, journal and periodical articles, and transactions. *Federal Register* notices, federal and state legislation, and congressional reports can usually be obtained from these libraries.

Documents such as theses, dissertations, foreign reports and translations, and non-NRC conference proceedings are available for purchase from the organization sponsoring the publication cited.

Single copies of NRC draft reports are available free upon written request to the Division of Technical Information and Document Control, U.S. Nuclear Regulatory Commission, Washington, DC 20555.

Copies of industry codes and standards used in a substantive manner in the NRC regulatory process are maintained at the NRC Library, 7920 Norfolk Avenue, Bethesda, Maryland, and are available there for reference use by the public. Codes and standards are usually copyrighted and may be purchased from the originating organization or, if they are American National Standards, from the American National Standards Institute, 1430 Broadway, New York, NY 10018.

GPO Printed copy price: $6.50

NUREG/CR-3272
PNL-4669
R3

LOCA Simulation in NRU Program

Data Report for the Fourth Materials Experiment (MT-4)

Manuscript Completed: May 1983
Date Published: July 1983

Prepared by
C. L. Wilson, C. L. Mohr*, G. M. Hesson, N. J. Wildung,
G. E. Russcher, B. J. Webb, M. D. Freshley

Pacific Northwest Laboratory
Richland, WA 99352

*Mohr and Associates, Kennewick, WA 99336

Prepared for
Division of Accident Evaluation
Office of Nuclear Regulatory Research
U.S. Nuclear Regulatory Commission
Washington, D.C. 20555
NRC FIN B2277

ACKNOWLEDGMENTS

The authors and project staff would like to thank Chalk River Nuclear Laboratories (CRNL) for their assistance in performing this experiment. A special acknowledgment is due to CRNL staff members J. P. Inglis, P. E. Kelly, J. W. Logie, D. T. Nishimura, and I. D. Ross, who made major contributions in keeping this test on schedule. The project staff would also like to thank CRNL staff members D. J. Axford, I. C. Martin, and S. J. McAuley for insuring a safe test. The helpful directives of R. Van Houten, the NRC program manager, and the consultations of T. Healey of the United Kingdom Central Electricity Generating Board and I. Gibson and P. Coddington of the United Kingdom Atomic Energy Authority are also very much appreciated. The authors would also like to acknowledge the efforts of L. D. Hochreiter and D. Burman of Westinghouse, who provided valuable assistance in selecting the test parameters and providing the technical background for obtaining industry-relevant test data.

The contributions of the following Pacific Northwest Laboratory staff members are also acknowledged:

- L. L. King and J. P. Pilger designed and constructed the test assembly.
- L. J. Parchen was responsible for quality assurance.
- R. K. Marshall designed the test assembly instrumentation.
- M. C. Wismer operated and made improvements to the data acquistion and control system.
- W. N. Rausch contributed to the fuel cladding deformation analysis.
- S. K. Edler edited this document and provided publication assistance.

ABSTRACT

A series of in-reactor experiments were conducted using full-length 32-rod pressurized water reactor (PWR) fuel bundles as part of the Loss-of-Coolant Accident (LOCA) Simulation Program by Pacific Northwest Laboratory (PNL). The fourth materials experiment (MT-4) was the seventh experiment in the series of thermal-hydraulic and materials deformation/rupture experiments conducted in the National Research Universal (NRU) reactor, Chalk River, Ontario, Canada. This experiment was funded by the U.S. Nuclear Regulatory Commission (NRC) to evaluate ballooning and rupture during adiabatic heatup in the temperature range of 1033 to 1200K (1400 to 1700°F). The 12 test rods in the center of the 32-rod bundle were initially pressurized to 4.62 MPa (670 psia) to insure rupture in the correct temperature range. All 12 test rods ruptured with an average strain of 43.7% at the maximum flow blockage elevation of 2.68 m (105.4 in.). Experimental data for the MT-4 transient experiment and post-test measurements and photographs of the fuel are presented in this report.

SUMMARY

The Loss-of-Coolant Accident (LOCA) Simulation Program was conducted by Pacific Northwest Laboratory (PNL) to evaluate the thermal-hydraulic and mechanical deformation behavior of full-length light-water reactor (LWR) fuel bundles under LOCA conditions. The test conditions were designed to simulate the heatup, reflood, and quench phases of a large-break LOCA. The experiments were performed in the National Research Universal (NRU) reactor using nuclear fission to simulate the low-level decay power that is typical of these conditions.

Data and initial results and analysis from the seventh experiment in the program--materials test-4 (MT-4)--are presented in this document. MT-4 was funded by the U.S. Nuclear Regulatory Commission (NRC) with the main objective of addressing NRC licensing requirements for ballooning and blockage.

The major objectives of the MT-4 experiment were to:

- Provide sufficient time in the alpha-Zircaloy ballooning window of 1033 to 1200K (1400 to 1700°F) to allow all 12 pressurized test fuel rods to rupture before reflood cooling was introduced.
- Demonstrate boiloff control of the test by alternately boiling down and filling the test assembly with water.
- Measure data to determine heat transfer coefficients for ballooned and ruptured fuel for boildown and refill conditions with very low reflood rates.
- Measure internal rod pressure as a function of time during deformation.
- Measure fuel rod deformation as a function of position for each of the deformed fuel rods.
- Determine the effects of grid spacers on limiting fuel rod deformations.

All of the major objectives of the experiment were accomplished. Test results indicated that all 12 pressurized test rods in the 32-rod bundle ruptured. The time in the ballooning window was ~58 s, and the temperature

history was almost identical to that of the TH-1.16 test. All 12 test rods were instrumented with pressure transducers to indicate pressure histories.

The results of the test demonstrated the successful use of liquid level feedback to control peak temperatures for extended periods of time. Oscillating boiloff conditions provided information on the range of reflood rates necessary to achieve a stable liquid level in the test bundle. There was no measurable effect of "liftoff" (a thermal decoupling of the cladding from the fuel that results in cooling of the cladding during deformation).

The average maximum test rod rupture strain (72.1%) was obtained using the measured rod strain on each side of the rupture zone. Peak rod rupture strains of up to 99.2% were obtained. Significant strains were detected over 0.189 m (7.42 in.) of rod length. The rupture sites were randomly distributed with no apparent flow channel or flux tilt bias. Test data are summarized below:

Failure time	52 to 58 s
Peak pressure	9.41 MPa (1365 psi)
Pressure at failure	5.58 to 6.48 MPa (810 to 940 psi)
Cladding temperature at failure	1077 to 1114K (1480 to 1547°F)
Maximum test rod rupture strain (rod 5C)	99.2%
Average maximum test rod rupture strain	72.1%
Standard deviation of test rod strain at maximum rupture Oite for each rod	11.9
Average test bundle strain for 12-rod cruciform; test rods at maximum blockage elevation of 2.68 m (105.4 in.)	43.7%

CONTENTS

ACKNOWLEDGMENTS....iii

ABSTRACT....v

SUMMARY....vii

INTRODUCTION....1

EXPERIMENT DESCRIPTION....5

TEST TRAIN ASSEMBLY....5

EXPERIMENT OPERATION....7

EXPERIMENT CONDITIONS AND RESULTS....19

HEAT TRANSFER COEFFICIENTS AND ASSOCIATED THERMAL-HYDRAULICS FOR BALLOONED AND RUPTURED FUEL....31

REFLOOD RATES....31

QUENCH-FRONT PROPAGATION AND LIQUID LEVEL....31

AXIAL POWER DISTRIBUTION....32

TEST ROD AND GUARD ROD TEMPERATURES....35

HEAT TRANSFER COEFFICIENTS....36

DESUPERHEATER SPRAY SYSTEM....38

FUEL ROD PLENUM PRESSURE MEASUREMENTS....51

DEFORMATION EXAMINATION AND ANALYSIS....55

GUARD ROD BUNDLE EXAMINATION....55

TEST ROD BUNDLE EXAMINATION....55

ANALYSIS OF FUEL CLADDING DEFORMATION....75

DESCRIPTION OF THE APPENDICES....77

REFERENCES....79

APPENDIX A - PRECONDITIONING TEST ASSEMBLY TEMPERATURES....A.1

APPENDIX B - PRETRANSIENT TEST ASSEMBLY TEMPERATURES.....B.1

APPENDIX C - TRANSIENT FUEL AND CLADDING TEMPERATURES.....C.1

APPENDIX D - TEST COOLANT AND SHROUD TEMPERATURES.....D.1

APPENDIX E - NEUTRON FLUX DATA.....E.1

APPENDIX F - REFLOOD FLOW MEASUREMENTS.....F.1

APPENDIX G - FUEL ROD DEFORMATION DATA.....G.1

FIGURES

1 Schematic of NRU Loss-of-Coolant Accident Test Assembly.....6

2 Instrumentation Levels for the MT-4 Test Assembly.....8

3 Instrumentation at Levels -0.2 Through 19.2 in the MT-4 Test Assembly.....9

4 Instrumentation at Levels 25.5 Through 46.5 in the MT-4 Test Assembly.....10

5 Instrumentation at Levels 49.0 Through 73.9 in the MT-4 Test Assembly.....11

6 Instrumentation at Levels 76.9 Through 90.0 in the MT-4 Test Assembly.....12

7 Instrumentation at Levels 93.9 Through 111.0 in the MT-4 Test Assembly.....13

8 Instrumentation at Levels 118.9 Through 156.0 in the MT-4 Test Assembly.....14

9 Instrumentation at Levels 168.7 and 187.4 in the MT-4 Test Assembly.....15

10 NRU Reactor Core Configuration.....18

11 Average Test Rod and Shroud Temperatures at Level 76.9 for Adiabatic Test MT-4.03.....20

12 Average Test Rod and Shroud Temperatures at Level 97.9 for Adiabatic Test MT-4.03.....21

13 Average Test Rod and Shroud Temperatures at Level 118.9 for Adiabatic Test MT-4.03.....22

14 Hot Spot Sensor Averages--Levels 97.9 and 118.9--and Demand and Actual Reflood Flow Rates for Initial 90 s of MT-4.04.....23

15 Hot Spot Sensor Averages--Levels 97.9 and 118.9--and Demand and Actual Reflood Flow Rates for 1500 s of MT-4.04; DACS Control 72 s After Steam Off....24

16 Average Test Rod Temperatures at Levels 76.9, 97.9, and 118.9 for Initial 90 s of MT-4.04....25

17 Average Test Rod Temperatures at Levels 76.9, 97.9, and 118.9 for 1500 s of MT-4.04....26

18 Time Domain Reflectometry Instrumentation Liquid Level Response for 1500 s of MT-4.04....27

19 Average Cladding Temperatures at Level 76.9 for MT-1, MT-2.2, MT-3.06, and MT-4.04....28

20 Average Cladding Temperatures at Level 97.9 for MT-1, MT-2.2, MT-3.06, and MT-4.04....29

21 Average Cladding Temperatures at Level 118.9 for MT-1, MT-2.2, MT-3.06, and MT-4.04....30

22 Measured Reflood Rate Versus Time for the MT-4.04 Transient....33

23 Comparison of MT-4 Quench-Front Elevation for the Guard Rods and the Shroud....34

24 Comparison of MT-4 Liquid Level Detector Readings and Guard Rod and Shroud Quench-Front Behavior as a Function of Time....34

25 Comparison of MT-4 Heatup Rate-Based, SPND, Flux Wire, NRU Reactor Preconditioning, and Calculated Axial Power Profiles....35

26 Comparison of Maximum and Minimum Test Rod and Guard Rod Temperatures at Level 76.9 for MT-4....36

27 Comparison of Maximum and Minimum Test Rod and Guard Rod Temperatures at Level 97.9 for MT-4....37

28 Comparison of Maximum and Minimum Test Rod and Guard Rod Temperatures at Level 118.9 for MT-4....38

29 Comparison of Test Rod Temperatures at Level 97.9 for MT-1, MT-2.2, MT-3.06, and MT-4.04....39

30 Comparison of Test Rod Heat Transfer Coefficients at Level 97.9 for MT-1, MT-2.2, MT-3.06, and MT-4.04.....40

31 Comparison of Guard Rod Temperatures at Level 97.9 for MT-1, MT-2.2, MT-3.06, and MT-4.04.....41

32 Comparison of Guard Rod Heat Transfer Coefficients at Level 97.9 for MT-1, MT-2.2, MT-3.06, and MT-4.04.....42

33 Comparison of Test Rod Temperatures at Level 118.9 for MT-1, MT-2.2, MT-3.06, and MT-4.04.....43

34 Comparison of Test Rod Heat Transfer Coefficients at Level 118.9 for MT-1, MT-2.2, MT-3.06, and MT-4.04.....44

35 Comparison of Guard Rod Temperatures at Level 118.9 for MT-1, MT-2.2, MT-3.06, and MT-4.04.....45

36 Comparison of Guard Rod Heat Transfer Coefficients at Level 118.9 for MT-1, MT-2.2, MT-3.06, and MT-4.04.....46

37 Comparison of Heat Transfer Coefficients at Level 76.9 for Nondeformed Guard Rods and Deformed Test Rods for MT-4.04.....47

38 Comparison of Heat Transfer Coefficients at Level 97.9 for Nondeformed Guard Rods and Deformed Test Rods for MT-4.04.....48

39 Comparison of Heat Transfer Coefficients at Level 118.9 for Nondeformed Guard Rods and Deformed Test Rods for MT-4.04.....49

40 Desuperheater Spray Indication and Associated Steam Temperatures.....50

41 Pressure Data at Level 156.0 for Rods 2C, 2D, 3B, and 3C.....52

42 Pressure Data at Level 156.0 for Rods 3D, 3E, 4B, and 4C.....53

43 Pressure Data at Level 156.0 for Rods 4D, 4E, 5B, and 5C.....54

44 MT-4 Bundle Cross Sections Before and After Deformation at Axial Elevation Z = 81.12 in.....57

45 MT-4 Bundle Cross Sections Before and After Deformation at Axial Position Z = 100.70 in.....58

46 Test Rod Bundle Rupture Zones--Sides A, 6, F, and 1.....59

47 Rupture Zone for Test Rod 2C.....60

48 Rupture Zone for Test Rod 2D.....61

49 Rupture Zone for Test Rod 3B.....62
50 Rupture Zone for Test Rod 3C.....63
51 Rupture Zone for Test Rod 3D.....64
52 Rupture Zone for test Rod 3E.....65
53 Rupture Zone for Test Rod 4B.....66
54 Rupture Zone for Test Rod 4C.....67
55 Rupture Zone for Test Rod 4D.....68
56 Rupture Zone for Test Rod 4E.....69
57 Rupture Zone for Test Rod 5C.....70
58 Rupture Zone for Test Rod 5D.....71
59 Comparison of Rupture Zones for Test Rods 2C, 2D, 3B, and 3C.....72
60 Comparison of Rupture Zones for Test Rods 3D, 3E, 4B, and 4C.....73
61 Comparison of Rupture Zones for Test Rods 4D, 4E, 5C, and 5D.....74
62 Cladding Deformation Profiles for MT-4.....75
63 DILATE Calculations for MT-4.....76

TABLES

1 Test Fuel Rod Design Variables.....7

2 Instrumentation at Each Level in the MT-4 Test Assembly.....16

3 Instrumentation Array in the MT-4 Test Assembly.....17

4 Sensors That Failed in the MT-4 Experiment.....17

5 Experiment Conditions for the MT-4.04 Transient.....32

6 Summary of Pressure Switch and Pressure Transducer Rod Failure Data for MT-4.04.....51

7 Summary of Failure Conditions.....56

INTRODUCTION

The Loss-of-Coolant Accident (LOCA) Simulation Program was conducted in the National Research Universal (NRU) reactor at Chalk River Nuclear Laboratories (CRNL),[a] Chalk River, Ontario, Canada, by Pacific Northwest Laboratories (PNL).[b] The program was sponsored by the U.S. Nuclear Regulatory Commission (NRC) to evaluate the thermal-hydraulic and mechanical deformation behavior of full-length, 3% enriched 17 x 17 pressurized water reactor (PWR) fuel bundles during the heatup, reflood, and quench phases of a LOCA. Low-level nuclear fission heat was used to simulate the decay heat in the fuel and cladding that is typical of a LOCA.[1]

Three thermal-hydraulic and four cladding materials deformation experiments were performed. The initial thermal-hydraulic experiment (TH-1) was performed in October 1980 and provided a data base for predicting the quenching characteristics of Zircaloy-clad fuel rods under various reflood conditions.[2]

The first materials experiment (MT-1) was performed in April 1981 and used a pressurized cruciform of 11 rods pressurized to 3.21 MPa (465 psia), 1 water tube, and 20 guard rods sealed at atmospheric pressure. The delay time and the reflood rate were selected to duplicate the TH-1.10 experiment, which reached a peak fuel cladding[c] temperature of 1144K (1600°F). These conditions were achieved, 6 of the 11 rods ruptured, and all 11 pressurized test rods deformed significantly.[3] The average peak rupture strain was 43%, the average rupture time was 43 s, and the average rupture temperature was 1145K (1601°F).

In the second materials experiment (MT-2), which was performed in July 1981, the MT-1 guard rod and shroud assembly was reconstituted underwater and reused with a new cruciform test bundle. The 12 test rods were pres surized to 3.21 MPa (465 psia). One of the test objectives was to perform a low-temperature--1089K (1500°F)--test using variable reflood rates. A malfunction of the test loop resulted in higher temperatures than desired, and 8 of the 11 rods ruptured.[4] The average peak rupture strain was 43%, the average rupture time was 65 s, and the average rupture temperature was 1156K (1623°F).

The fourth experiment (TH-2) was conducted in October 1981 and used a new thermal-hydraulic test bundle sealed at atmospheric pressure that was reconstituted in the MT-1/MT-2 guard rod and shroud assembly.[5] This experiment evaluated the reflood rates necessary to obtain a "flat top" or extended transient from 1033 to 1103K (1400 to 1525°F). The delay time and automatic control system used to control the variable reflood rate in this experiment demonstrated the capability of holding temperatures above 1033K (1400°F) for periods of up to 280 s. The test conditions approached a steady-state boiloff condition.

(a) Operated by Atomic Energy of Canada Ltd. (AECL).
(b) Operated for the U.S. Department of Energy (DOE) by Battelle Memorial Institute.
(c) Fuel cladding subsequently referred to as cladding.

The fifth experiment (TH-3) used the same test bundle as TH-2; several new thermocouples (TCs) and a spray desuperheater were added. Several modifications were also made to the loop control logic to improve the reflood rate control and extend the length of the flat top transient. TH-3 was performed just prior to MT-3 to verify the loop control system (LCS) and the data acquisition and control system (DACS) instrumentation and operation. TH-3 and MT-3 were both performed in November 1981. TH-3 also verified test assembly power levels and the changes to the DACS control performance. The results of the TH-3 experiment made it possible to extend the time above 1033K (1400°F) from 280 s in TH-2.14 to 340 s in TH-3.03. In addition, the transient time-temperature history was modified to provide more two-phase cooling at the start of the transient. The desuperheater modification to the TH-3 assembly controlled exit steam temperatures.

The primary objective of the MT-3 experiment was to determine the deformation and flow channel restrictions for a flat top transient using pressurized fuel rods. Peak cladding temperatures were maintained above 1033K (1400°F) for 180 s. The MT-3 experiment repeated the test conditions demonstrated by the TH-3.03 test using a completely new test train with 12 fuel rods pressurized to 3.90 MPa (565 psia). All 12 test rods ruptured during the active two-phase cooling regime. The average peak rupture strain was 46%, the average rupture time was 133 s, and the average failure temperature was 1067K (1461°F). The MT-3 experiment had a lower average failure temperature and a longer failure time than any of the other materials experiments due to the significant amount of reflood water that was introduced early in the transient (reflood delay time was 7 s). The active strain region was spread over 2.03 m (80 in.) of fuel, and no lack of coolability due to coplanar blockage or liftoff[a] was observed.

The MT-4 experiment was conducted in May 1982. Its primary objective was to evaluate cladding ballooning and rupture during adiabatic heatup in the temperature range from 1033 to 1200K (1400 to 1700°F). The 12 test rods in the 32-rod bundle were initially pressurized to 4.62 MPa (670 psia) at 296K (72°F) to assure rupture in the correct temperature range. All 12 test rods ruptured with an average peak rod strain of 72.1%. The active strain region was spread over 0.189 m (7.42 in.), the average failure time was 55 s, and the average failure temperature was 1094K (1511°F). The MT-4 experiment was most similar to the MT-2 experiment, except for three differences: 1) MT-4 rods were pressurized to 4.62 MPa (670 psia) whereas MT-2 rods were pressurized to 3.21 MPa (465 psia); 2) after the adiabatic heatup transient and temperature turnaround, peak cladding temperatures were stabilized to measure heat transfer characteristics of the deformed (and ruptured) fuel rods, and 3) self-powered neutron detectors (SPNDs) mounted on the shroud were moved to grid elevations to minimize axial neutron power distortion.

The MT-4 experiment used a new cruciform bundle of 12 pressurized test fuel rods and the guard fuel rods and shroud previously used in MT-3. Test operations most closely followed the operating conditions of TH-1.16, where

(a) Liftoff is a thermal decoupling of the cladding from the fuel that results in cooling of the cladding during deformation.

reflood cooling was used to terminate the heatup transient temperature at ~1200K (1700°F). Stabilized post-transient operations closely followed the operating conditions used in the MT-3 experiment.

The results from MT-4 provide thermal-hydraulic and materials deformation response data for full-length PWR nuclear-heated cladding in the high alpha temperature range for variable reflood conditions. These conditions extend the existing data base on thermal-hydraulic and mechanical response to LOCA operating conditions not previously investigated by other out-of-reactor test programs. The MT-4 test series has resulted in valuable information on 1) the control of quench fronts and two-phase cooling that will be used for subsequent thermal-hydraulic and materials experiments and 2) the quench characteristics of deformed rods as compared with nondeformed rods for the flow conditions covered in these experiments.

Data from MT-4 will be used in conjunction with previous test results to assess various calculational models for reactor safety analyses and conclusions derived from the large series of electrically heated tests and smaller scale in-reactor tests being conducted elsewhere. The experimental results of the program address 17 specific items outlined in the Code of Federal Regulations 10 CFR 50.46 and 10 CFR 50, Appendix K. These results will be used to provide additional data for model calibration and to help define the primary heat transfer mechanisms for new analytical models. The major contribution of these tests to light-water reactor (LWR) technology is to quantify the uncertainty on licensing criteria and offer the potential for raising the operating limits on some commercial LWRs.

EXPERIMENT DESCRIPTION

This section describes the components of the test assembly that were used for the MT-4 experiment and details the instrumentation that was provided. The experiment operation, which consisted of four separate tests, is also described; and experimental conditions and results are discussed.

TEST TRAIN ASSEMBLY

A schematic of the test train used for the LOCA program is depicted in Figure 1. The test train (including the head closure, hanger tube, and fuel assembly) was ~9 m (~30 ft) long. The closure region provided the primary pressure boundary and included penetrations for 183 instrumentation leads. The hanger tube was used to suspend the fuel assembly and shroud from the head closure plug, and instrument leads were attached to the hanger to protect them during transport and testing. The shroud, which supported the fuel assembly and served as a protective liner during the experiment and during transfer operations, also provided proper coolant flow distribution during various stages of the experiment. The stainless steel (SS) shroud consisted of two halves that were clamped together at 17.8-cm (7-in.) intervals and attached at the end fittings. The split shroud design made it possible to disassemble, examine, and reassemble the fuel assembly underwater after its irradiation. The highly instrumented shroud and fuel assembly was ~4 m (14 ft) long.

The fuel assembly consisted of a 6 x 6 segment of a 17 x 17 PWR fuel assembly with the four corner rods removed (Figure 1) and provided a basic fuel array of 32 rods. The 20 unpressurized guard rods in the outer row isolated the inner 12 test rods and reduced the heat transfer from the test rods to the shroud during the test. The 12 test rods, which were arranged in a cruciform pattern, were pressurized with helium to 4.62 MPa (670 psia) to provide the necessary internal cladding stresses that would result in test rod failure at the desired temperature (Table 1).

Test train instrumentation included: 24 SPNDs, 143 TCs, 12 fuel rod pressure sensors, 1 liquid level detector, and 4 flux wires. The instrumentation was located at 37 elevations or levels along the test assembly; 36 of these levels are defined in Figure 2 and detailed in Figures 3 through 9. An additional level was located in the test assembly closure where four TCs measured the closure region temperatures. Instrumentation for the 36 levels is shown in Table 2; the instrumentation array, in Table 3; and failed sensors, in Table 4.

Turbine flowmeters and TCs provided the main source of thermal-hydraulic data. Local coolant temperatures were measured with steam probe TCs that

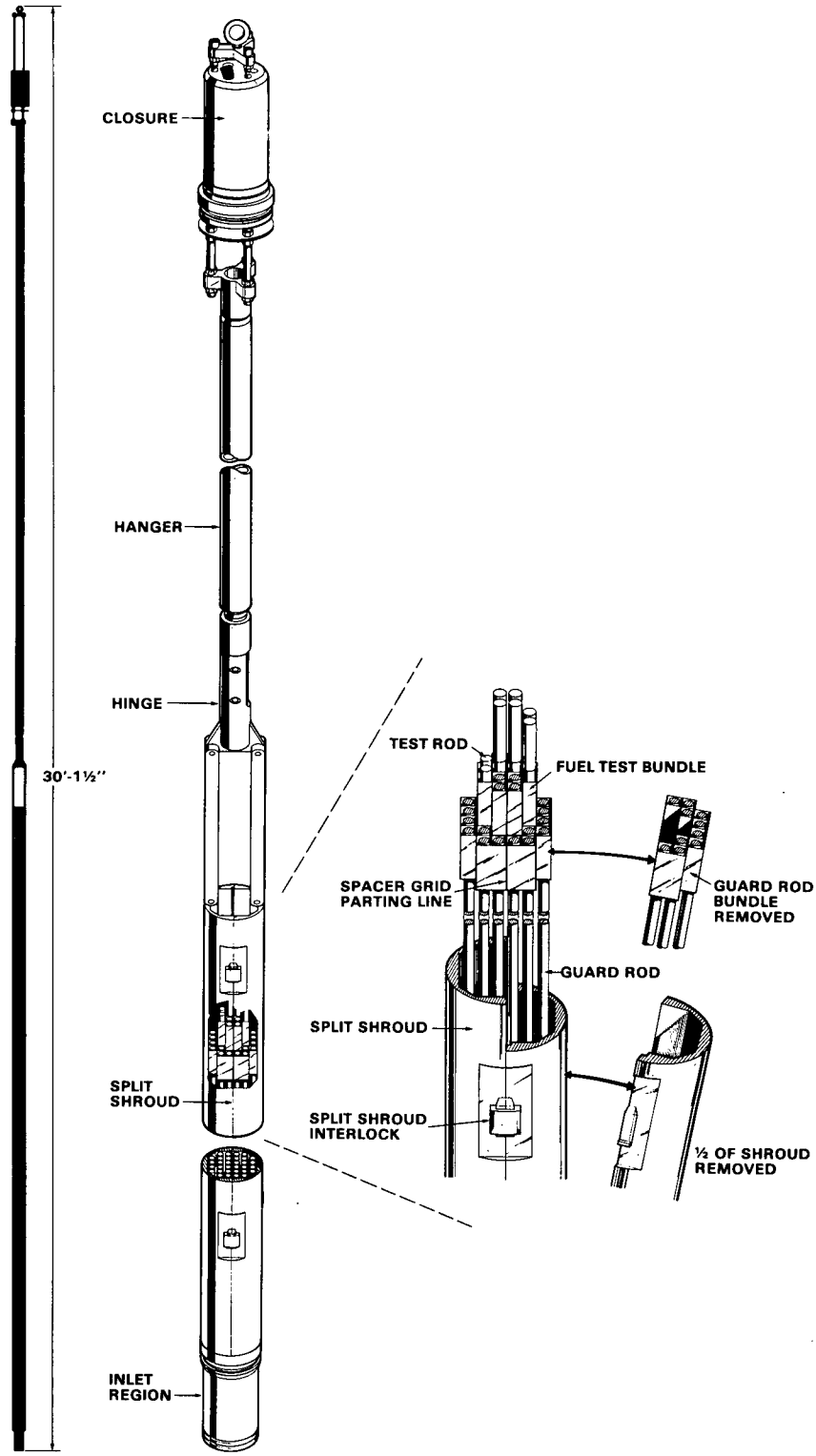

FIGURE 1. Schematic of NRU Loss-of-Coolant Accident Test Assembly

TABLE 1. Test Fuel Rod Design Variables

Cladding material	Zircaloy-4
Cladding outside diameter (OD)	0.963 cm (0.379 in.)
Cladding inside diameter (ID)	0.841 cm (0.331 in.)
Pitch (rod to rod)	1.275 cm (0.502 in.)
Fuel pellet OD	0.826 cm (0.325 in.)
Fuel pellet length	0.953 cm (0.375 in.)
Active fuel length	3.66 m (12 ft)
Total shroud length	4.33 m (14.18 ft)
Helium pressurization	4.62 MPa (670 psia) at 296K (73°F)
Fuel enrichment	2.93% ^{235}U

protruded into the coolant channel and with TCs attached to the shroud. TCs were also spot welded to the inside of the cladding surface. These cladding TCs monitored the cladding temperature without interference from fuel pellet chips or unintentional TC relocation. TCs were also located at the fuel centerline.

SPNDs provided neutron flux measurements within the fuel bundle. They could also detect coolant density variations (through flux changes) associated with the quench front that passed each SPND during the reflood phase of the transient. SPND data with regard to coolant density could potentially be correlated to liquid level. The four flux wires provided additional information on the axial flux distribution.

A liquid level detector measured changes in the liquid level in the fuel bundle during the test. The detector, which is based on time domain reflectometry (TDR), is described in more detail in Reference 6.

EXPERIMENT OPERATION

The MT-4 experiment consisted of a preconditioning phase, three preliminary tests, and a test in which all test rods ruptured (MT-4.04). The experiment was performed in the L-24 site in the NRU reactor (Figure 10). The assembly was oriented in the reactor with side F (side that has fuel rods designated F) facing north.

The preconditioning phase was initiated May 26, 1982. Two rises to full NRU power operation and two conditional reactor trips assured fuel pellet cracking and good fuel/cladding mechanical contact.

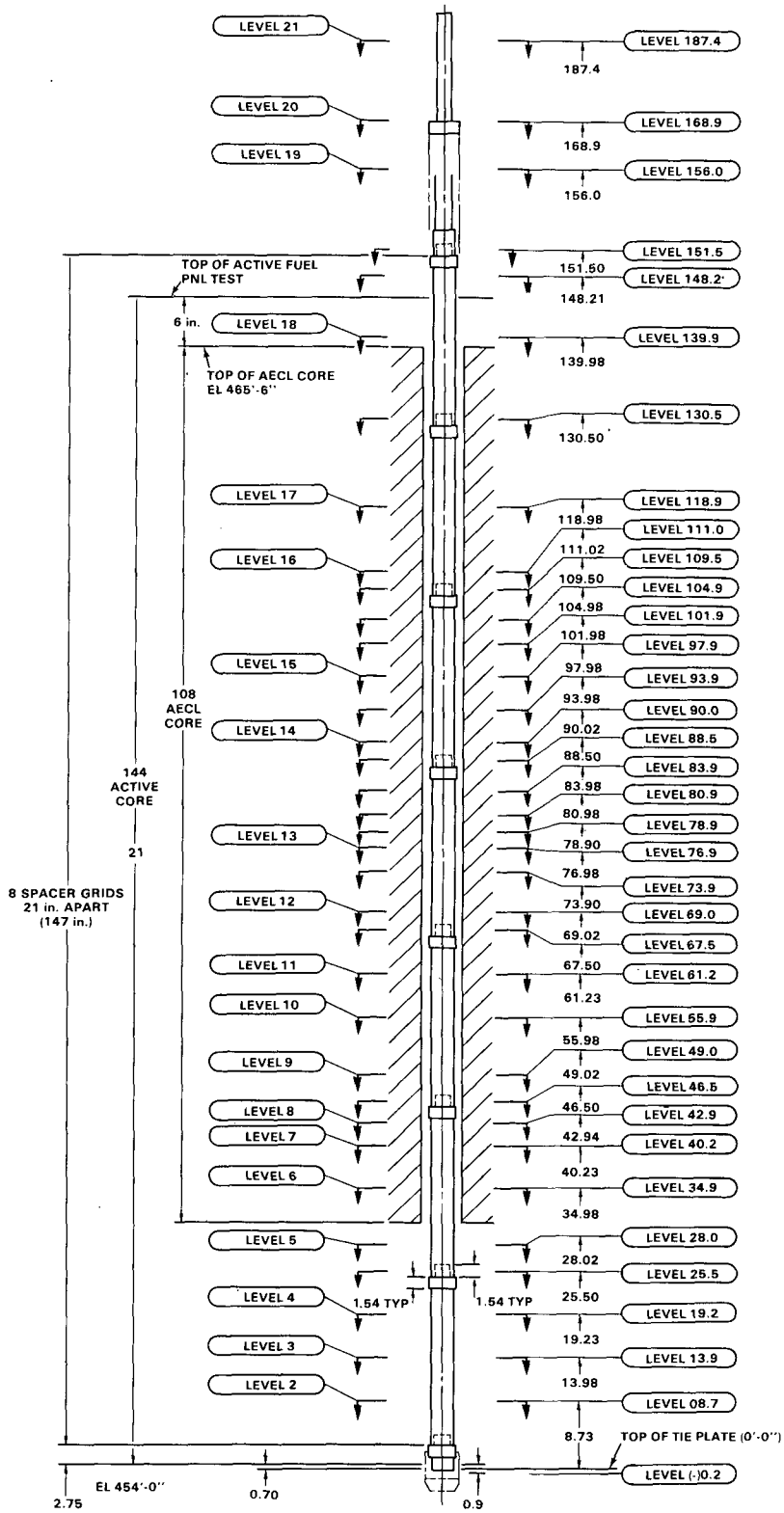

FIGURE 2. Instrumentation Levels for the MT-4 Test Assembly

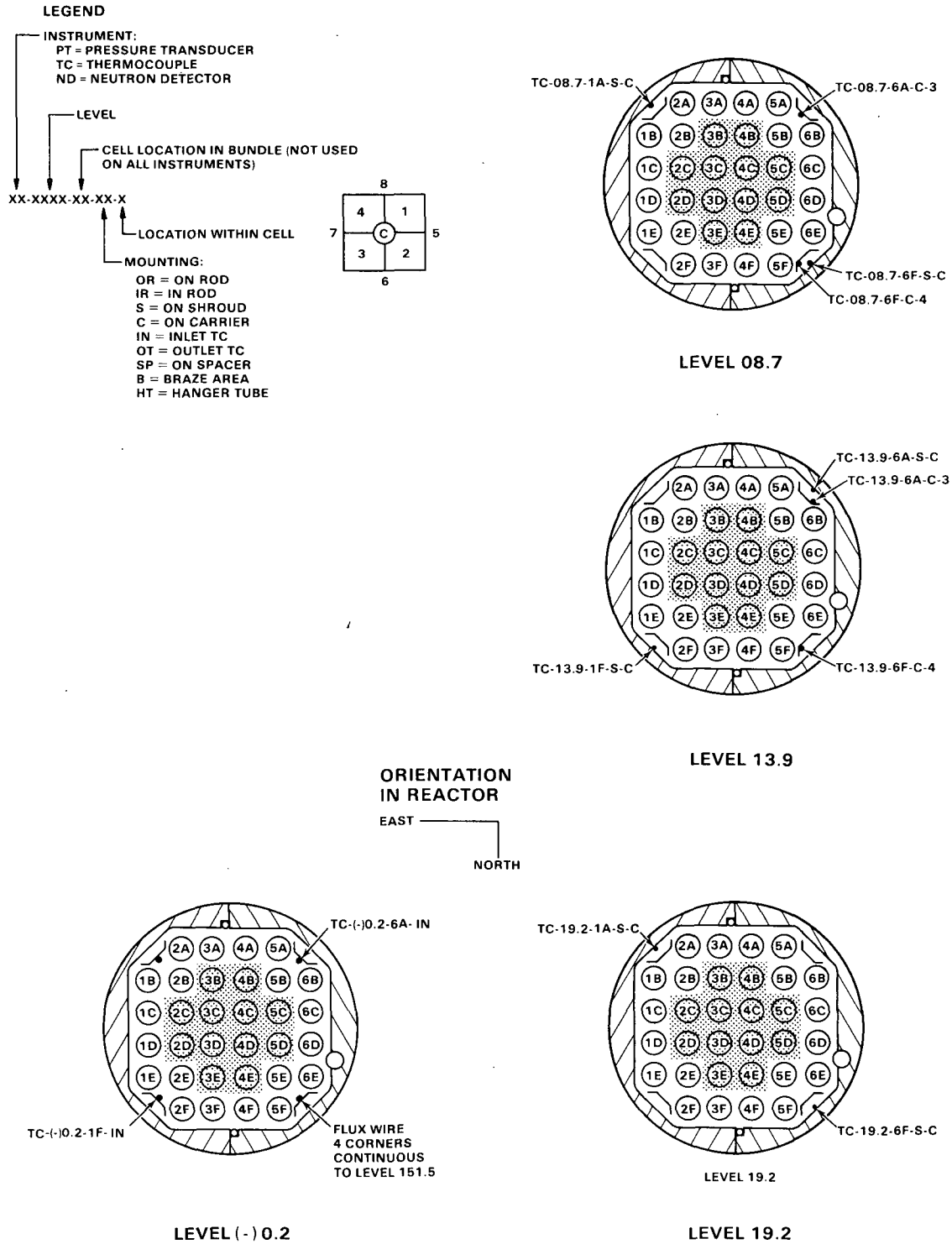

FIGURE 3. Instrumentation at Levels -0.2 Through 19.2 in the MT-4 Test Assembly

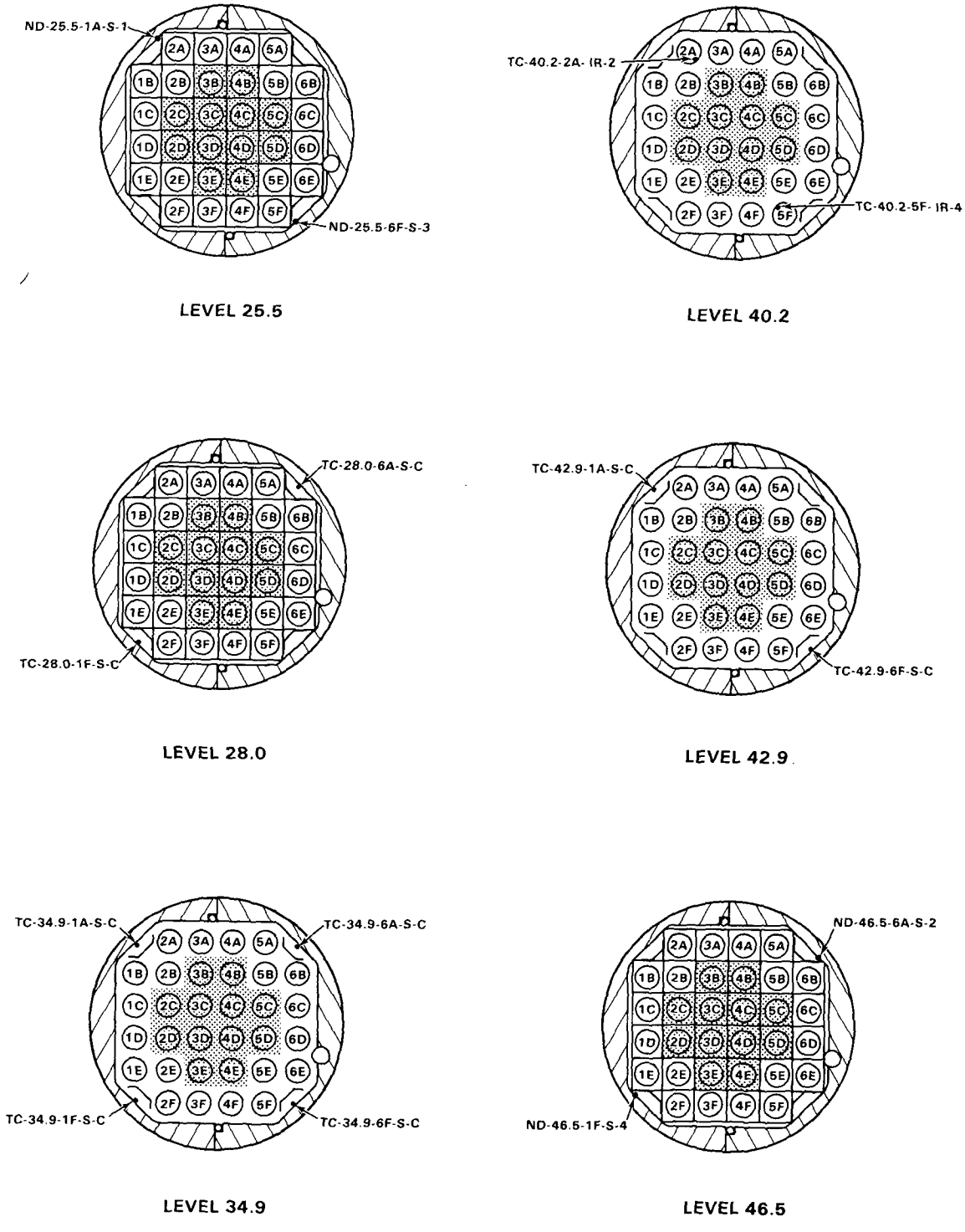

FIGURE 4. Instrumentation at Levels 25.5 Through 46.5 in the MT-4 Test Assembly

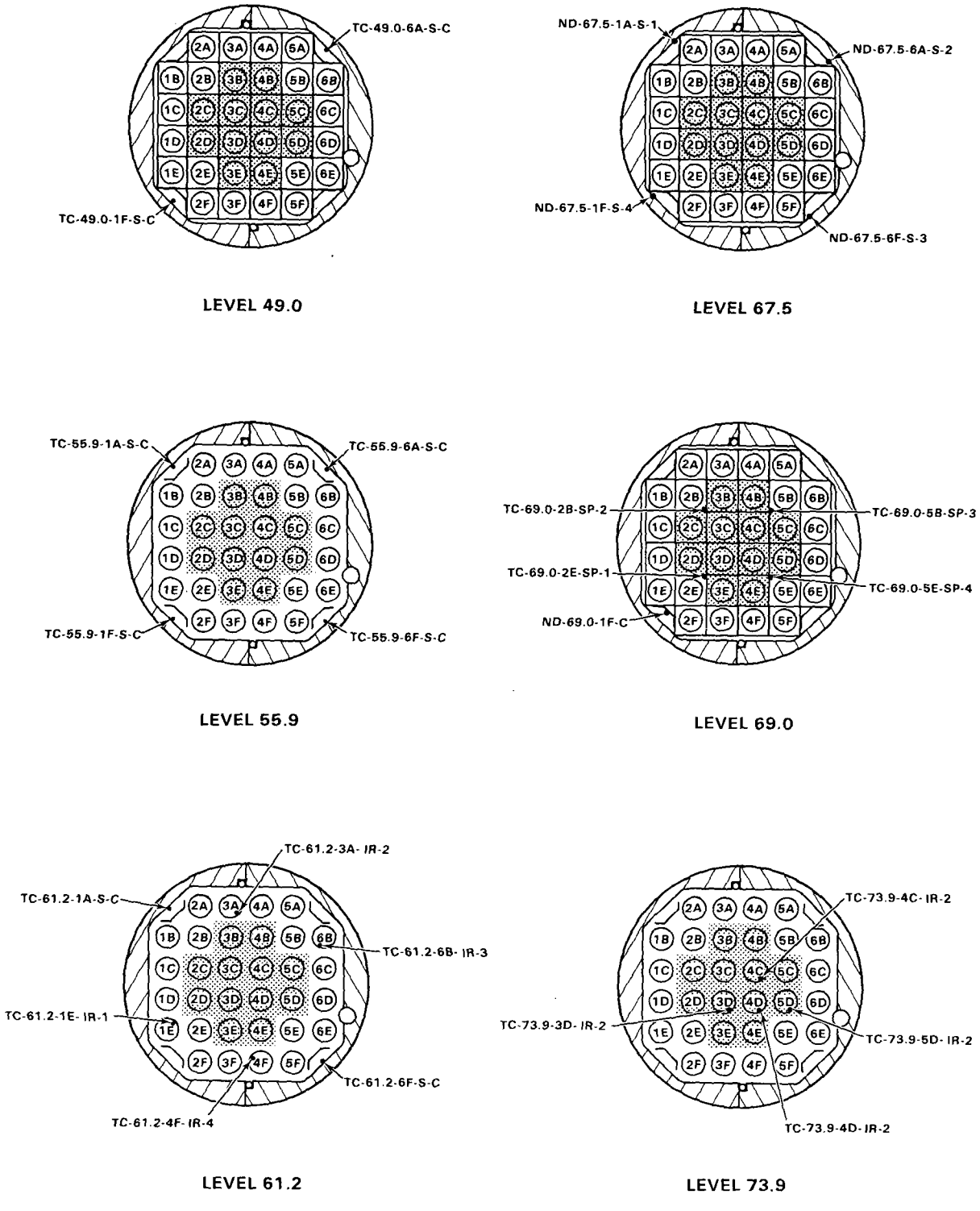

FIGURE 5. Instrumentation at Levels 49.0 Through 73.9 in the MT-4 Test Assembly

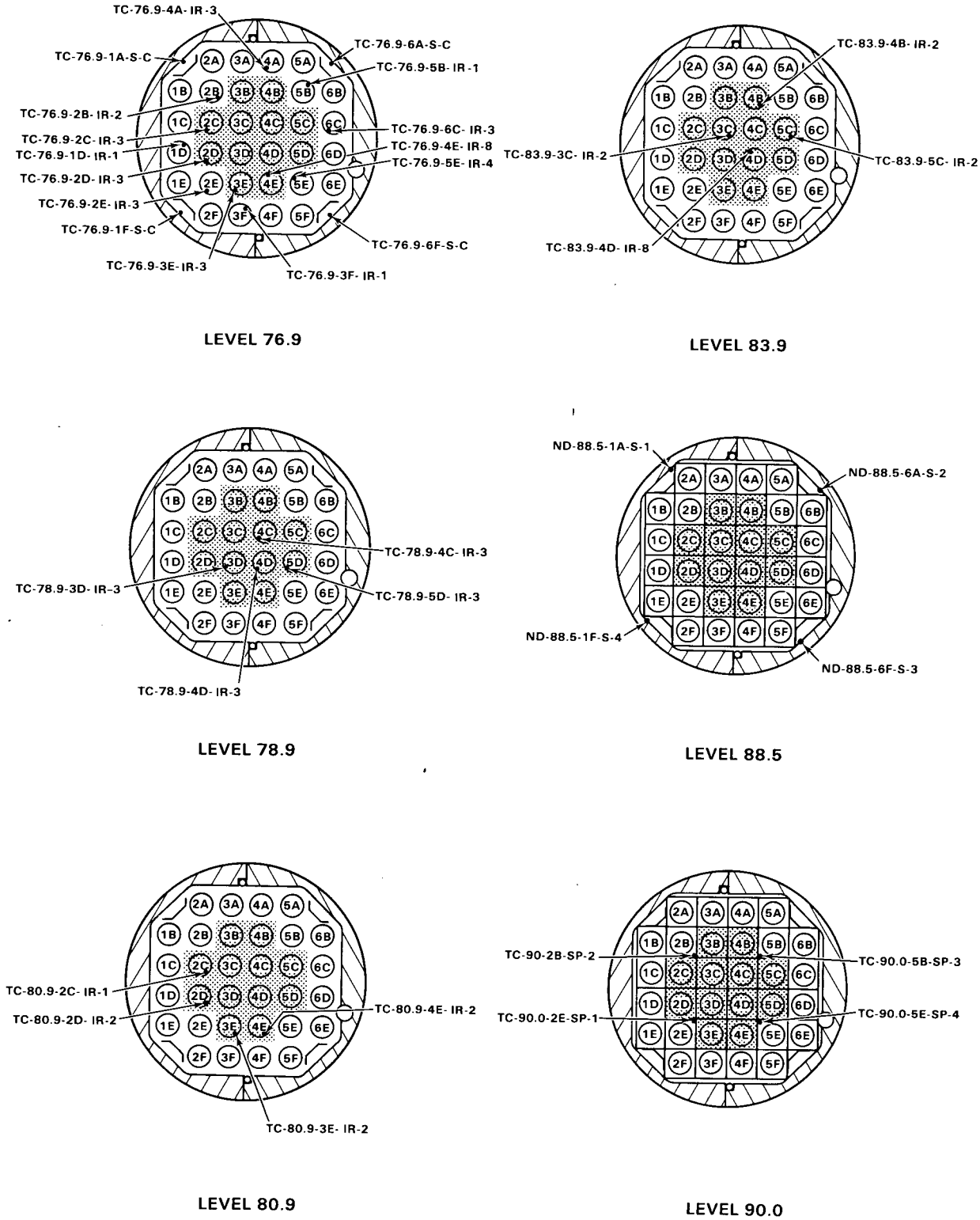

FIGURE 6. Instrumentation at Levels 76.9 Through 90.0 in the MT-4 Test Assembly

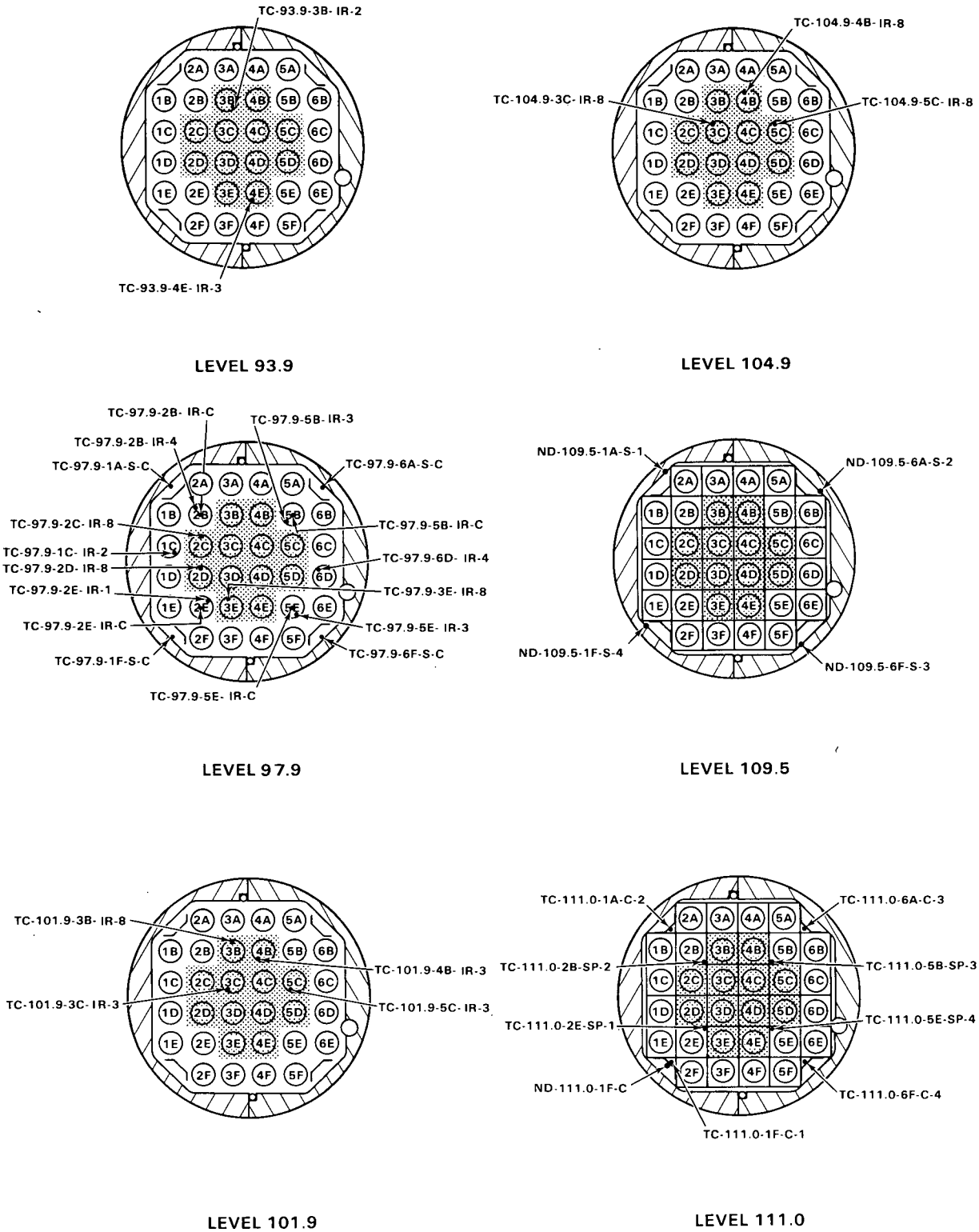

FIGURE 7. Instrumentation at Levels 93.9 Through 111.0 in the MT-4 Test Assembly

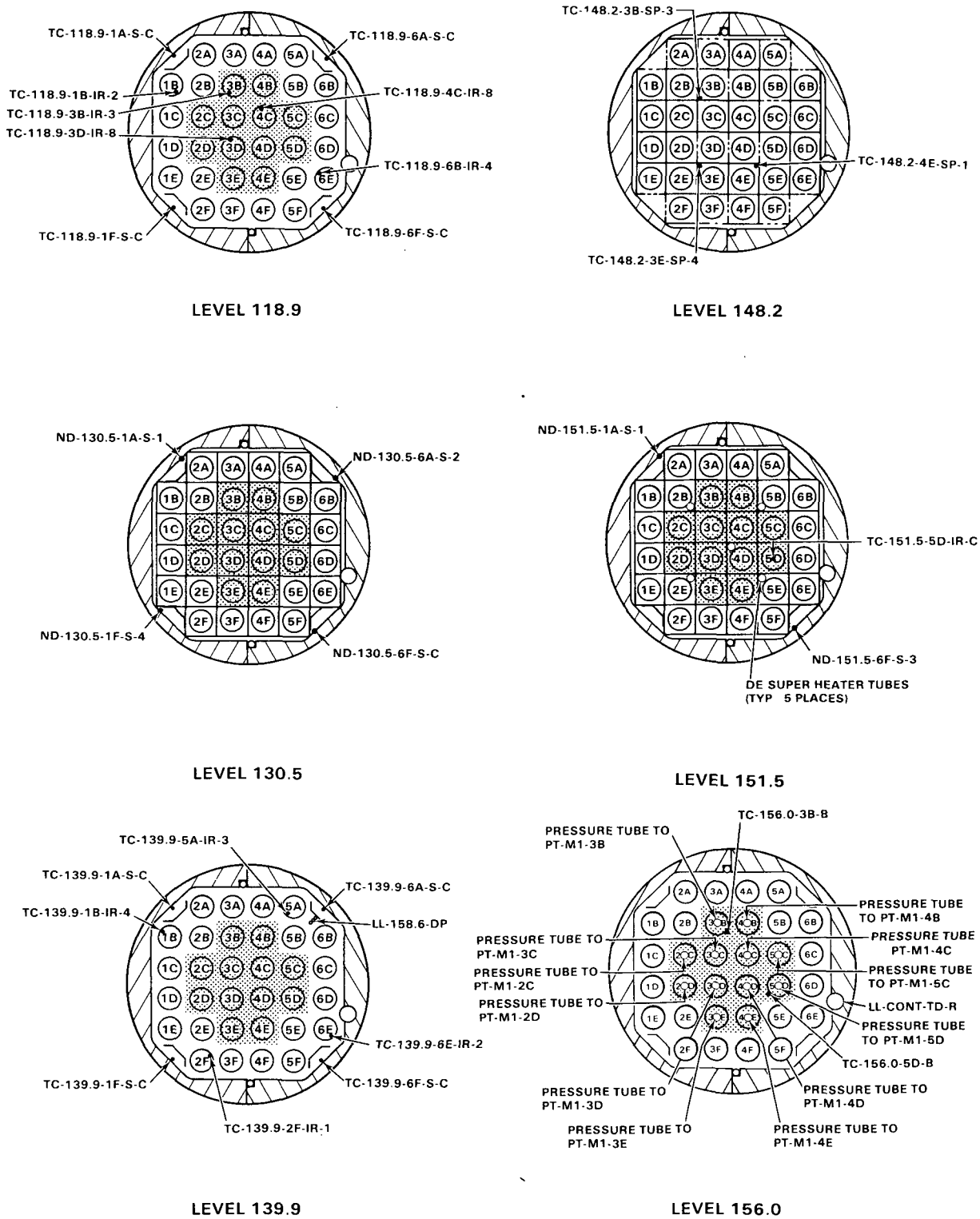

FIGURE 8. Instrumentation at Levels 118.9 Through 156.0 in the MT-4 Test Assembly

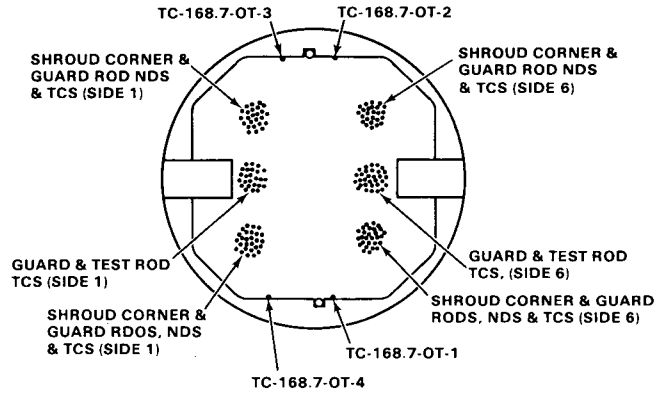

LEVEL 168.7

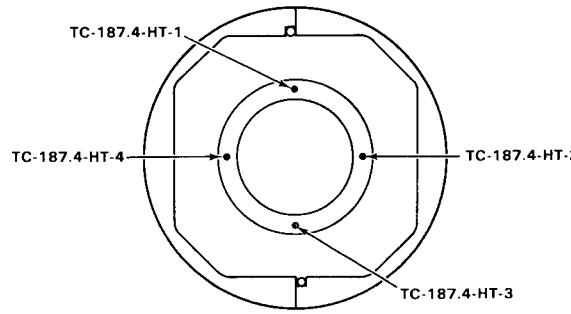

LEVEL 187.4

FIGURE 9. Instrumentation at Levels 168.7 and 187.4 in the MT-4 Test Assembly

The first transient test sequence--MT-4.01--consisted of two phases: a reflood calibration at 0.123 m/s (4.8 in./s) with no power and an interrupted steady-state test at power using a reflood rate of 0.123 m/s. The transient never reached steady state because the power was so high that the reactor tripped at a cladding temperature of 867K (1100°F). Reprogramming the LCS led to an error in the steam cooling flow rate indication, which resulted in a high reactor power setting. MT-4.02 was an adiabatic heatup test with heatup rates of ~10.3K/s (18.5°F/s). These heatup rates showed that test fuel powers were still higher than required for the reflood transient test. MT-4.03 was an adiabatic heatup test that achieved maximum cladding heatup rates of ~8.3K/s

TABLE 2. Instrumentation at Each Level in the MT-4 Test Assembly

Level	Cladding Inside Diameter TCs	Cladding Outside Diameter TCs	Fuel Centerline TCs	Shroud TCs	Carrier TCs	Steam Probe TCs	SPNDs
-0.2 (1)					2		
8.7 (2)				2	2		
13.9 (3)				2	2		
19.2 (4)				2			
25.5							2
28.0 (5)				2			
34.9 (6)				4			
40.2 (7)	2						
42.9 (8)				2			
46.5							2
49.0 (9)				2			
55.9 (10)				4			
61.2 (11)	4			2			
67.5							4
69.0 (12)						4	1
73.9	4						
76.9 (13)	12			4			
78.9	4						
80.9	4						
83.9	4						
88.5							4
90.0 (14)						4	
93.9	2						
97.9 (15)	9		4	4			
101.9	4						
104.9	3						
109.5							4
111.0 (16)					4	4	1
118.9 (17)	5			4			
130.5							4
139.9 (18)	4			4			
148.2						3	
151.5							2
156.0 (19)		2					
168.7 (20)				4			
Total	61	2	4	42	10	15	24

Note:
Four flux wires ran from Level -0.2 to Level 151.5; 12 fuel plenum pressure taps were at Level 156.0; 5 desuperheater tube outlets and 1 fuel plenum TC were at Level 151.5; 4 hanger tube TCs were at Level 187.4; and 4 TCs were located in the closure region.

TABLE 3. Instrumentation Array in the MT-4 Test Assembly

	TCs	SPNDs	Pressure Transducers
Guard bundle	30		
Test bundle	35		12
Shroud	42	22	
Hanger tube	4		
Carrier	10	2	
Fuel plenum	1		
Spacer grid	15		
Fuel rod braze	2		
Closure head	4		
Total	143	24	12

TABLE 4. Sensors That Failed in the MT-4 Experiment

Failed Sensor	Time of Failure
TC-40.2-2A-IR-2	before MT-4.01
TC-76.9-3F-IR-1	before MT-4.01
TC-76.9-5B-IR-1	before MT-4.01
TC-80.9-2D-IR-2	before MT-4.01
TC-83.9-3C-IR-2	before MT-4.01
TC-90.0-2B-SP-2	before MT-4.01
TC-97.9-6D-IR-4	before MT-4.01
TC-111.0-1A-C-2	before MT-4.01
TC-118.9-6E-IR-4	before MT-4.01
TC-139.9-5A-IR-3	before MT-4.01
ND-25.5-6F-S-3	before MT-4.01
ND-67.5-6F-S-3	before MT-4.01
ND-67.5-6A-S-2	before MT-4.01
ND-67.5-6F-S-3	before MT-4.01
ND-88.5-1A-S-1	before MT-4.01
ND-88.5-1F-S-4	before MT-4.01
ND-109.5-1A-S-1	during MT-4.03
ND-151.5-6F-S-3	before MT-4.01

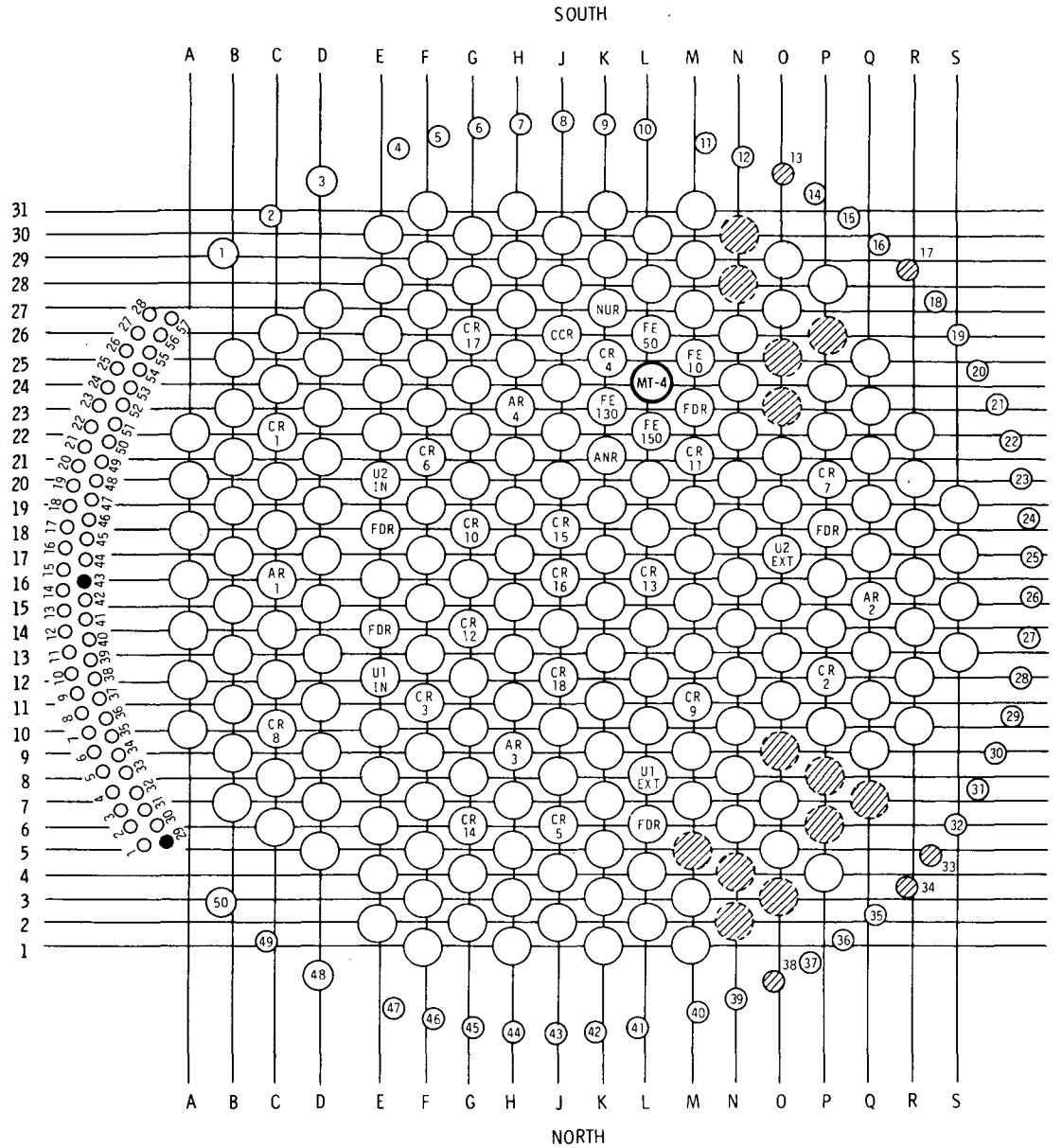

CR CONTROL ROD

AR ADJUSTER ROD

FDR FLUX DETECTOR ROD

U-1 IN, U-2 IN — DOWN FLOW CHANNEL-DUMMY FUEL

U-1 EXT, U-2 EXT — UP FLOW CHANNEL-DUMMY FUEL

STANDARD LATTICE POSITION

BLOCKED CHANNEL-NOT FUELED

CCR COBALT CARRIER ROD

NUR NATURAL URANIUM ROD

ANR ALUMINUM NITRIDE ROD

FE 50 FUEL ELEMENT - 50 MWd BURNUP

FE 10 FUEL ELEMENT - 10 MWd BURNUP

FE 130 FUEL ELEMENT - 130 MWd BURNUP

FE 150 FUEL ELEMENT - 150 MWd BURNUP

FIGURE 10. NRU Reactor Core Configuration

(15°F/s)--rates desired for the final transient (MT-4.04). MT-4.04 consisted of two phases: a short heatup phase that lasted ~1.5 min and a longer phase at temperature that lasted ~20 min. Tests MT-4.01 through MT-4.04 were all performed on May 27, 1982.

EXPERIMENT CONDITIONS AND RESULTS

The MT-4 experiment consisted of four separate tests. The first three tests were preliminary evaluation runs performed to determine reactor power and reflood rates and to check loop control performance. The last test--MT-4.04--was the final transient test where all 12 pressurized test rods ruptured during the heatup phase.

The test conditions measured for MT-4.03 are summarized in Figures 11 through 13. These figures indicate the average temperature versus time histories for the shroud and the test rods at Levels 76.9, 97.9, and 118.9. The MT-4.03 test was an adiabatic heatup run using a stagnant steam environment. The results of this test were used to set the reactor power for transient test MT-4.04. The temperature ramp rates for the test rods and the shroud indicate the assembly power and the degree of coupling between the test rods and the shroud.

The MT-4.04 transient test used a combination of LCS preprogrammed reflood rate control and DACS reflood control logic. After a reflood delay of 57 s, the LCS controlled the reflood rate at 0.203 m/s (8 in./s) for 6 s, 0.102 m/s (4 in./s) for 6 s, and then 0.00254 m/s (1 in./s) for 3 s. The DACS then took over using variable reflood rates to control cladding temperatures for the boiloff portion of the test.

The fuel failed in the 52- to 58-s range; the reflood coolant delay time was 57 s; and all but one rod ruptured during the adiabatic heatup (Figure 14). Fuel failure temperatures ranged from 1077 to 1114K (1480 to 1547°F). Five of the 12 test rods ruptured before leaving the 1033 to 1088K (1400 to 1500°F) ballooning window and seven ruptured shortly afterwards. The measured temperatures for the hot spot TC sensors used in the control logic for the 20-min duration of MT-4.04 are plotted in Figure 15. The peak control temperatures changed from Level 95.9 to Level 118.9. Boiloff was controlled by alternately boiling down and filling the test assembly with water (Figures 15 through 18). Average test rod inside cladding temperatures at Levels 76.9, 97.9, and 118.9 are shown in Figures 19 through 21 for MT-1, MT-2.2, MT-3.06, and MT-4.04. These plots demonstrate test repeatability using DACS control. The extended time at temperature for MT-4.04 demonstrates the feasibility of controlling a boildown test.

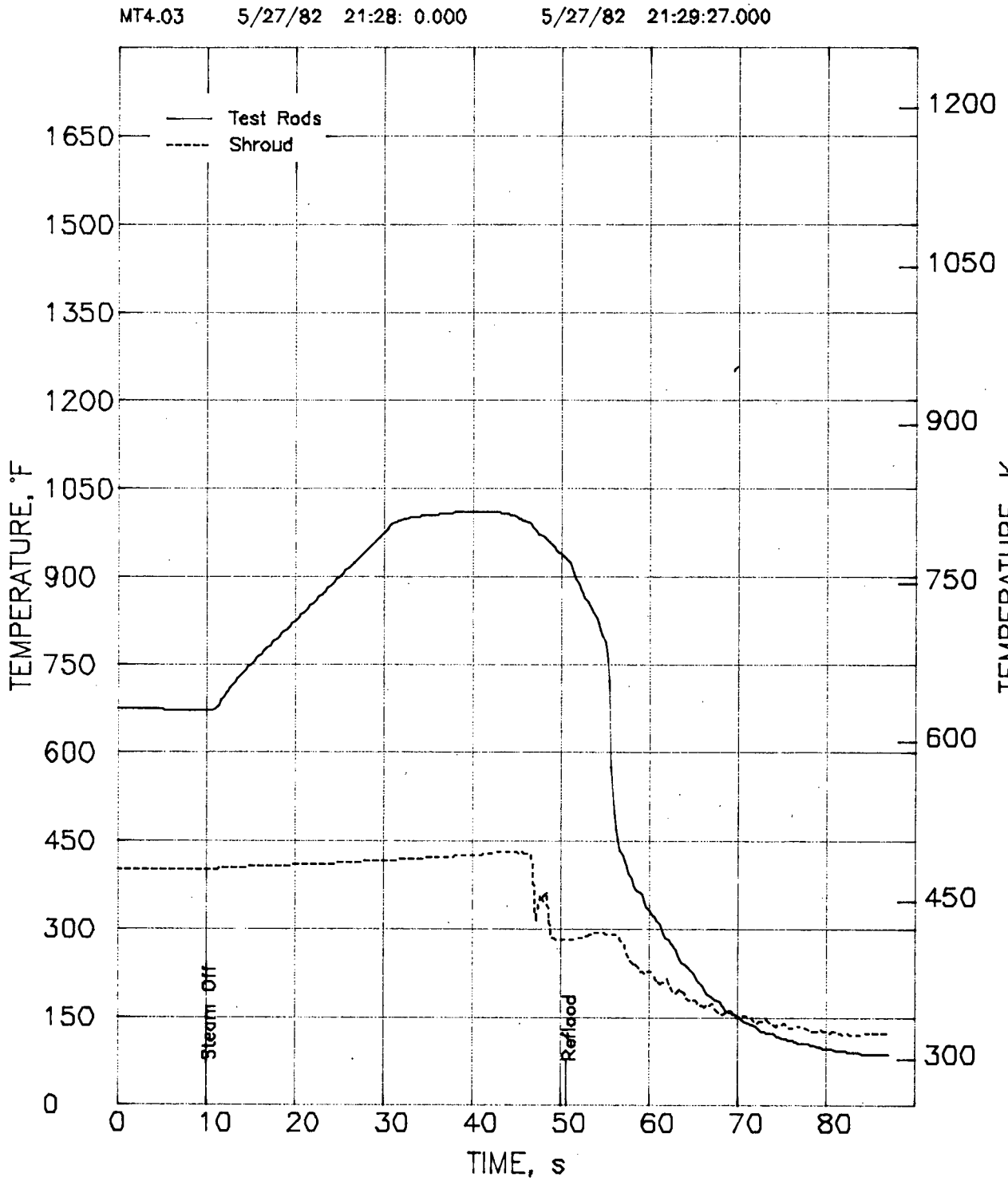

FIGURE 11. Average Test Rod and Shroud Temperatures at Level 76.9 for Adiabatic Test MT-4.03

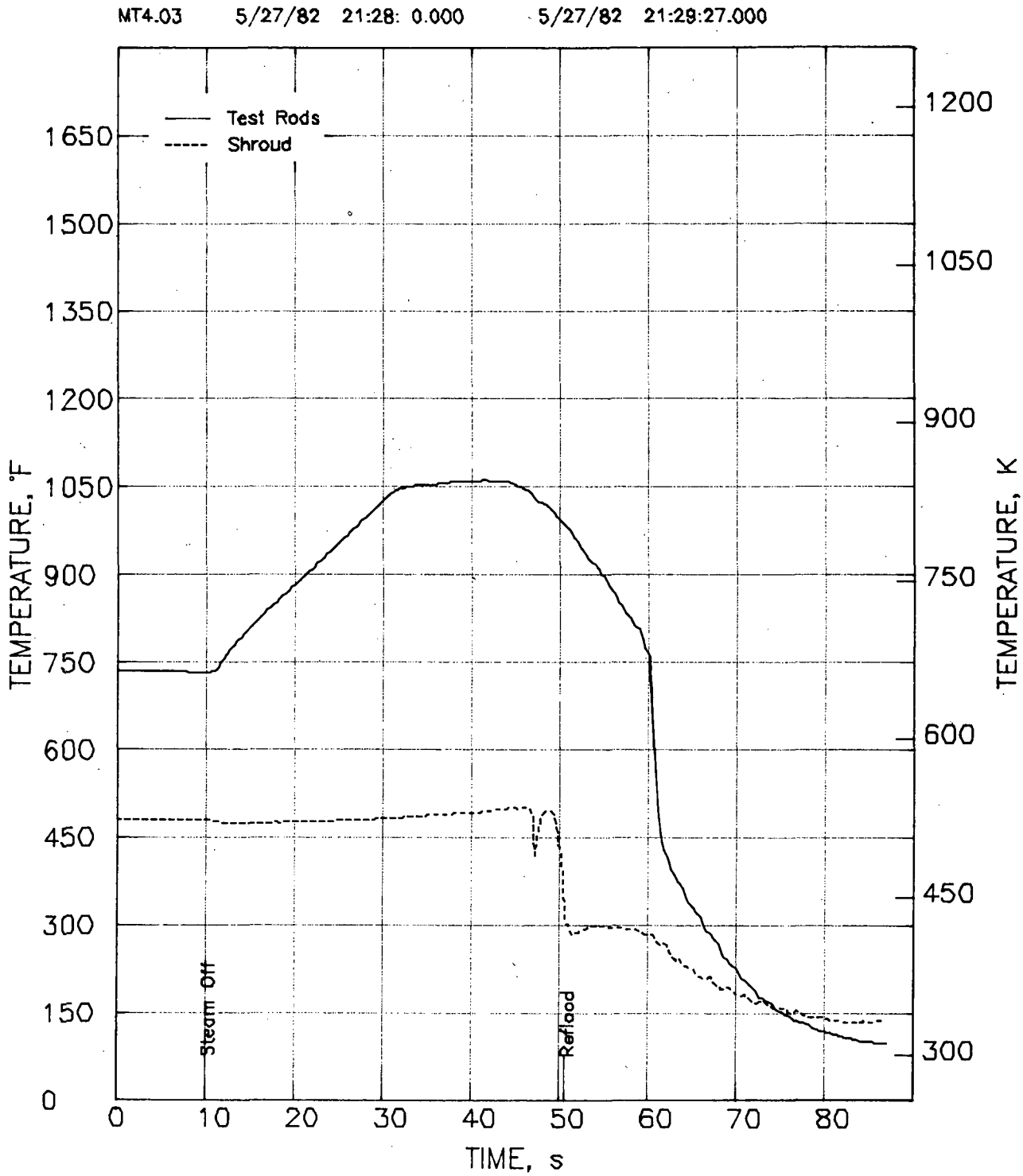

FIGURE 12. Average Test Rod and Shroud Temperatures at Level 97.9 for Adiabatic Test MT-4.03

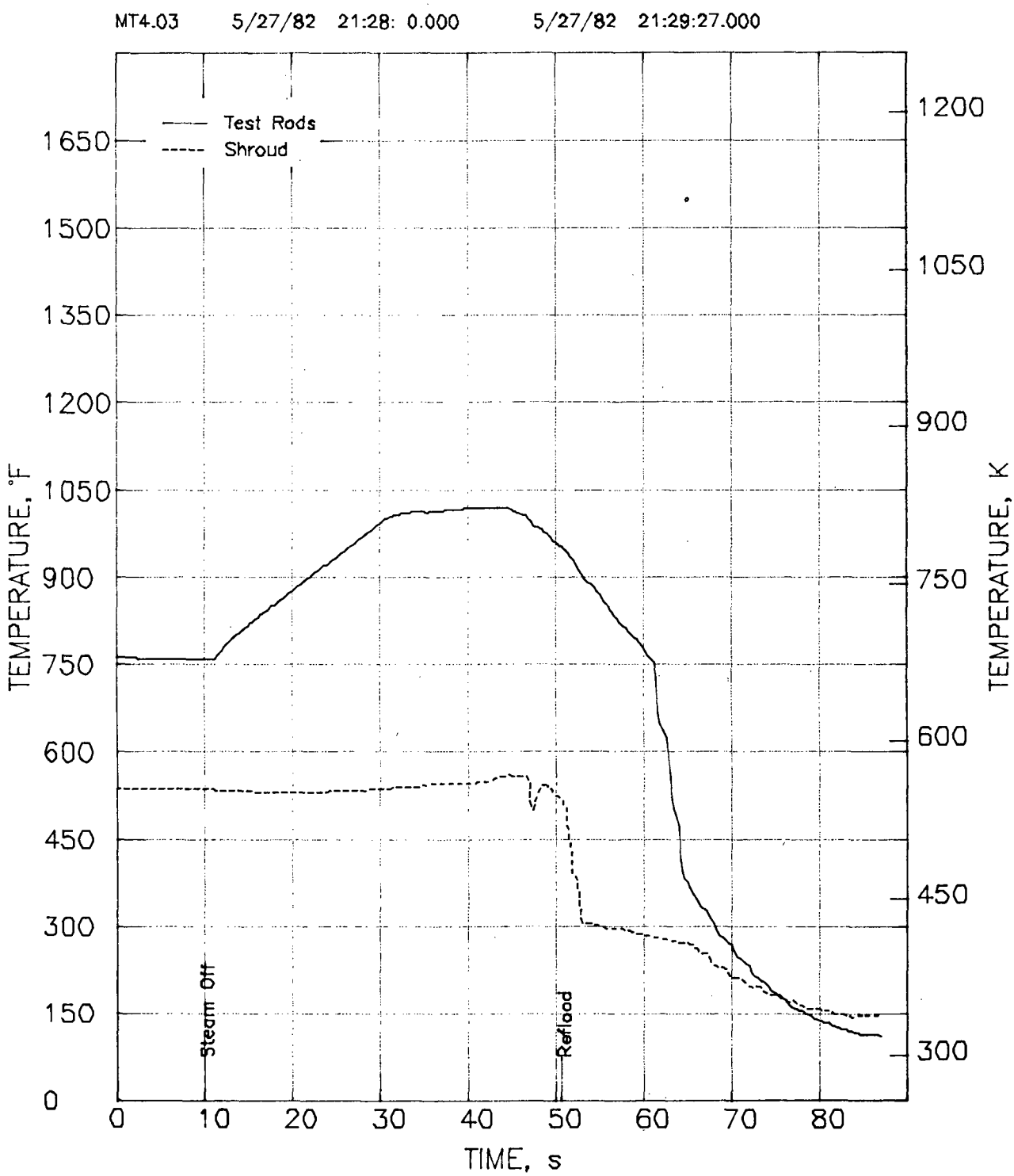

FIGURE 13. Average Test Rod and Shroud Temperatures at Level 118.9 for Adiabatic Test MT-4.03

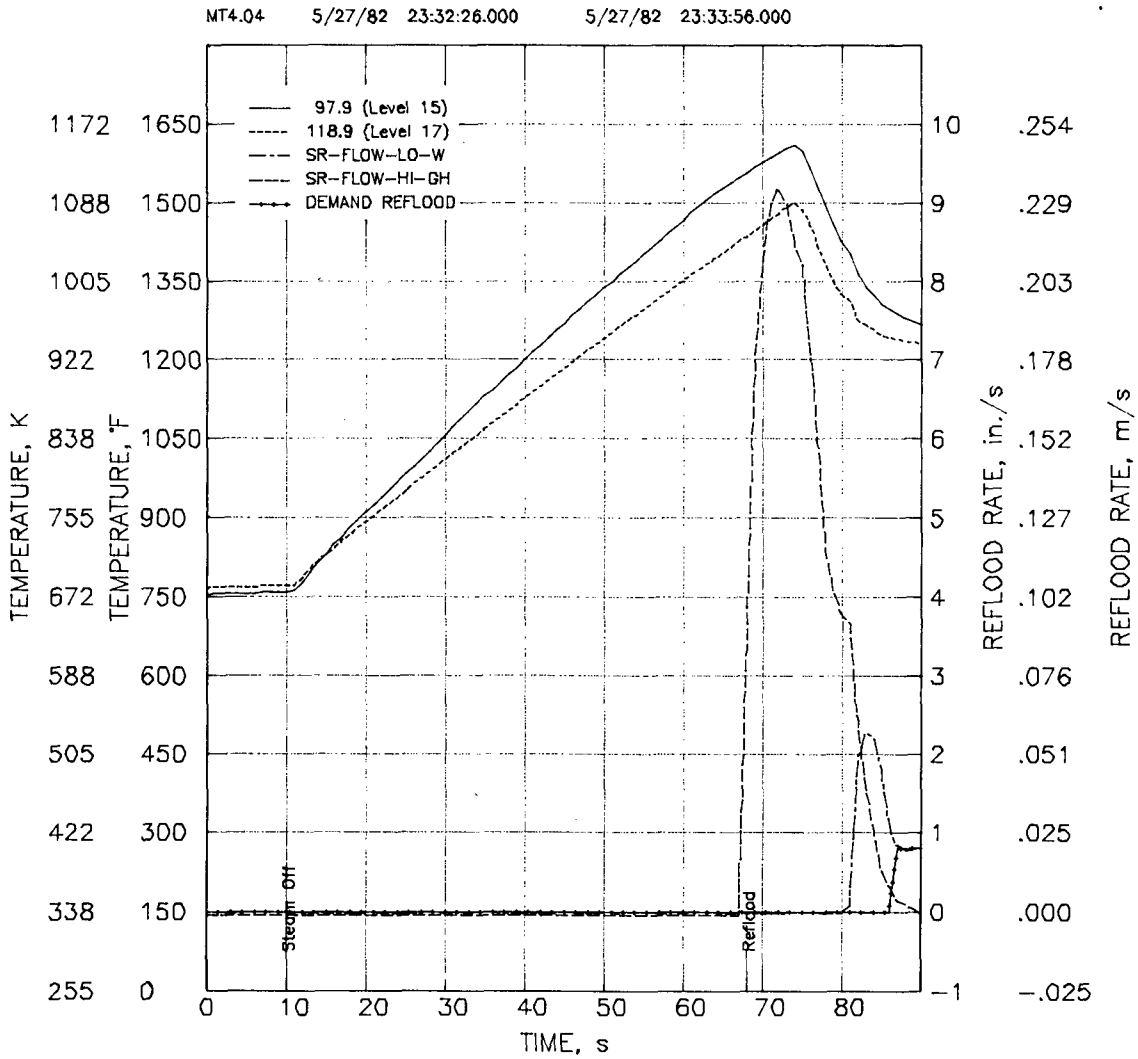

FIGURE 14. Hot Spot Sensor Averages--Levels 97.9 and 118.9--and Demand and Actual Reflood Flow Rates for Initial 90 s of MT-4.04

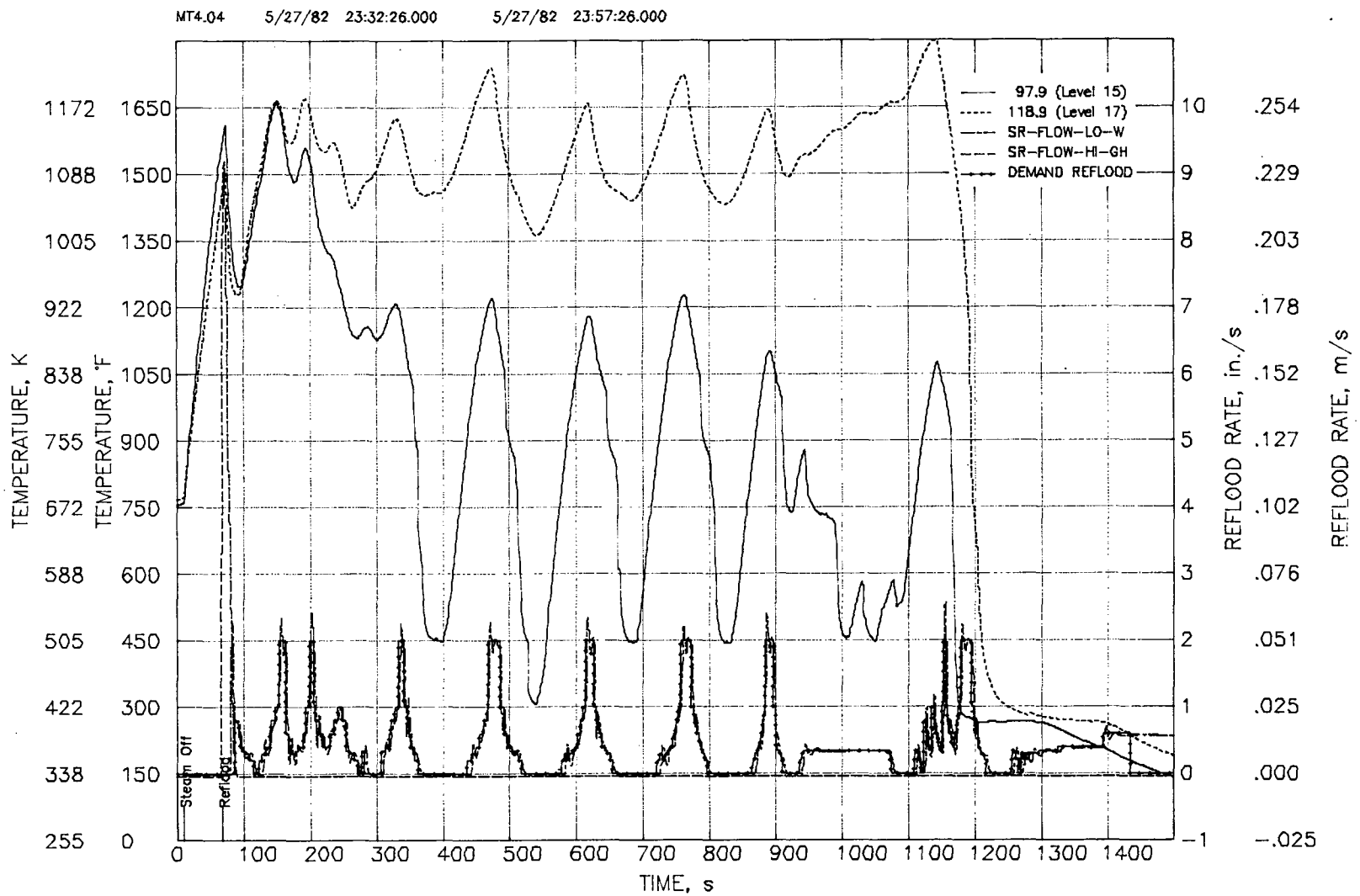

FIGURE 15. Hot Spot Sensor Averages--Levels 97.9 and 118.9--and Demand and Actual Reflood Flow Rates for 1500 s of MT-4.04; DACS Control 72 s After Steam Off

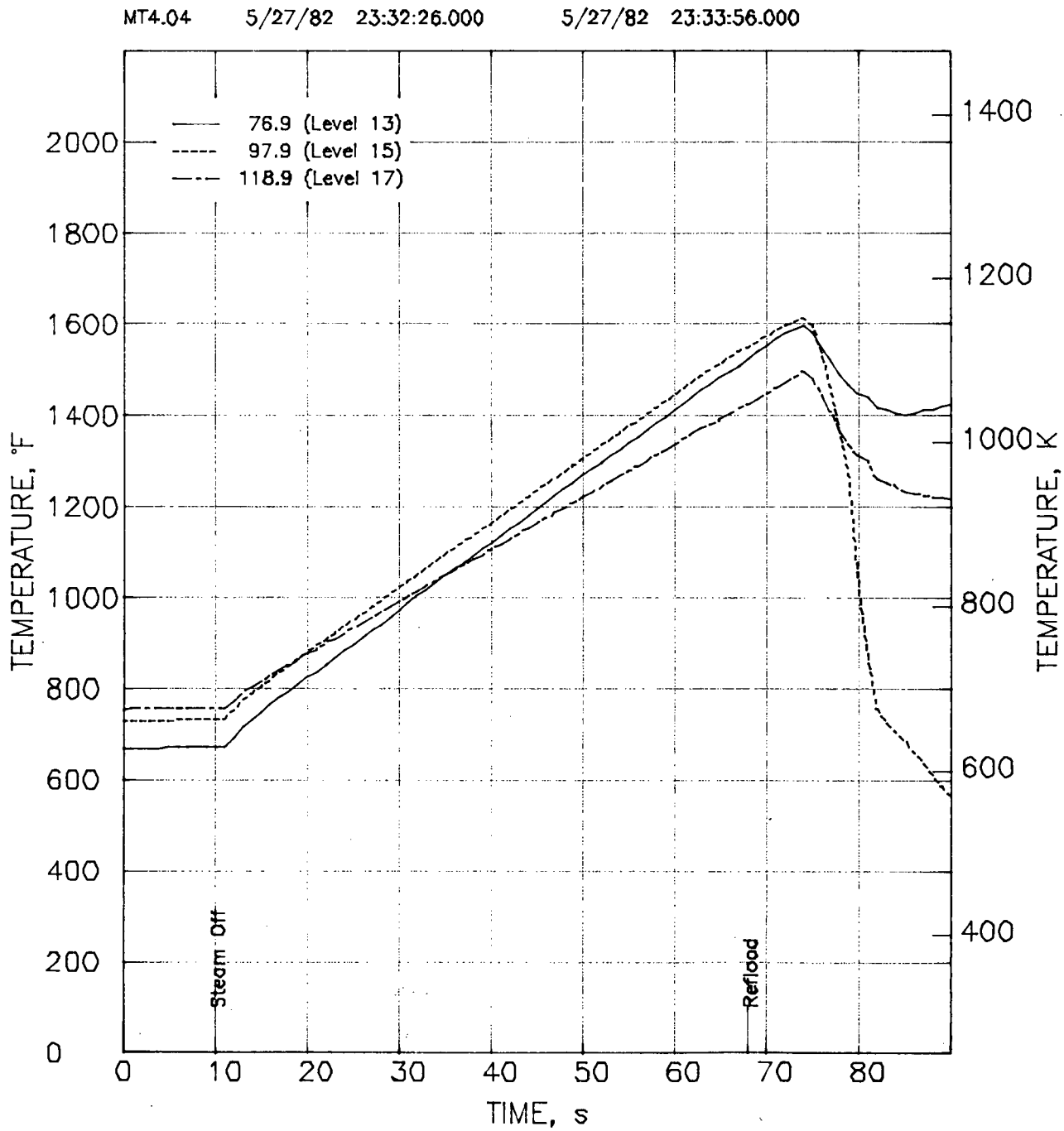

FIGURE 16. Average Test Rod Temperatures at Levels 76.9, 97.9, and 118.9 for Initial 90 s of MT-4.04

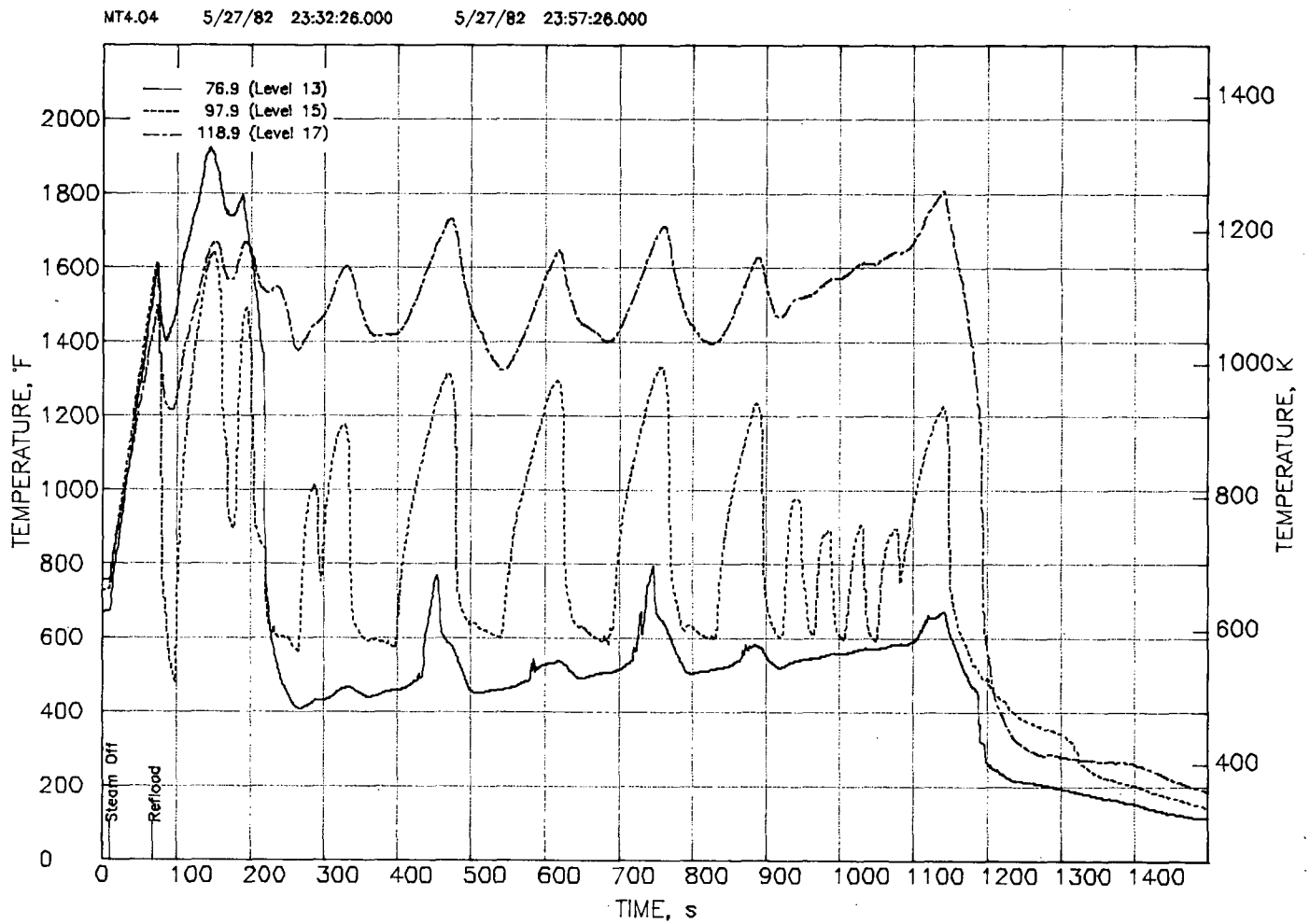

FIGURE 17. Average Test Rod Temperatures at Levels 76.9, 97.9, and 118.9 for 1500 s of MT-4.04

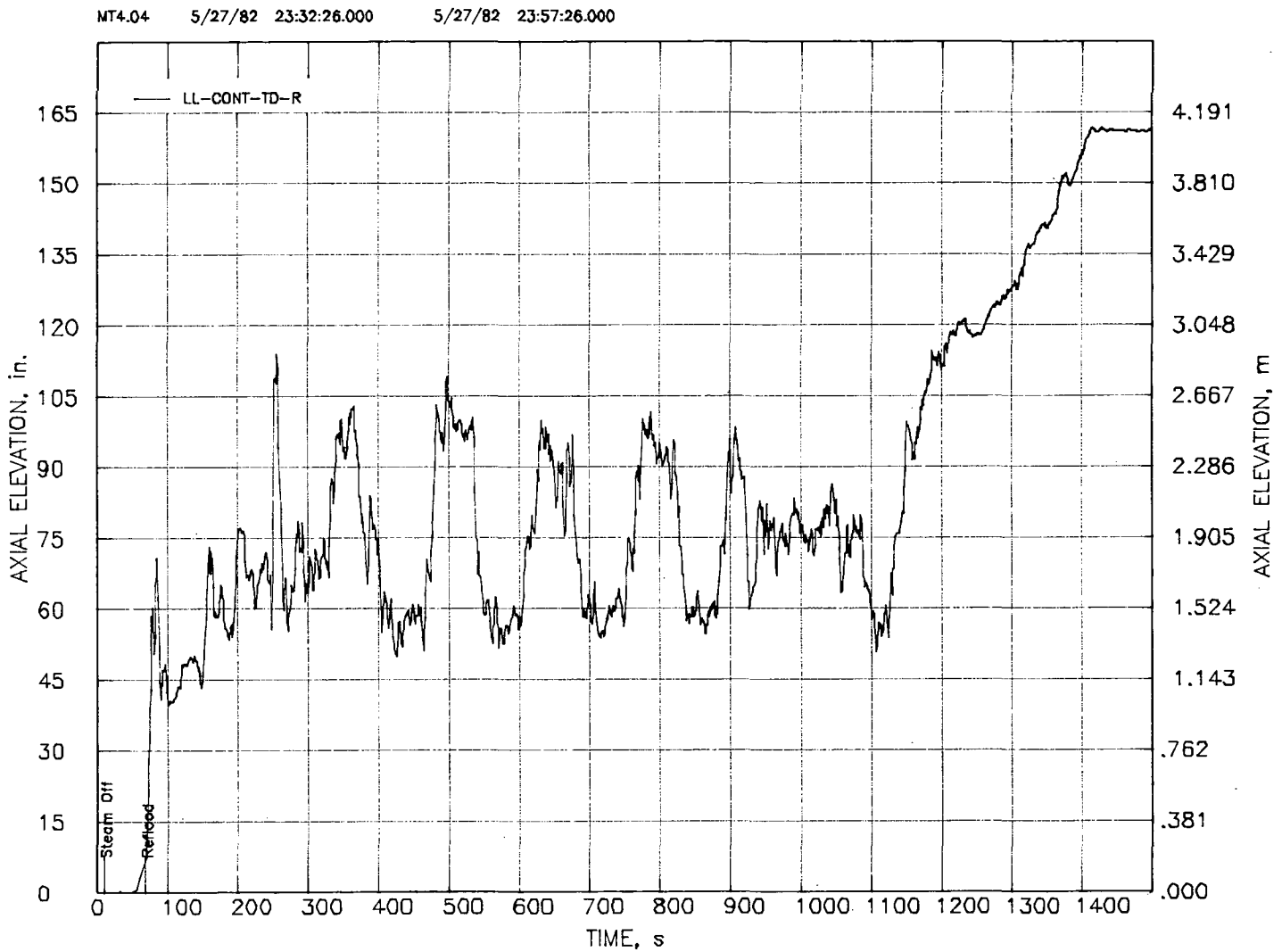

FIGURE 18. Time Domain Reflectometry Instrumentation Liquid Level Response for 1500 s of MT-4.04

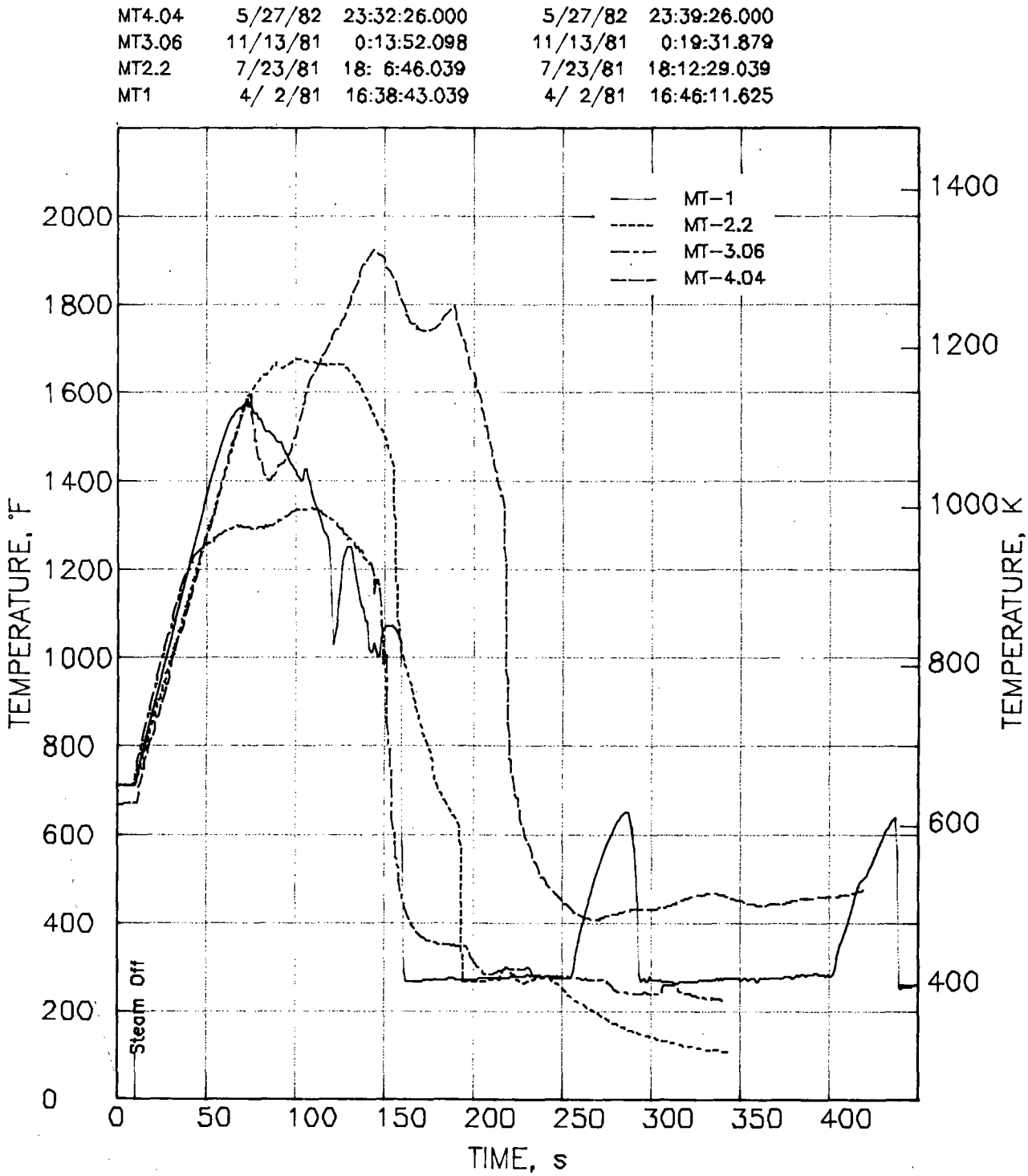

FIGURE 19. Average Cladding Temperatures at Level 76.9 for MT-1, MT-2.2, MT-3.06, and MT-4.04

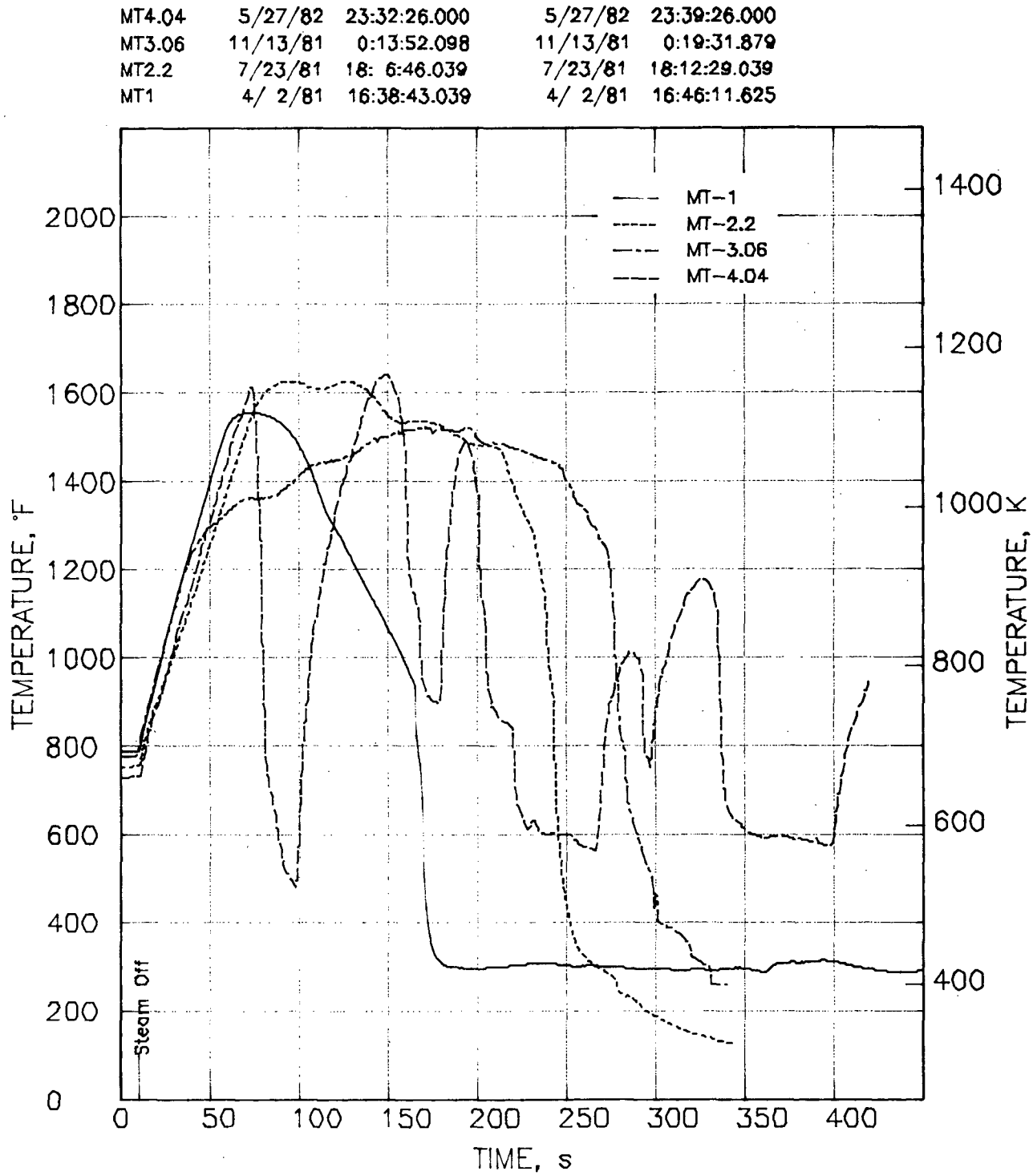

FIGURE 20. Average Cladding Temperatures at Level 97.9 for MT-1, MT-2.2, MT-3.06, and MT-4.04

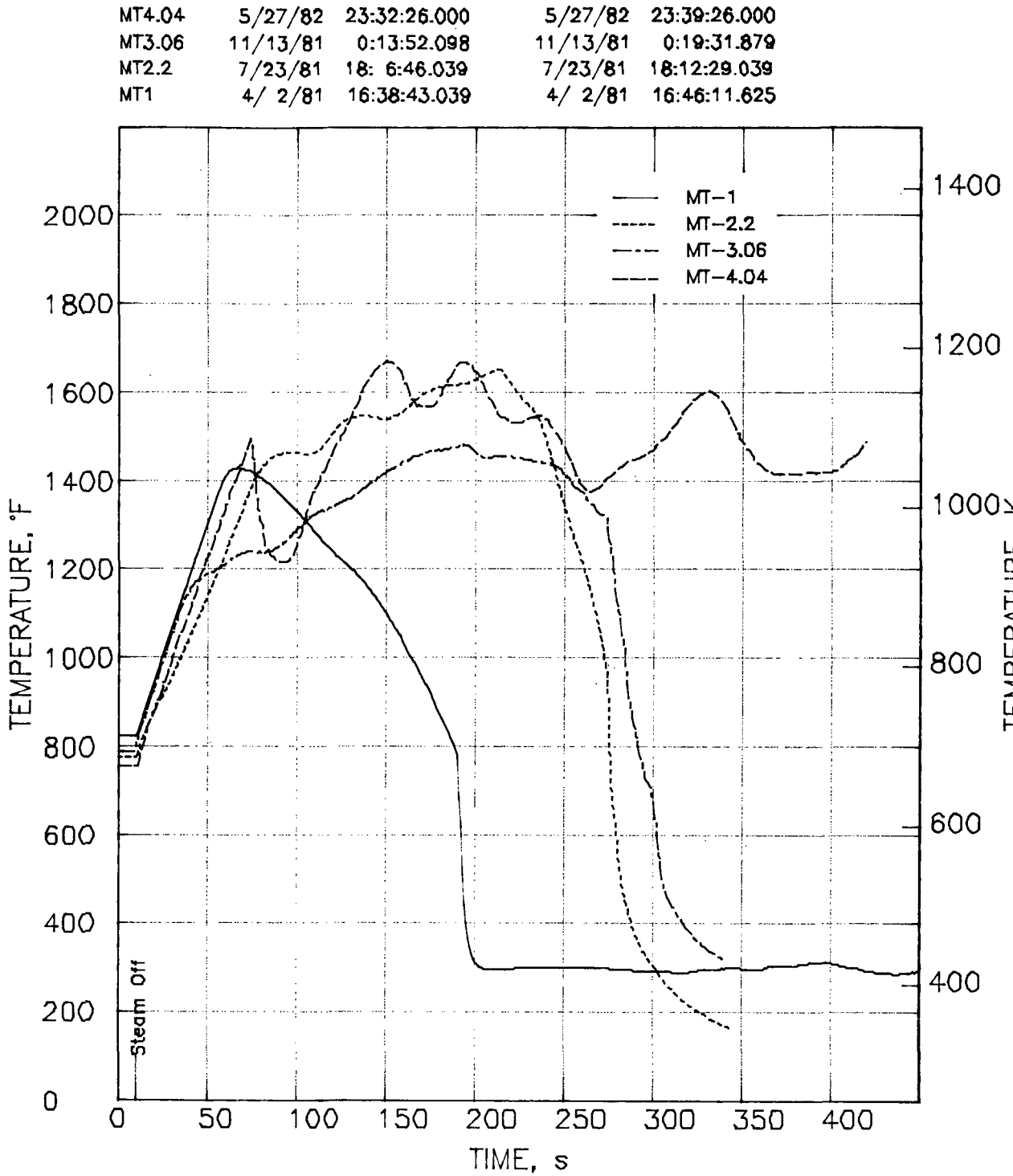

FIGURE 21. Average Cladding Temperatures at Level 118.9 for MT-1, MT-2.2, MT-3.06, and MT-4.04

HEAT TRANSFER COEFFICIENTS AND ASSOCIATED THERMAL-HYDRAULICS FOR BALLOONED AND RUPTURED FUEL

The MT-4.04 experiment operation closely followed the operating conditions of the TH-1.16 test to provide the desired ballooned and ruptured fuel for heat transfer characterization. Following the heatup transient temperature turn-around, the peak cladding temperatures were controlled using variable reflood to provide the required boildown and refill conditions. This test environment provided the opportunity to determine the heat transfer characteristics associated with ballooned and ruptured full-length nuclear-heated fuel during reflood and boildown transient modes.

Data on reflood rate, quench-front propagation, liquid level, axial power, fuel rod temperature, and heat transfer coefficients are presented in this section. The data represent the test environment for which heat transfer conditions were determined. The test conditions for TH-1.16 and MT-4.04 are compared in Table 5. Desuperheater spray system data are also presented, establishing that the pressure tube surrounding the test assembly was in a safe environment at all times.

REFLOOD RATES

The reflood rates used in the MT-4 experiment were selected to stabilize the peak cladding temperatures so that the heat transfer characteristics of the deformed (and ruptured) fuel bundle could be measured. In addition, latter portions of the test were devoted to gaining experience with boildown transient behavior. The measured reflood rates during the MT-4 transient are illustrated in Figure 22.

QUENCH-FRONT PROPAGATION AND LIQUID LEVEL

During the reflood and boildown phases of the transient, the fuel bundle and shroud quenched and dried out. The time history of the quench-front level in the fuel bundle is an approximation of the water level in the fuel bundle for very low reflood rates. Quench-front movement for the shroud will be much faster than for the fuel bundle and will give an indication of the liquid entrainment effects in the steam during the reflood and boildown operations. The average guard rod and shroud quench-front elevations as a function of time are shown in Figure 23.

A liquid level detector was used to determine the liquid level during the course of the transient. The average guard rod and shroud quench-front behaviors and the liquid level detector indications are compared in Figure 24.

TABLE 5. Experiment Conditions for the MT-4.04 Transient

Parameter	TH-1.16	MT-4.04
Average rod power,[a] kW/ft	0.316	0.367
Delay time, s	65	57
Reflood rate, m/s (in./s)	0.104 (4.1)	Variable
Peak temperature elevation, m (in.)	2.47 (97.3)	2.05 (80.9)
Peak temperature, K (°F)	1204 (1707)	1459 (2166)
Average peak temperature, K (°F)	1182 (1668)	1418 (2092)
Peak rod temperature, K (°F)		
Start of test	720 (836)	636 (686)
Start of reflood	1089 (1500)	1103 (1526)
Average temperature at peak location, K (°F)		
Start of test	682 (768)	639 (690)
Start of reflood	1121 (1558)	1105 (1529)
Nominal system pressure, MPa (psia)	0.276 (40)	0.276 (40)
Nominal inlet coolant temperature, K (°F)	311 (100)	311 (100)

(a) Based on heatup rate method; from adiabatic portion of MT-4.

AXIAL POWER DISTRIBUTION

The axial power distribution in the fuel assembly was evaluated using normalized local heatup rates, assembly SPND measurements, assembly flux wire data, and a series of measurements taken by a transit flux probe during the preconditioning phase of the experiment in the NRU reactor. Local axial powers were calculated using the adiabatic period heatup rates and the fuel rod mass and specific heat. These normalized readings are plotted against a computed power profile based on core physics calculations prior to the test in Figure 25.

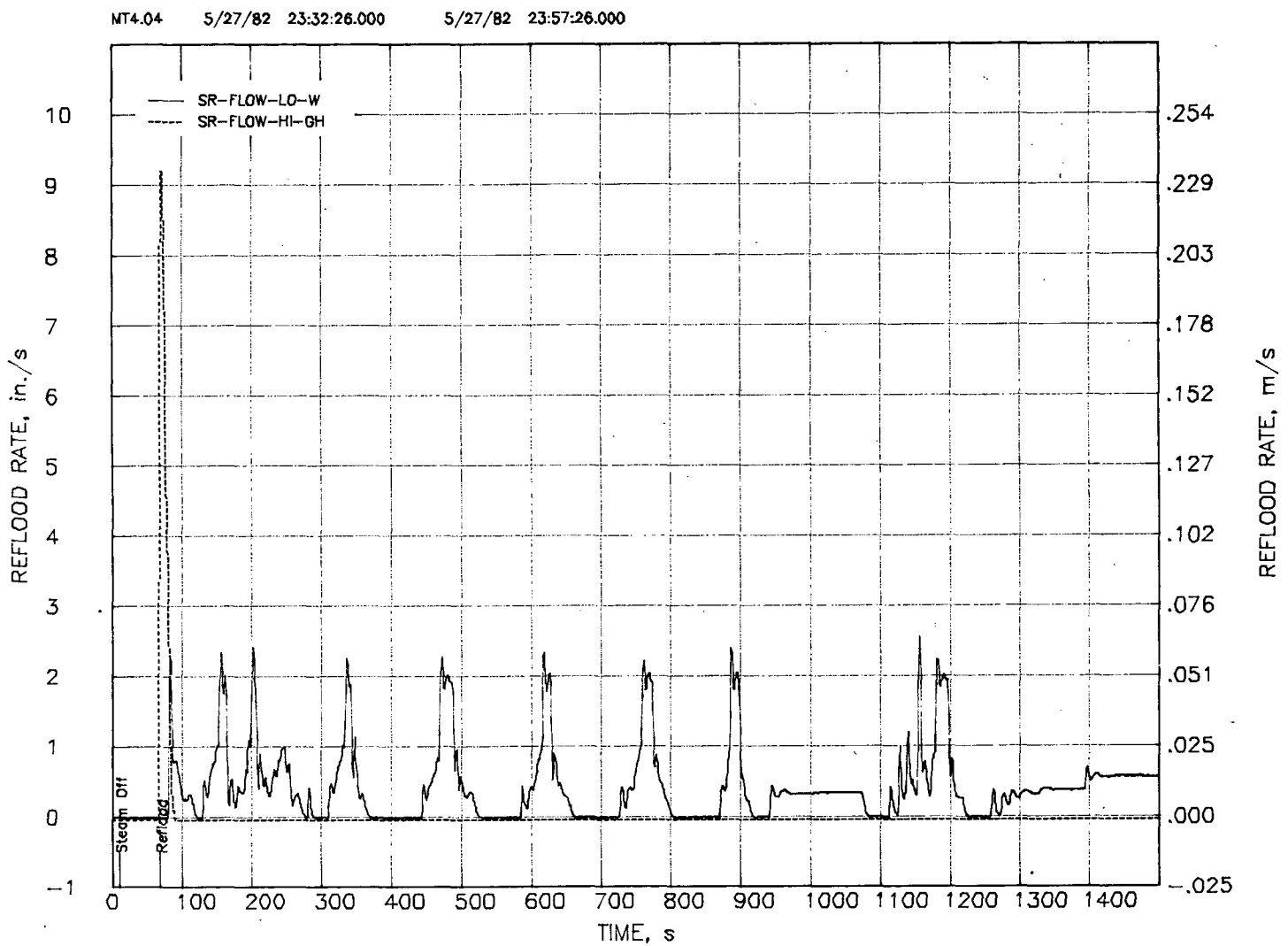

FIGURE 22. Measured Reflood Rate Versus Time for the MT-4.04 Transient

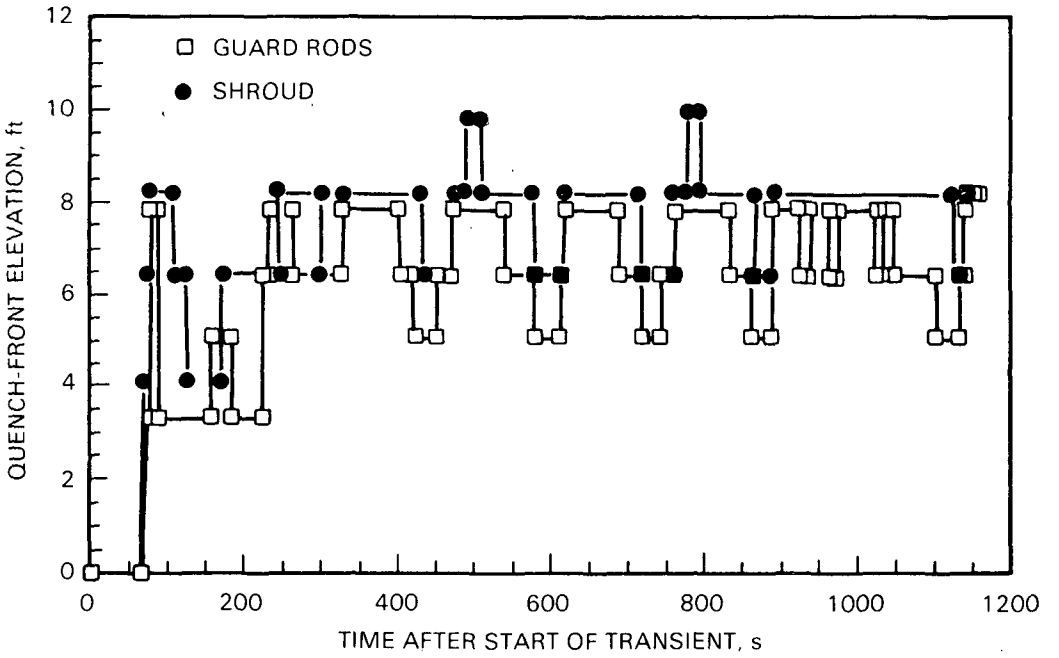

FIGURE 23. Comparison of MT-4 Quench-Front Elevation for the Guard Rods and the Shroud

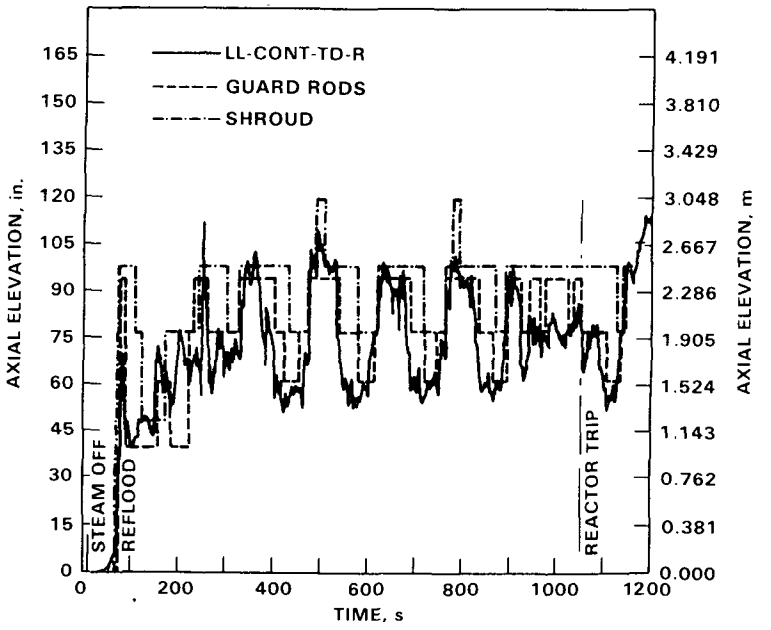

FIGURE 24. Comparison of MT-4 Liquid Level Detector Readings and Guard Rod and Shroud Quench-Front Behavior as a Function of Time

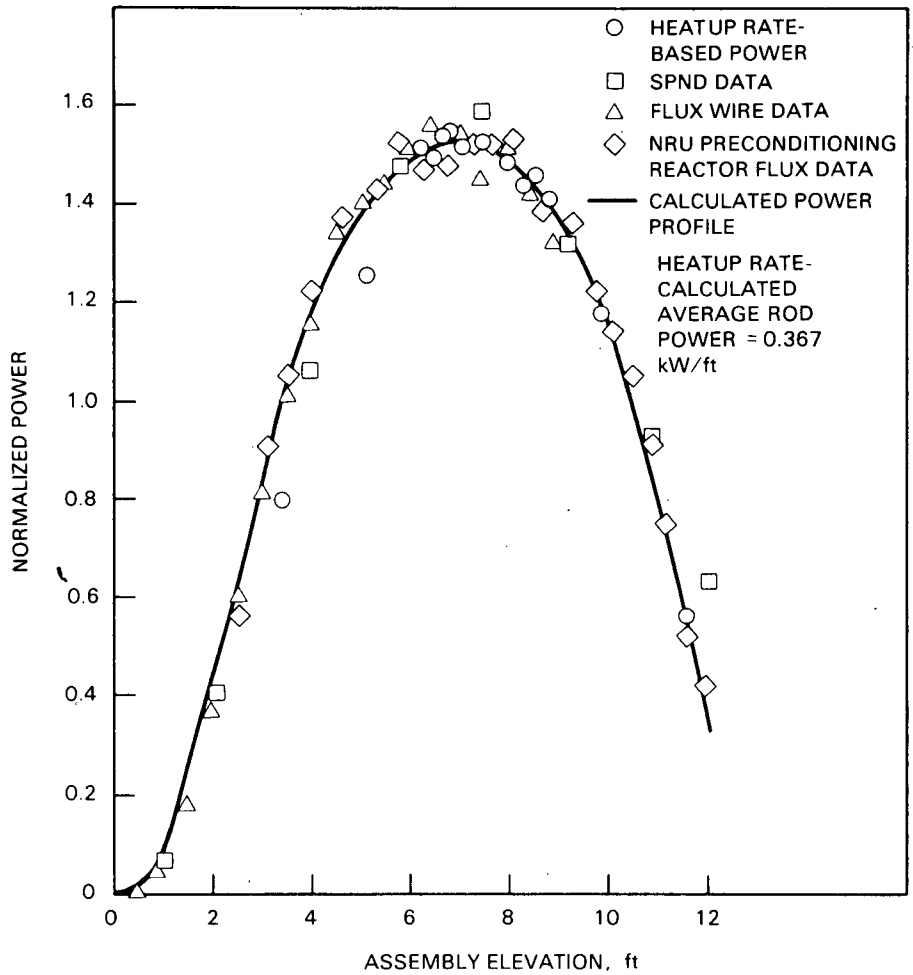

FIGURE 25. Comparison of MT-4 Heatup Rate-Based, SPND, Flux Wire, NRU Reactor Preconditioning, and Calculated Axial Power Profiles

TEST ROD AND GUARD ROD TEMPERATURES

The maximum and minimum test rod and guard rod temperatures at Levels 76.9, 97.9, and 118.9 are compared in Figures 26 through 28, respectively. The shaded areas show the range between the maximum and minimum rod temperatures. There does not appear to be any significant effect of the ballooning and rupture on the measured higher cladding temperatures between nonpressurized nondeformed guard rods and pressurized deformed test rods.

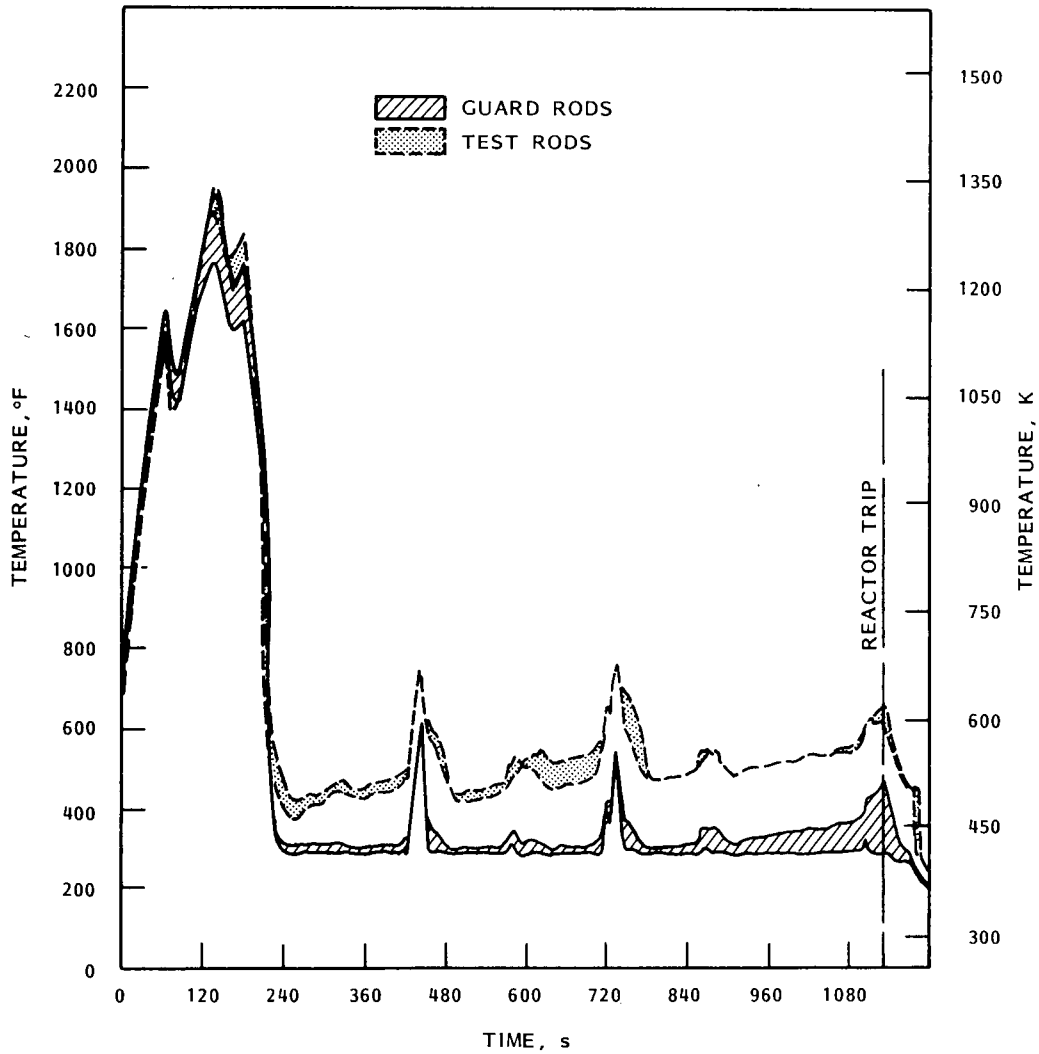

FIGURE 26. Comparison of Maximum and Minimum Test Rod and Guard Rod Temperatures at Level 76.9 for MT-4

HEAT TRANSFER COEFFICIENTS

The evaluation of the thermal conditions in the fuel cladding as a function of time is characterized by the local heat transfer coefficients. The heat transfer coefficients presented are from an analysis that used saturation temperatures and measured local cladding temperatures. The saturation temperature is defined by the system operating pressures and remained constant throughout the experiment at 0.276 MPa (40 psi).

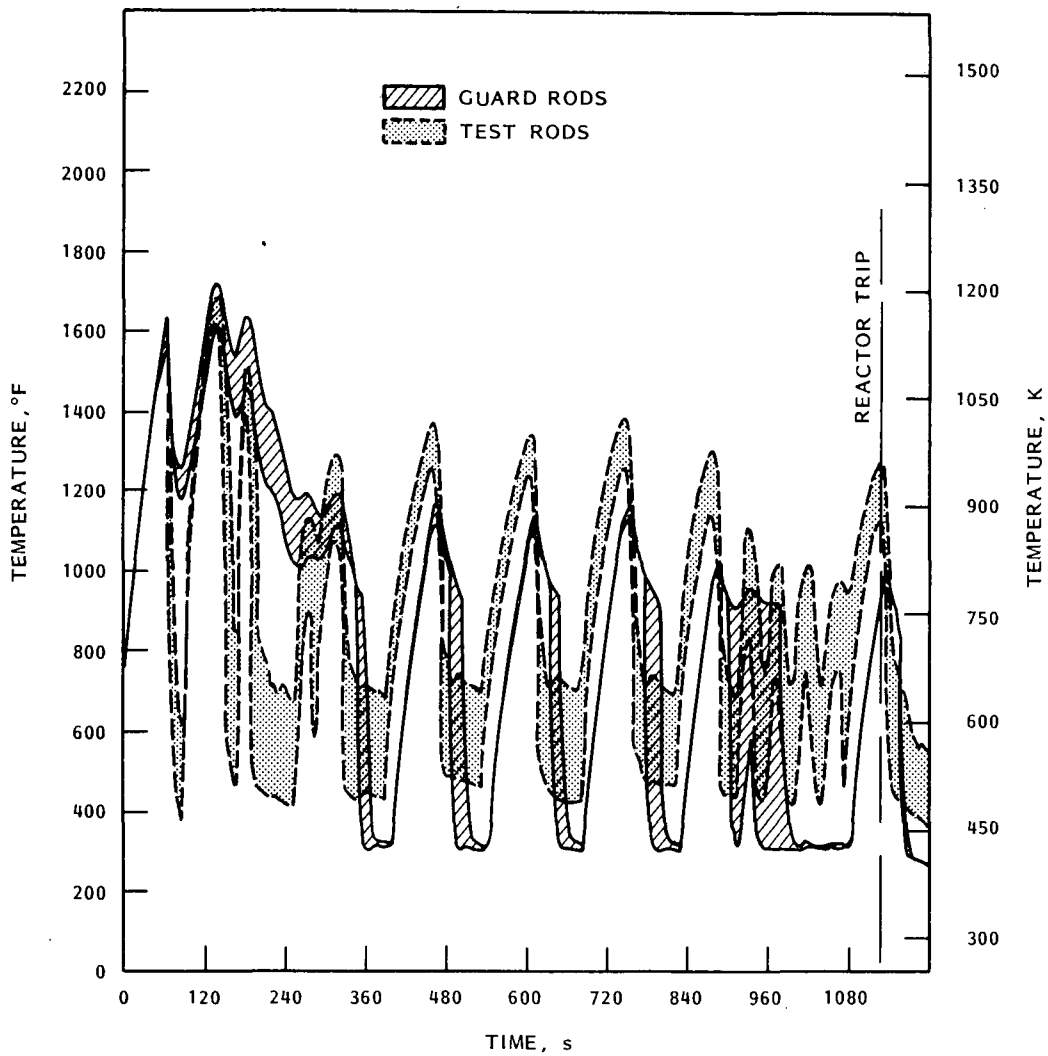

FIGURE 27. Comparison of Maximum and Minimum Test Rod and Guard Rod Temperatures at Level 97.9 for MT-4

Temperatures and local heat transfer coefficients are shown in Figures 29 through 39. Computed results are compared for the deformed test bundle rods and for the nondeformed guard bundle rods at Levels 76.9, 97.9, and 118.9. These plots also contain information from the MT-1, MT-2, and MT-3 experiments. The different results for guard and test rods at Levels 76.9 and 97.9 are caused more by the earlier quenching of guard rods than by deformation differences. Heat transfer for deformed versus nondeformed rods can be best compared by evaluating deformed test rod behavior versus nondeformed guard rod behavior for the same test at higher elevations (Figure 39).

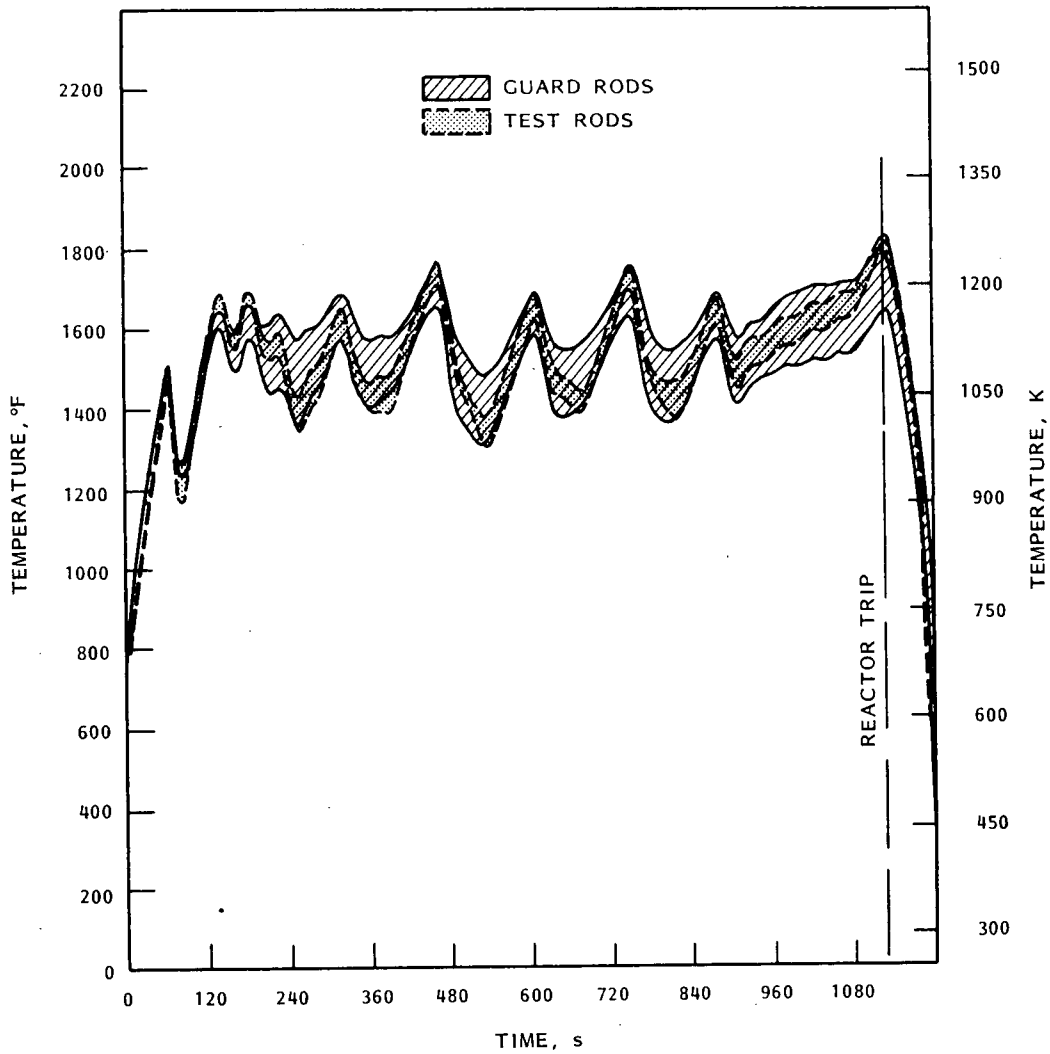

FIGURE 28. Comparison of Maximum and Minimum Test Rod and Guard Rod Temperatures at Level 118.9 for MT-4

DESUPERHEATER SPRAY SYSTEM

A desuperheater spray system was installed in the MT-4 test assembly at the 151.5-in. elevation as an engineered safety feature. The system insured that steam did not heat the pressure tube in the upper region above 700K (800°F). Subcooled water was injected into the outlet steam to maintain a temperature of 589 ±56K (600 ±100°F). The system was controlled by the DACS, which monitored several TCs in the upper region and activated the spray injection. The average steam temperatures at the 148.2-, 156.0-, 168.7-, and 187.4-in. elevations are shown in comparison to the desuperheater activation signal during the MT-4 transient in Figure 40.

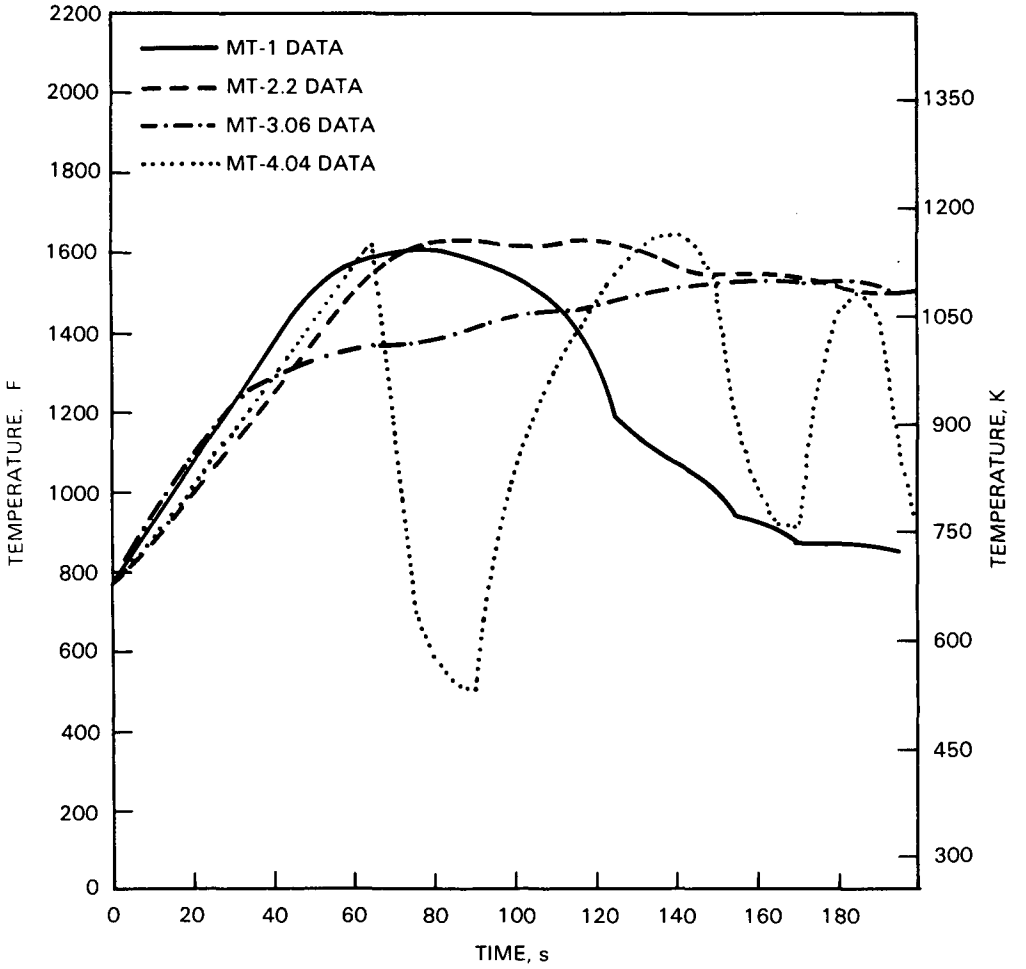

FIGURE 29. Comparison of Test Rod Temperatures at Level 97.9 for MT-1, MT-2.2, MT-3.06, and MT-4.04

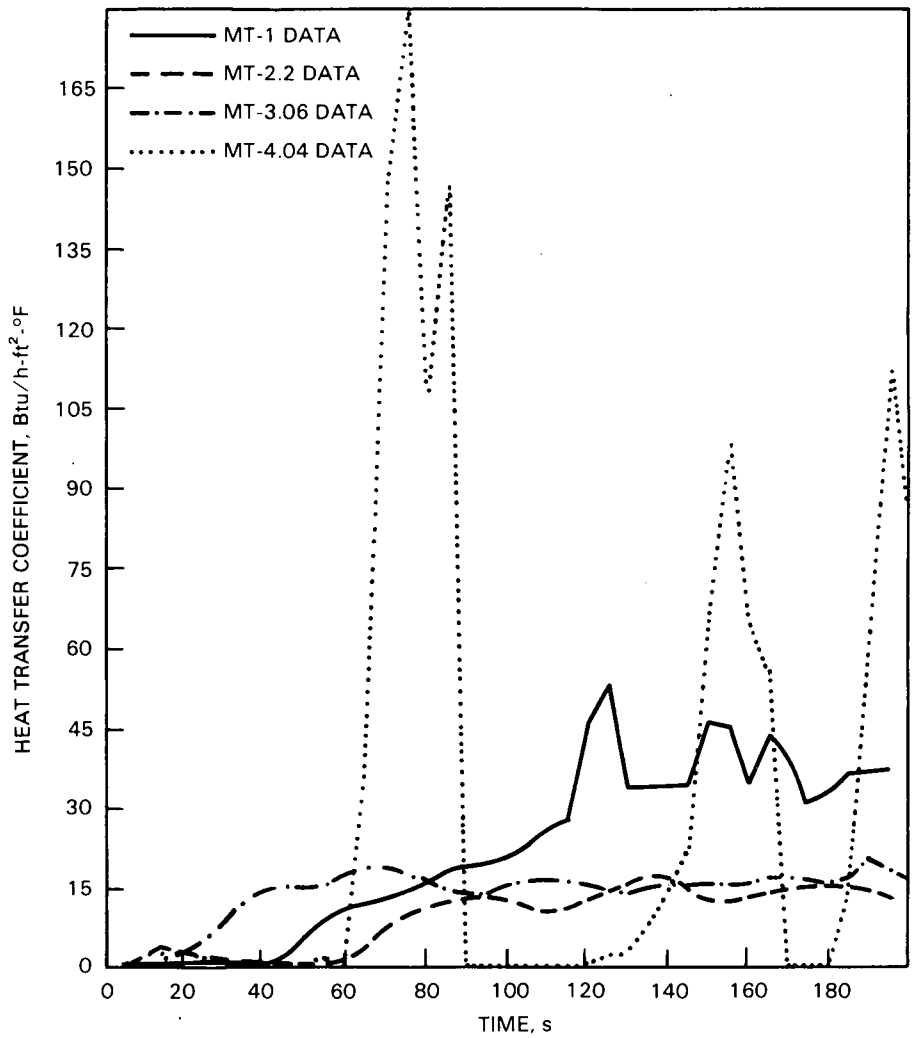

FIGURE 30. Comparison of Test Rod Heat Transfer Coefficients at Level 97.9 for MT-1, MT-2.2, MT-3.06, and MT-4.04 ($Btu/h\text{-}ft^2\text{-}°F \times 5.678263 = W/m^2\text{-}K$)

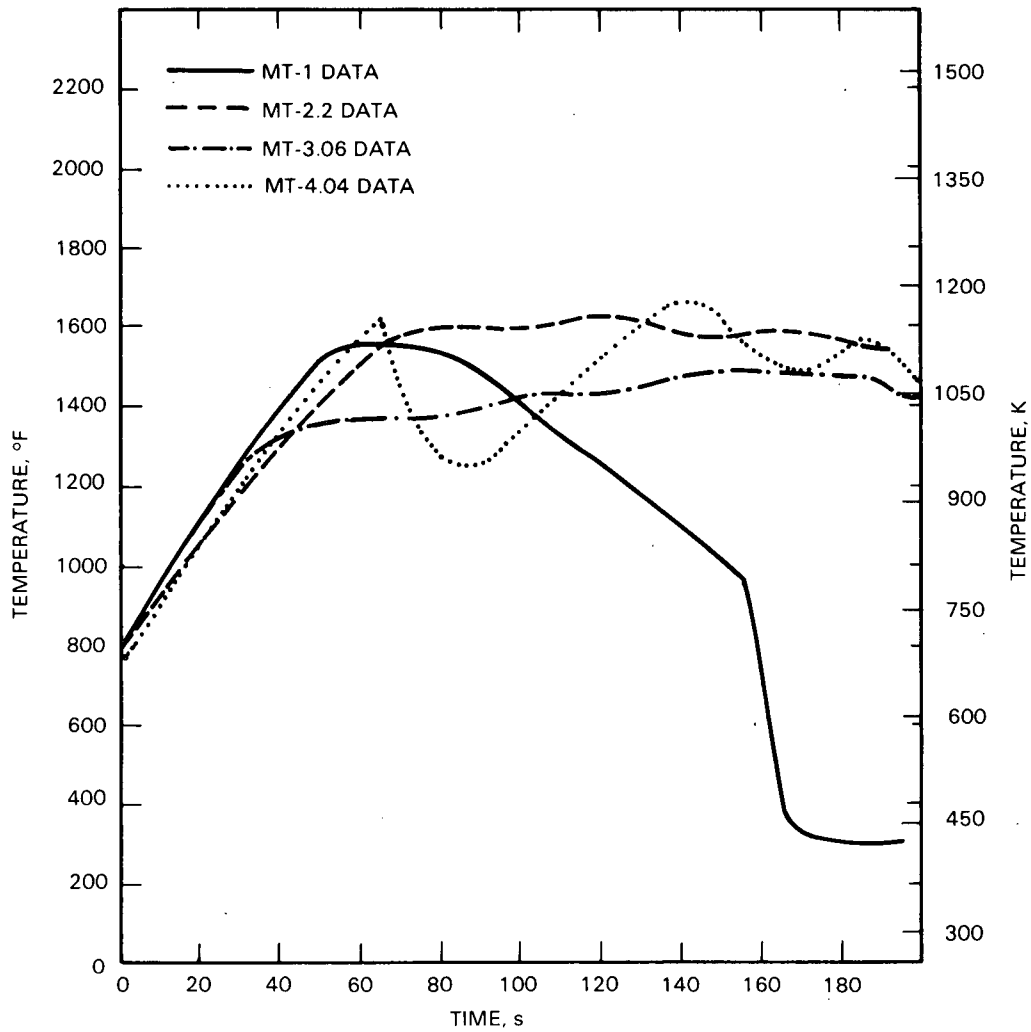

FIGURE 31. Comparison of Guard Rod Temperatures at Level 97.9 for MT-1, MT-2.2, MT-3.06, and MT-4.04

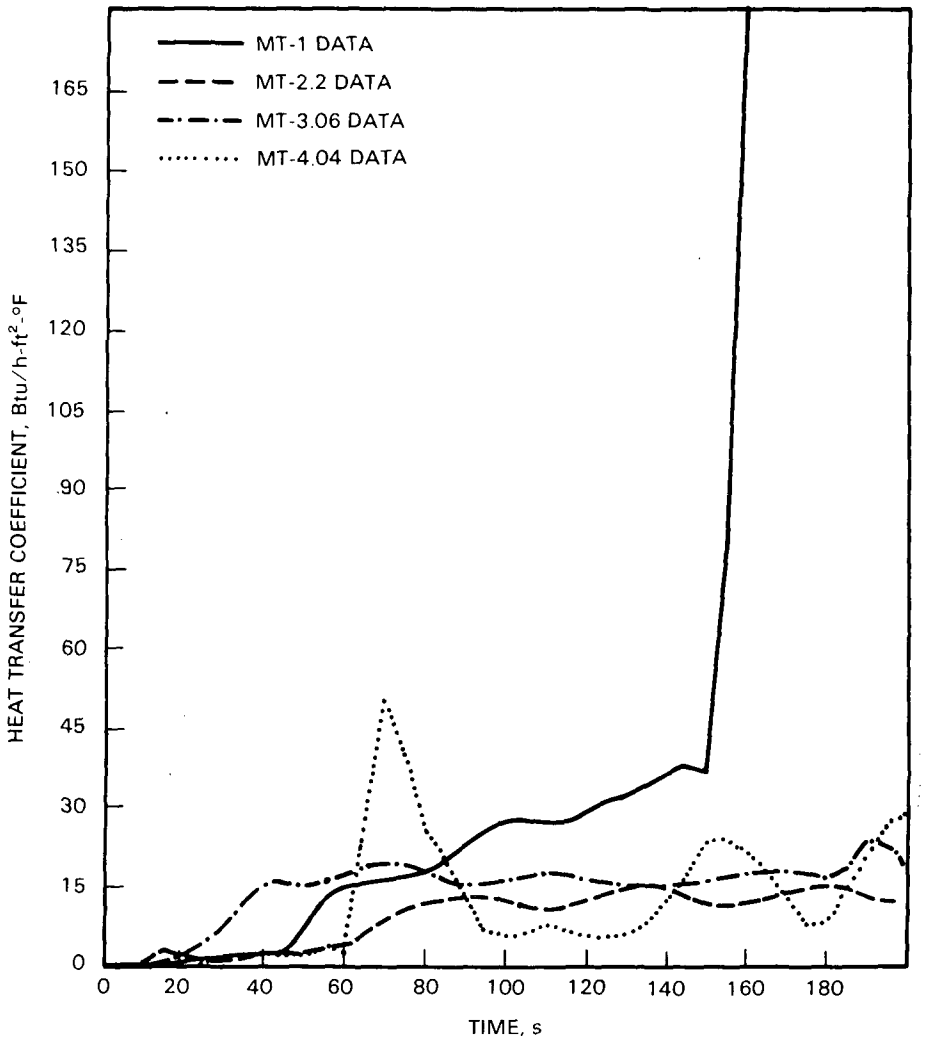

FIGURE 32. Comparison of Guard Rod Heat Transfer Coefficients at Level 97.9 for MT-1, MT-2.2, MT-3.06, and MT-4.04 (Btu/h-ft^2-°F x 5.678263 = W/m^2-K)

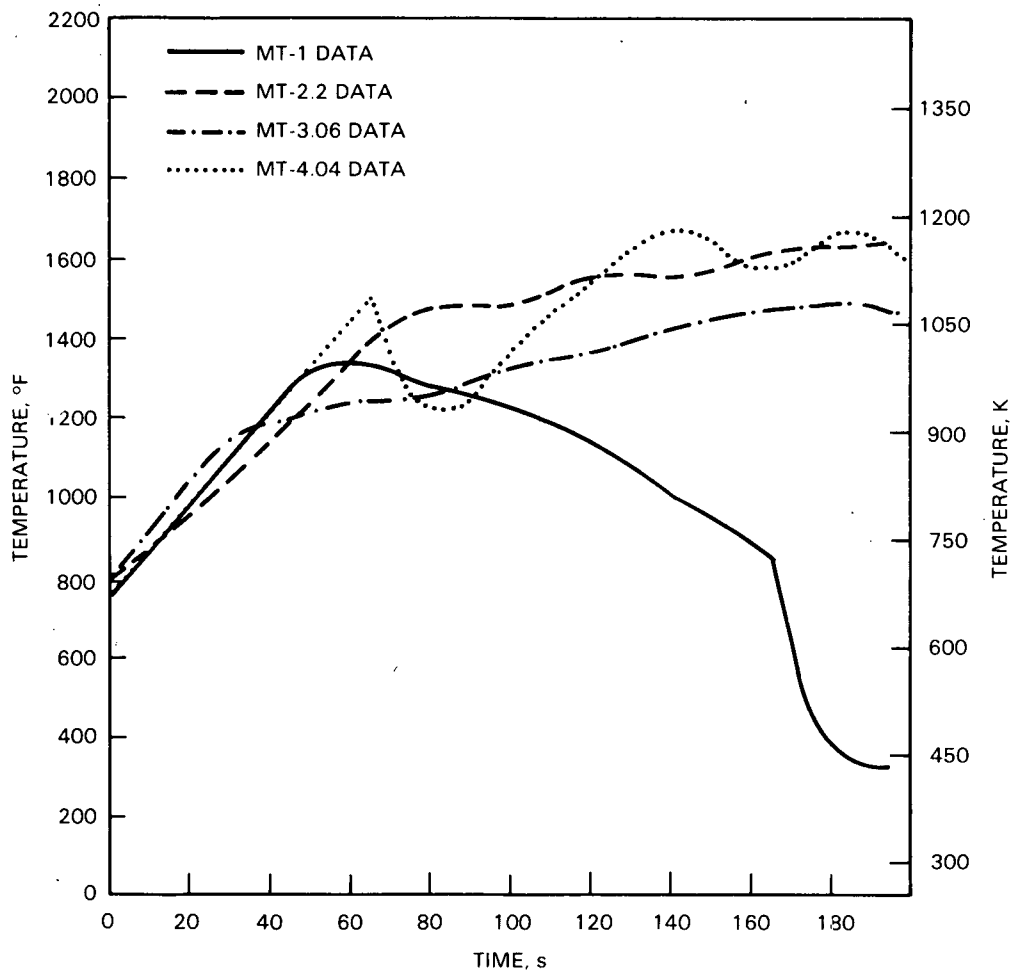

FIGURE 33. Comparison of Test Rod Temperatures at Level 118.9 for MT-1, MT-2.2, MT-3.06, and MT-4.04

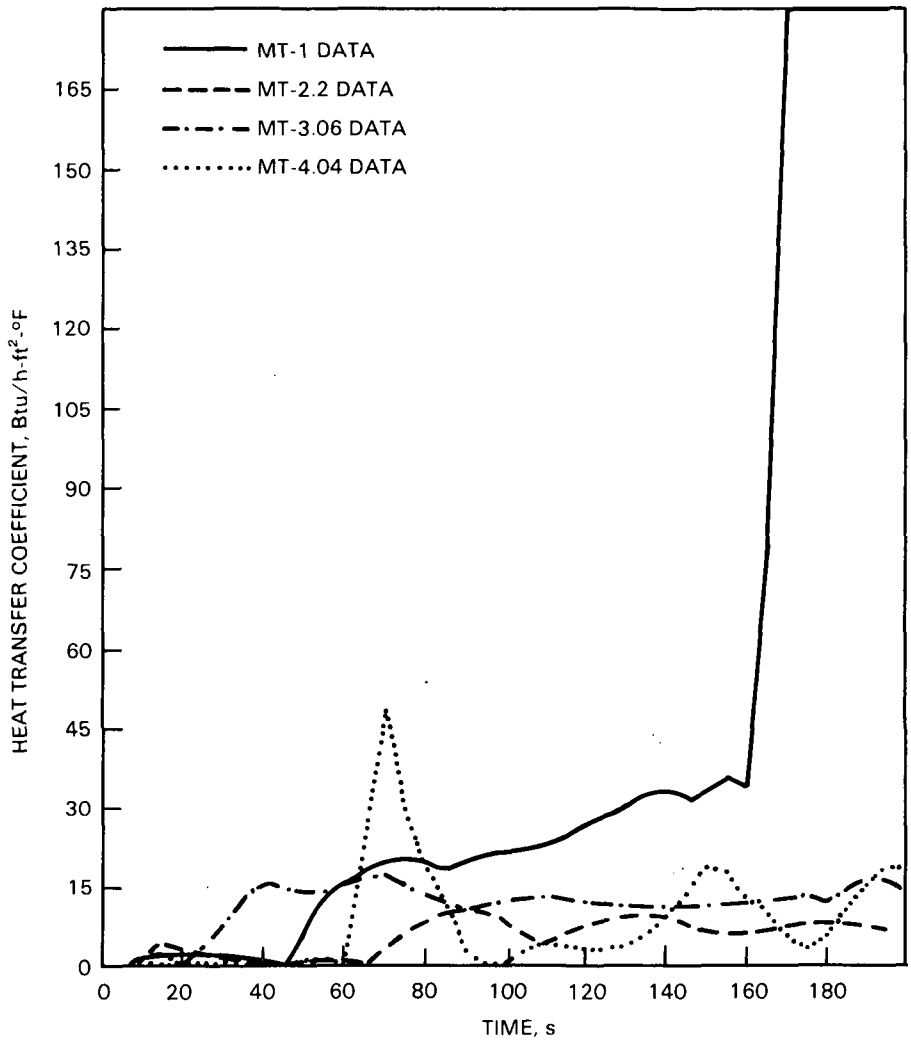

FIGURE 34. Comparison of Test Rod Heat Transfer Coefficients at Level 118.9 for MT-1, MT-2.2, MT-3.06, and MT-4.04 ($Btu/h\text{-}ft^2\text{-}°F \times 5.678263 = W/m^2\text{-}K$)

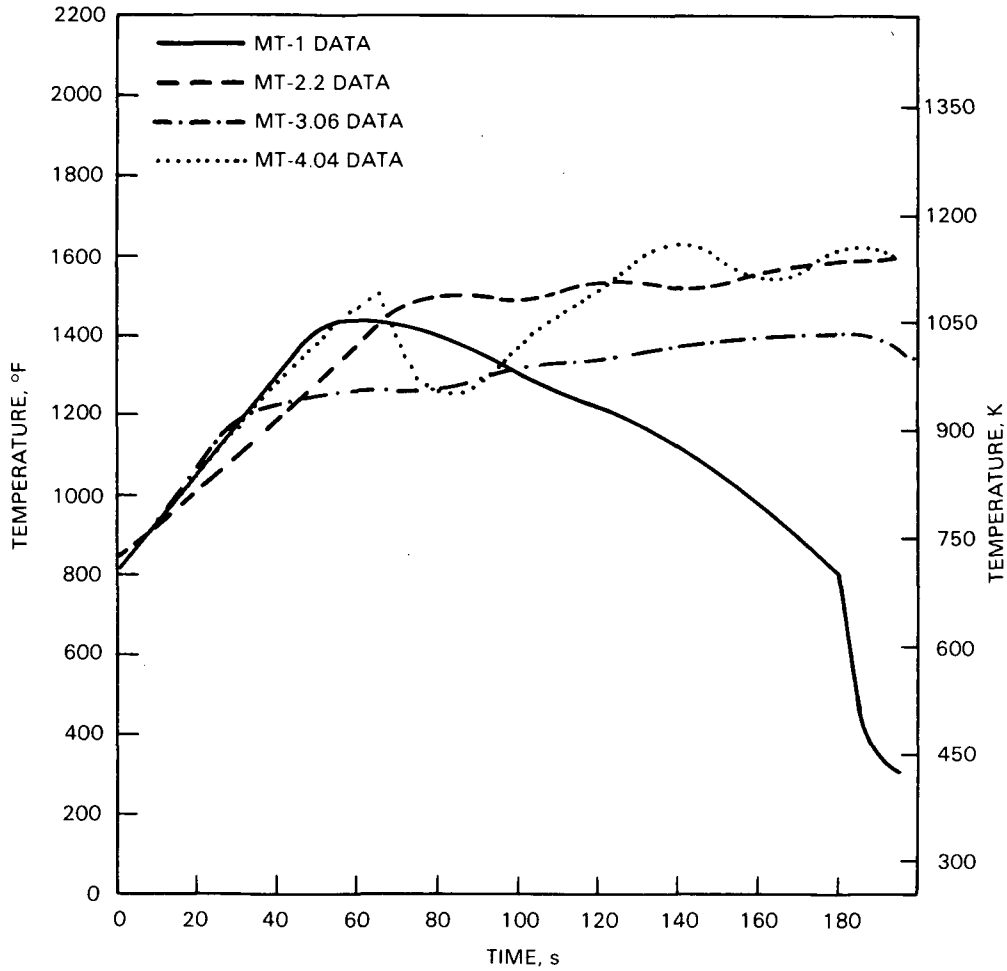

FIGURE 35. Comparison of Guard Rod Temperatures at Level 118.9 for MT-1, MT-2.2, MT-3.06, and MT-4.04

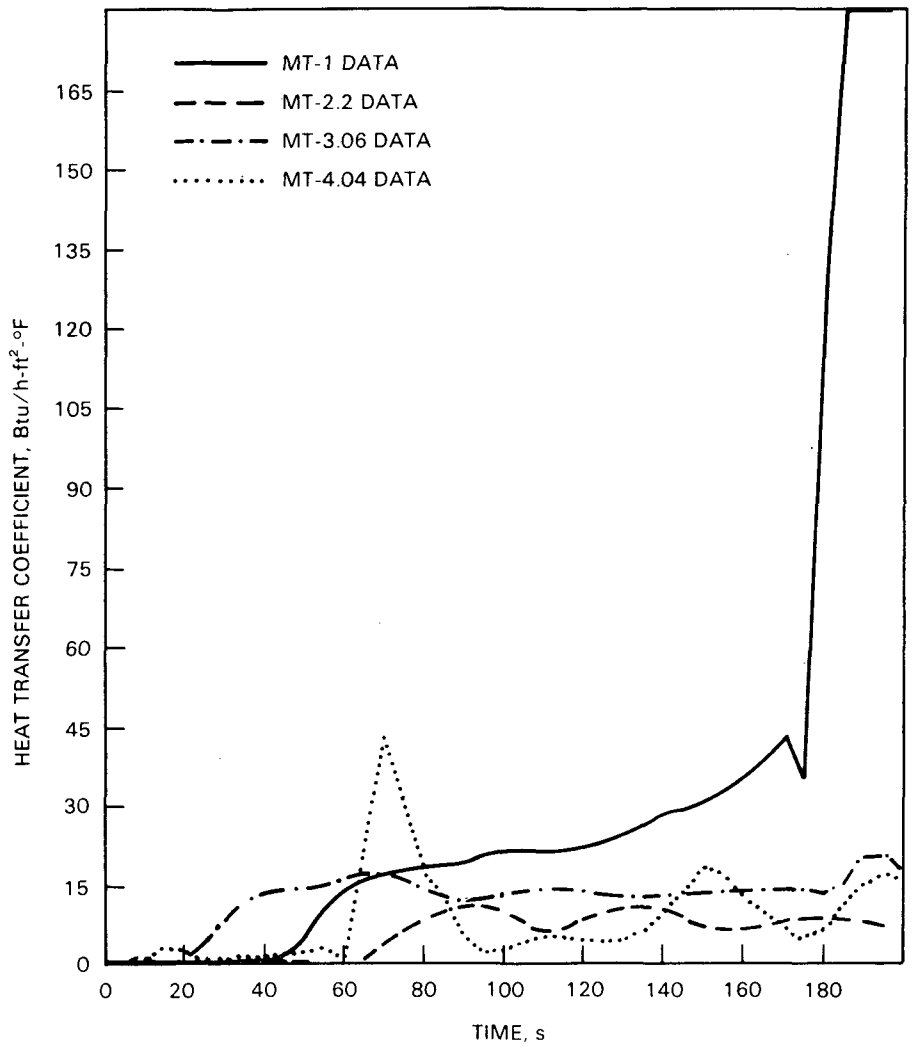

FIGURE 36. Comparison of Guard Rod Heat Transfer Coefficients at Level 118.9 for MT-1, MT-2.2, MT-3.06, and MT-4.04 ($Btu/h\text{-}ft^2\text{-}°F \times 5.678263 = W/m^2\text{-}K$)

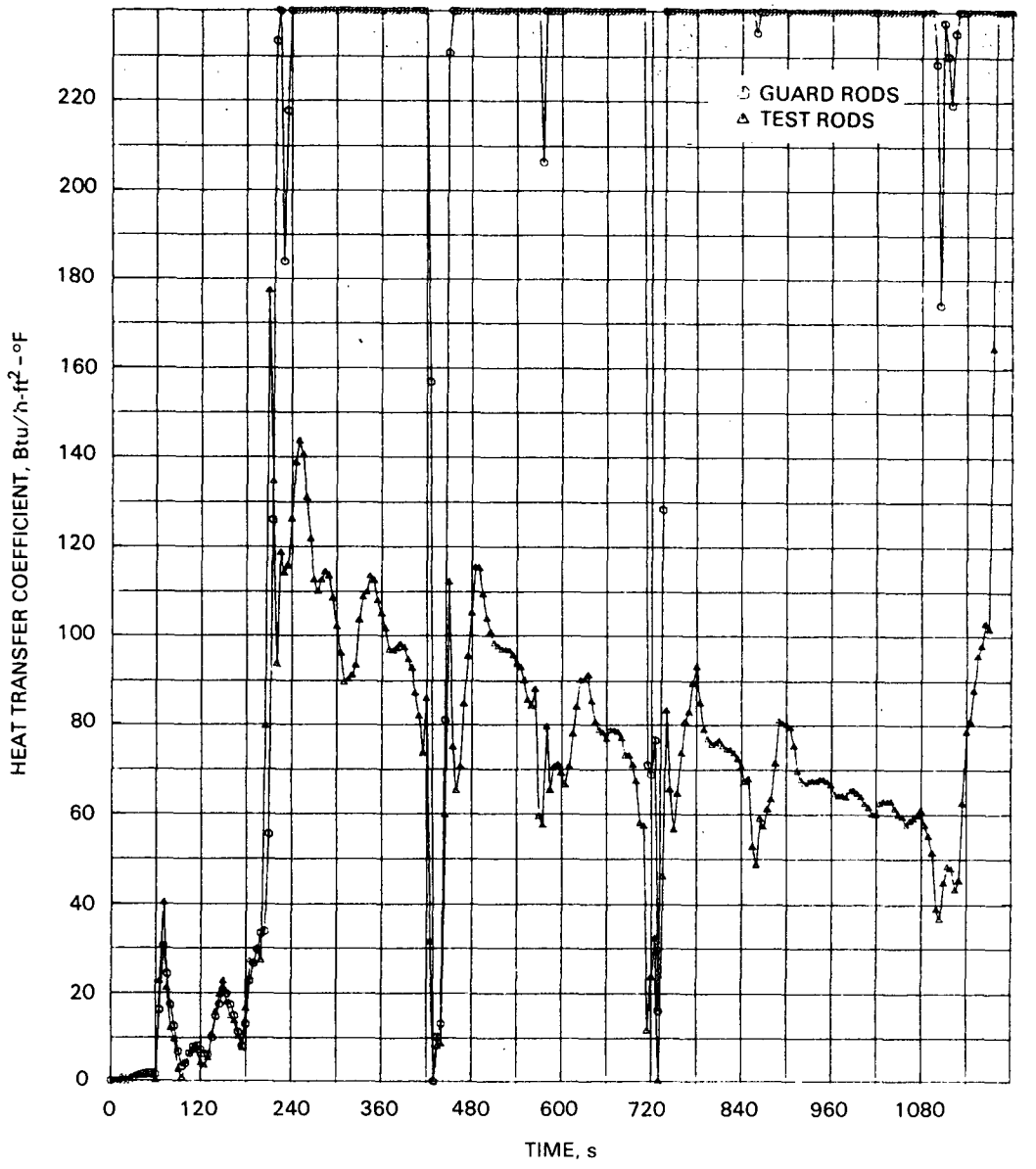

FIGURE 37. Comparison of Heat Transfer Coefficients at Level 76.9 for Nondeformed Guard Rods and Deformed Test Rods for MT-4.04 (Btu/h-ft^2-°F x 5.678263 = W/m^2-K)

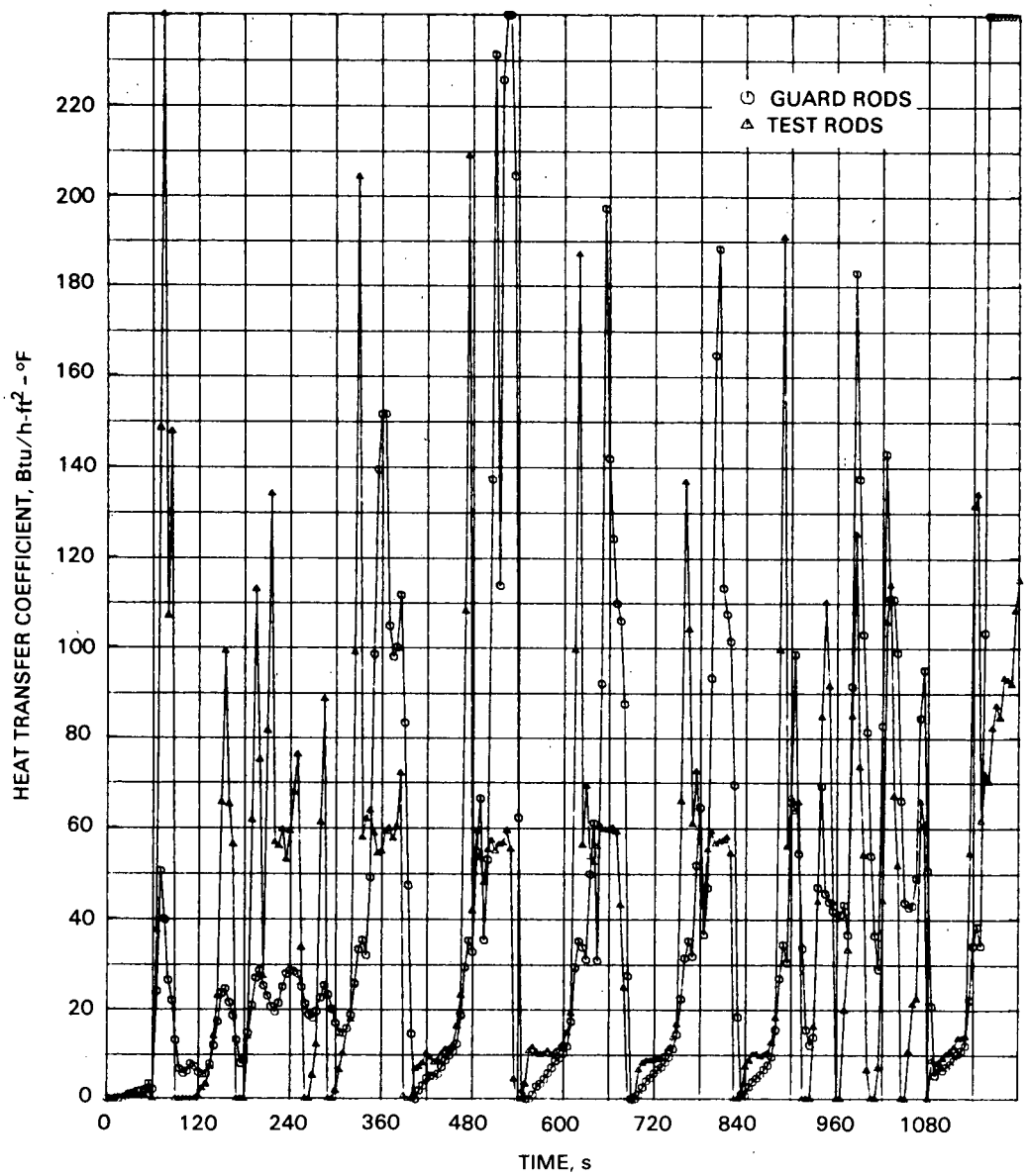

FIGURE 38. Comparison of Heat Transfer Coefficients at Level 97.9 for Nondeformed Guard Rods and Deformed Test Rods for MT-4.04 (Btu/h-ft^2-°F x 5.678263 = W/m^2-K)

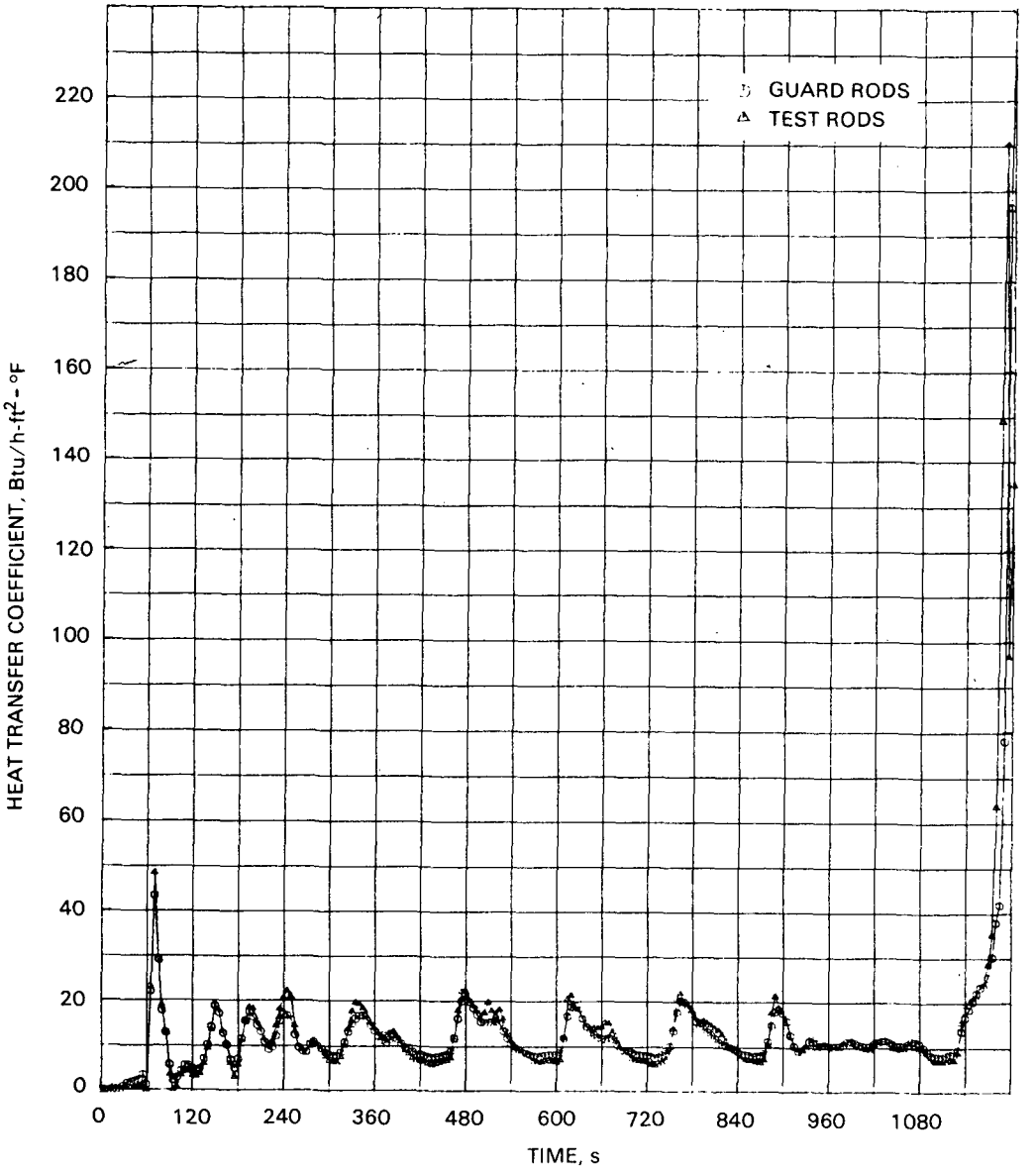

FIGURE 39. Comparison of Heat Transfer Coefficients at Level 118.9 for Nondeformed Guard Rods and Deformed Test Rods for MT-4.04 (Btu/h-ft^2-°F x 5.678263 = W/m^2-K)

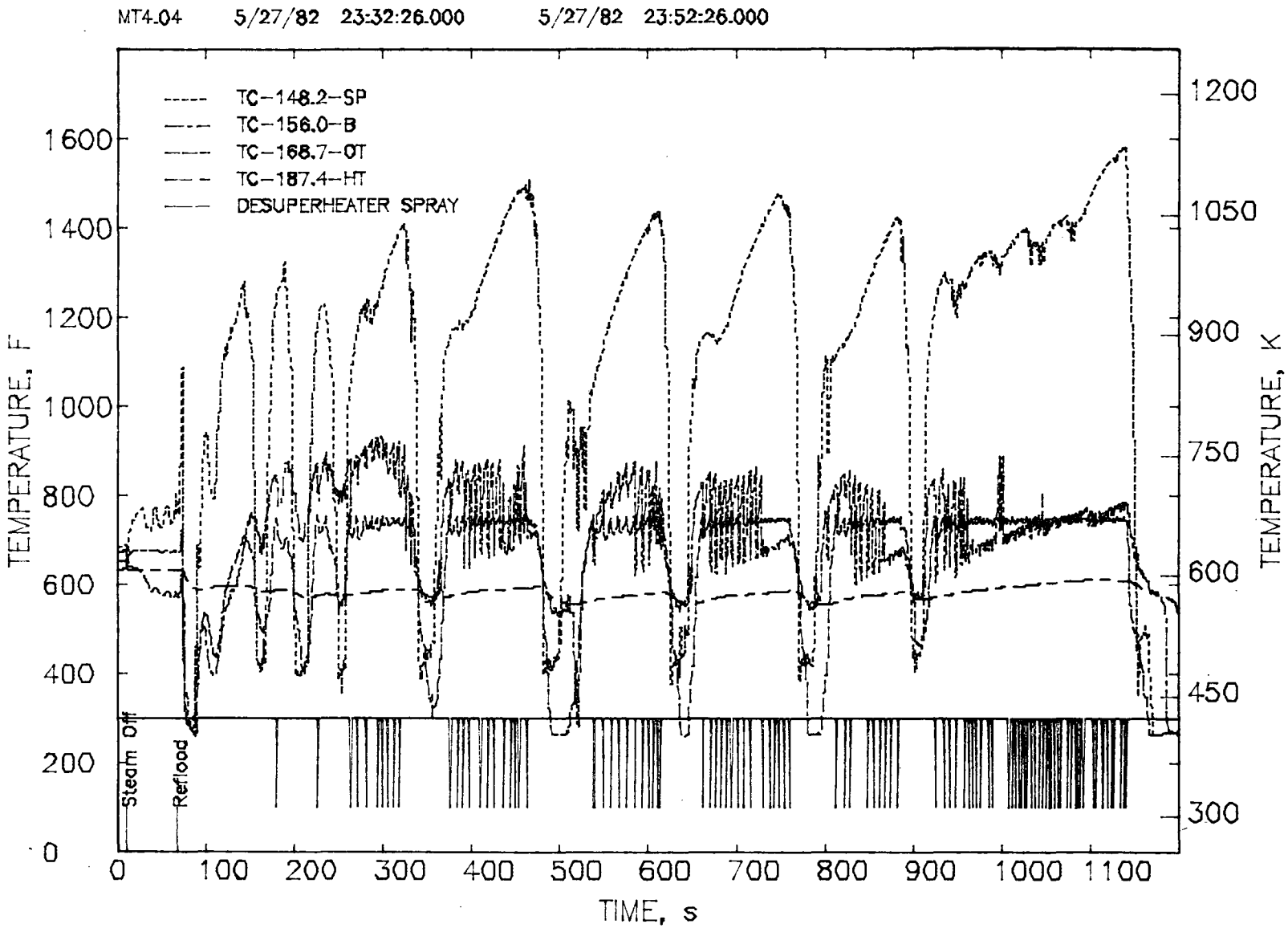

FIGURE 40. Desuperheater Spray Indication and Associated Steam Temperatures

FUEL ROD PLENUM PRESSURE MEASUREMENTS

Gas pressure changes as a function of time in the plenums of the 12 test rods were measured using an out-of-reactor pressure transducer on each rod. All 12 test rods were initially filled with helium to a pressure of 0.243 to 0.384 MPa (35.3 to 55.7 psia) at room temperature and sealed. This same initial fill gas was maintained throughout preconditioning and tests MT-4.01 through MT-4.03. Prior to the final transient test (MT-4.04), the 12 test rods were pressurized to 4.62 MPa (670 psia) at 296K (72°F).

The pressure transducers indicated rod failure data as summarized in Table 6. Post-test examinations using the DERM[a] showed that all of the pressurized rods ruptured, which indicated that all test rods were pressurized during the test. The test rods were fitted with Thurman Hydronics pressure transducers (strain gauge design). The pressure transducers were located outside the reactor above the test assembly and were connected to the fuel rod plenum by capillary tubes. Pressure transducer data are shown in Figures 41 through 43; fuel rod failures occurred where pressure traces drop dramatically.

TABLE 6. Summary of Pressure Switch and Pressure Transducer Rod Failure Data for MT-4.04

Rod Number	Time to Failure, s	Temperature at Failure, K (°F)	Differential Failure Pressure, MPa (psi)	Fill Pressure, MPa (psia)
2C	57	1114 (1547)	5.58 (810)	4.62 (670)
2D	56	1099 (1520)	6.13 (890)	4.62 (670)
3B	53	1092 (1508)	6.23 (905)	4.62 (670)
3C	56	1094 (1510)	6.03 (875)	4.62 (670)
3D	57	1110 (1540)	6.30 (915)	4.62 (670)
3E	55	1095 (1512)	6.48 (940)	4.62 (670)
4B	52	1077 (1480)	6.37 (925)	4.62 (670)
4C	56	1088 (1500)	6.06 (880)	4.62 (670)
4D	58	1088 (1500)	5.79 (840)	4.62 (670)
4E	55	1101 (1524)	6.06 (880)	4.62 (670)
5C	54	1086 (1497)	5.82 (845)	4.62 (670)
5D	54	1086 (1497)	6.10 (885)	4.62 (670)

(a) DERM - dissassembly, examination, reassembly machine.

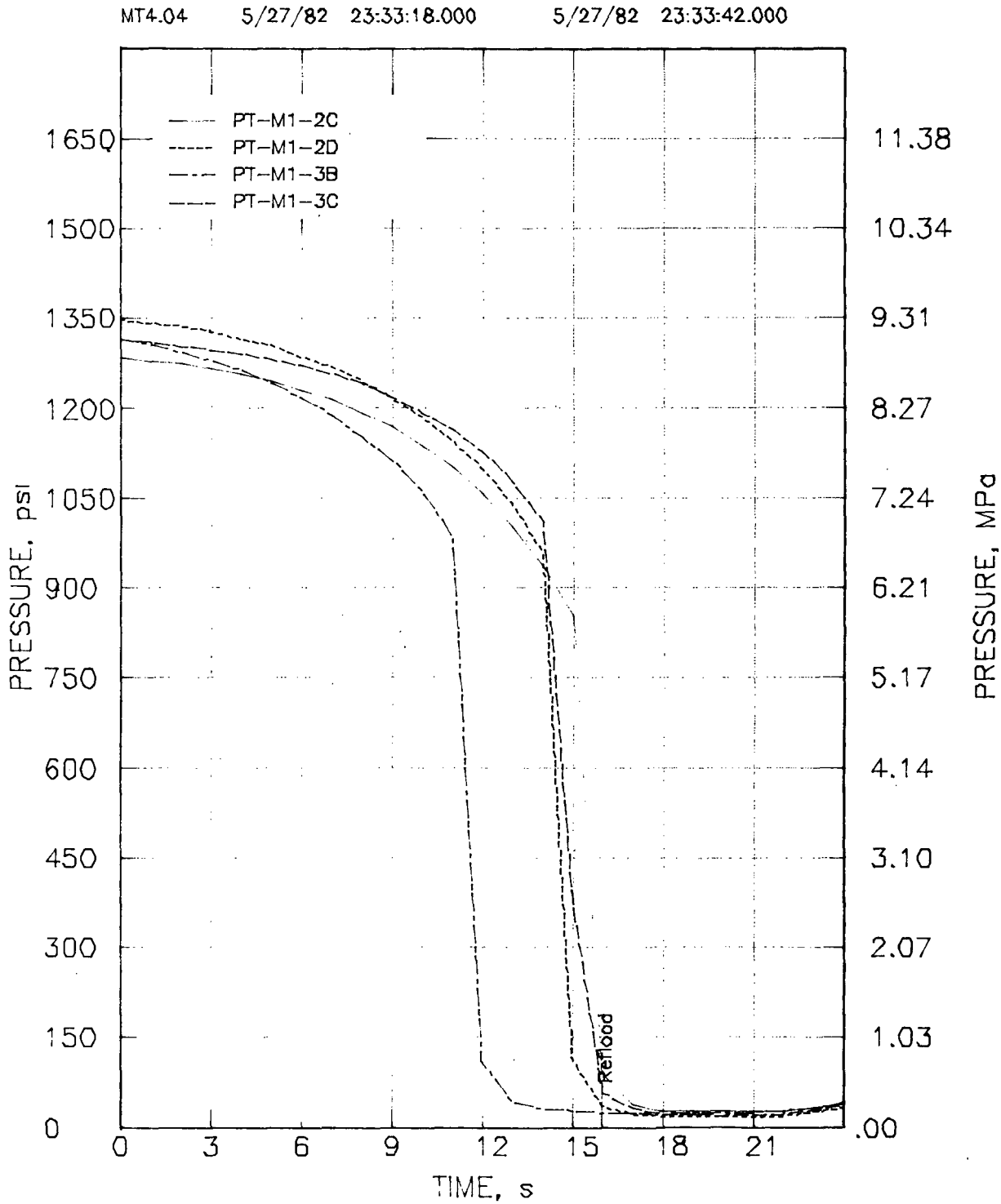

FIGURE 41. Pressure Data at Level 156.0 for Rods 2C, 2D, 3B, and 3C

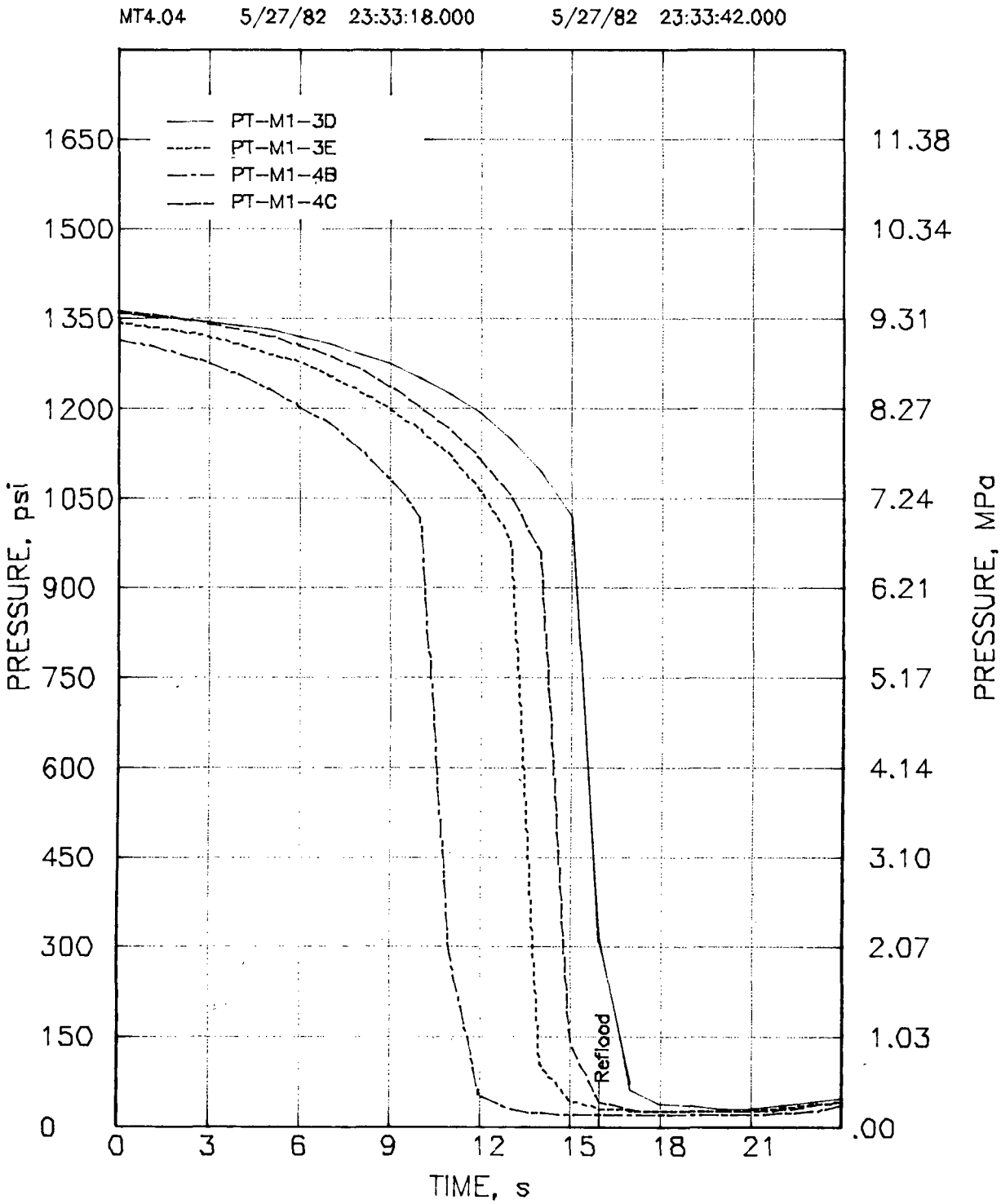

FIGURE 42. Pressure Data at Level 156.0 for Rods 3D, 3E, 4B, and 4C

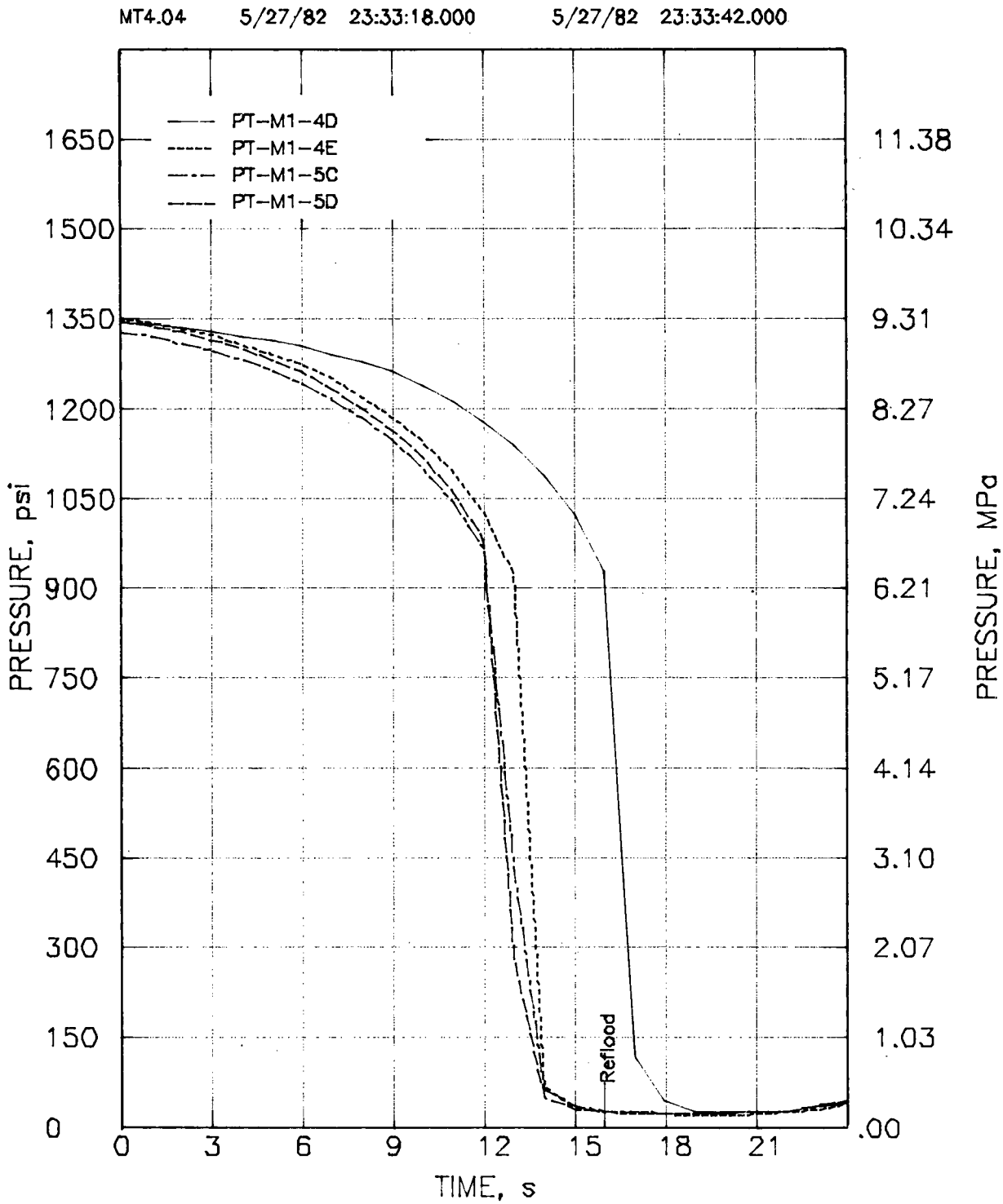

FIGURE 43. Pressure Data at Level 156.0 for Rods 4D, 4E, 5B, and 5C

DEFORMATION EXAMINATION AND ANALYSIS

The examination and measurement of the MT-4 test assembly was performed using the DERM--a computer-controlled device that provides remote, detailed measurement data on individual fuel rods under ~2 m (6.0 ft) of water. The DERM is located in the spent fuel storage bay at CRNL. Detailed photographic and mechanical measurement data were obtained on the cruciform test bundle and on each of the 12 ruptured fuel rods. Television scans of the guard bundle, the test bundle, and some of the individual rod examinations were also obtained. Detailed DERM rod deformation data are included in Appendix G.

The photographic information on the MT-4 test assembly is summarized in this section of the report. The rupture strains in each rod are also summarized. The deformation of one fuel rod (rod 2C) is analyzed to show the relationship among local heat transfer conditions, temperature history, mechanical properties, and constitutive laws analysis techniques.

GUARD ROD BUNDLE EXAMINATION

The guard rod bundle was examined during the disassembly process to determine if the bundle and shroud were reusable and to detect any abnormal appearances. Visual inspections and television scans were made of one side of the bundle when the top half of the shroud was removed; however, no photographs were taken. Although visual examination indicated some distortion of the guard rods in the vicinity of Levels 76.9, 97.9, and 118.9, this distortion was <0.102 cm (0.040 in.). The results of this examination indicated that the guard bundle and shroud were in excellent condition and could be used again.

TEST ROD BUNDLE EXAMINATION

Visual examination of the test rod bundle verified that all 12 rods had ruptured; failure conditions are summarized in Table 7. The peak test bundle strain for the 12-rod region was 43.7% at an elevation of 2.68 m (105.4 in.). The active strain region was spread over 0.189 m (7.42 in.) of fuel, and no indication of coplanar blockage was observed. Bundle cross sections before and after deformation at rupture elevations are shown in Figures 44 and 45 as viewed from the bottom of the test assembly. The sides of the test bundle were photographed from the outside; sides A, 6, F, and 1 are shown for the rupture region in Figure 46. Several views of the rupture zones for each of the 12 test rods are shown in Figures 47 through 58. The rupture zones for individual rods are compared in Figures 59 through 61. In these figures, a 0°

TABLE 7. Summary of Failure Conditions

Rod Number	Center of Rupture, cm (in.)	Rupture Length, cm (in.)	Lower End of Rupture Axial Position, cm (in.)	Upper End of Rupture Axial Position, cm (in.)	Failure Time, s	Failure Temperature, K (°F)	Peak Rupture Strain, %	Differential Failure Pressure, MPa (psi)
2C	242.38 (95.43)	1.52 (0.60)	241.623 (95.127)	243.139 (95.724)	57	1114 (1547)	76.2	5.58 (810)
2D	241.66 (95.14)	2.06 (0.81)	240.627 (94.735)	242.682 (95.544)	56	1099 (1520)	67.6	6.13 (890)
3B	240.99 (94.88)	2.19 (0.86)	239.888 (94.444)	242.082 (95.308)	53	1092 (1508)	64.6	6.23 (905)
3C	241.16 (94.95)	2.55 (1.01)	239.888 (94.444)	242.440 (95.449)	56	1094 (1510)	53.0	6.03 (875)
3D	241.14 (94.94)	3.09 (1.22)	239.588 (94.326)	242.682 (95.544)	57	1110 (1540)	59.4	6.30 (915)
3E	240.37 (94.63)	1.95 (0.77)	239.390 (94.248)	241.343 (95.017)	55	1095 (1512)	73.7	6.48 (940)
4B	257.21 (101.27)	2.06 (0.81)	256.184 (100.860)	258.242 (101.670)	52	1077 (1480)	68.4	6.37 (925)
4C	241.13 (94.93)	1.76 (0.69)	240.246 (94.585)	242.004 (95.277)	56	1088 (1500)	99.2	6.06 (880)
4D	254.97 (100.38)	2.39 (0.94)	253.771 (99.910)	256.159 (100.85)	58	1088 (1500)	78.5	5.79 (840)
4E	240.69 (94.76)	2.19 (0.86)	239.598 (94.330)	241.783 (95.190)	55	1101 (1524)	81.5	6.06 (880)
5C	254.58 (100.23)	3.81 (1.50)	252.677 (99.479)	256.489 (100.980)	54	1086 (1497)	66.0	5.82 (845)
5D	255.02 (100.40)	2.69 (1.06)	253.672 (99.871)	256.362 (100.93)	54	1086 (1497)	77.3	6.10 (885)

(a) All measurements are from the top of the tie plate that supports the fuel rods.

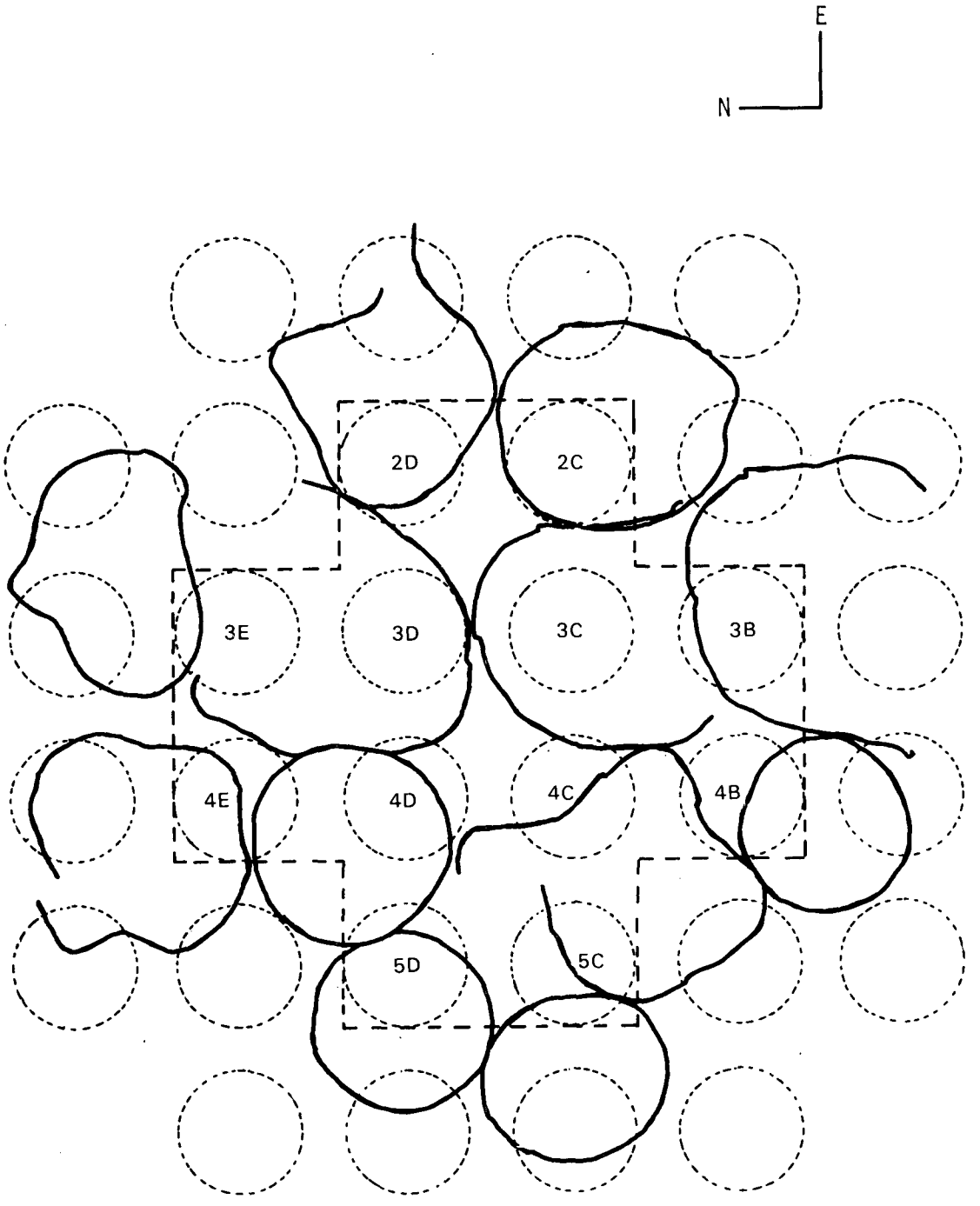

FIGURE 44. MT-4 Bundle Cross Sections Before and After Deformation at Axial Elevation Z = 81.12 in.

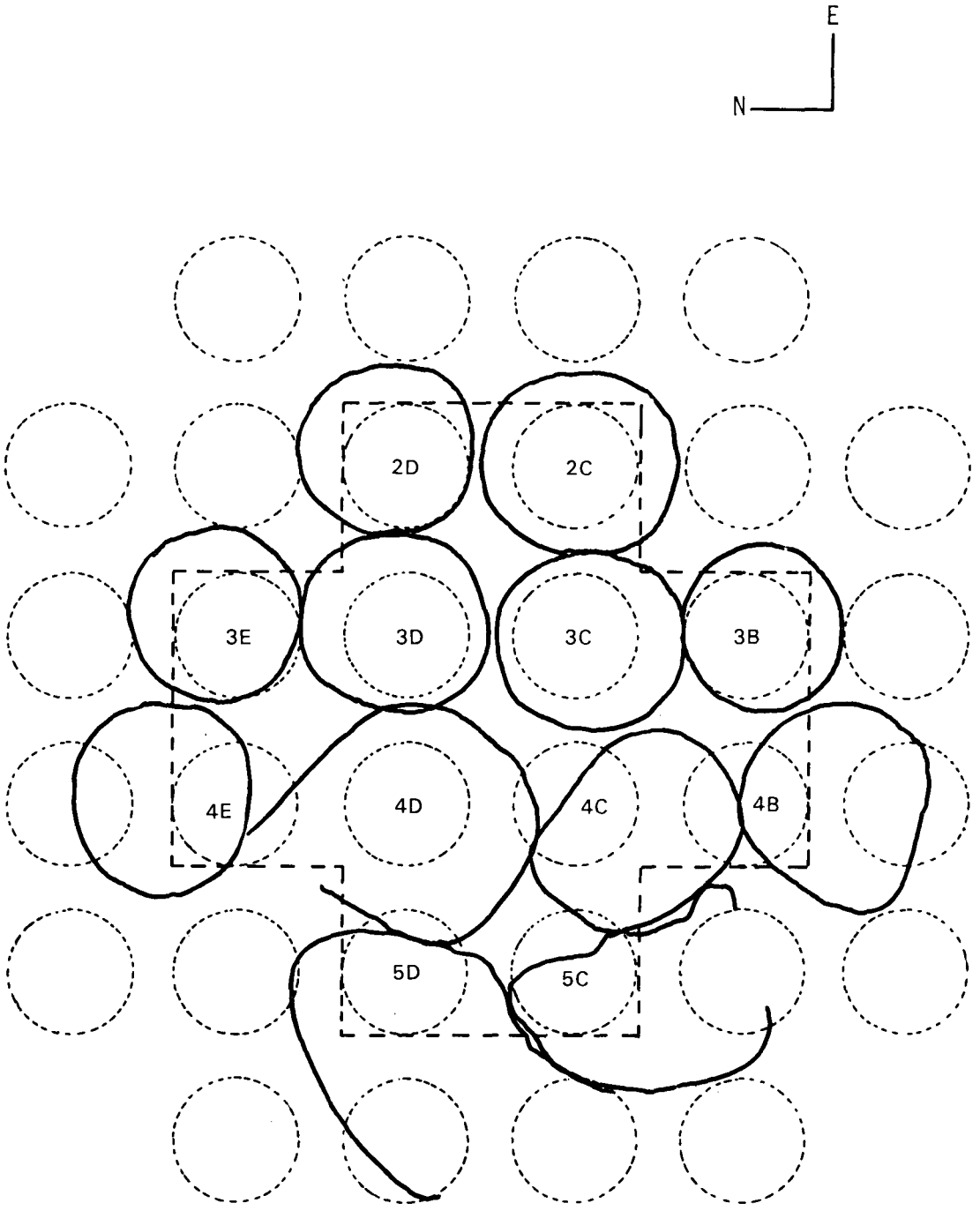

FIGURE 45. MT-4 Bundle Cross Sections Before and After Deformation at Axial Position Z = 100.70 in.

MT-4 TEST BUNDLE RUPTURE REGION

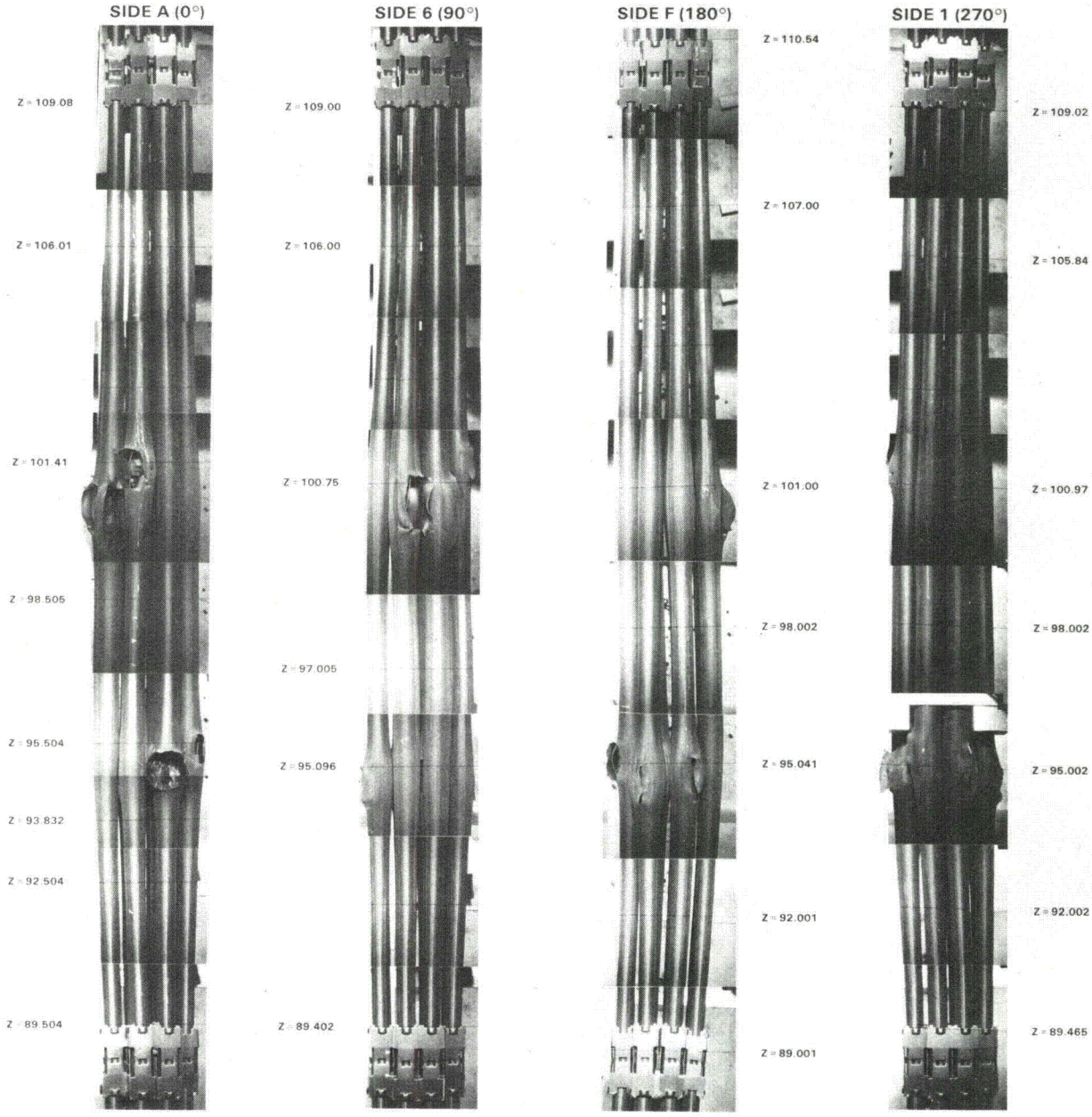

FIGURE 46. Test Rod Bundle Rupture Zones--Sides A, 6, F, and 1

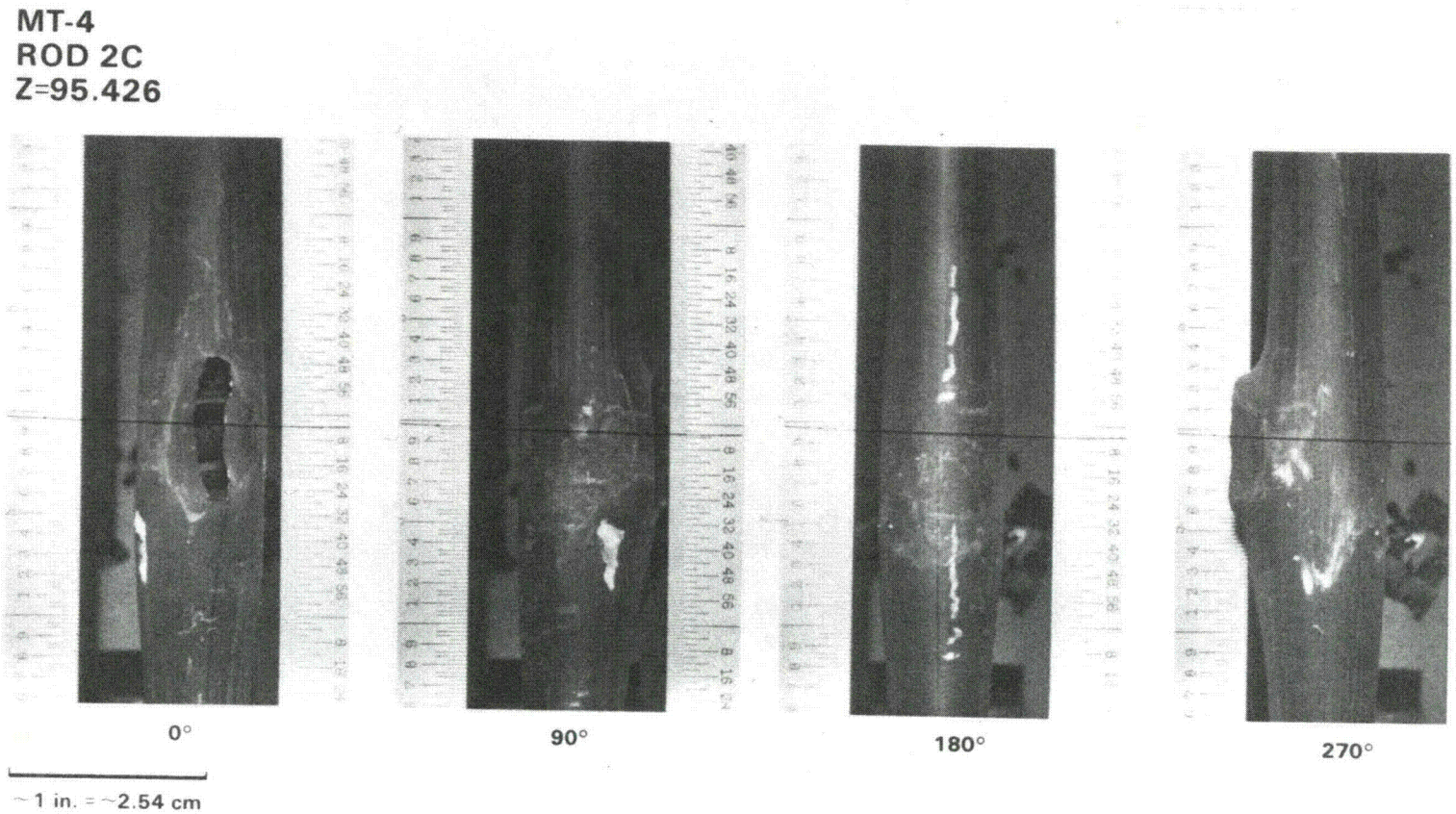

FIGURE 47. Rupture Zone for Test Rod 2C (Z = 95.426)

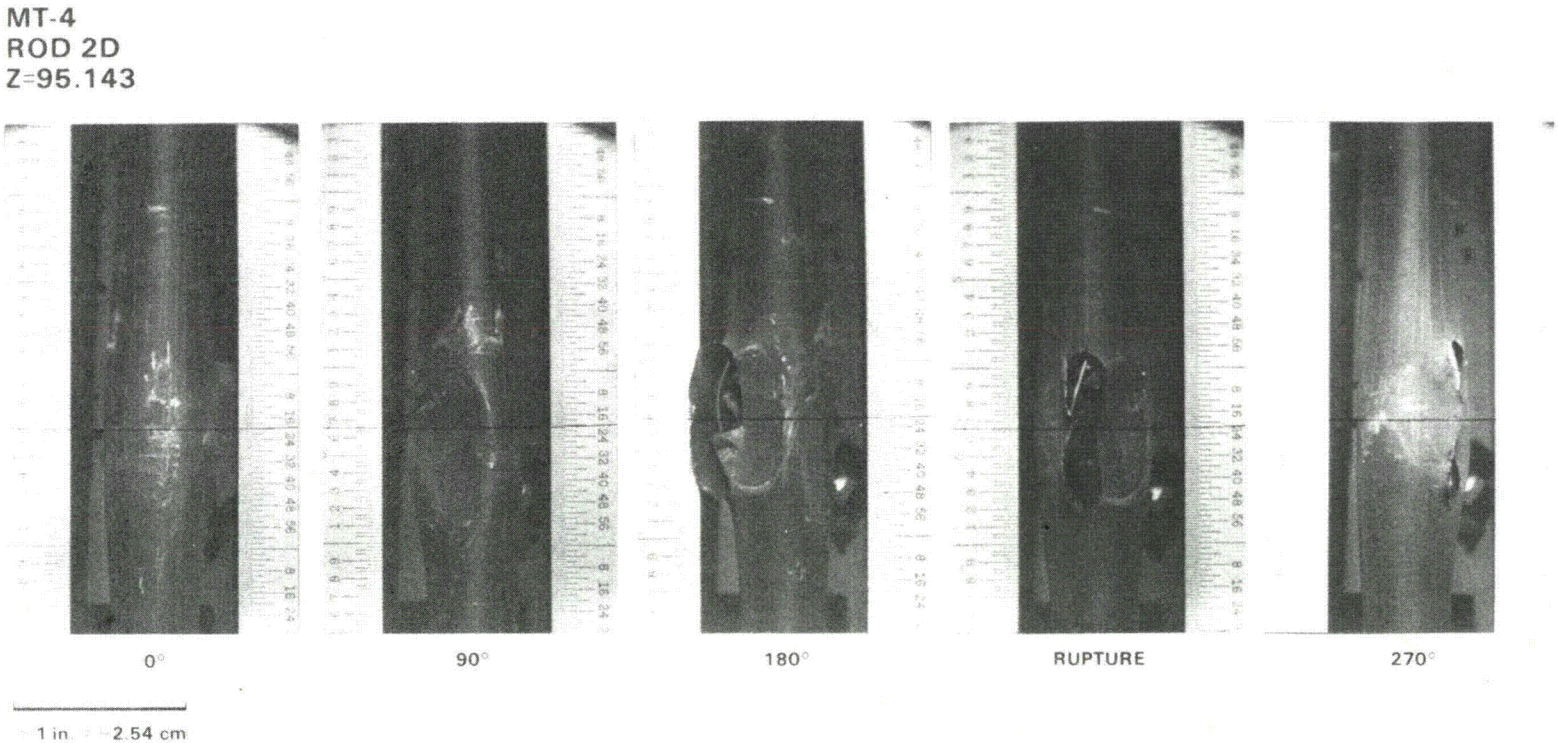

FIGURE 48. Rupture Zone for Test Rod 2D (Z = 95.143)

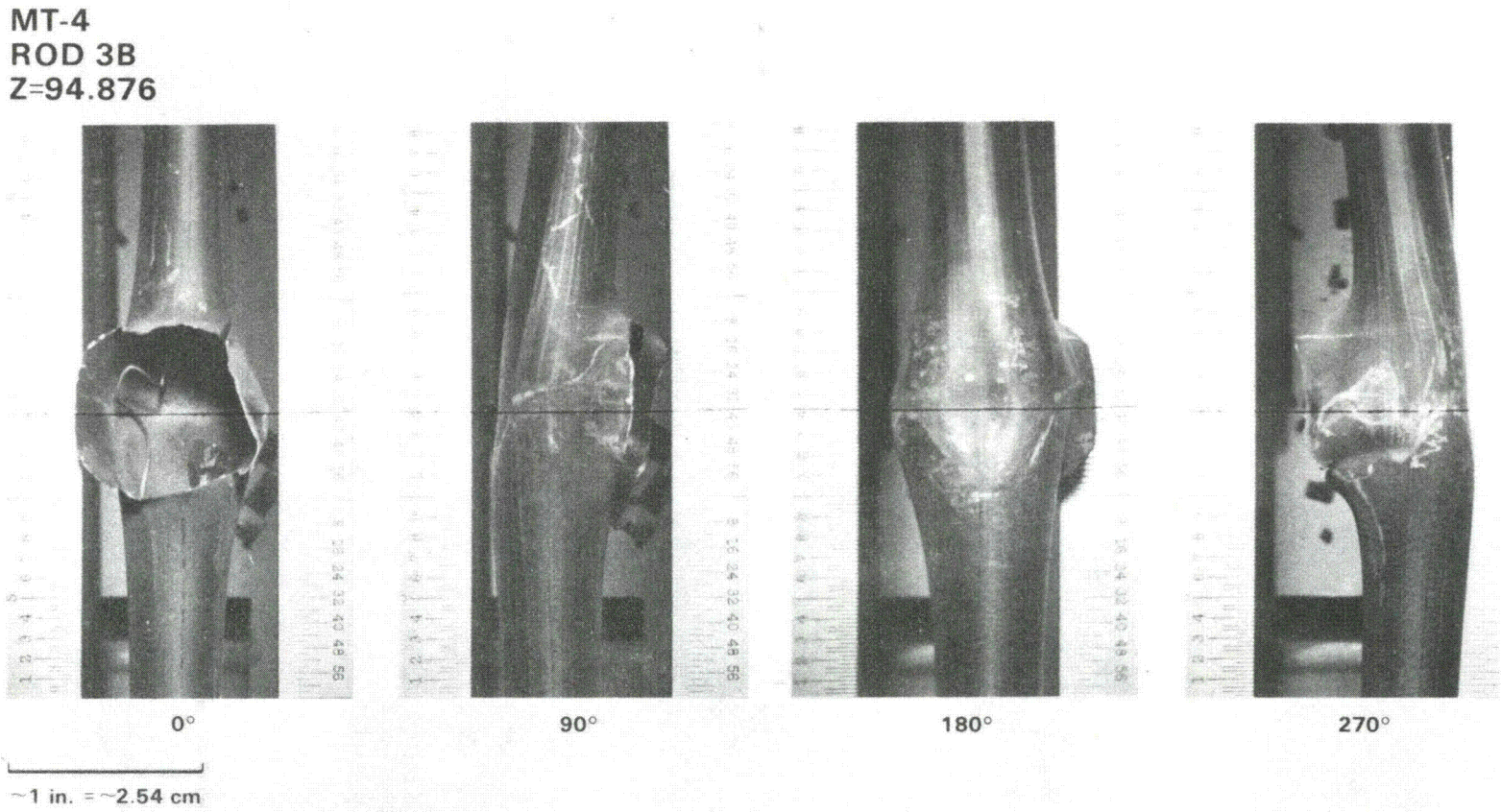

FIGURE 49. Rupture Zone for Test Rod 3B (Z = 94.876)

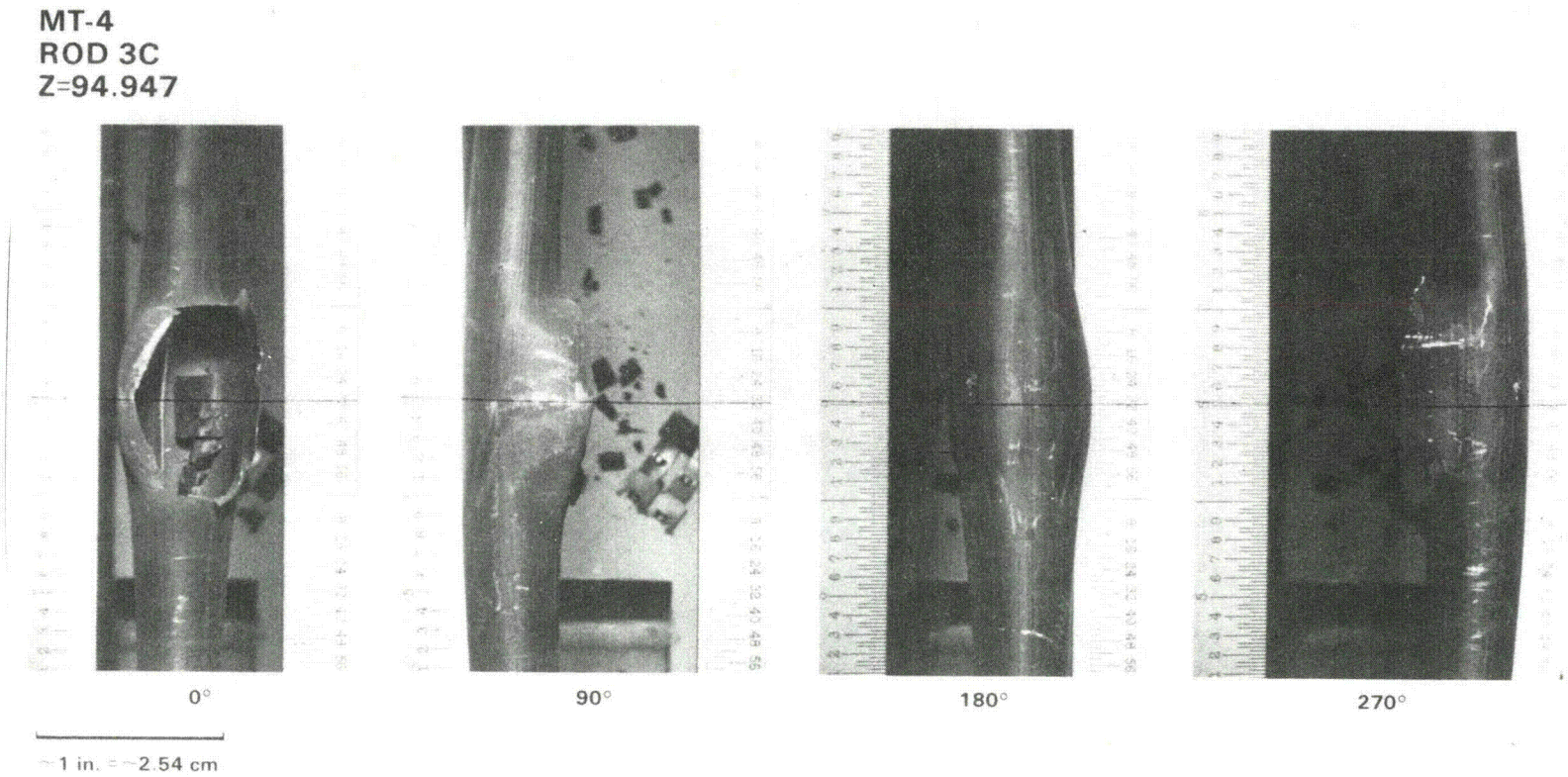

FIGURE 50. Rupture Zone for Test Rod 3C (Z = 94.947)

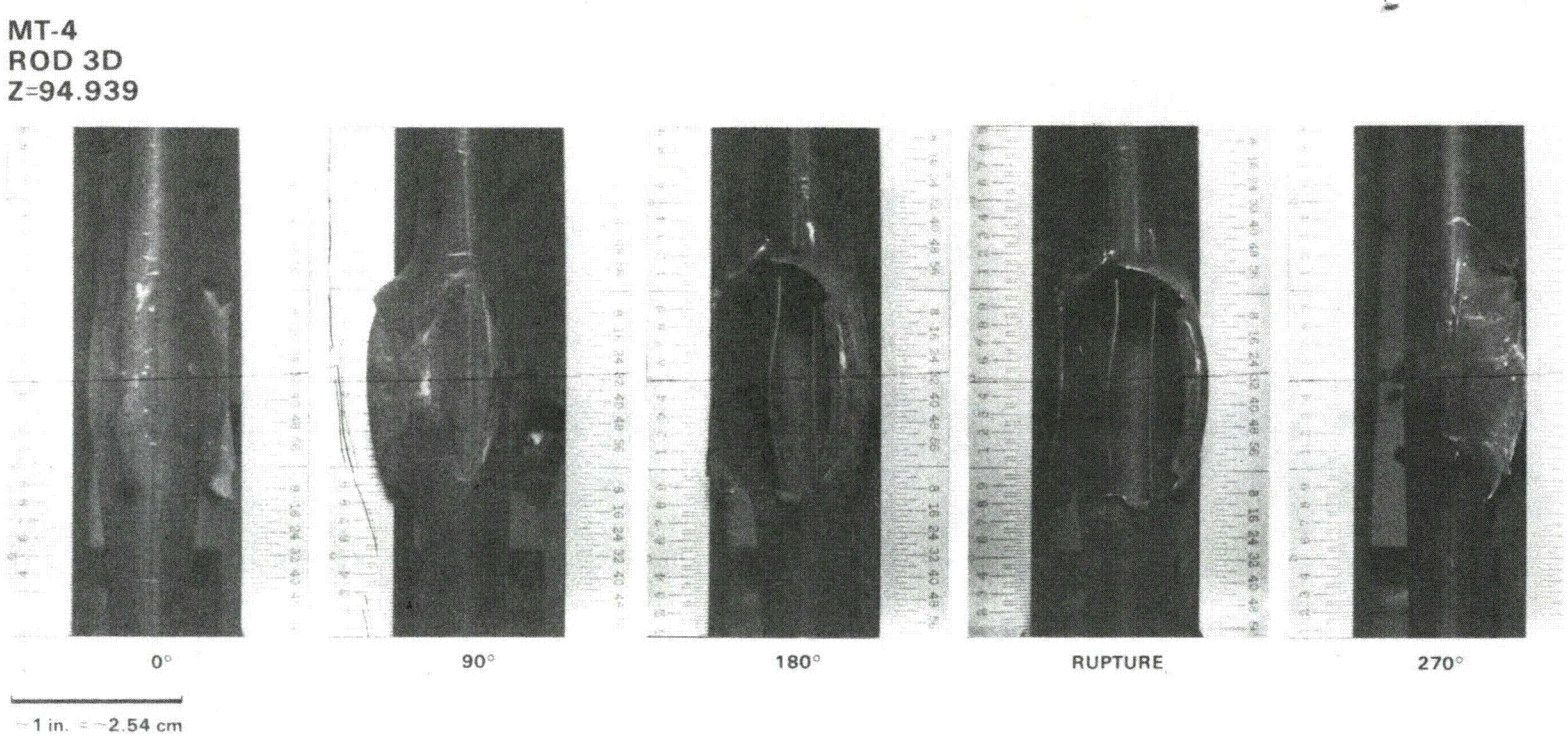

FIGURE 51. Rupture Zone for Test Rod 3D (Z = 94.939)

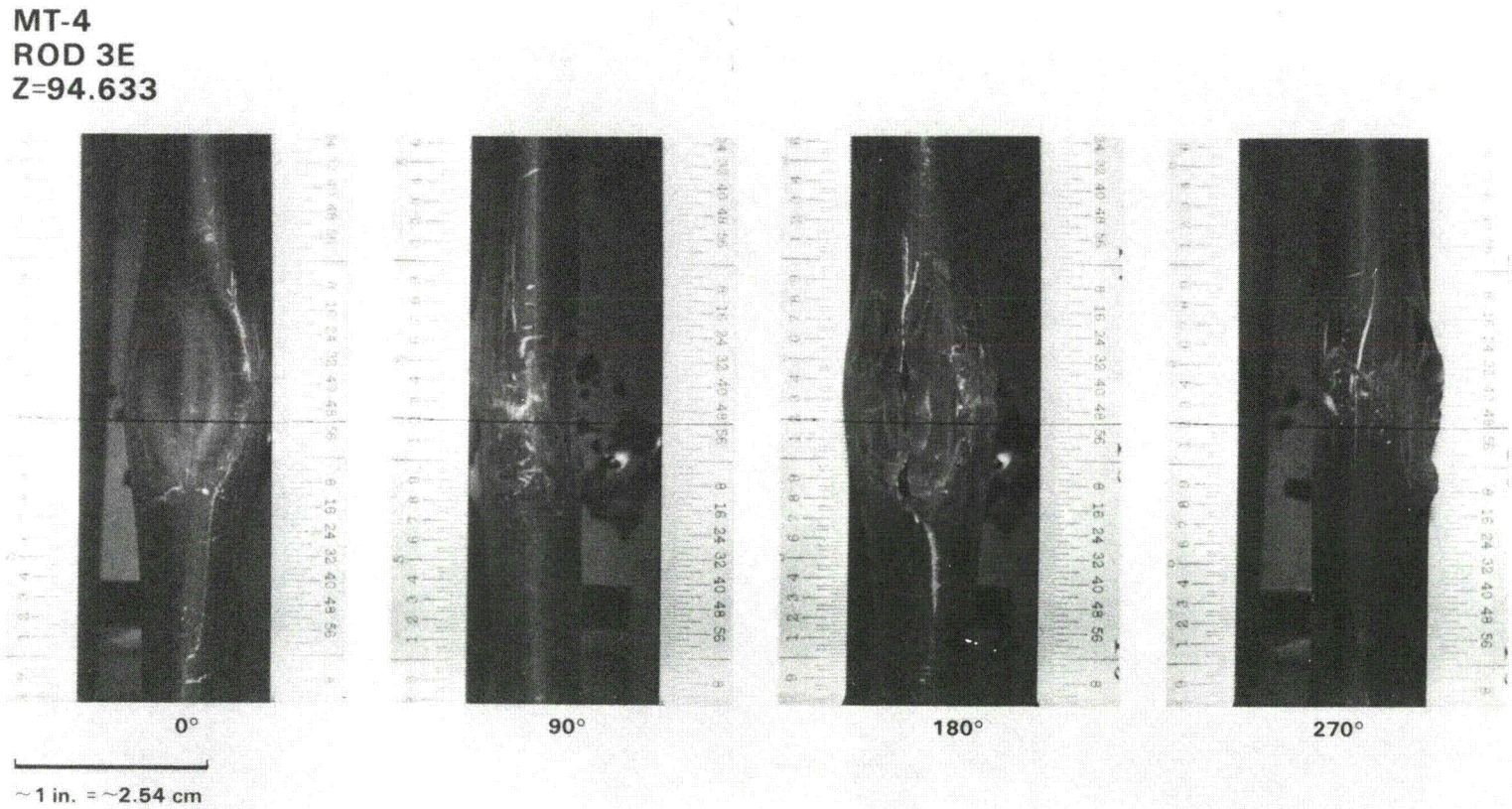

FIGURE 52. Rupture Zone for Test Rod 3E (Z = 94.633)

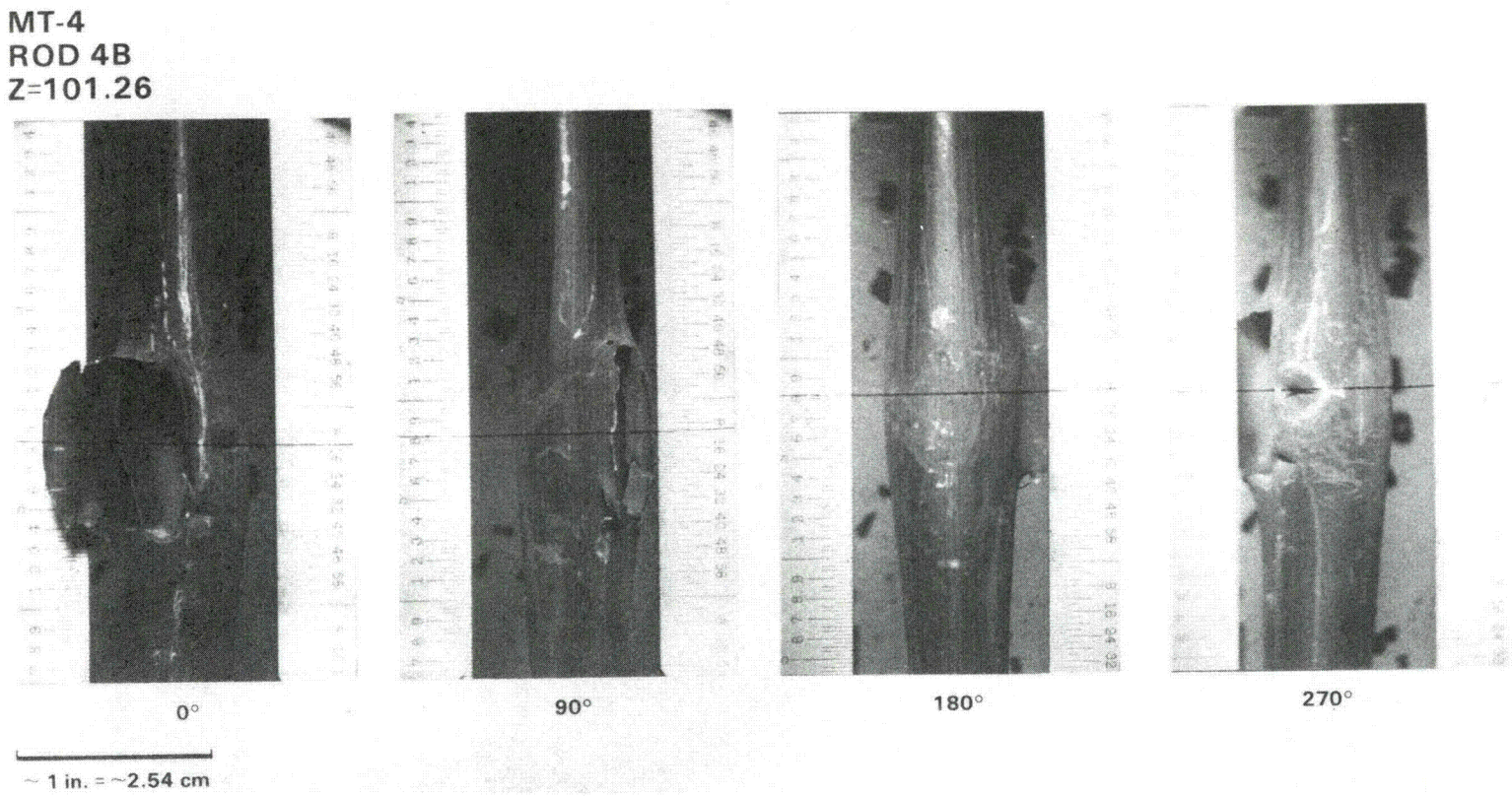

FIGURE 53. Rupture Zone for Test Rod 4B (Z = 101.26)

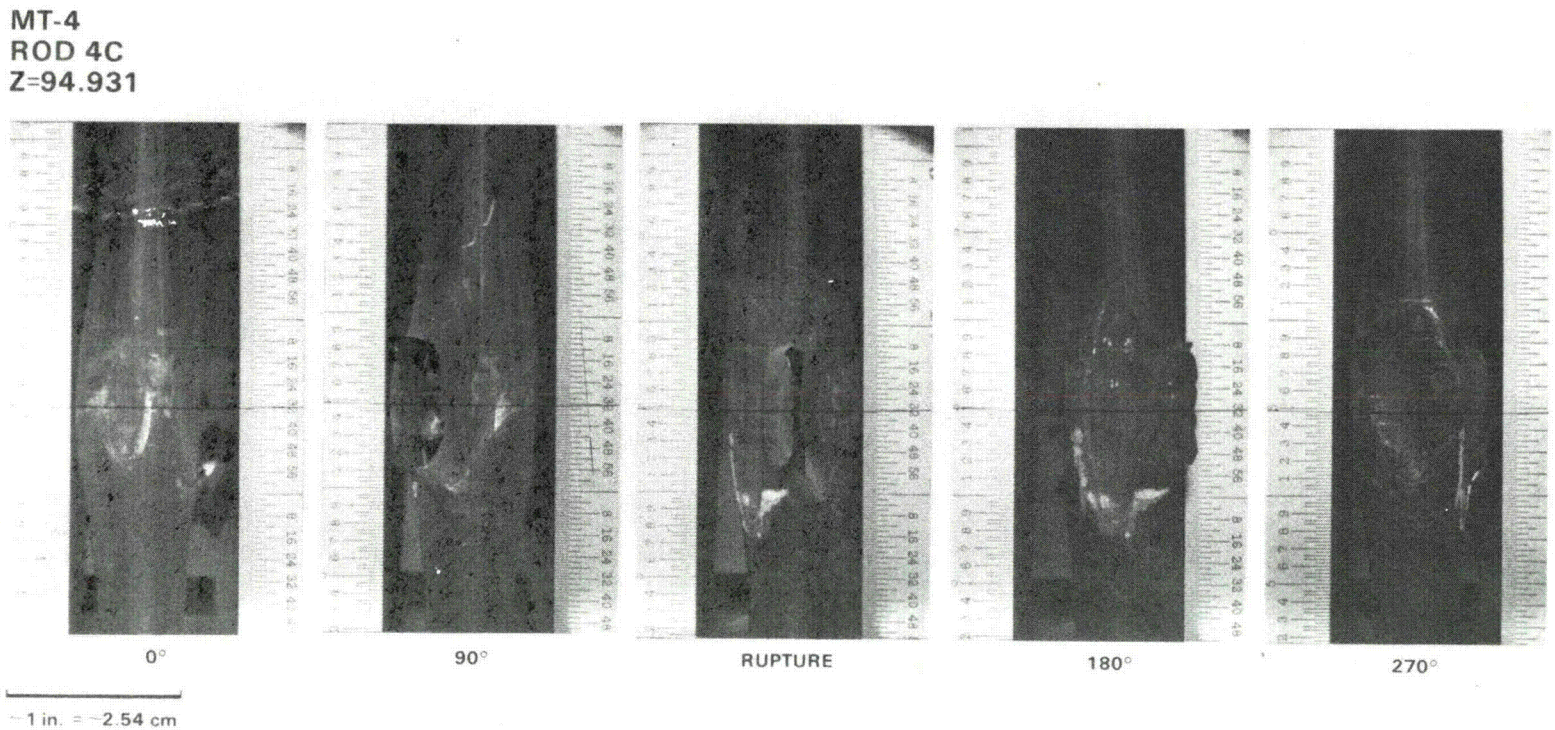

FIGURE 54. Rupture Zone for Test Rod 4C (Z = 94.931)

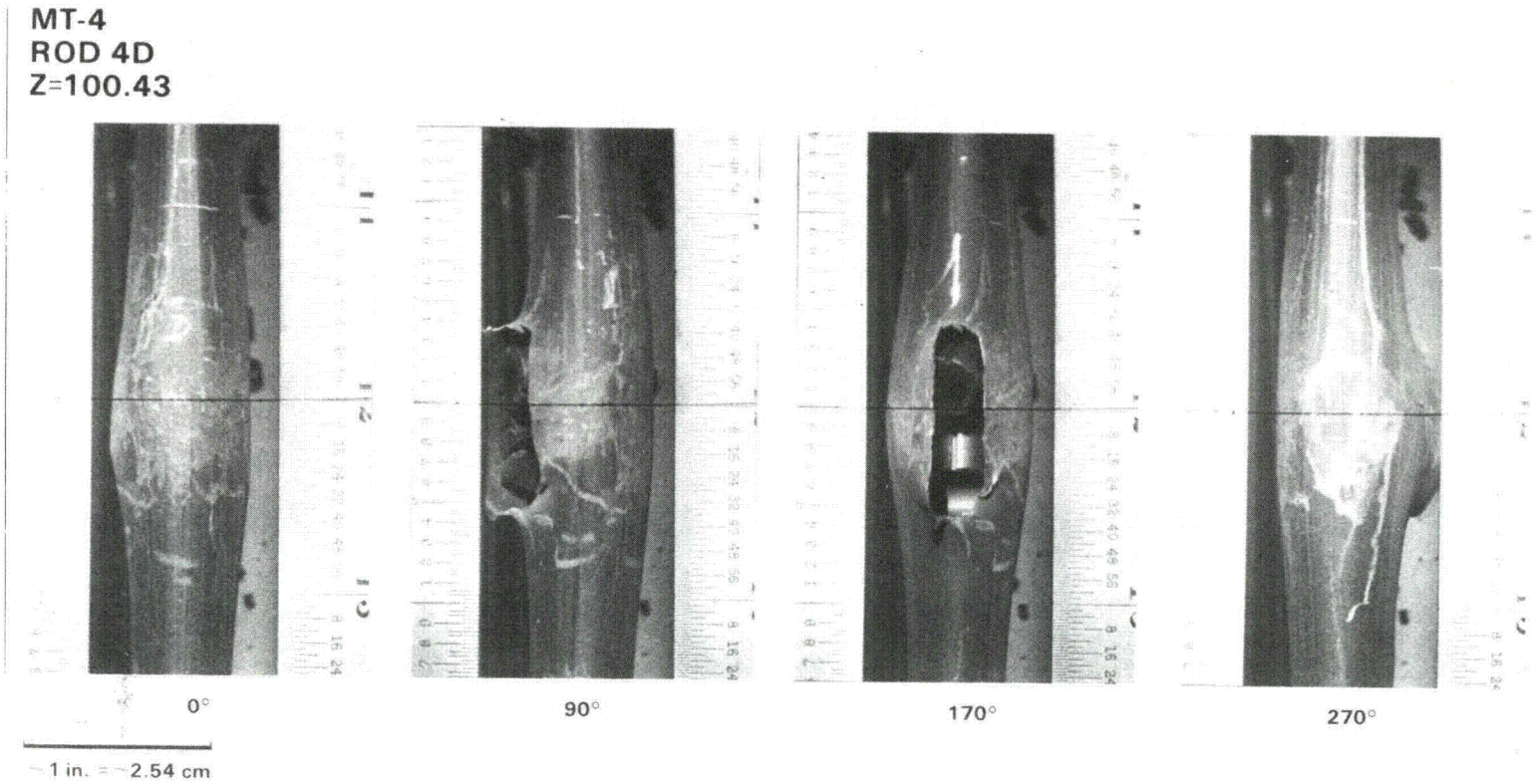

FIGURE 55. Rupture Zone for Test Rod 4D (Z = 100.430)

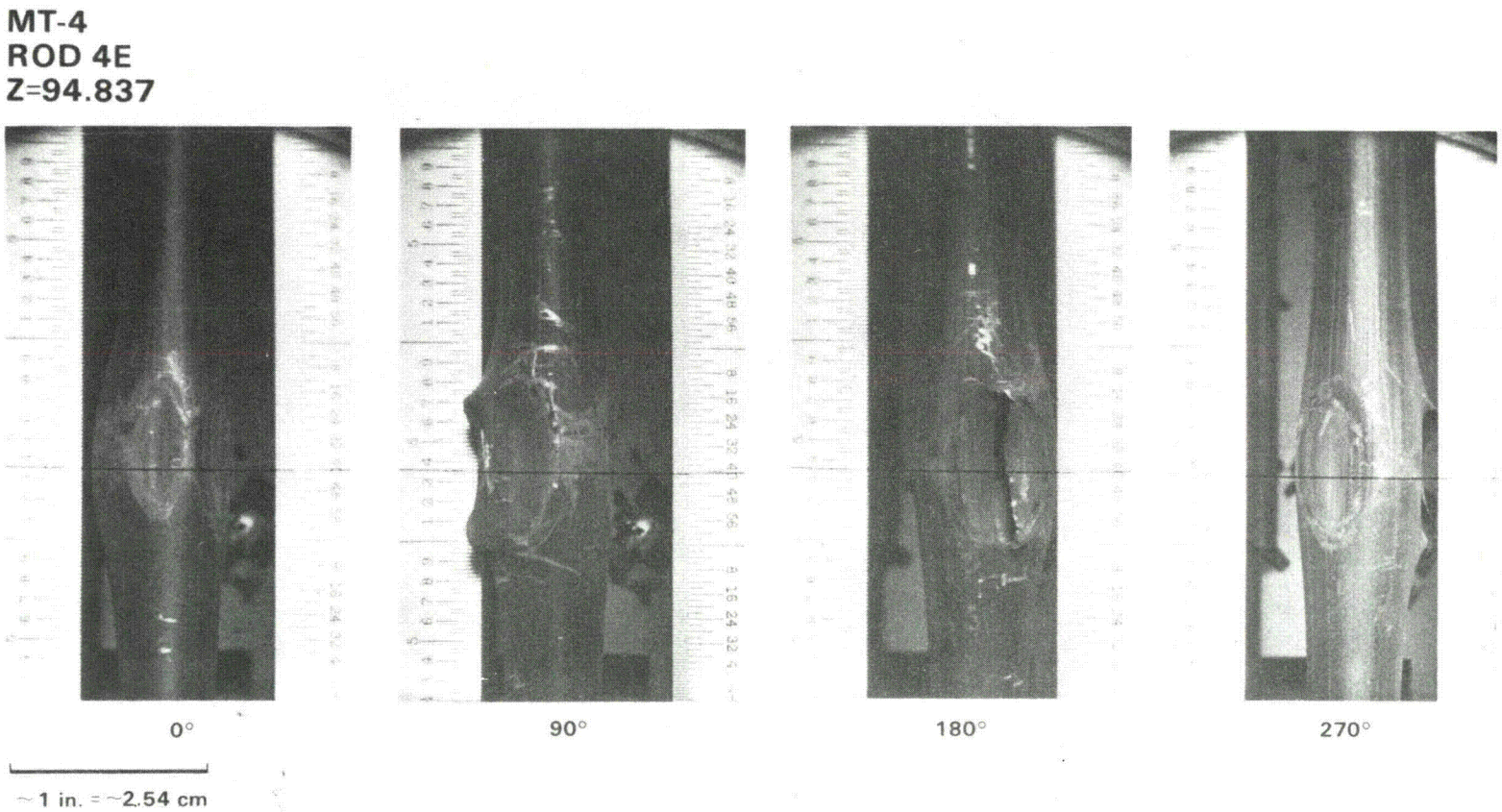

FIGURE 56. Rupture Zone for Test Rod 4E (Z = 94.837)

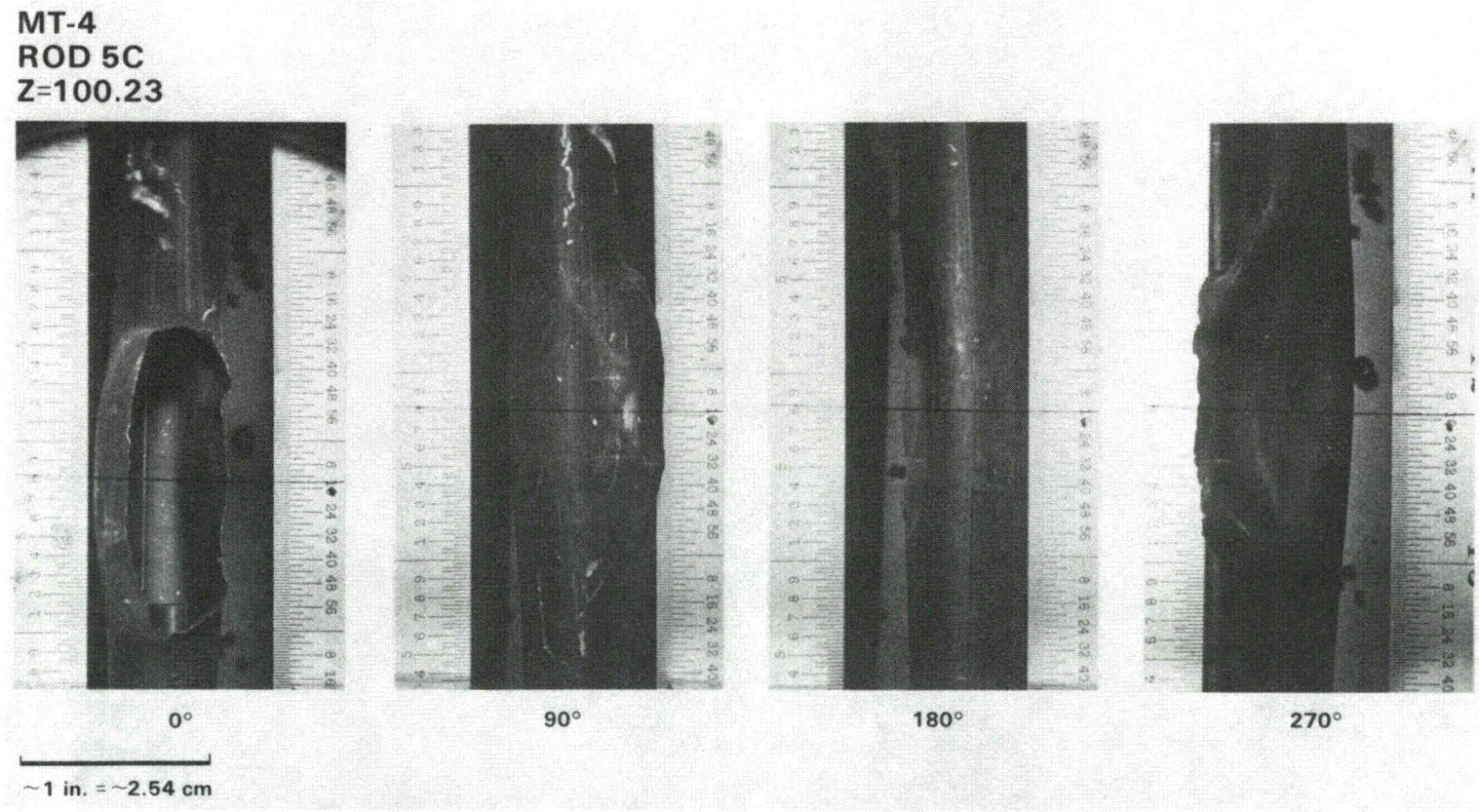

FIGURE 57. Rupture Zone for Test Rod 5C (Z = 100.230)

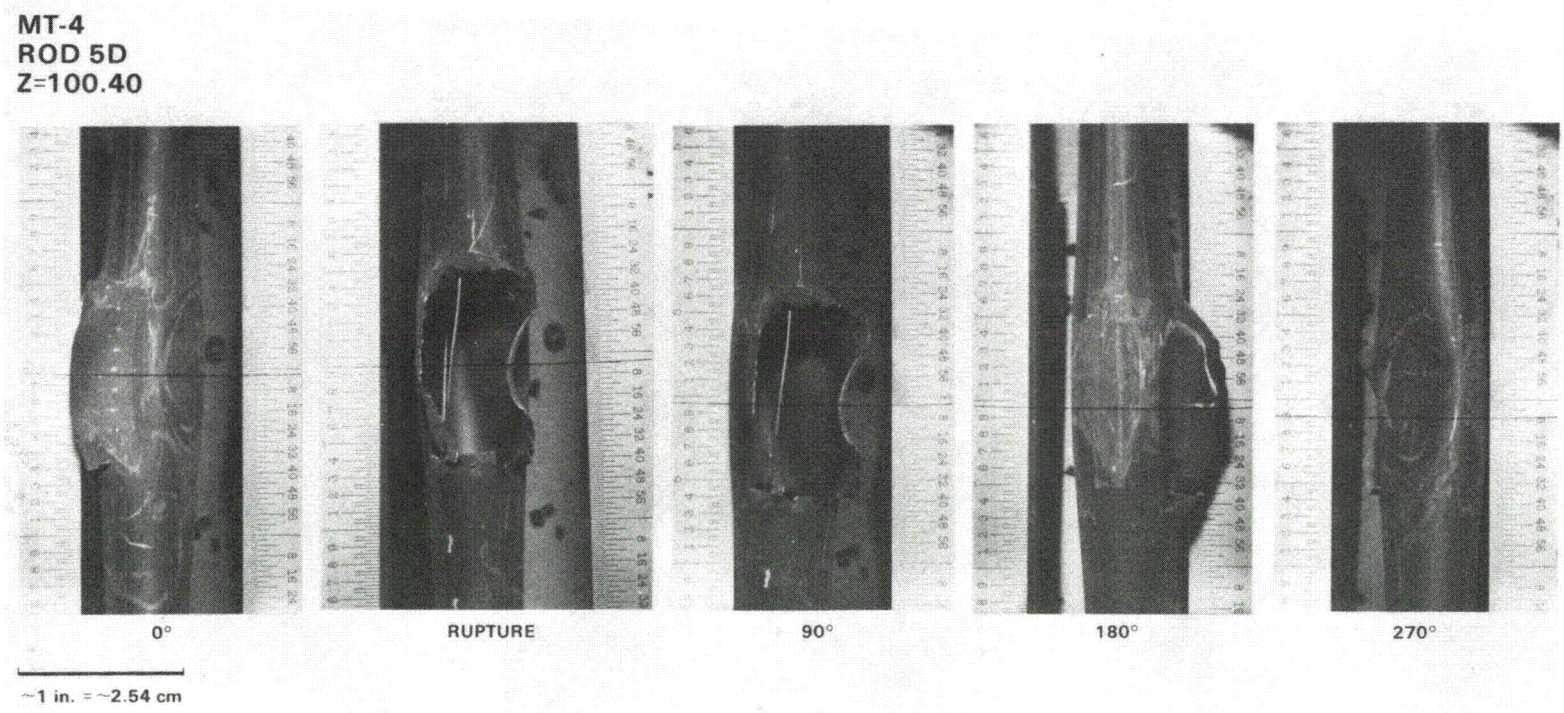

FIGURE 58. Rupture Zone for Test Rod 5D (Z = 100.40)

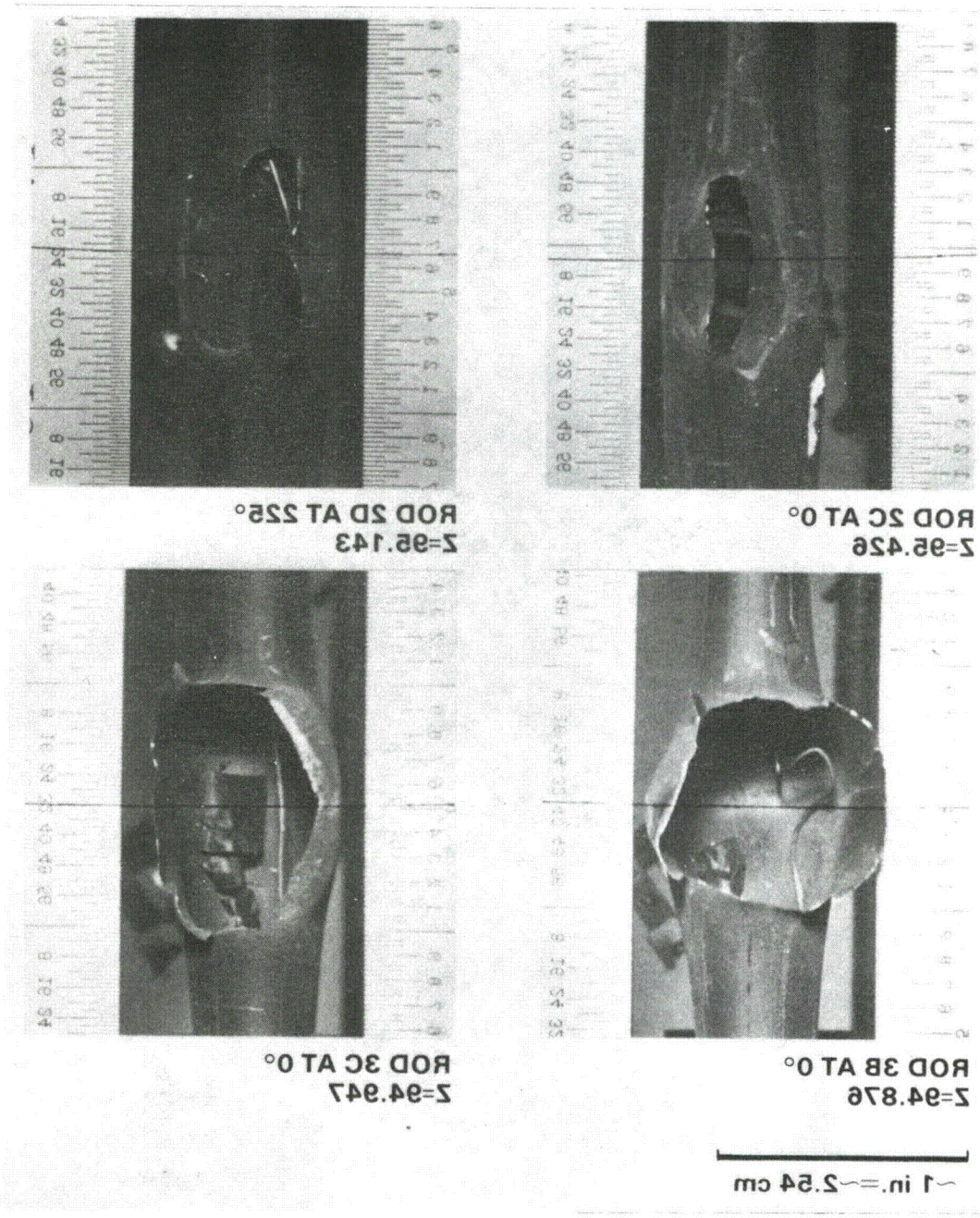

FIGURE 59. Comparison of Rupture Zones for Test Rods 2C, 2D, 3B, and 3C

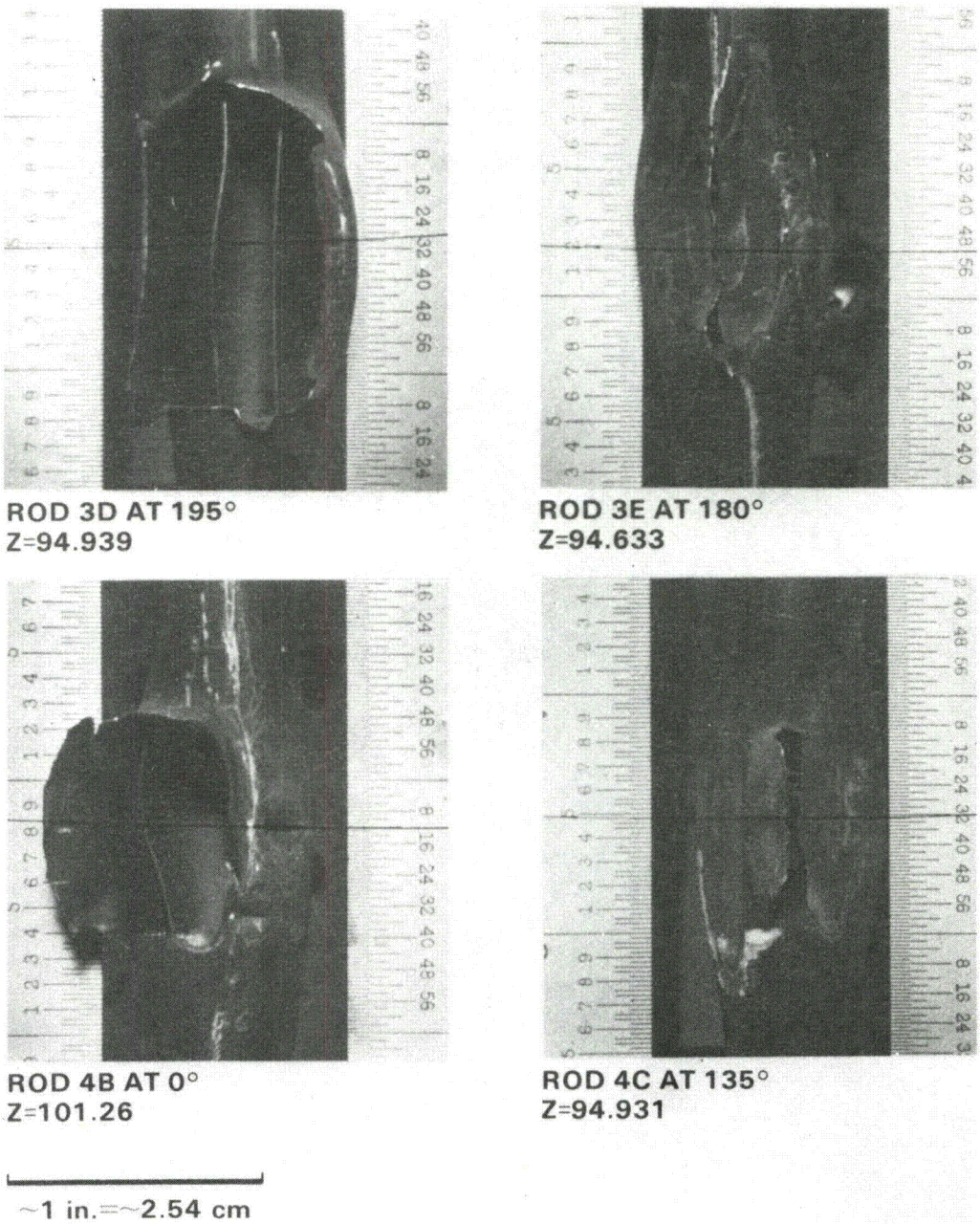

FIGURE 60. Comparison of Rupture Zones for Test Rods 3D, 3E, 4B, and 4C

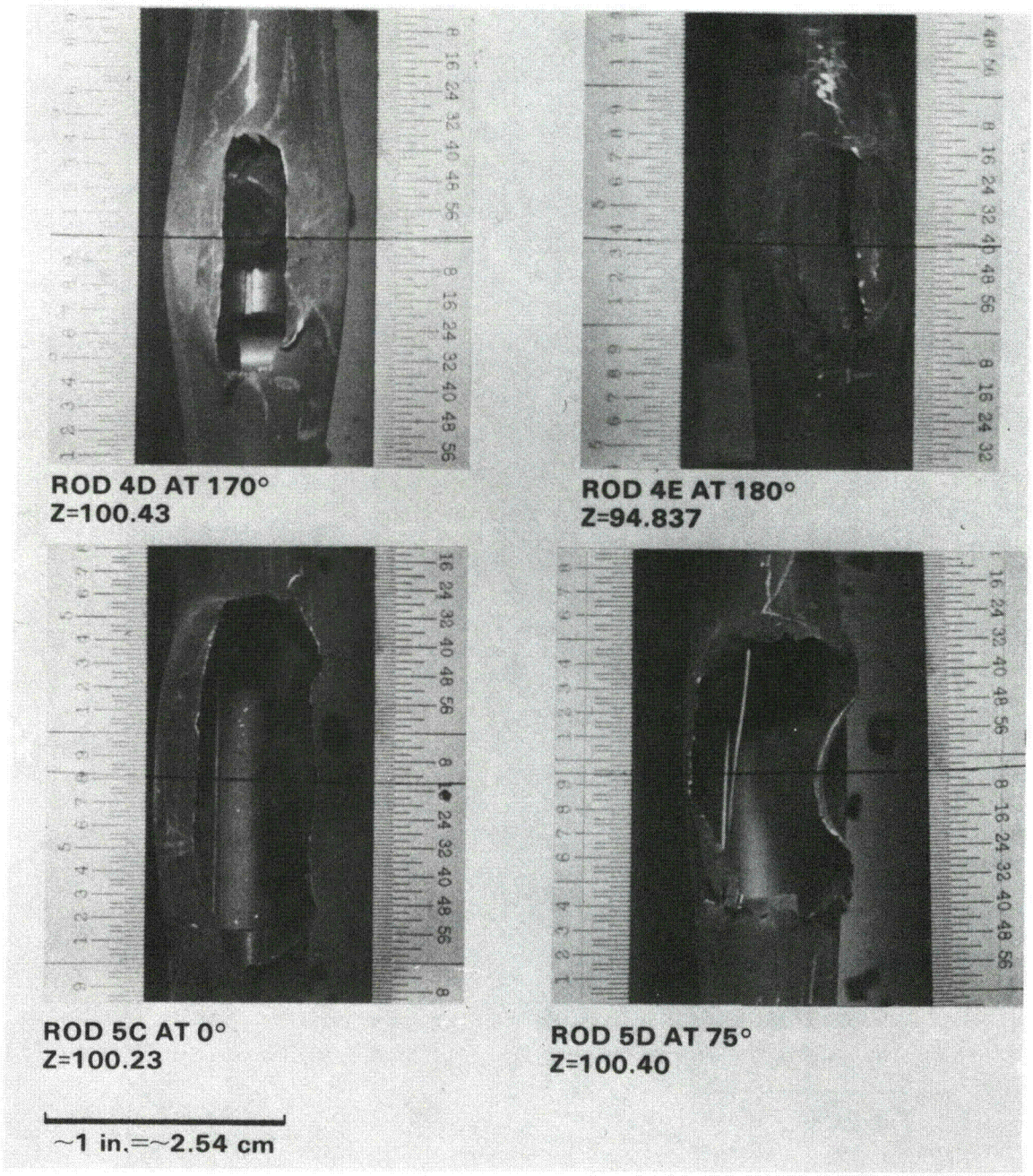

FIGURE 61. Comparison of Rupture Zones for Test Rods 4D, 4E, 5C, and 5D

orientation represents the view looking toward the north; 90°, the east; 180°, the south; and 270°, the west. The tops of all the photographs are the upper ends of the rods.

ANALYSIS OF FUEL CLADDING DEFORMATION

The 12 test rods in the MT-4 experiment deformed significantly before the cladding burst. The measured cladding strain profile for a typical test rod is shown in Figure 62. This measured strain provides a good data base for testing the predictive capabilities of transient cladding deformation computer programs. One such code--DILATE--was run to simulate the MT-4 experiment. The results of the simulation are shown in Figure 63. The code underpredicted the actual strains by a large margin. Calculated strains were again much less than by experiment when using the original EPRI data base[7] or the relationships developed by Donaldson, Horwood, and Healey.[8] A more complete description of DILATE and these data can be found in References 7, 8, and 9.

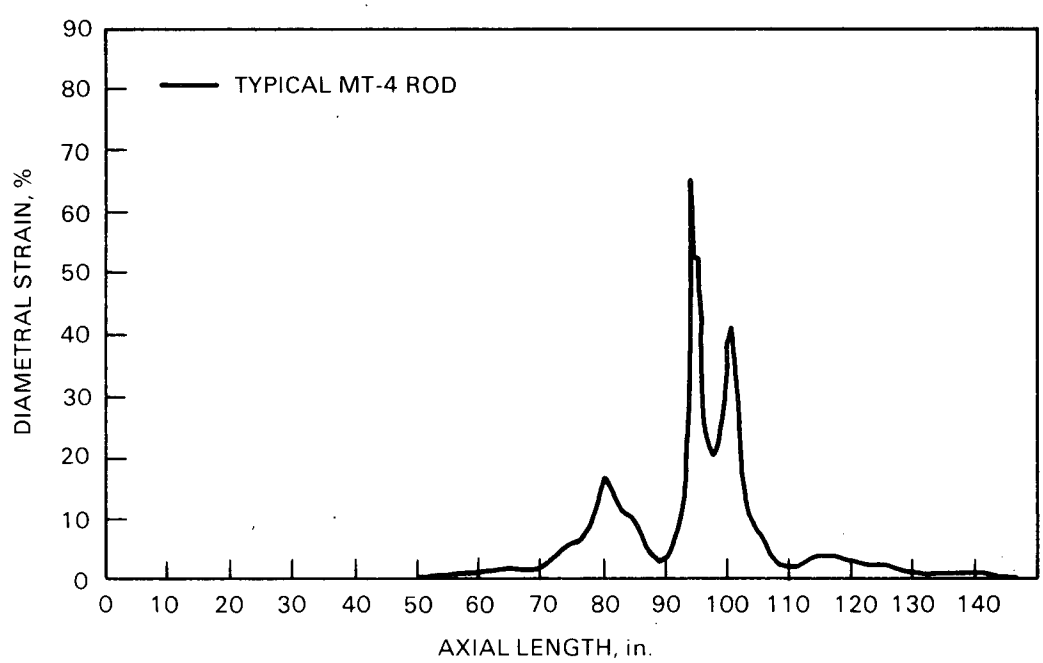

FIGURE 62. Cladding Deformation Profiles for MT-4

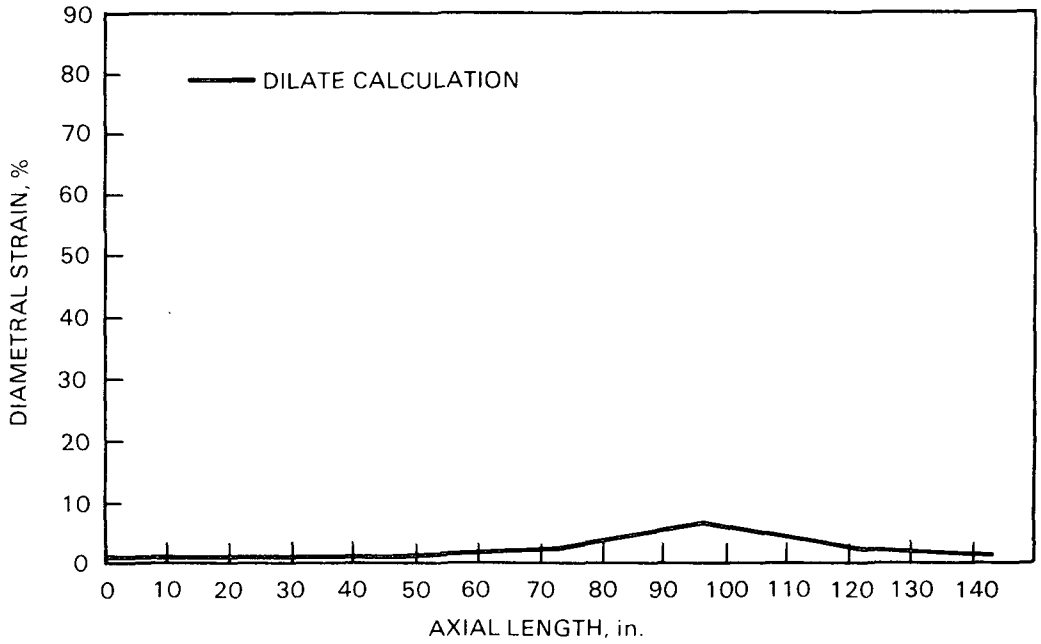

FIGURE 63. DILATE Calculations for MT-4

DESCRIPTION OF THE APPENDICES

Appendices A through G summarize the data resulting from the MT-4 experiment. The data are arranged as follows:

Appendix A - Preconditioning Test Assembly Temperatures
Appendix B - Pretransient Test Assembly Temperatures
Appendix C - Transient Fuel and Cladding Temperatures
Appendix D - Test Coolant and Shroud Temperatures
Appendix E - Neutron Flux Data
Appendix F - Reflood Flow Measurements
Appendix G - Fuel Rod Deformation Data

REFERENCES

1. Hann, C. R. 1979. Program Plan for LOCA Simulation in the National Research Universal (NRU) Reactor. PNL-3056, Pacific Northwest Laboratory, Richland, Washington.

2. Mohr, C. L., et al. April 1981. Prototypic Thermal-Hydraulic Experiment in NRU to Simulate Loss-of-Coolant Accidents. NUREG/CR-1882, PNL-3681, Pacific Northwest Laboratory, Richland, Washington.

3. Russcher, G. E., et al. October 1981. LOCA Simulation in the NRU Reactor - Materials Test-1. NUREG/CR-2152, Vol. 1, PNL-3835, Pacific Northwest Laboratory, Richland, Washington.

4. Barner, J. O., et al. March 1982. LOCA Simulation in the NRU Reactor - Materials Test-2. NUREG/CR-2509, PNL-4155, Pacific Northwest Laboratory, Richland, Washington.

5. Russcher, G. E., et al. September 1981. Experiment Operations Plan for a Loss-of-Coolant Accident Simulation in the National Research Universal Reactor. Addendum 1: Materials Tests 1 and 2. NUREG/CR-1735, PNL-3765, Pacific Northwest Laboratory, Richland, Washington.

6. Marshall, R. K., et al. 1983. The Continuous Measurement of Coolant Liquid Level During the MT-4 LOCA Experiment in the NRU Reactor. NUREG/CR-3183, PNL-4650, Pacific Northwest Laboratory, Richland, Washington.

7. Mohr, C. L., et al. 1978. Transient Deformation Properties of Zircaloy for LOCA Simulation. NP 526, Vol. 5, prepared for the Electric Power Research Institute, Palo Alto, California, by Battelle, Pacific Northwest Laboratories, Richland, Washington.

8. Donaldson, A. T., R. A. Horwood, and T. Healey. March 1982. Biaxial Creep Deformation of Zircaloy-4 in the High Alpha Phase Temperature Range. Presented at the IAEA Specialists Meeting on Water Reactor Fuel Element Performance Computer Modeling, Preston, England.

9. Mohr, C. L., et al. April 1983. LOCA Simulation in the National Research Universal Reactor Program - Data Report for the Third Materials Experiment (MT-3). NUREG/CR-2528, PNL-4166, Pacific Northwest Laboratory, Richland, Washington.

APPENDIX A

PRECONDITIONING TEST ASSEMBLY TEMPERATURES

APPENDIX A

PRECONDITIONING TEST ASSEMBLY TEMPERATURES

Data from the fourth materials experiment (MT-4) were recorded during the power ascensions and during the full-power, steady-state preconditioning phases of National Research Universal (NRU) reactor operation. Two preconditioning rises to power were performed. This appendix contains plots showing the test assembly environment at the second and final rise to full power. U-2 loop water at 16.3 kg/s (129,400 lbm/h) and 827 MPa (1200 psig) was used to cool the fuel. The average axial temperature profile for the test assembly shroud is shown in Figure A.1, and the individual corner channel axial temperature profiles are presented in Figure A.2. Modest coolant temperature gradients less than 12K (22°F) across the test assembly are evident from this comparison of individual corner channel temperatures. Radial coolant temperatures were measured by steam probe thermocouples (TCs) (Figure A.3); axial fuel and steam probe temperatures are shown in Figure A.4. The upper fuel TC in Figure A.4 was located in the fuel plenum.

The remainder of this appendix consists of the following graphical data:

FIGURE A.1. Average Axial Temperature Profile for the Shroud During Preconditioning (second rise to power) for MT-4

FIGURE A.2. Corner Axial Temperature Profiles for the Shroud During Preconditioning (second rise to power) for MT-4

FIGURE A.3. Radial Temperature Profiles Across Test Assembly Coolant at Levels 90.0, 111.0, and 148.2 During Preconditioning (second rise to power) for MT-4

FIGURE A.4. Average Fuel Rod Cladding Temperature Profiles for Interior and Centerline Thermocouples and Average Steam Probe Temperatures During Preconditioning (second rise to power) for MT-4

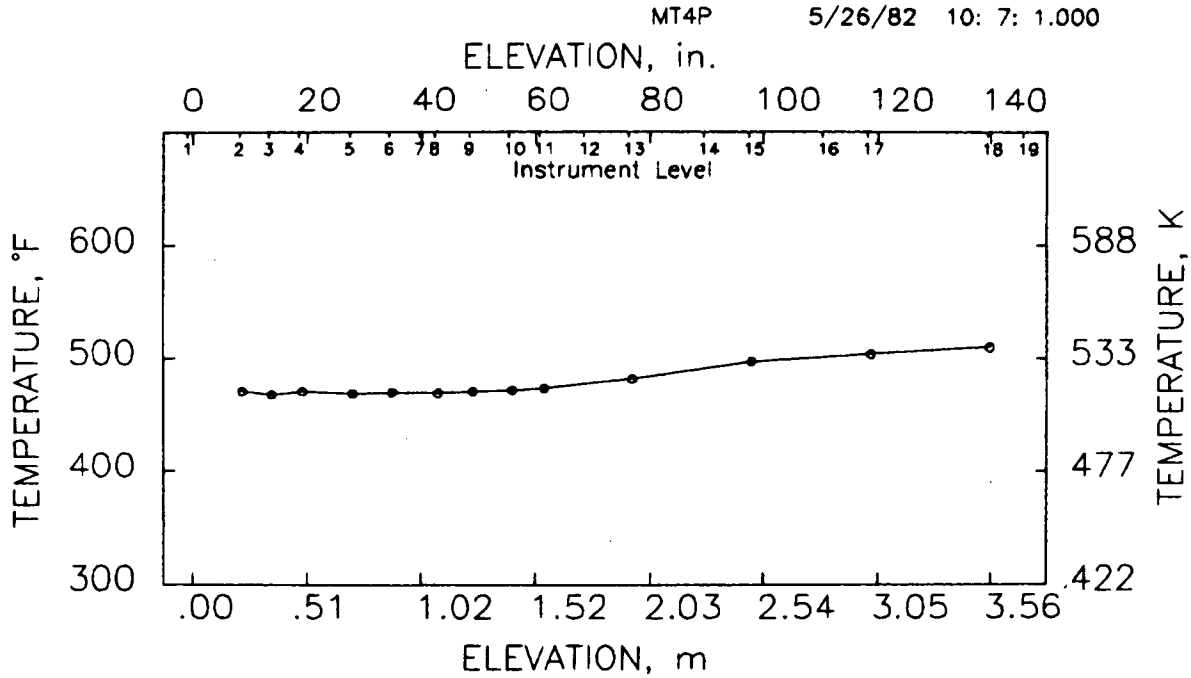

FIGURE A.1. Average Axial Temperature Profile for the Shroud During Preconditioning (second rise to power) for MT-4

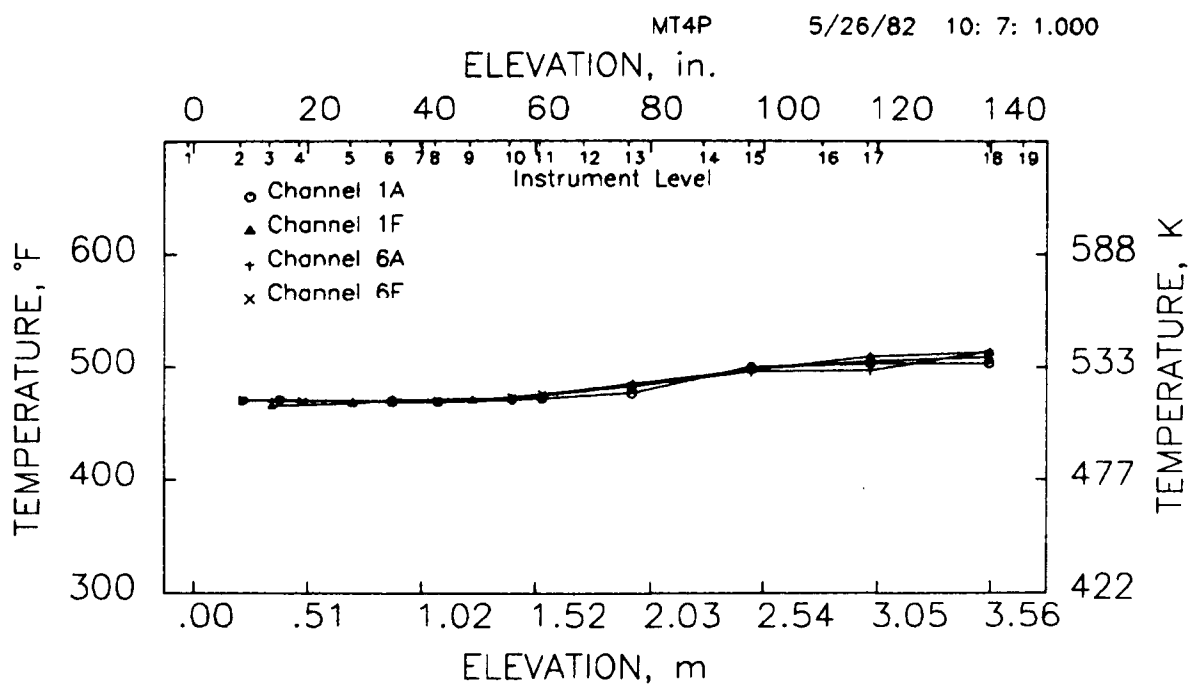

FIGURE A.2. Corner Axial Temperature Profiles for the Shroud During Preconditioning (second rise to power) for MT-4

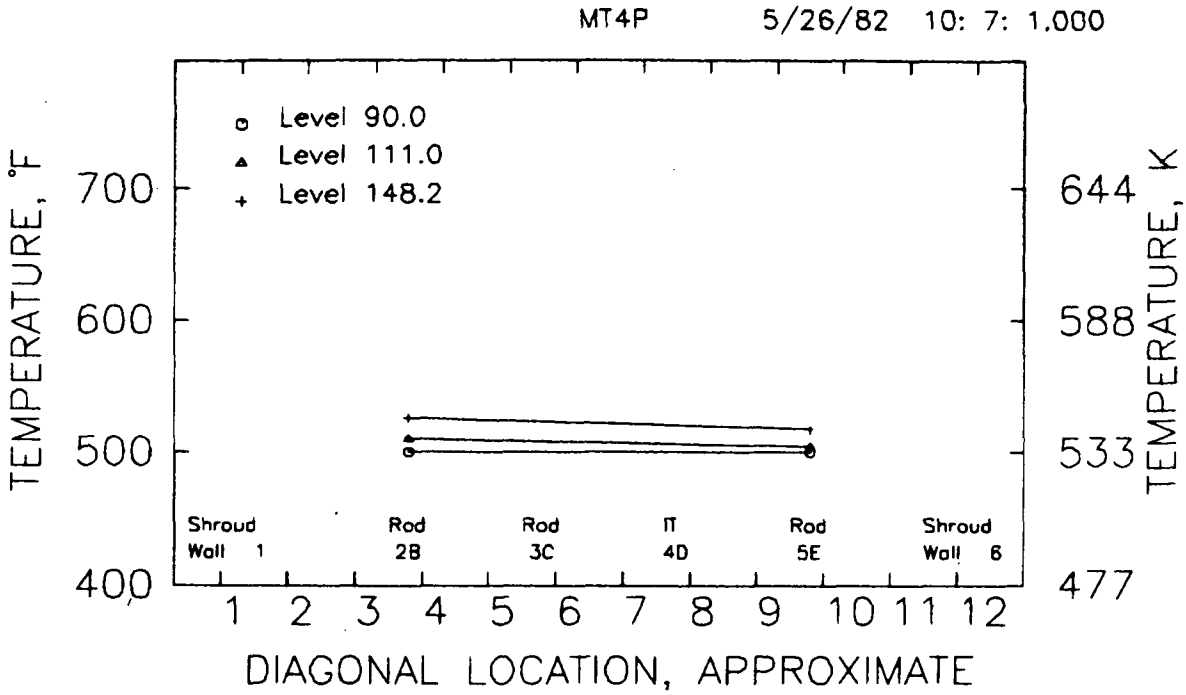

FIGURE A.3. Radial Temperature Profiles Across Test Assembly Coolant at Levels 90.0, 111.0, and 148.2 During Preconditioning (second rise to power) for MT-4

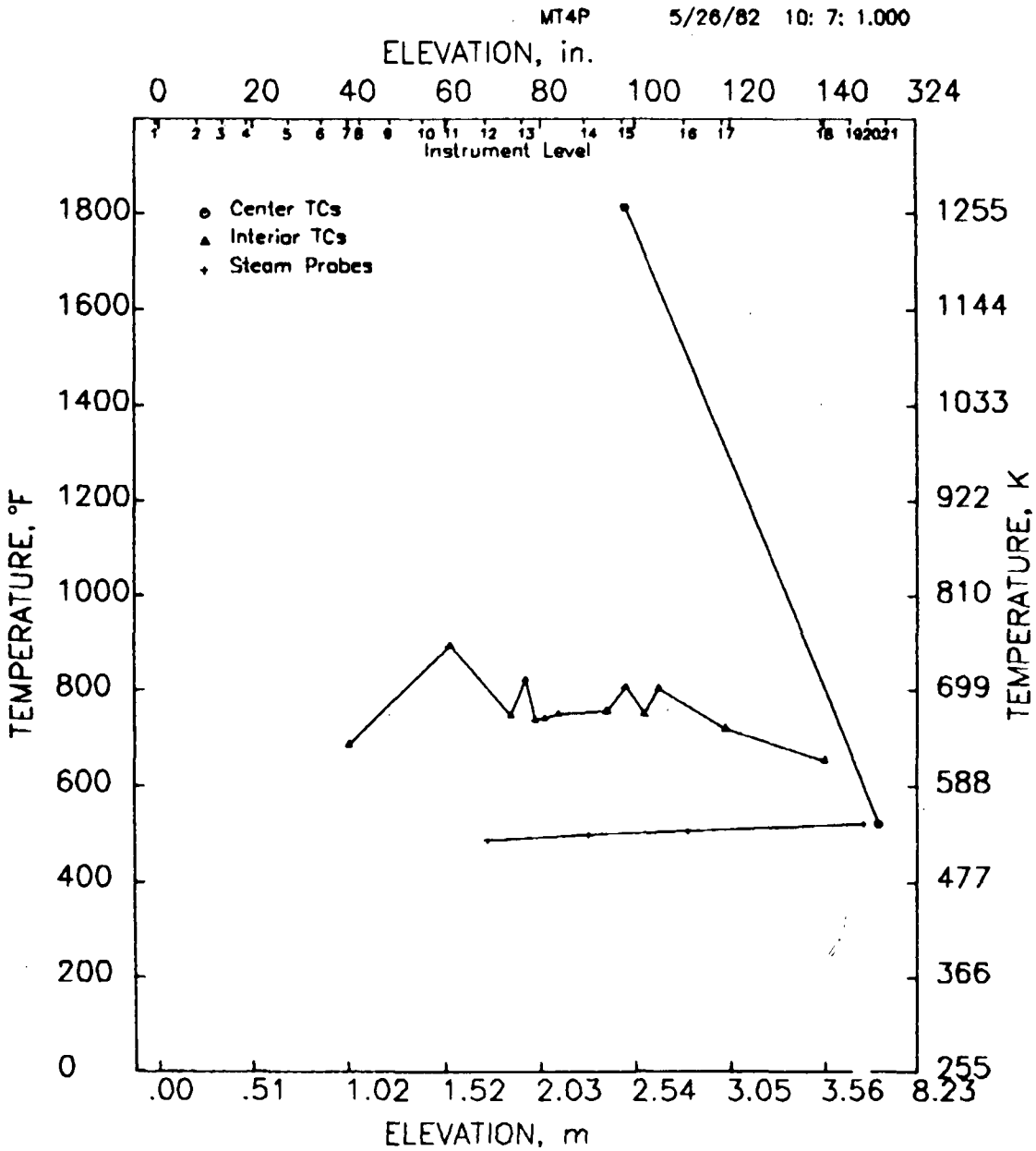

FIGURE A.4. Average Fuel Rod Cladding Temperature Profiles for Interior and Centerline Thermocouples and Average Steam Probe Temperatures During Preconditioning (second rise to power) for MT-4

APPENDIX B

PRETRANSIENT TEST ASSEMBLY TEMPERATURES

APPENDIX B

PRETRANSIENT TEST ASSEMBLY TEMPERATURES

Pretransient temperature data summaries are presented in this appendix. Steam at ~0.378 kg/s (3000 lbm/h) was used to cool the test assembly, and test assembly backpressure was maintained at ~0.28 MPa (40 psia).

Pretransient axial temperatures for the shroud are shown for adiabatic tests MT-4.02 and MT-4.03 and for the final test MT-4.04 (Figures B.1, B.2, and B.3, respectively). Individual corner channel axial temperature profiles are presented in Figures B.4 through B.6. Modest coolant temperature gradients (in steam) across the test assembly are evident. Radial coolant channel temperatures were measured by steam probe thermocouples (TCs) (Figures B.7 through B.9). Average fuel cladding temperatures for interior and centerline TCs and average steam probe temperatures during the pretransients are shown in Figures B.10 through B.12. The upper level TC was located in the fuel rod plenum.

The remainder of this appendix consists of the following graphical data:

FIGURE B.1. Average Axial Temperature Profile for the Shroud During Pretransient for Adiabatic Test MT-4.02

FIGURE B.2. Average Axial Temperature Profile for the Shroud During Pretransient for Adiabatic Test MT-4.03

FIGURE B.3. Average Axial Temperature Profile for the Shroud During Pretransient for MT-4.04

FIGURE B.4. Corner Axial Temperature Profiles for the Shroud During Pretransient for Adiabatic Test MT-4.02

FIGURE B.5. Corner Axial Temperature Profiles for the Shroud During Pretransient for Adiabatic Test MT-4.03

FIGURE B.6. Corner Axial Temperature Profiles for the Shroud During Pretransient for MT-4.04

FIGURE B.7. Radial Temperature Profiles Across Test Assembly Coolant at Levels 90.0, 111.0, and 148.2 During Pretransient for Adiabatic Test MT-4.02

FIGURE B.8. Radial Temperature Profiles Across Test Assembly Coolant at Levels 90.0, 111.0, and 148.2 During Pretransient for Adiabatic Test MT-4.03

FIGURE B.9. Radial Temperature Profiles Across Test Assembly Coolant at Levels 90.0, 111.0, and 148.2 During Pretransient for MT-4.04

FIGURE B.10. Average Fuel Rod Cladding Temperature Profiles for Interior and Centerline Thermocouples and Average Steam Probe Temperatures During Pretransient for Adiabatic Test MT-4.02

FIGURE B.11. Average Fuel Rod Cladding Temperature Profiles for Interior and Centerline Thermocouples and Average Steam Probe Temperatures During Pretransient for Adiabatic Test MT-4.03

FIGURE B.12. Average Fuel Rod Cladding Temperature Profiles for Interior and Centerline Thermocouples and Average Steam Probe Temperatures During Pretransient for MT-4.04

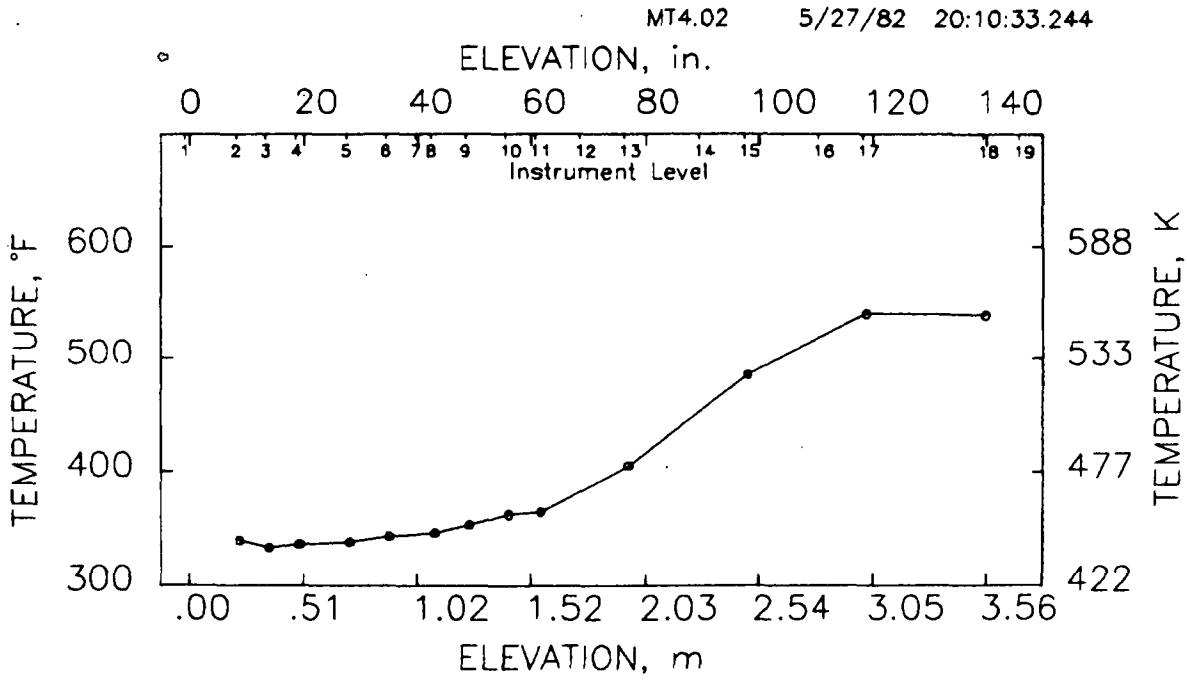

FIGURE B.1. Average Axial Temperature Profile for the Shroud During Pretransient for Adiabatic Test MT-4.02

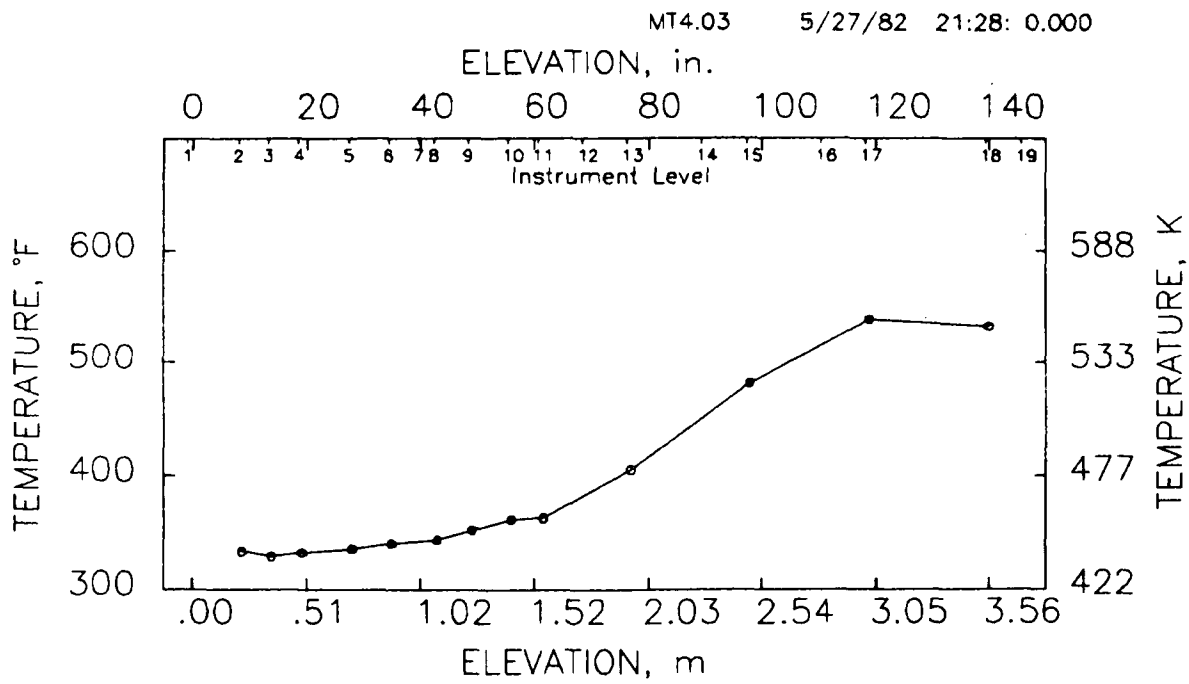

FIGURE B.2. Average Axial Temperature Profile for the Shroud During Pretransient for Adiabatic Test MT-4.03

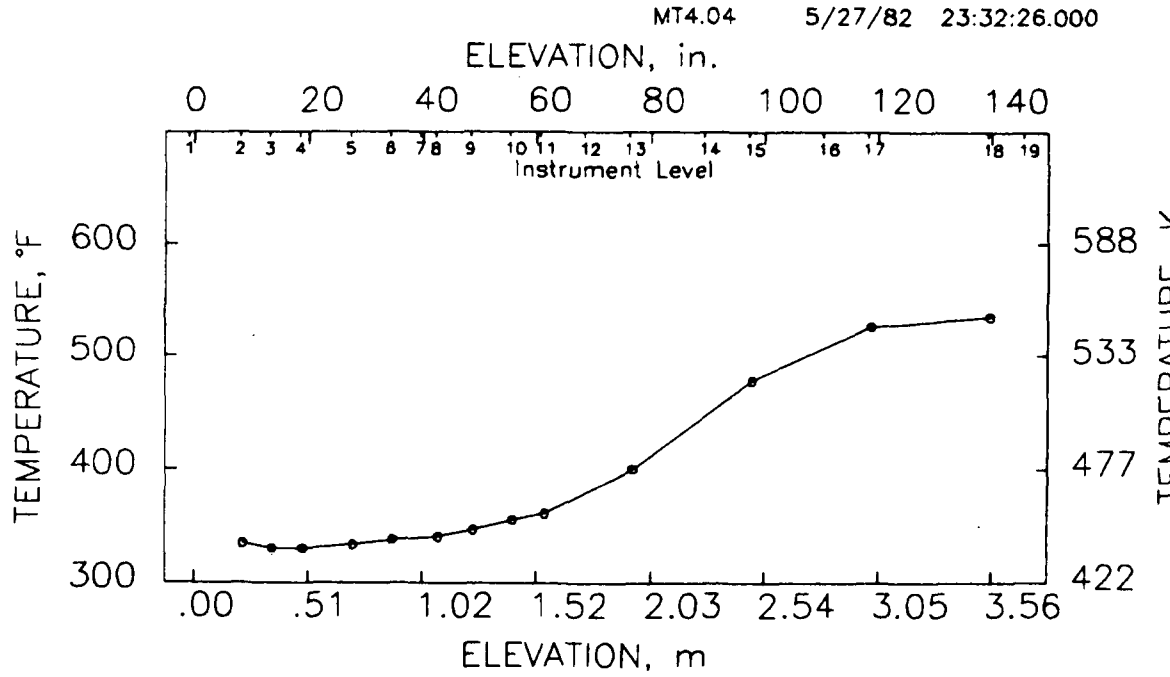

FIGURE B.3. Average Axial Temperature Profile for the Shroud During Pretransient for MT-4.04

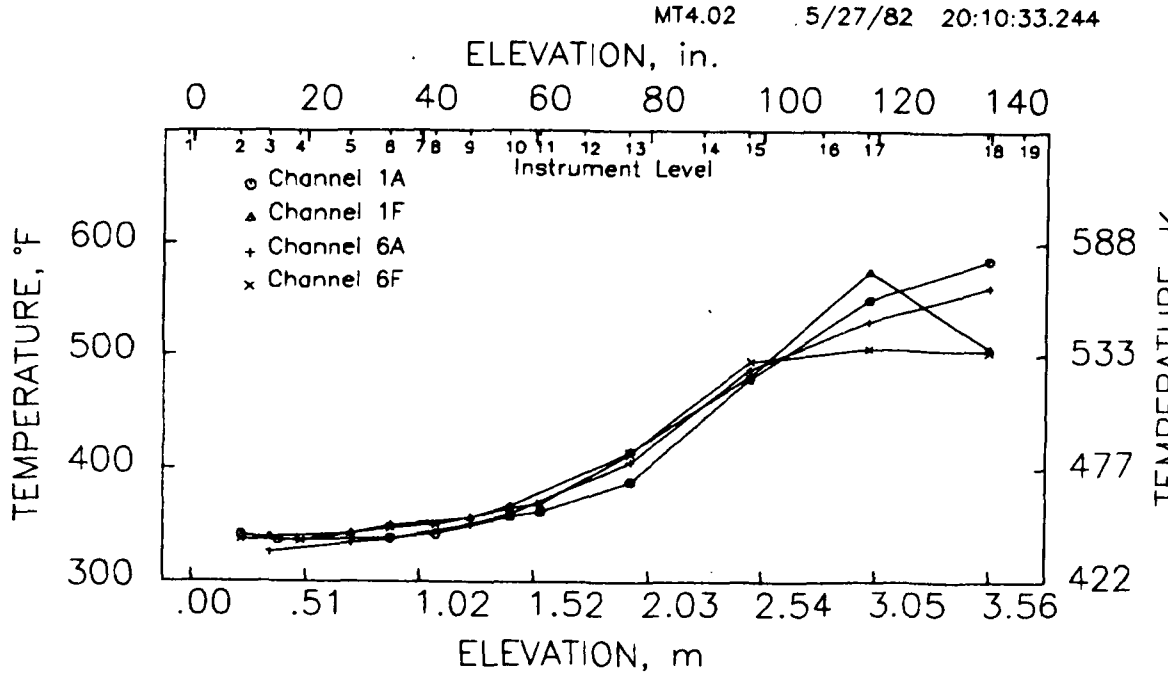

FIGURE B.4. Corner Axial Temperature Profiles for the Shroud During Pretransient for Adiabatic Test MT-4.02

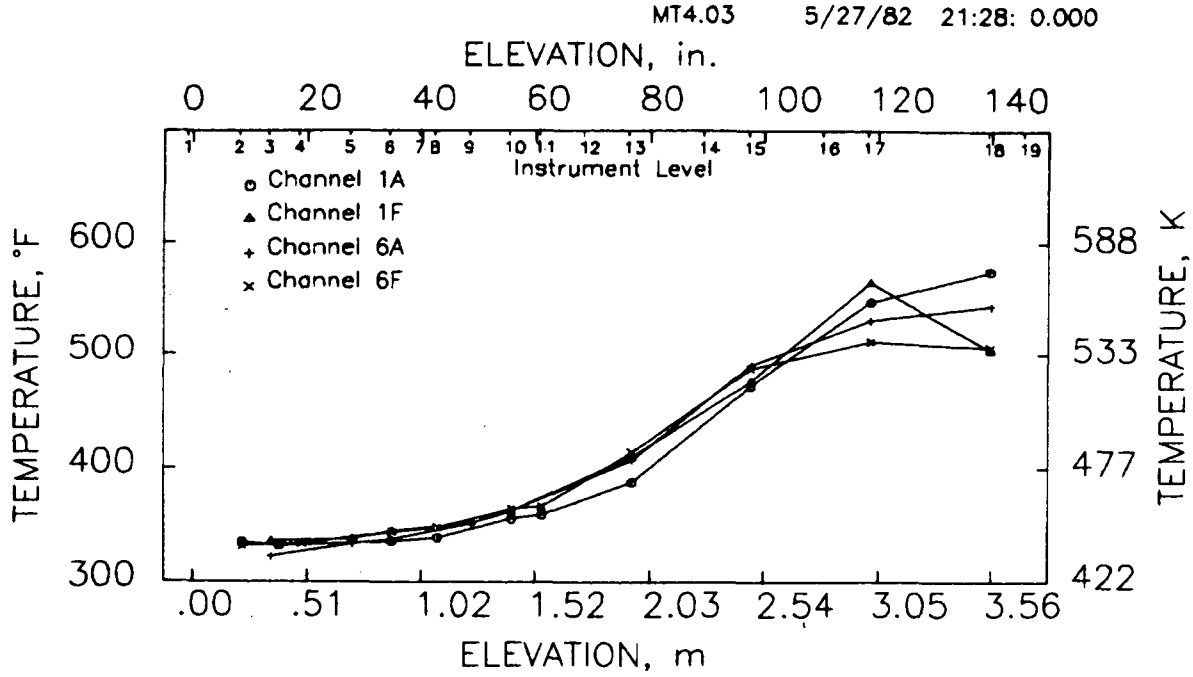

FIGURE B.5. Corner Axial Temperature Profiles for the Shroud During Pretransient for Adiabatic Test MT-4.03

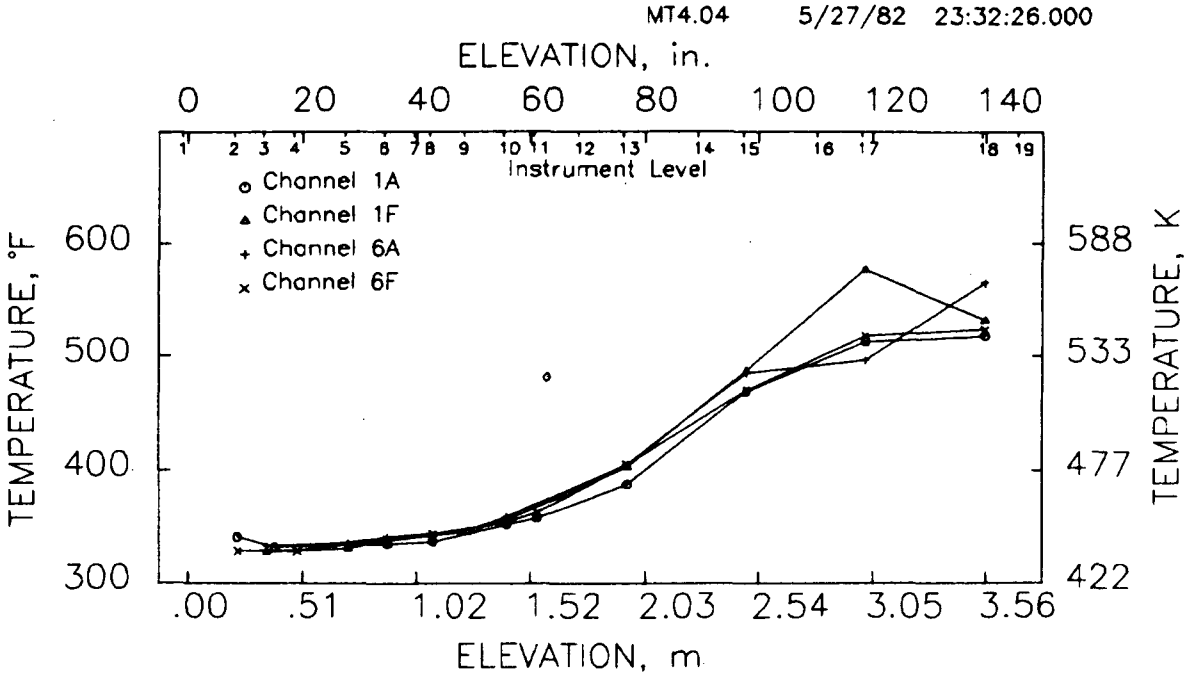

FIGURE B.6. Corner Axial Temperature Profiles for the Shroud During Pretransient for MT-4.04

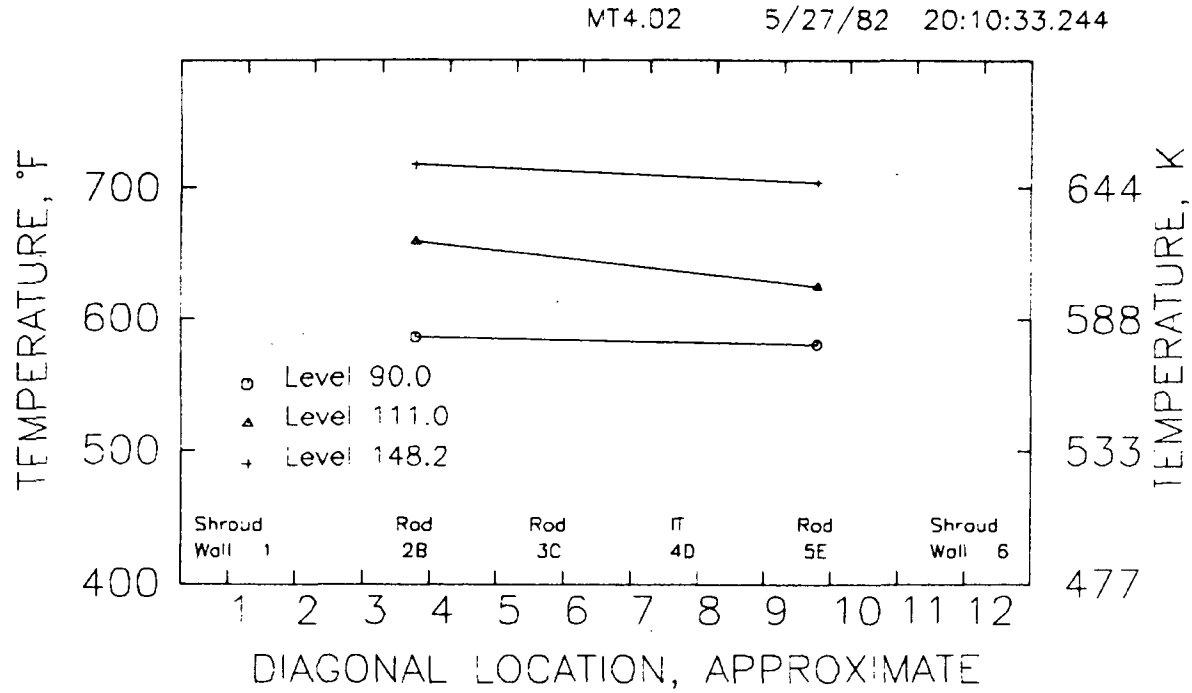

FIGURE B.7. Radial Temperature Profiles Across Test Assembly Coolant at Levels 90.0, 111.0, and 148.2 During Pretransient for Adiabatic Test MT-4.02

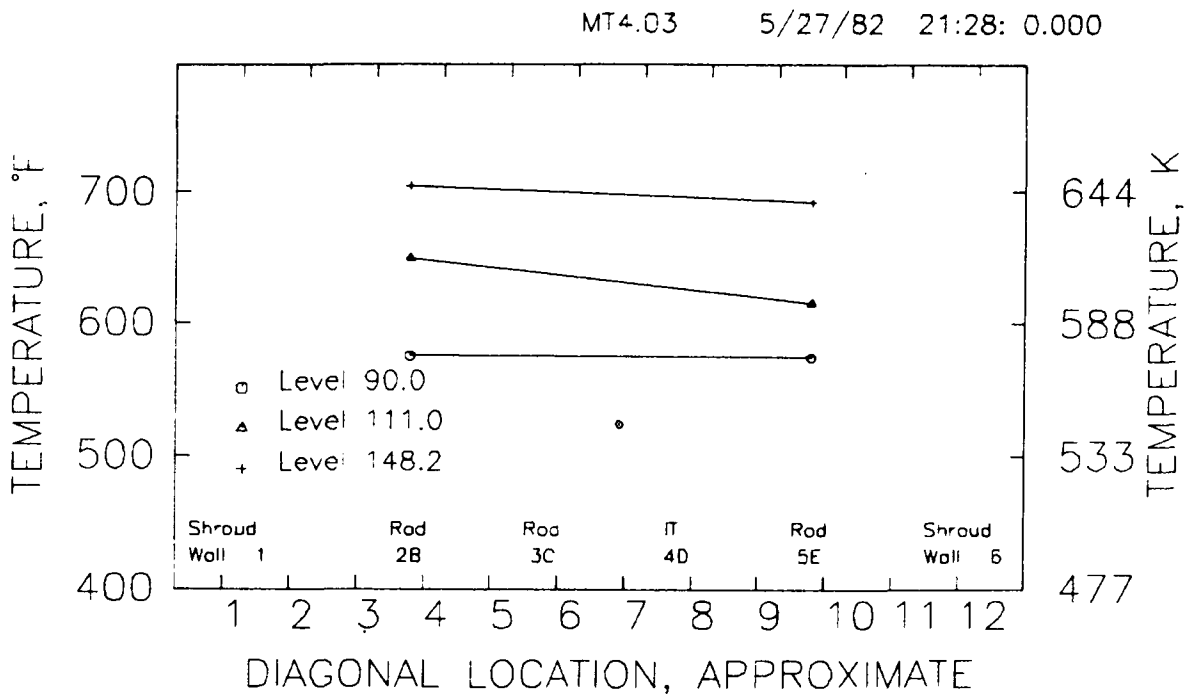

FIGURE B.8. Radial Temperature Profiles Across Test Assembly Coolant at Levels 90.0, 111.0, and 148.2 During Pretransient for Adiabatic Test MT-4.03

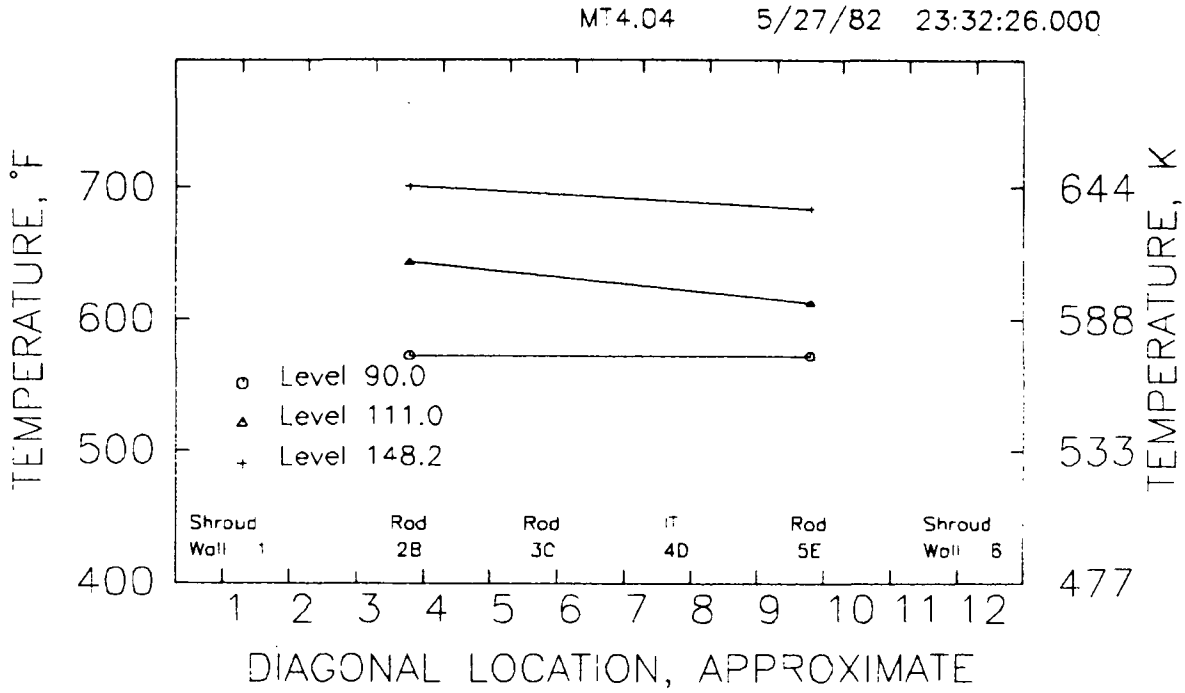

FIGURE B.9. Radial Temperature Profiles Across Test Assembly Coolant at Levels 90.0, 111.0, and 148.2 During Pretransient for MT-4.04

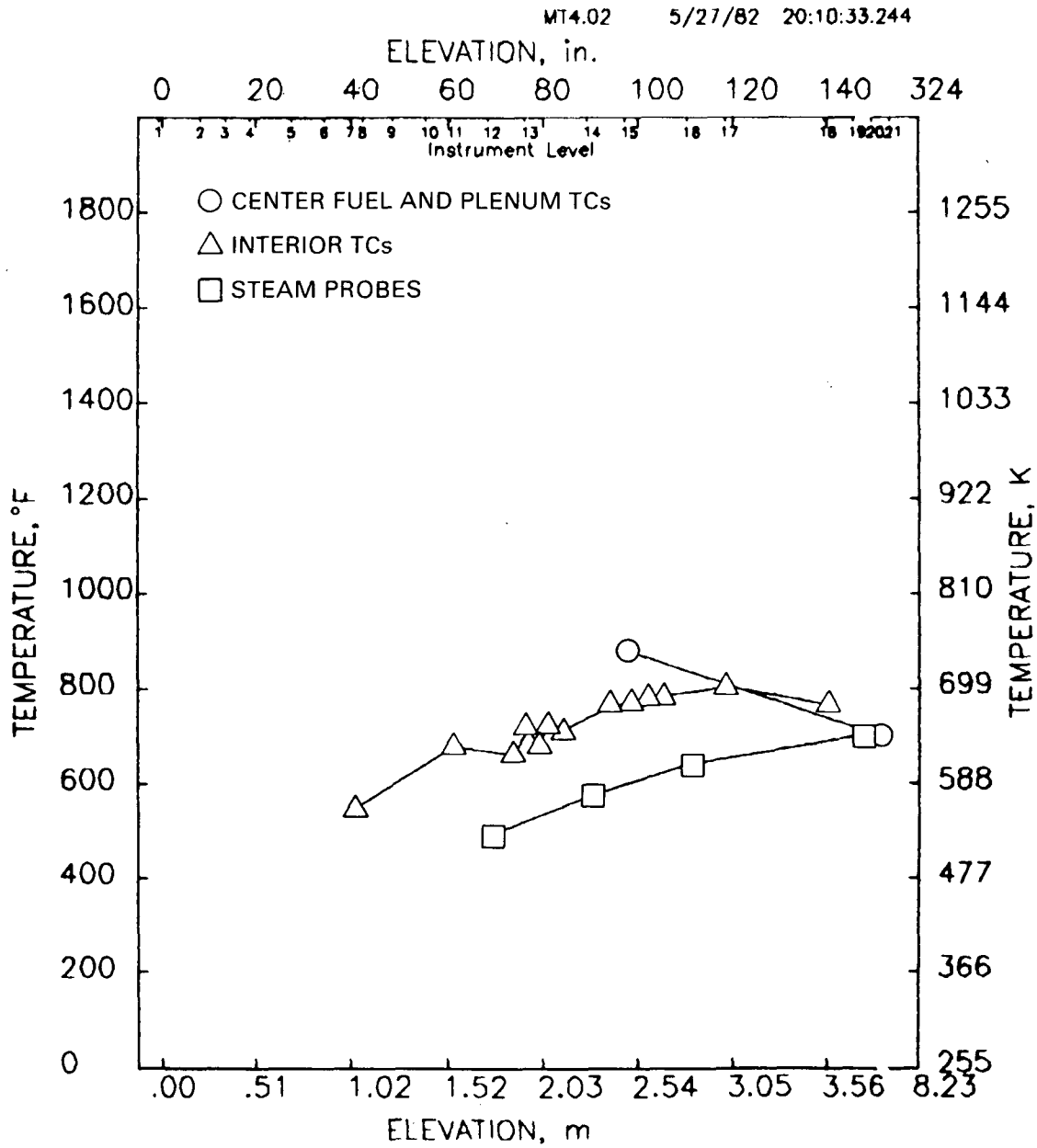

FIGURE B.10. Average Fuel Rod Cladding Temperature Profiles for Interior and Centerline Thermocouples and Average Steam Probe Temperatures During Pretransient for Adiabatic Test MT-4.02

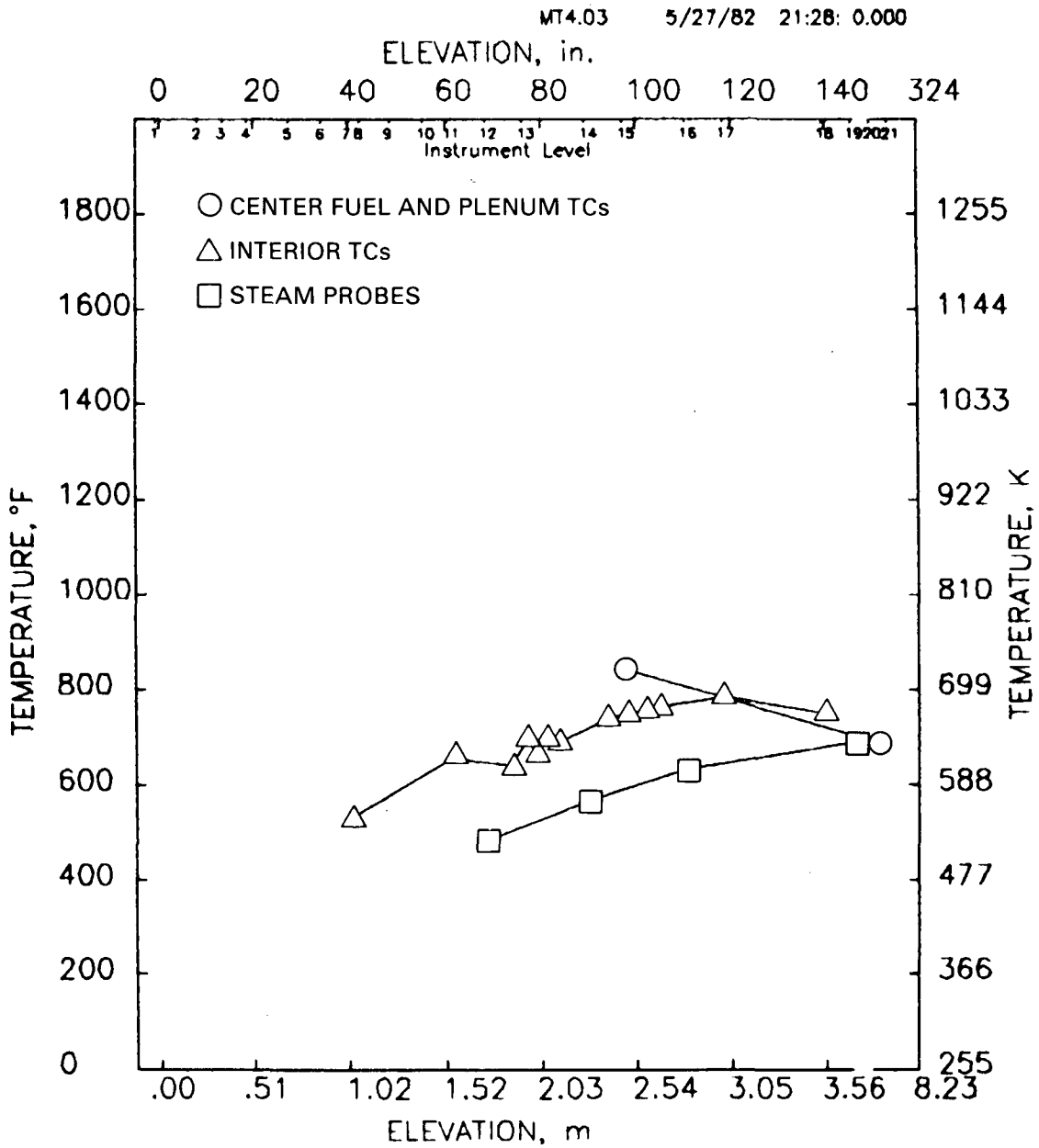

FIGURE B.11. Average Fuel Rod Cladding Temperature Profiles for Interior and Centerline Thermocouples and Average Steam Probe Temperatures During Pretransient for Adiabatic Test MT-4.03

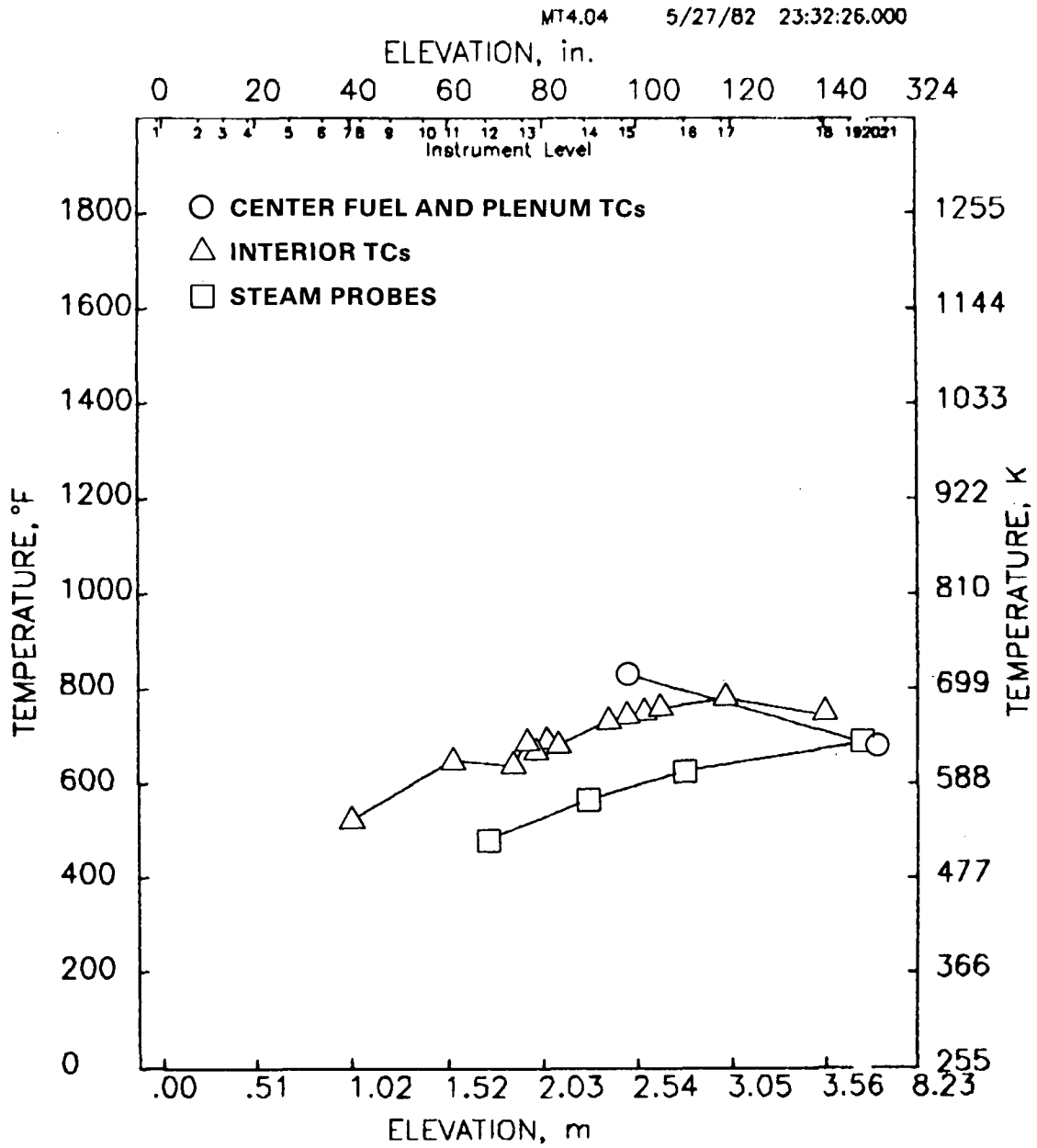

FIGURE B.12. Average Fuel Rod Cladding Temperature Profiles for Interior and Centerline Thermocouples and Average Steam Probe Temperatures During Pretransient for MT-4.04

APPENDIX C

TRANSIENT FUEL AND CLADDING TEMPERATURES

APPENDIX C

TRANSIENT FUEL AND CLADDING TEMPERATURES

Transient fuel centerline and cladding temperatures for adiabatic tests MT-4.02 and MT-4.03 and the final test MT-4.04 are presented in this appendix. The test assembly environment during the transient was steam, or water, or both with a changing neutron flux depending partially on control rod position and the changing reactivity of water and steam. The test assembly backpressure was maintained at ~0.28 MPa (40 psia). All of these environmental conditions affected the fuel and cladding temperatures during the transients.

Test rod interior cladding temperatures are shown for Levels 76.9, 97.9, and 118.9 in Figures C.1 through C.12 for MT-4.02, MT-4.03, and MT-4.04. Average fuel temperatures for test and guard rods at Levels 76.9, 97.9, and 118.9 are shown in Figures C.13 through C.24 for MT-4.02, MT-4.03, and MT-4.04. These figures demonstrate the resultant average guard and test fuel temperatures when using hot spot sensor feedback control. Fuel centerline and plenum temperatures for test rods 2B, 2E, 5E, and 5B are shown in Figures C.25 through C.32 for MT-4.02, MT-4.03, and MT-4.04. The temperatures of the brazes at the top of the fuel (Level 156.0) for MT-4.04 are shown in Figure C.33.

The remainder of this appendix consists of the following graphical data:

FIGURE C.1. Test Rod Interior Cladding Temperature Histories at Level 76.9 During Adiabatic Test MT-4.02

FIGURE C.2. Test Rod Interior Cladding Temperature Histories at Level 97.9 During Adiabatic Test MT-4.02

FIGURE C.3. Test Rod Interior Cladding Temperature Histories at Level 118.9 During Adiabatic Test MT-4.02

FIGURE C.4. Test Rod Interior Cladding Temperature Histories at Level 76.9 During Adiabatic Test MT-4.03

FIGURE C.5. Test Rod Interior Cladding Temperature Histories at Level 97.9 During Adiabatic Test MT-4.03

FIGURE C.6. Test Rod Interior Cladding Temperature Histories at Level 118.9 During Adiabatic Test MT-4.03

FIGURE C.7. Test Rod Interior Cladding Temperature Histories at Level 76.9 for First 90 s of MT-4.04

FIGURE C.8. Test Rod Interior Cladding Temperature Histories at Level 97.9 for First 90 s of MT-4.04

FIGURE C.9. Test Rod Interior Cladding Temperature Histories at Level 118.9 for First 90 s of MT-4.04

FIGURE C.10. Test Rod Interior Cladding Temperature Histories at Level 76.9 for 1500 s of MT-4.04

FIGURE C.11. Test Rod Interior Cladding Temperature Histories at Level 97.9 for 1500 s of MT-4.04

FIGURE C.12. Test Rod Interior Cladding Temperature Histories at Level 118.9 for 1500 s of MT-4.04

FIGURE C.13. Average Guard and Test Rod Interior Cladding Temperatures at Level 76.9 During Adiabatic Test MT-4.02

FIGURE C.14. Average Guard and Test Rod Interior Cladding Temperatures at Level 97.9 During Adiabatic Test MT-4.02

FIGURE C.15. Average Guard and Test Rod Interior Cladding Temperatures at Level 118.9 During Adiabatic Test MT-4.02

FIGURE C.16. Average Guard and Test Rod Interior Cladding Temperatures at Level 76.9 During Adiabatic Test MT-4.03

FIGURE C.17. Average Guard and Test Rod Interior Cladding Temperatures at Level 96.9 During Adiabatic Test MT-4.03

FIGURE C.18. Average Guard and Test Rod Interior Cladding Temperatures at Level 118.9 During Adiabatic Test MT-4.03

FIGURE C.19. Average Guard and Test Rod Interior Cladding Temperatures at Level 76.9 for First 90 s of MT-4.04

FIGURE C.20. Average Guard and Test Rod Interior Cladding Temperatures at Level 97.9 for First 90 s of MT-4.04

FIGURE C.21. Average Guard and Test Rod Interior Cladding Temperatures at Level 118.9 for First 90 s of MT-4.04

FIGURE C.22. Average Guard and Test Rod Interior Cladding Temperatures at Level 76.9 for 1500 s of MT-4.04

FIGURE C.23. Average Guard and Test Rod Interior Cladding Temperatures at Level 97.9 for 1500 s of MT-4.04

FIGURE C.24. Average Guard and Test Rod Interior Cladding Temperatures at Level 118.9 for 1500 s of MT-4.04

FIGURE C.25. Fuel Centerline Temperatures at Level 97.9 for Adiabatic Test MT-4.02

FIGURE C.26. Fuel Plenum Temperatures at Level 151.5 for Adiabatic Test MT-4.02

FIGURE C.27. Fuel Centerline Temperatures at Level 97.9 for Adiabatic Test MT-4.03

FIGURE C.28. Fuel Plenum Temperatures at Level 151.5 for Adiabatic Test MT-4.03

FIGURE C.29. Fuel Centerline Temperatures at Level 97.9 During First 90 s of MT-4.04

FIGURE C.30. Fuel Plenum Temperatures at Level 151.5 During First 90 s of MT-4.04

FIGURE C.31. Fuel Centerline Temperatures at Level 97.9 During 1500 s of MT-4.04

FIGURE C.32. Fuel Plenum Temperatures at Level 151.5 During 1500 s of MT-4.04

FIGURE C.33. Fuel Rod Upper End Cap Braze Temperatures at Level 156.0 for MT-4.04

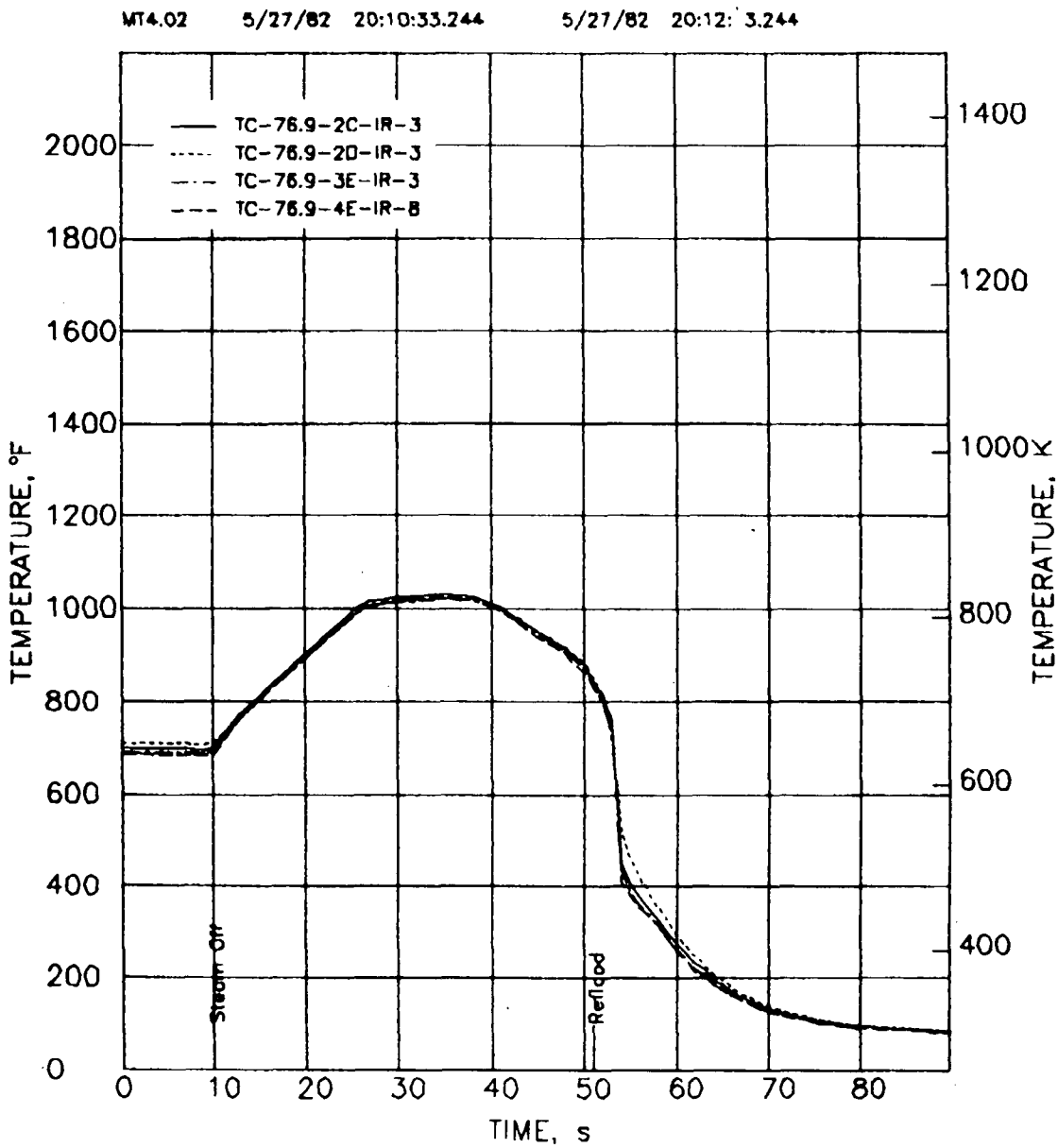

FIGURE C.1. Test Rod Interior Cladding Temperature Histories at Level 76.9 During Adiabatic Test MT-4.02

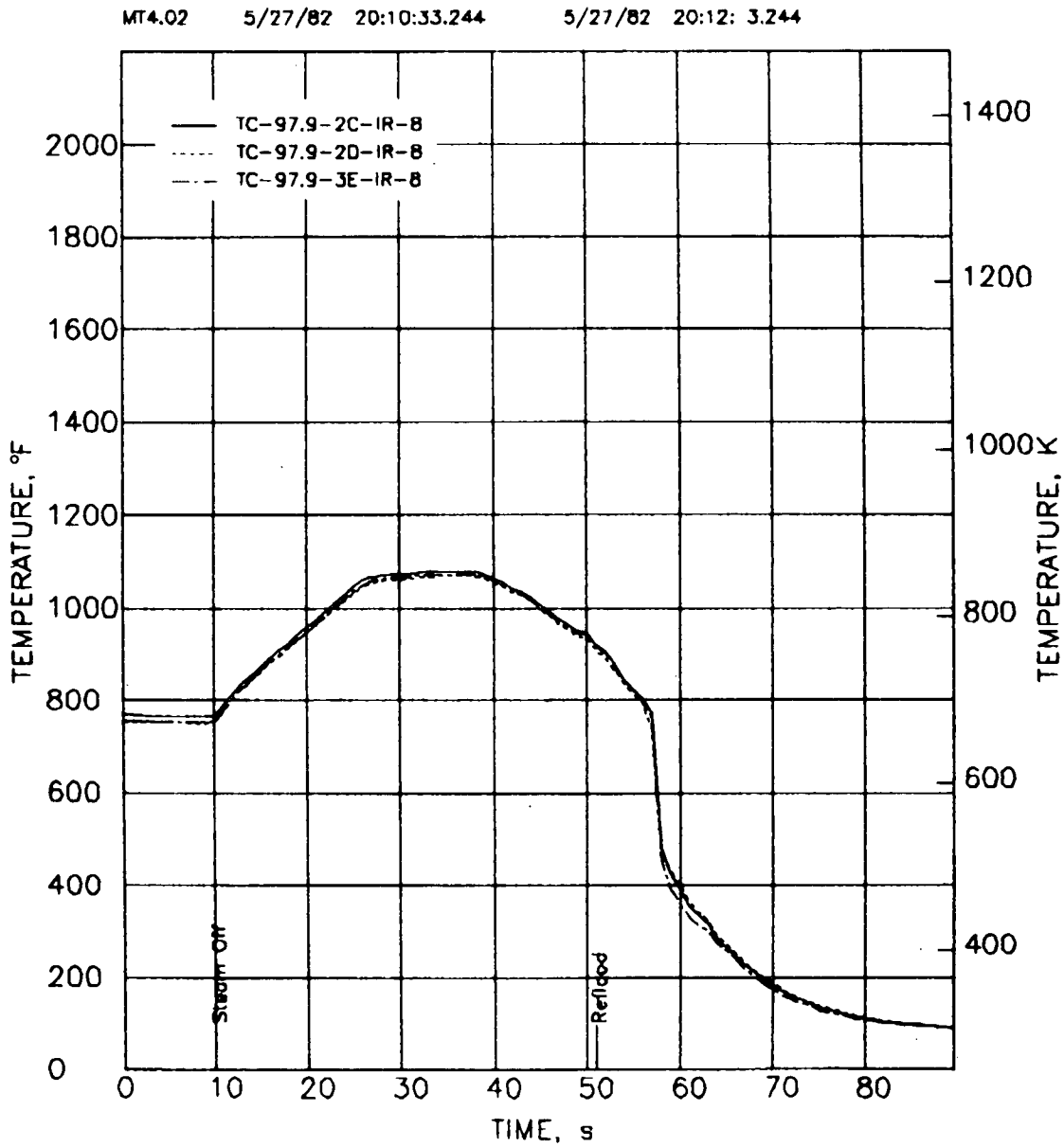

FIGURE C.2. Test Rod Interior Cladding Temperature Histories at Level 97.9 During Adiabatic Test MT-4.02

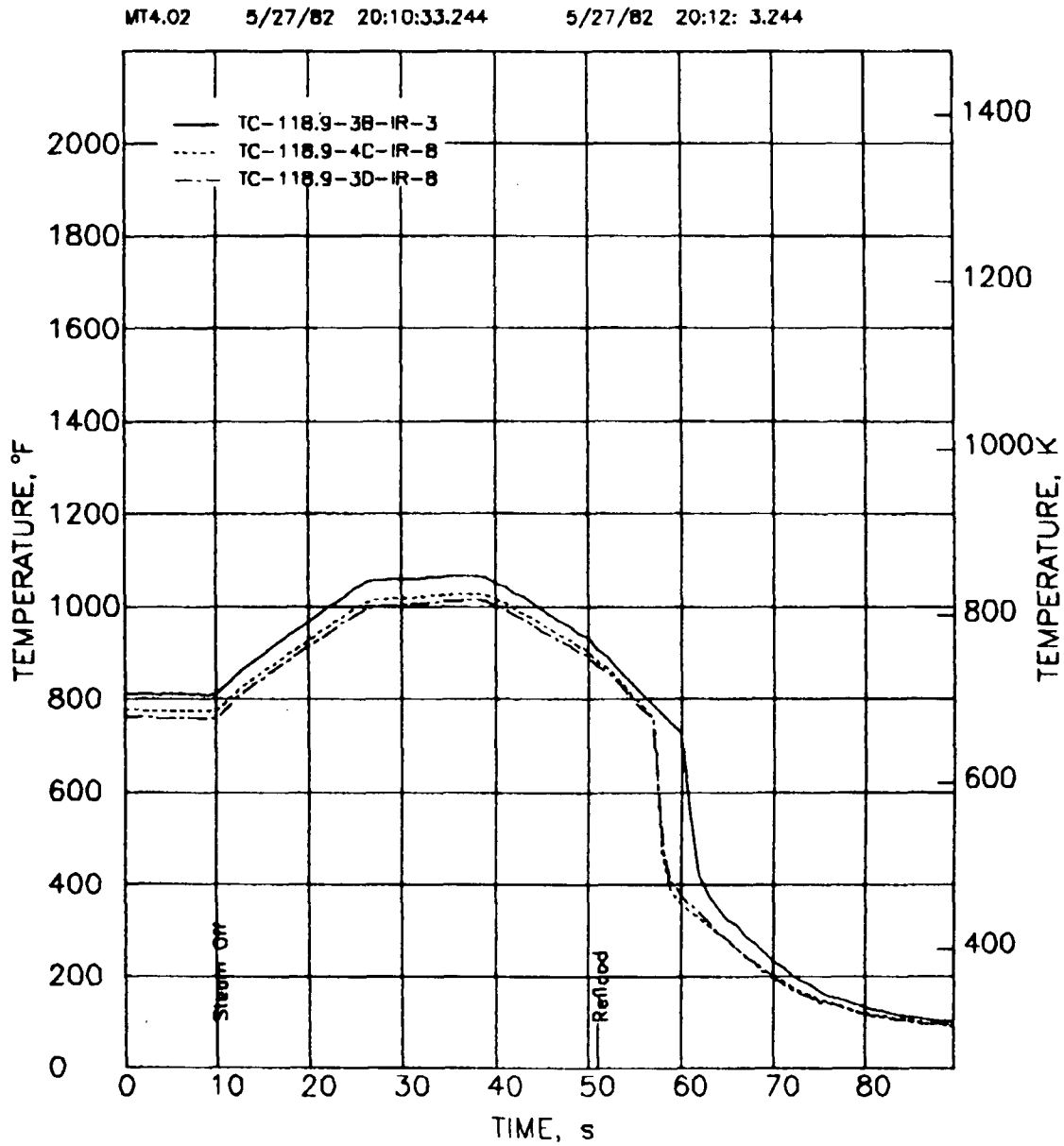

FIGURE C.3. Test Rod Interior Cladding Temperature Histories at Level 118.9 During Adiabatic Test MT-4.02

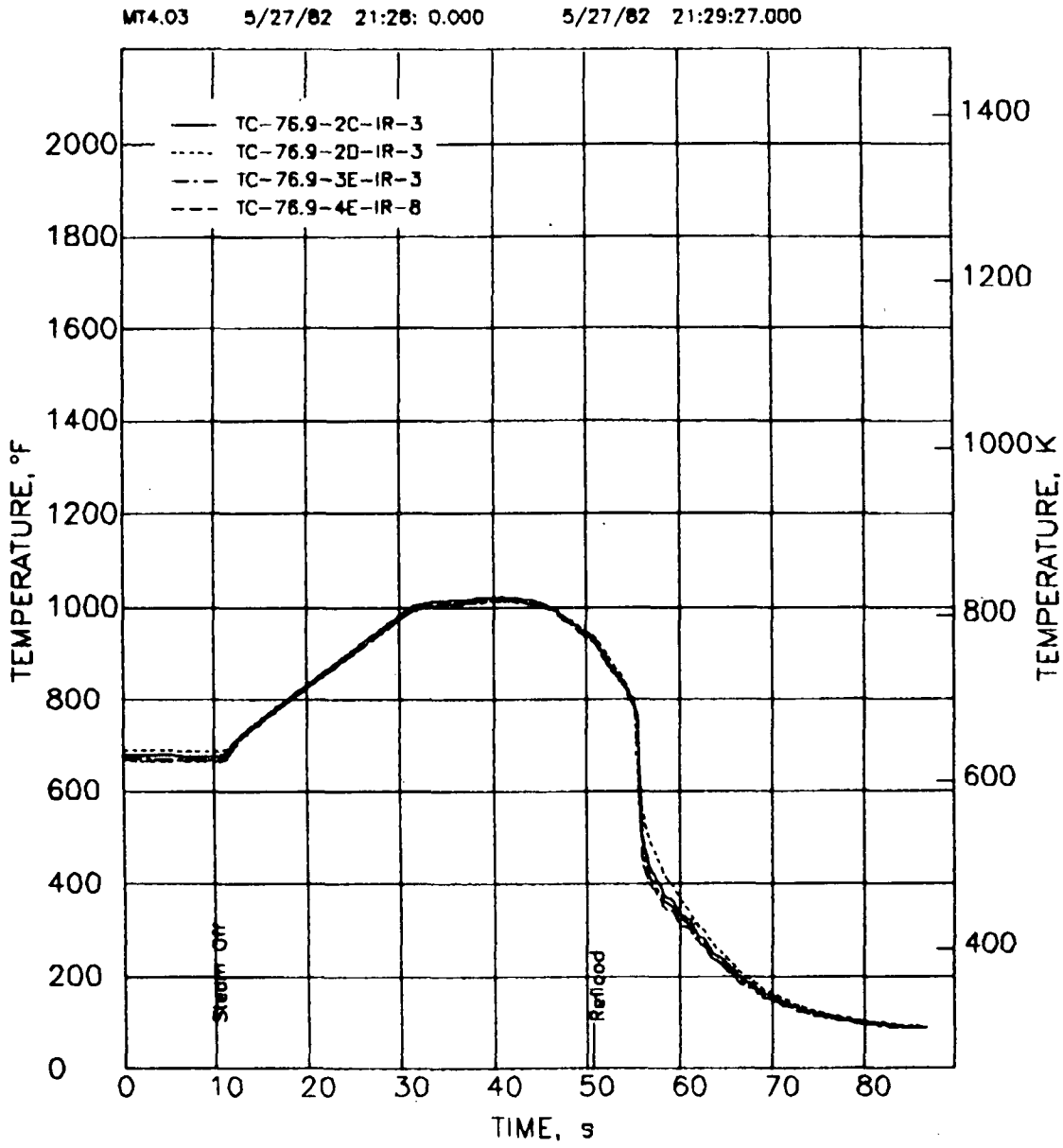

FIGURE C.4. Test Rod Interior Cladding Temperature Histories at Level 76.9 During Adiabatic Test MT-4.03

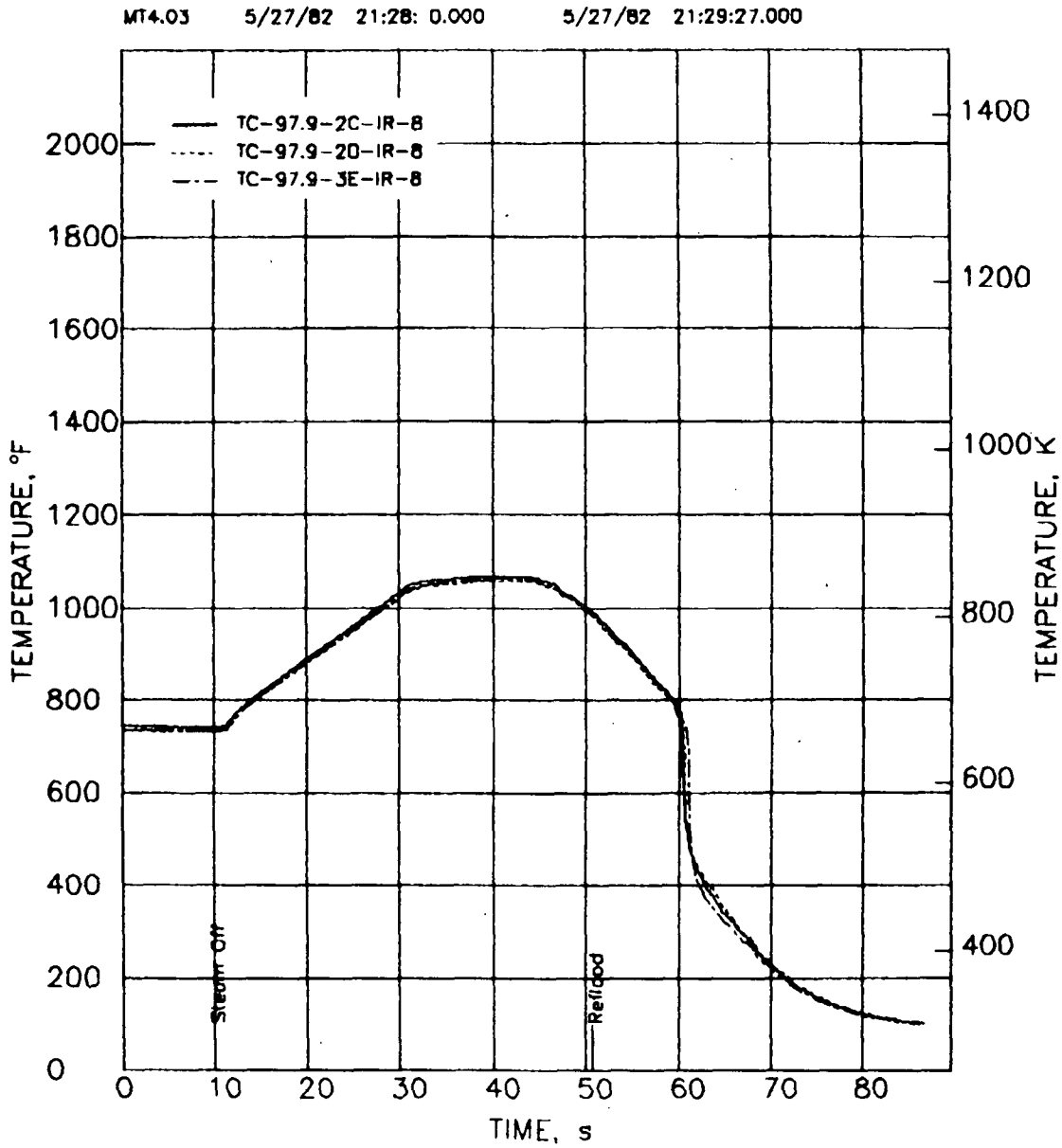

FIGURE C.5. Test Rod Interior Cladding Temperature Histories at Level 97.9 During Adiabatic Test MT-4.03

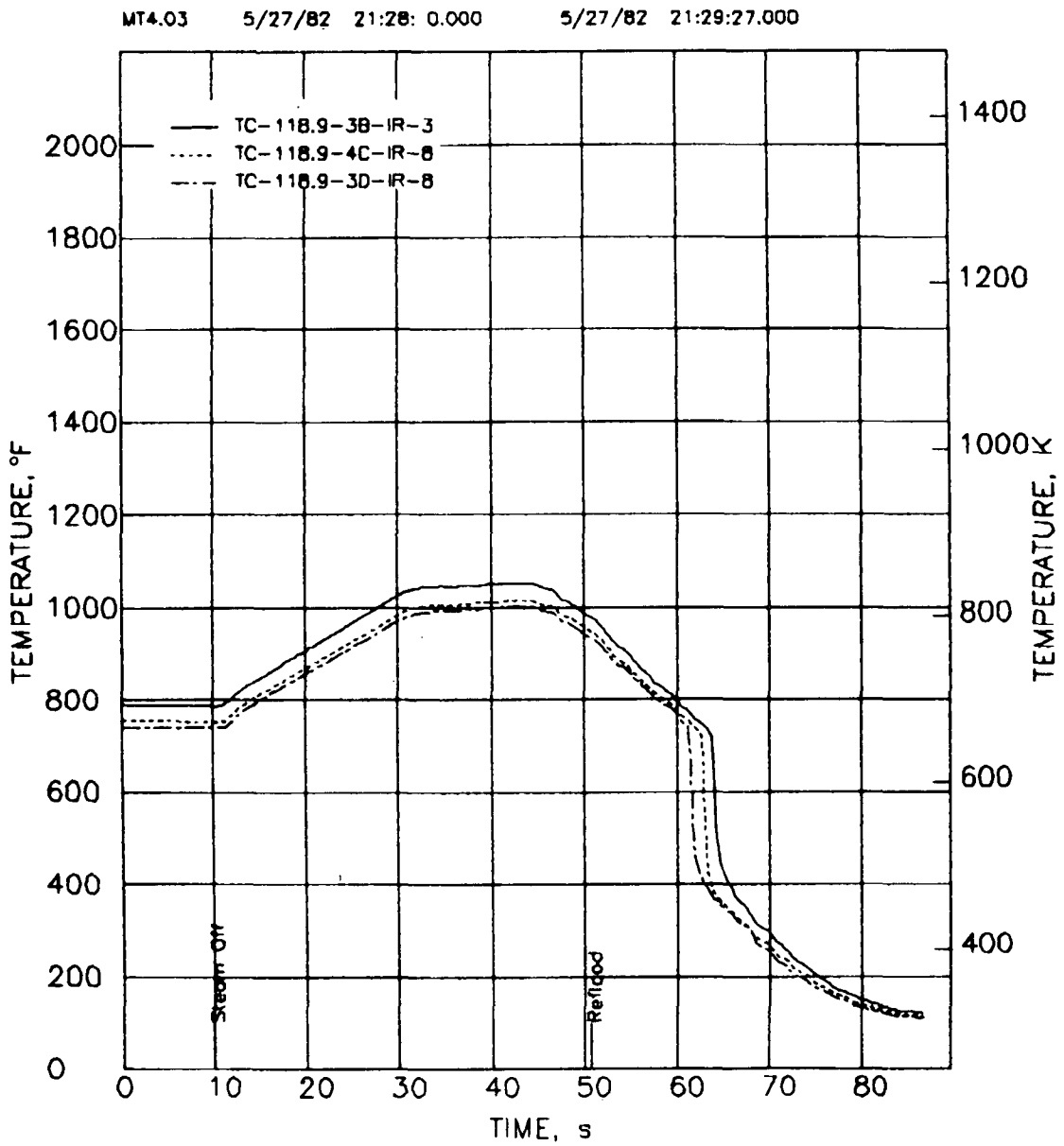

FIGURE C.6. Test Rod Interior Cladding Temperature Histories at Level 118.9 During Adiabatic Test MT-4.03

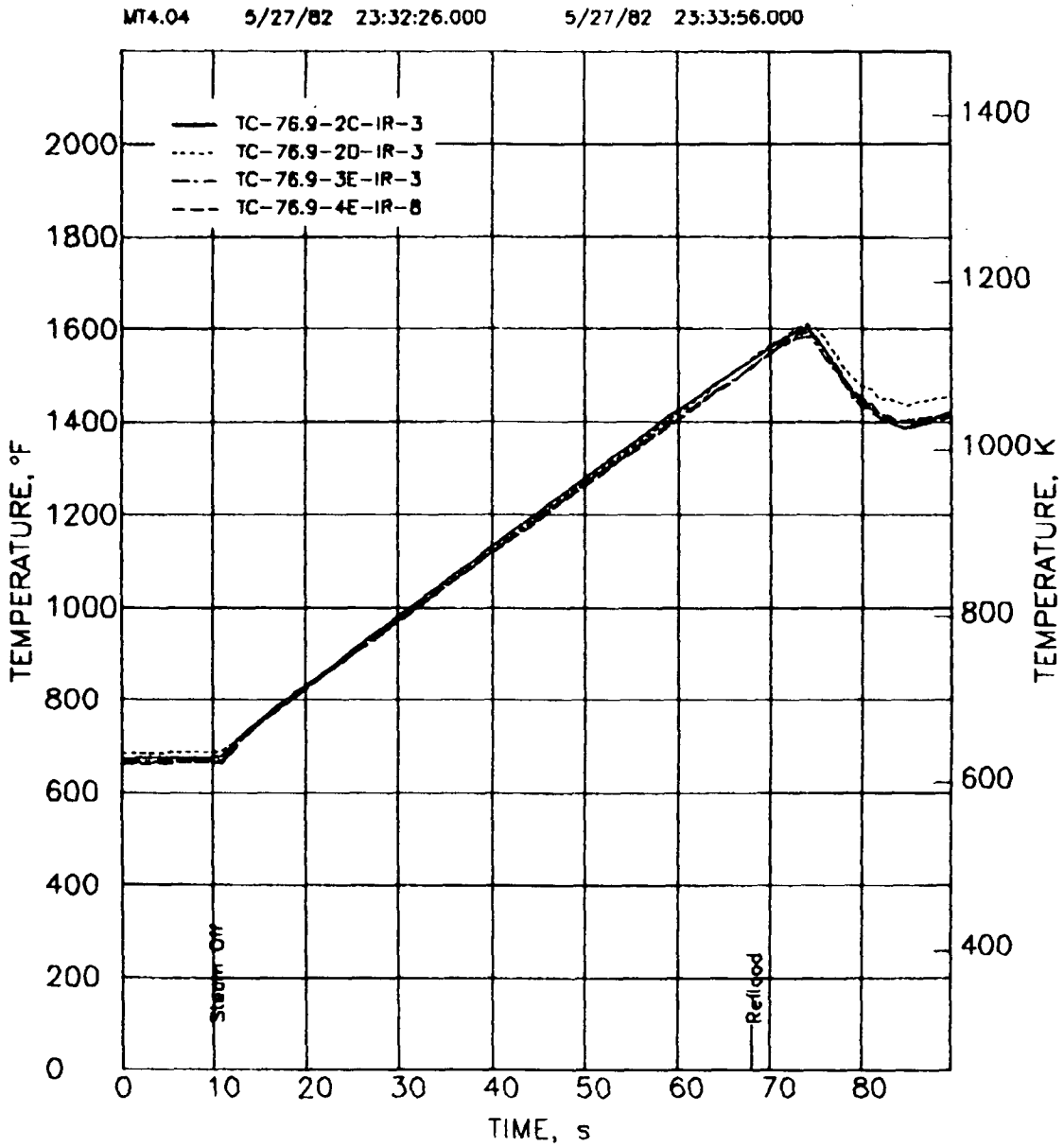

FIGURE C.7. Test Rod Interior Cladding Temperature Histories at Level 76.9 for First 90 s of MT-4.04

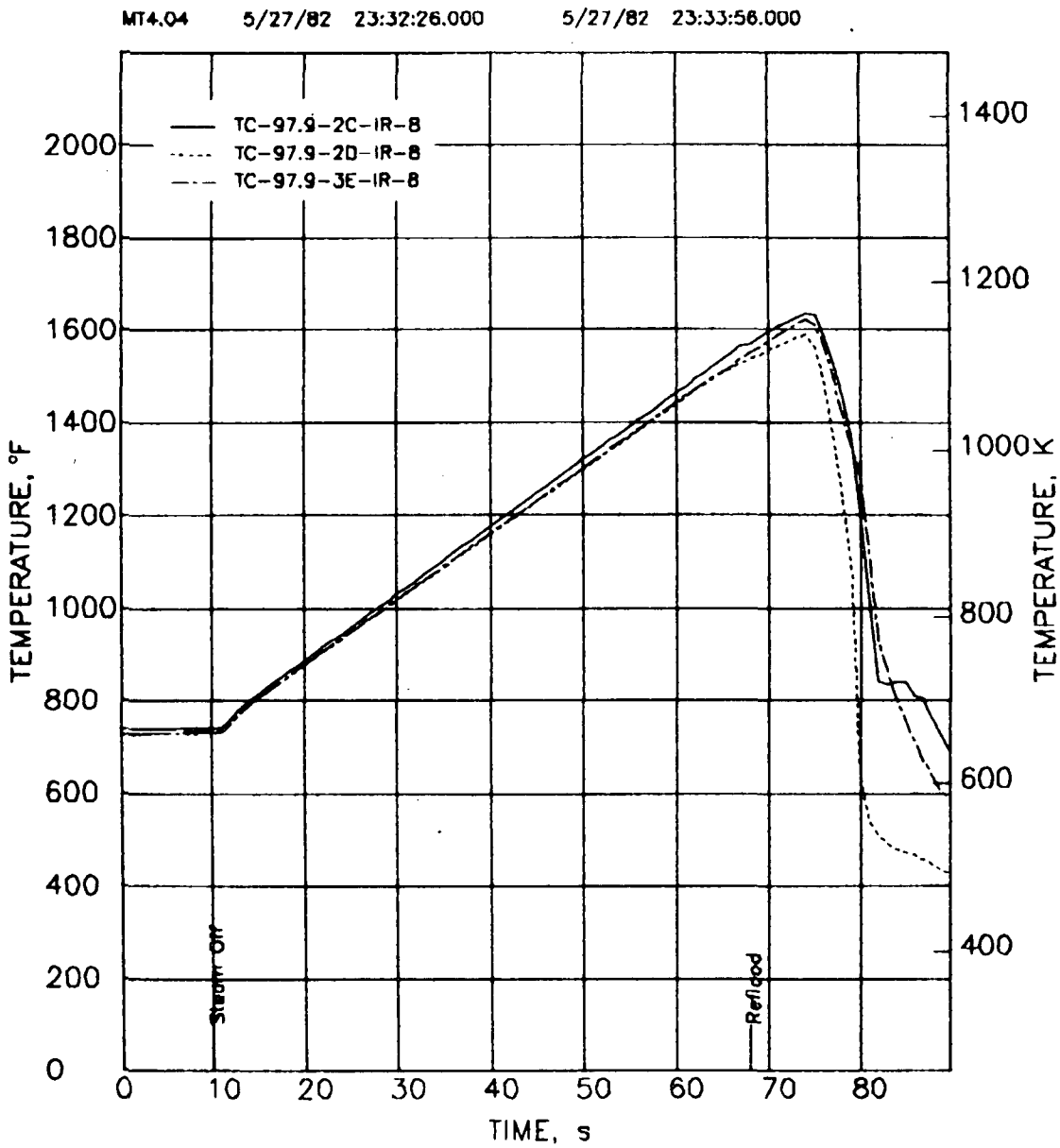

FIGURE C.8. Test Rod Interior Cladding Temperature Histories at Level 97.9 for First 90 s of MT-4.04

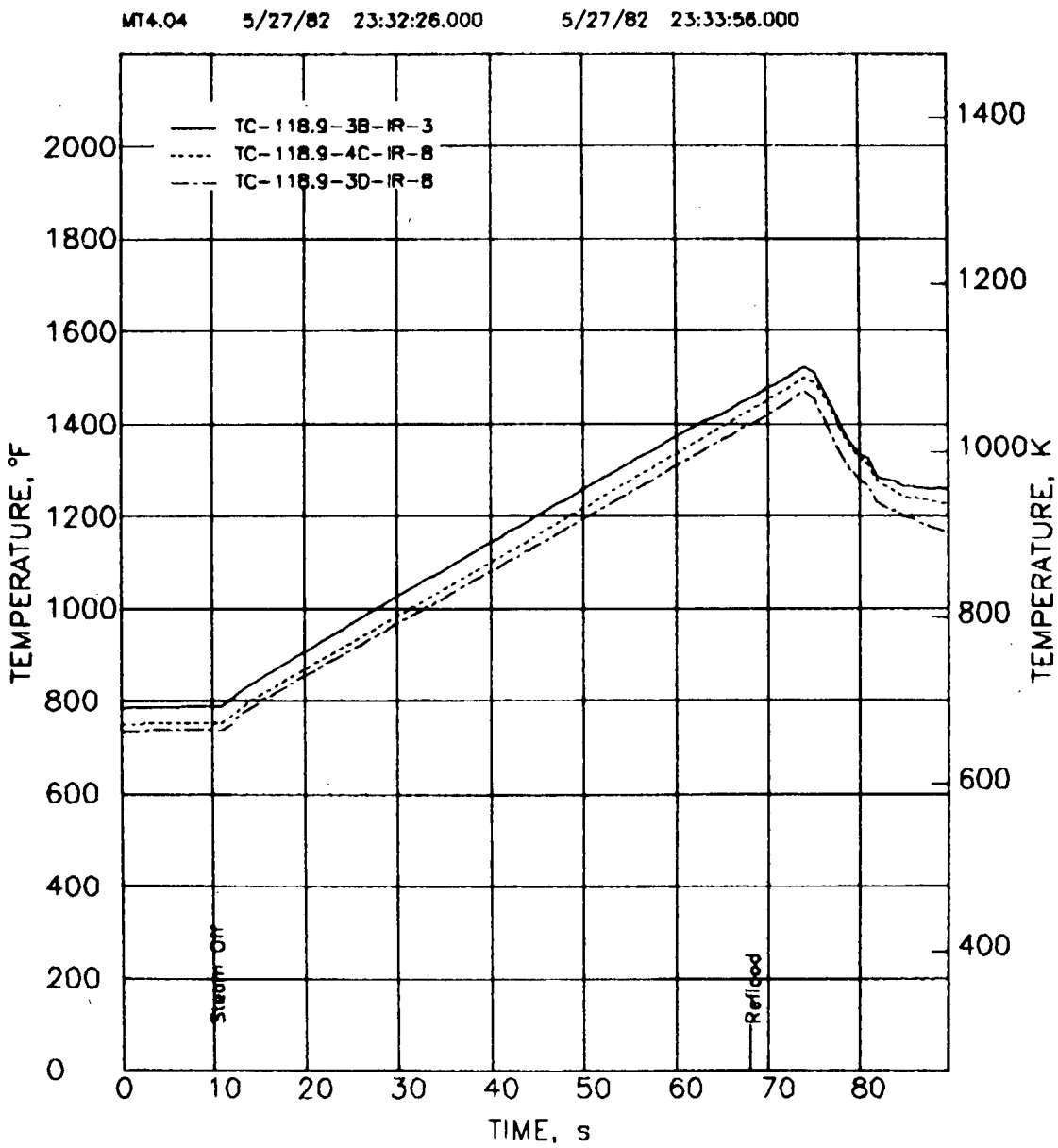

FIGURE C.9. Test Rod Interior Cladding Temperature Histories at Level 118.9 for First 90 s of MT-4.04

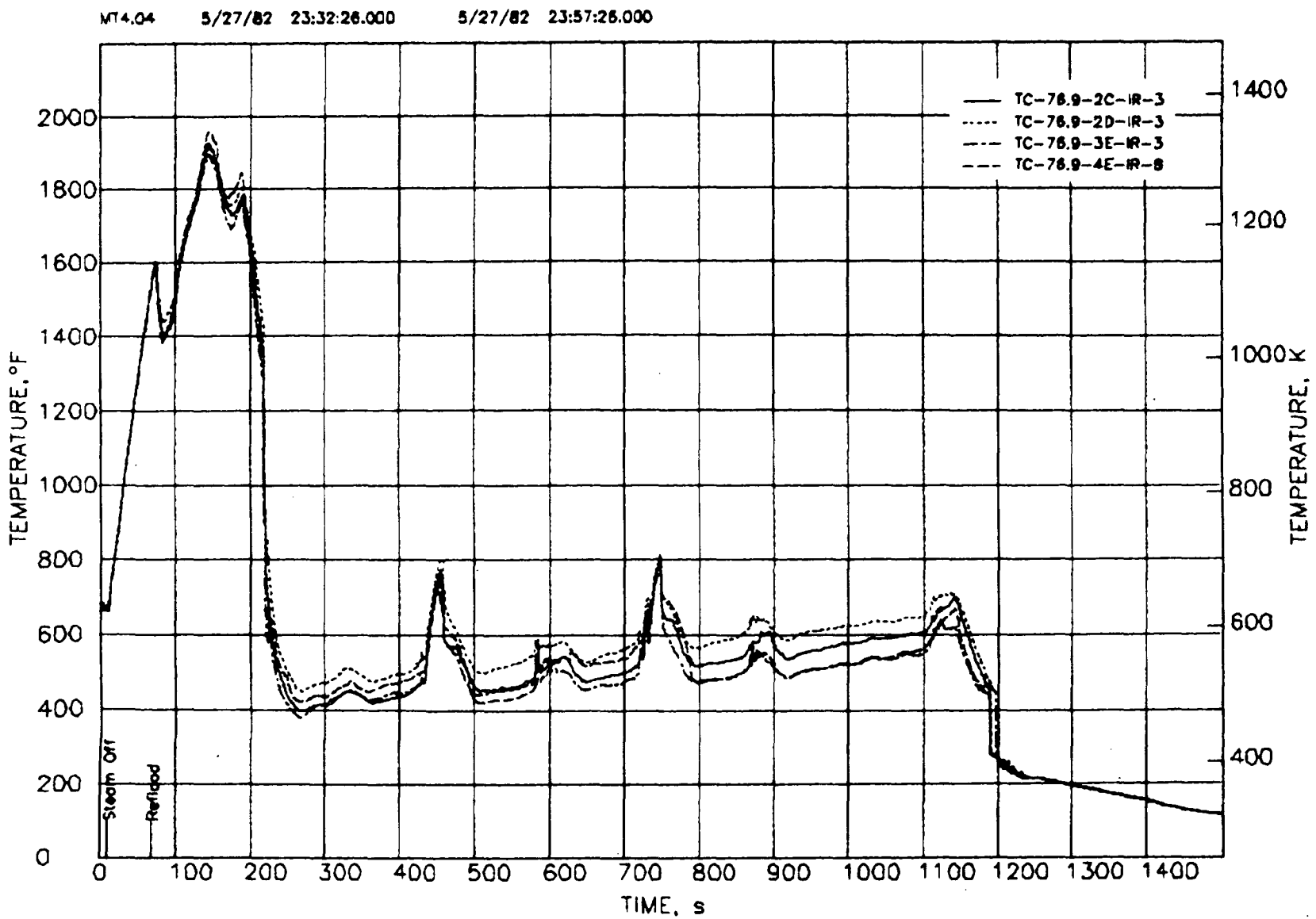

FIGURE C.10. Test Rod Interior Cladding Temperature Histories at Level 76.9 for 1500 s of MT-4.04

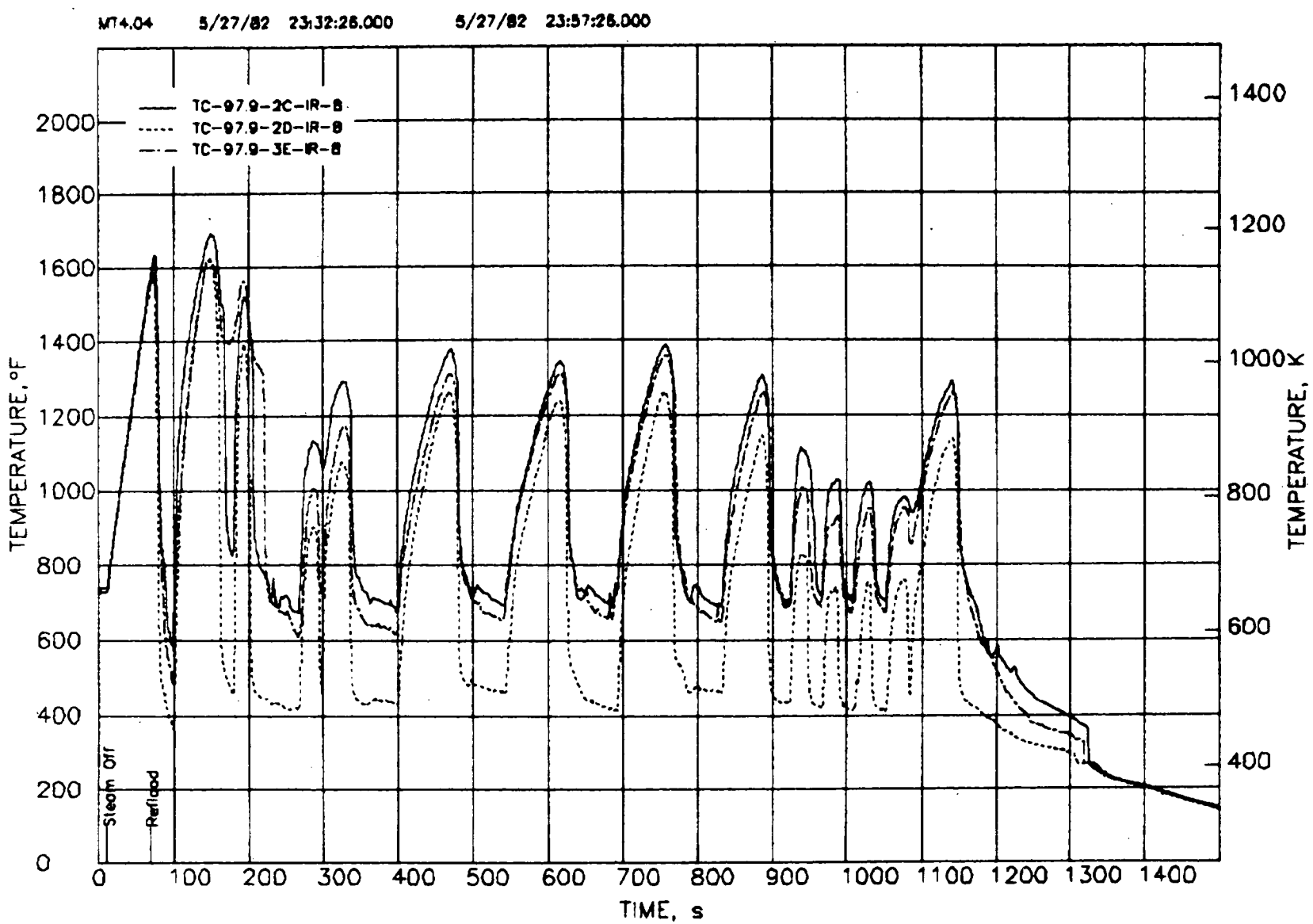

FIGURE C.11. Test Rod Interior Cladding Temperature Histories at Level 97.9 for 1500 s of MT-4.04

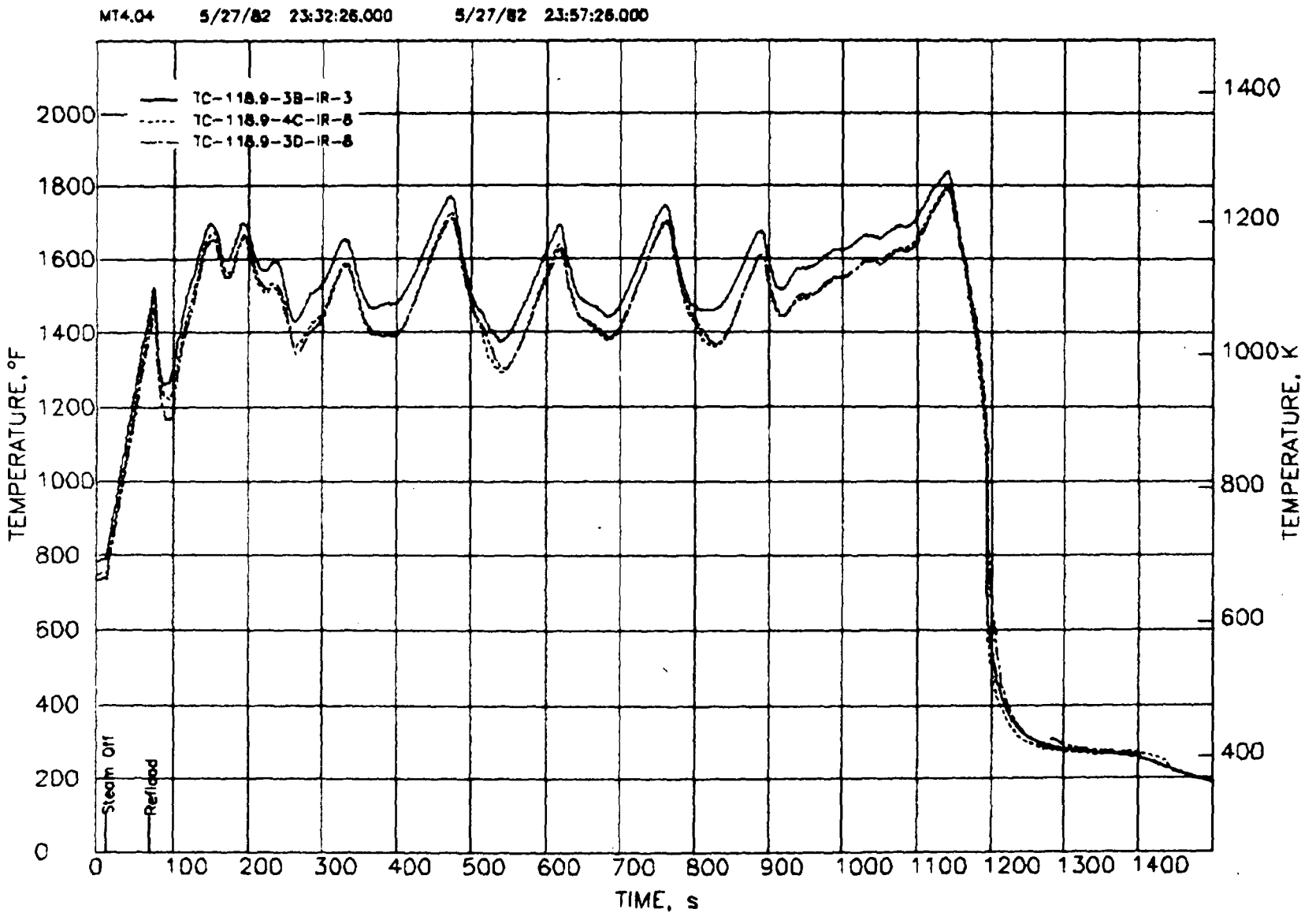

FIGURE C.12. Test Rod Interior Cladding Temperature Histories at Level 118.9 for 1500 s of MT-4.04

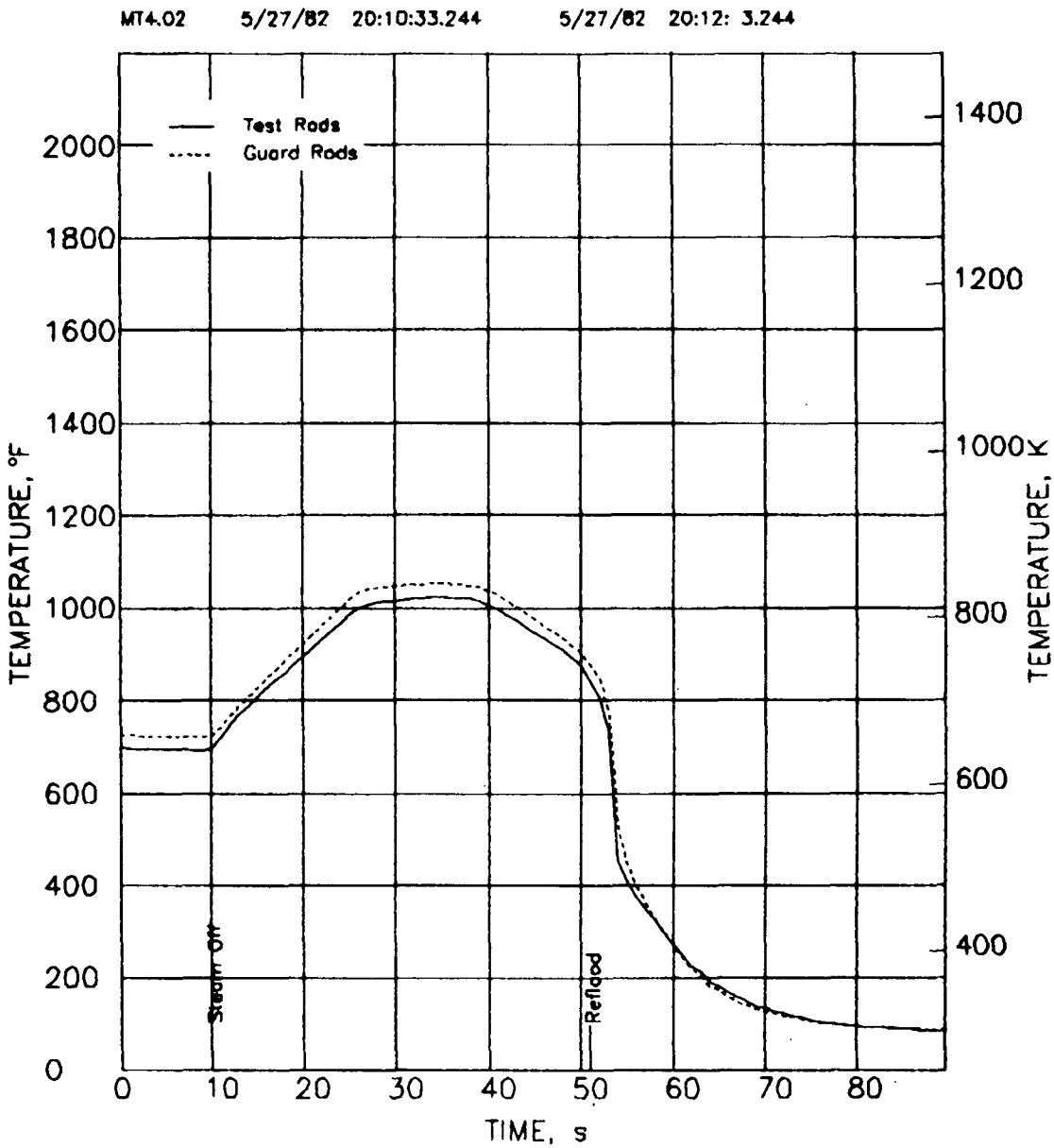

FIGURE C.13. Average Guard and Test Rod Interior Cladding Temperatures at Level 76.9 During Adiabatic Test MT-4.02

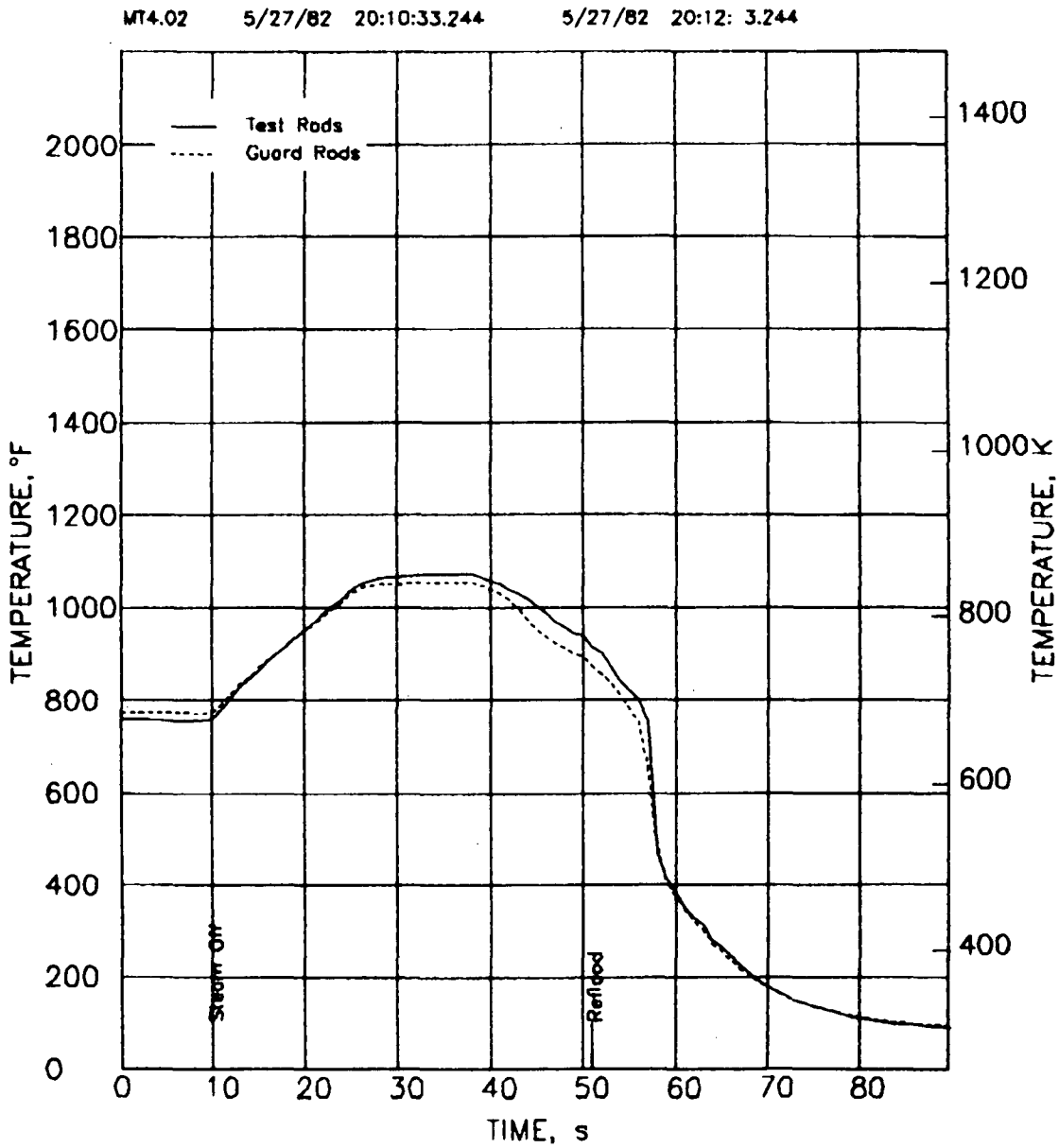

FIGURE C.14. Average Guard and Test Rod Interior Cladding Temperatures at Level 97.9 During Adiabatic Test MT-4.02

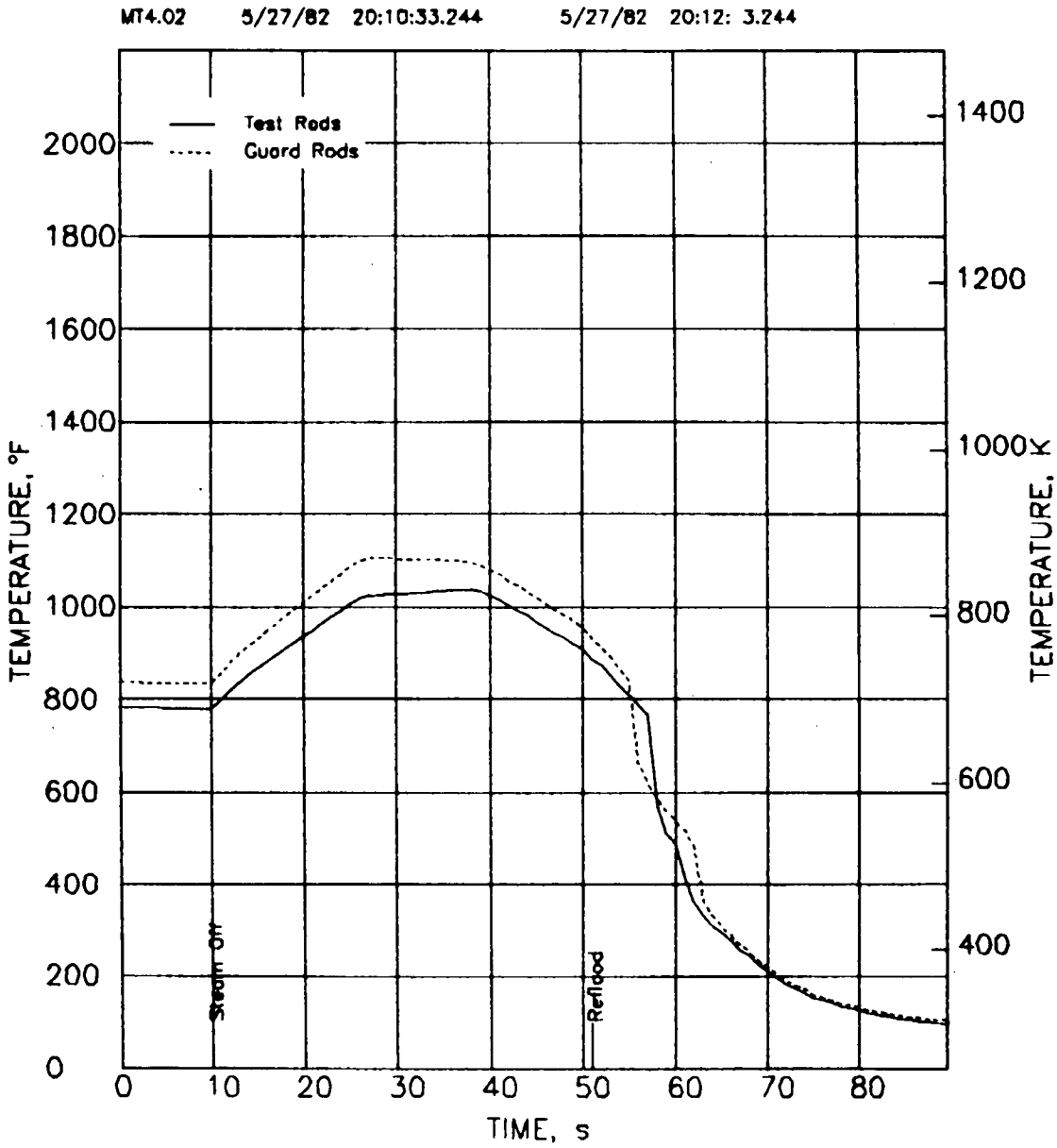

FIGURE C.15. Average Guard and Test Rod Interior Cladding Temperatures at Level 118.9 During Adiabatic Test MT-4.02

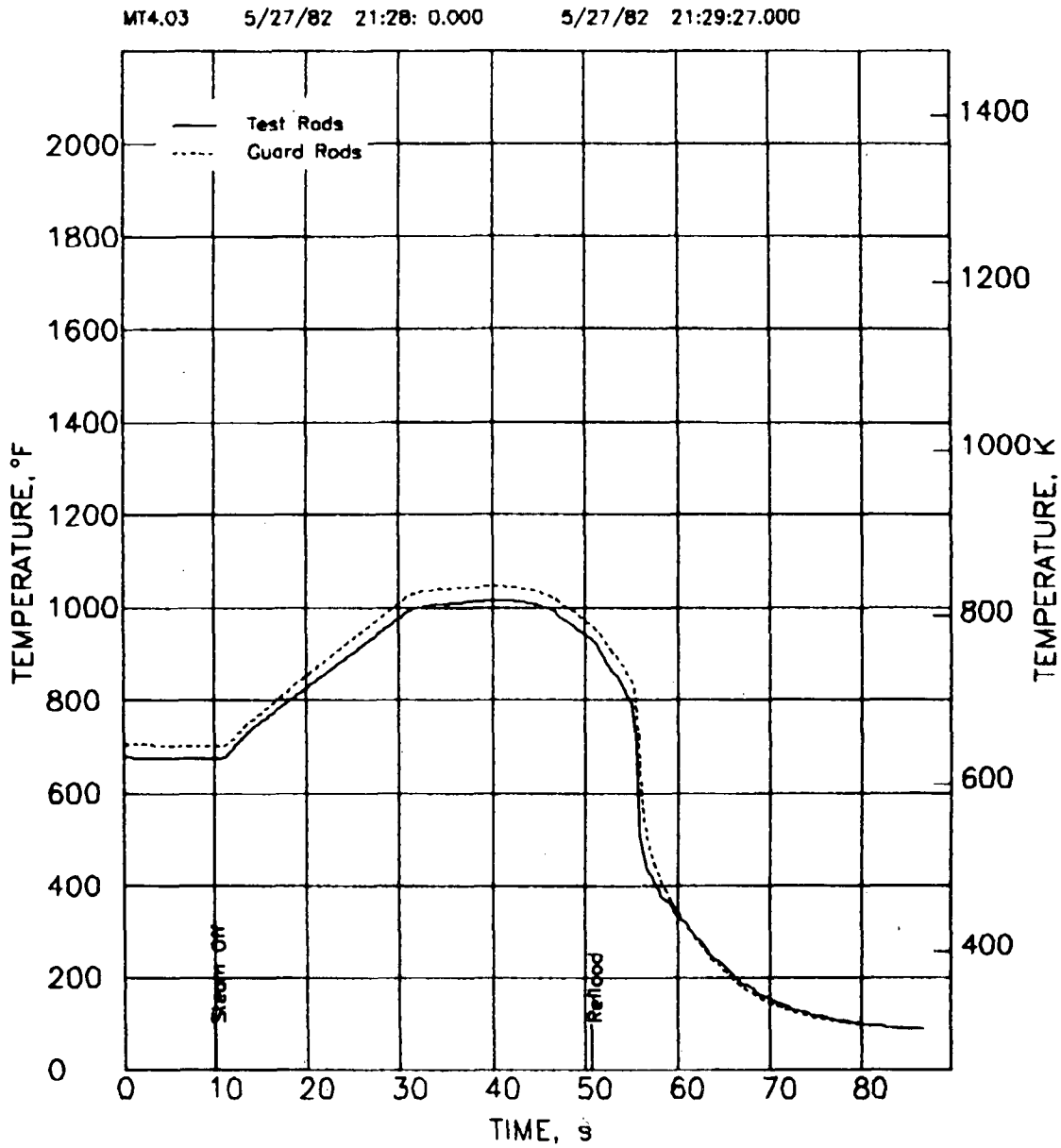

FIGURE C.16. Average Guard and Test Rod Interior Cladding Temperatures at Level 76.9 During Adiabatic Test MT-4.03

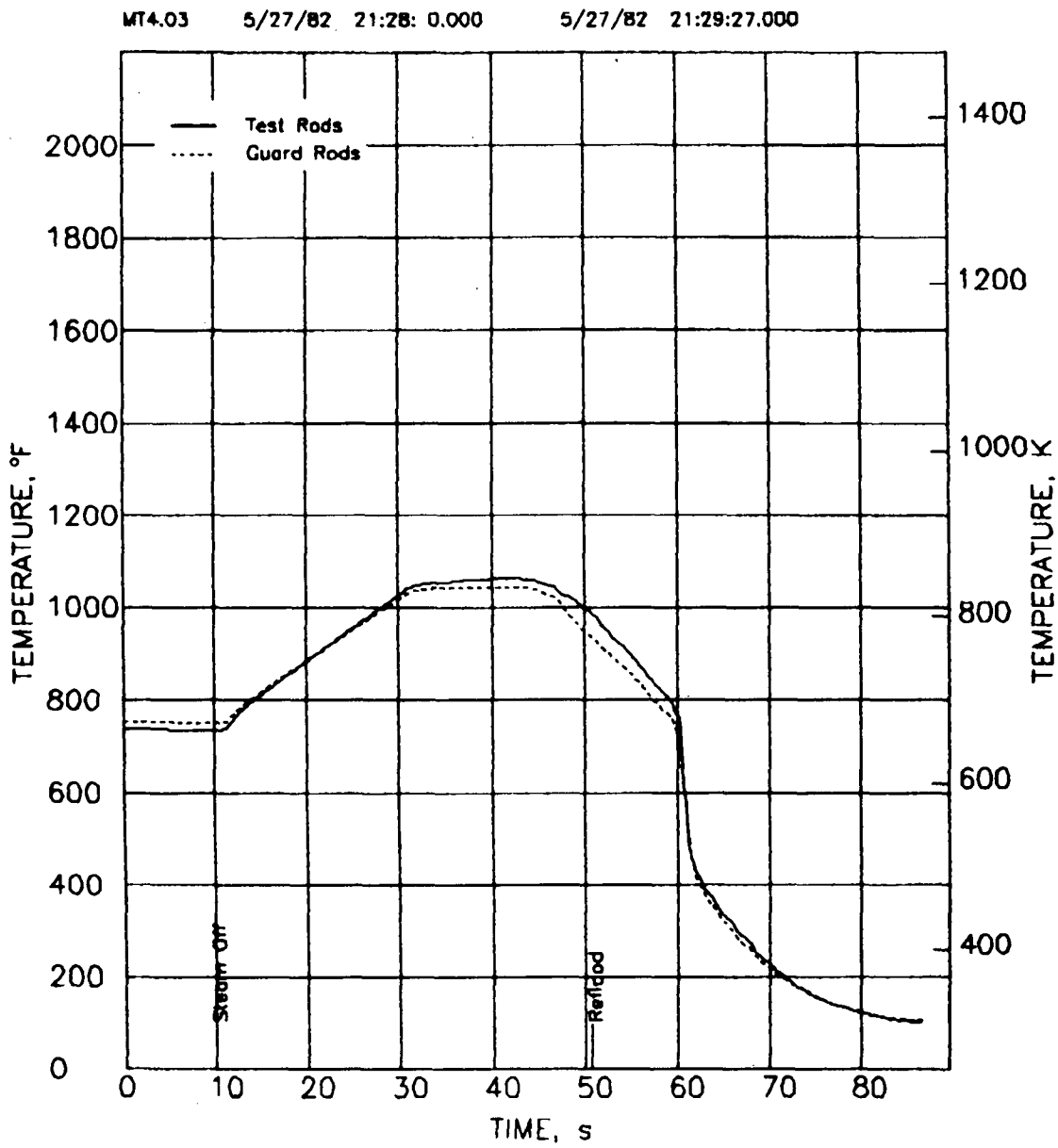

FIGURE C.17. Average Guard and Test Rod Interior Cladding Temperatures at Level 96.9 During Adiabatic Test MT-4.03

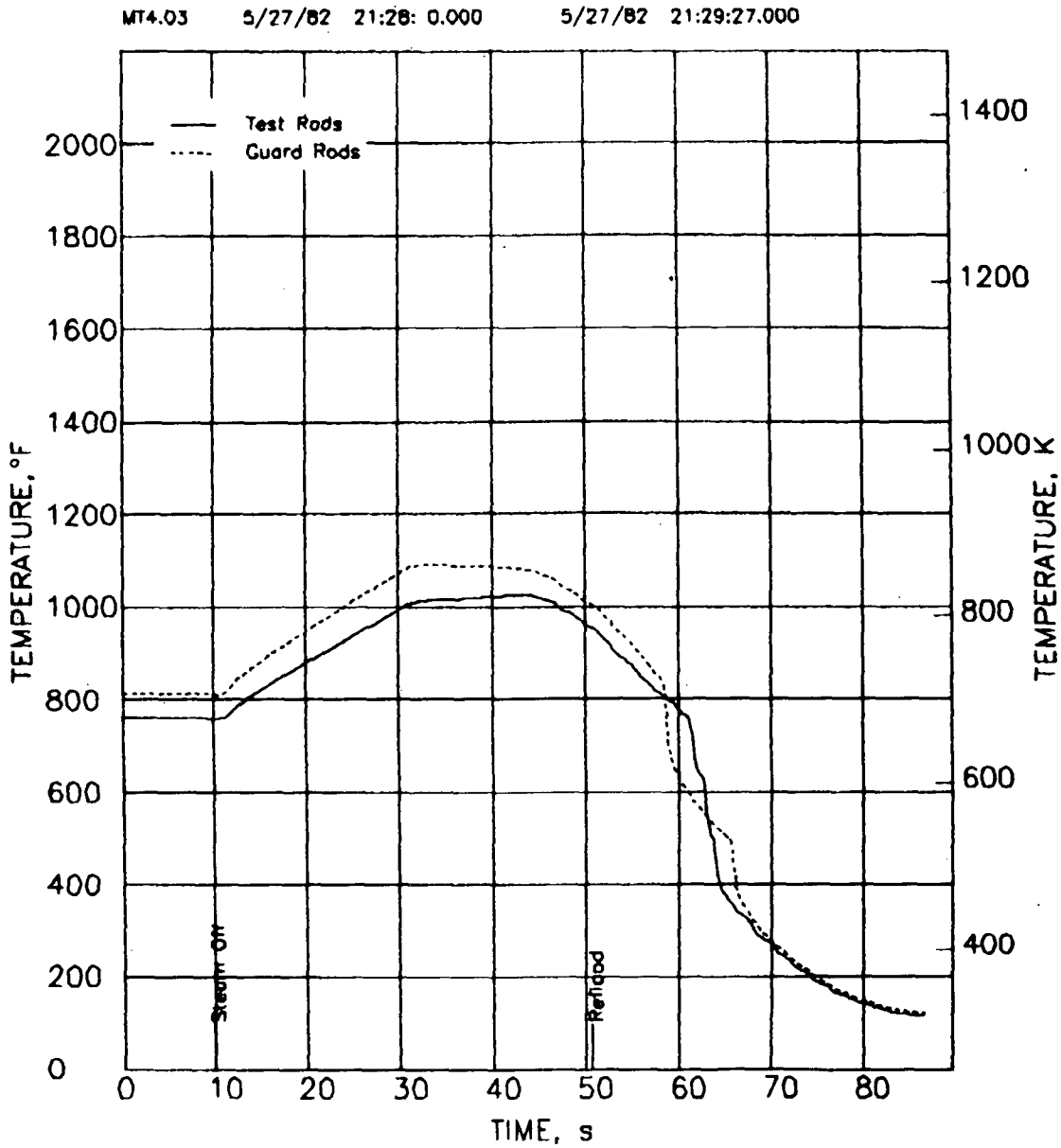

FIGURE C.18. Average Guard and Test Rod Interior Cladding Temperatures at Level 118.9 During Adiabatic Test MT-4.03

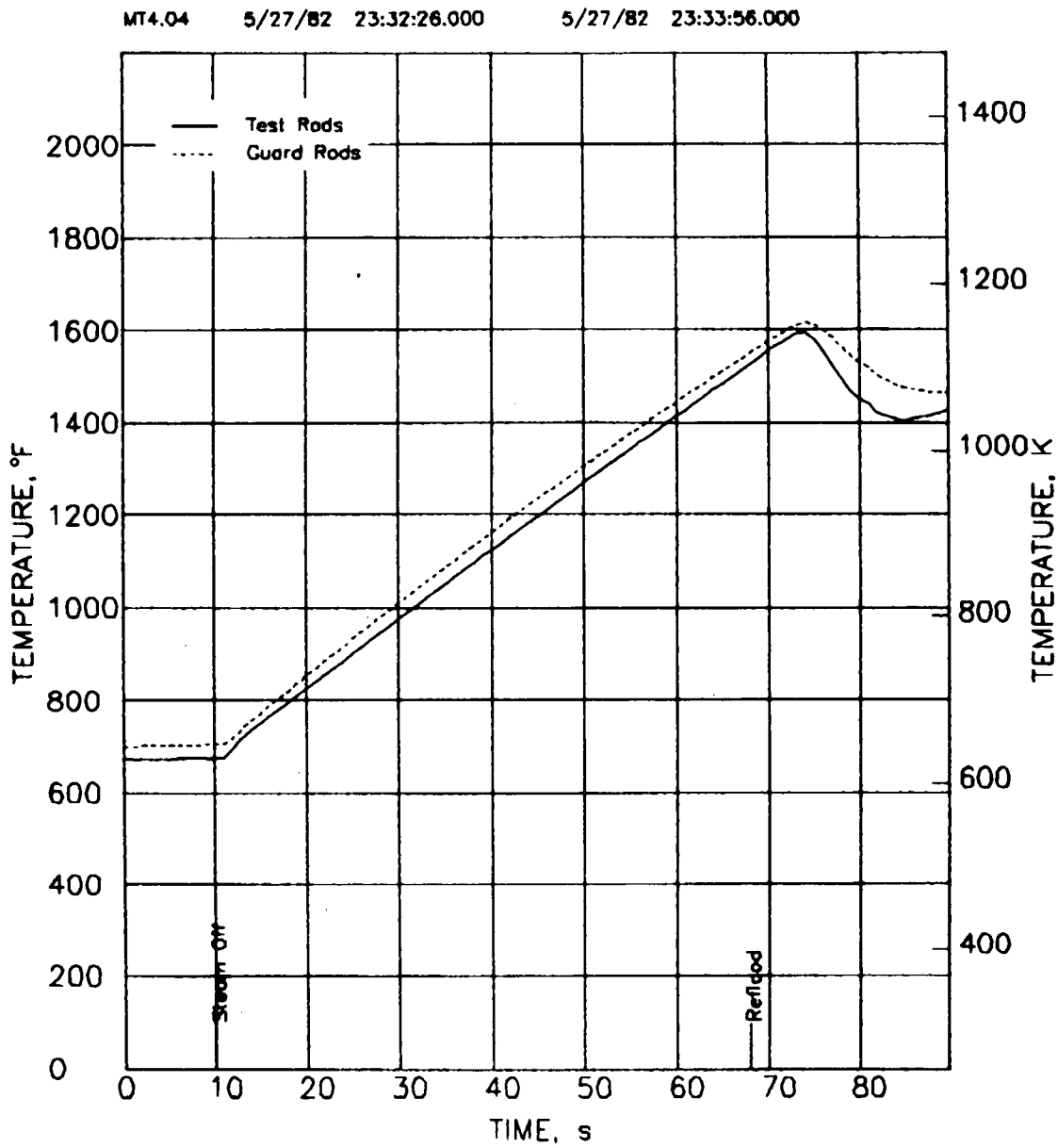

FIGURE C.19. Average Guard and Test Rod Interior Cladding Temperatures at Level 76.9 for First 90 s of MT-4.04

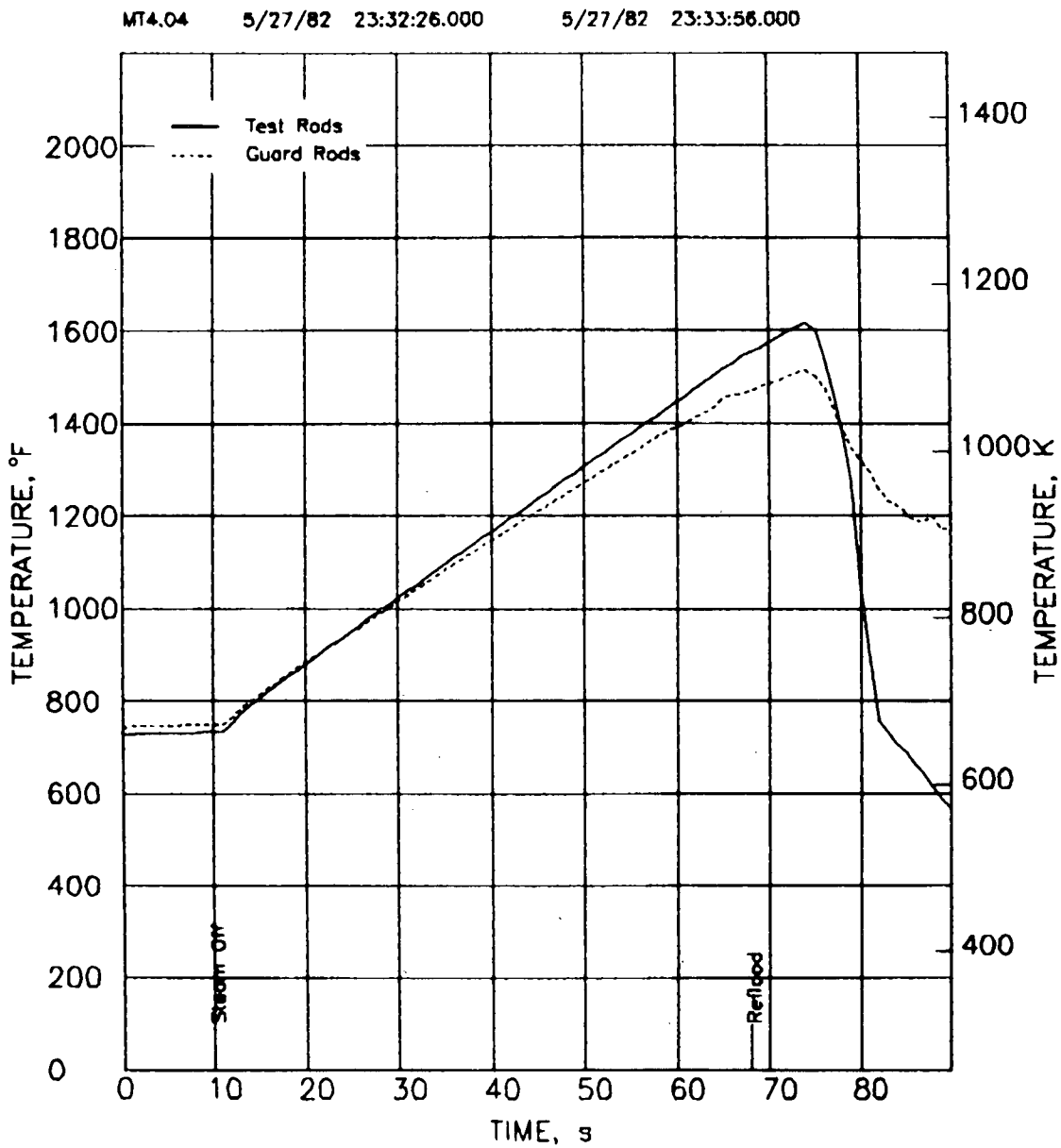

FIGURE C.20. Average Guard and Test Rod Interior Cladding Temperatures at Level 97.9 for First 90 s of MT-4.04

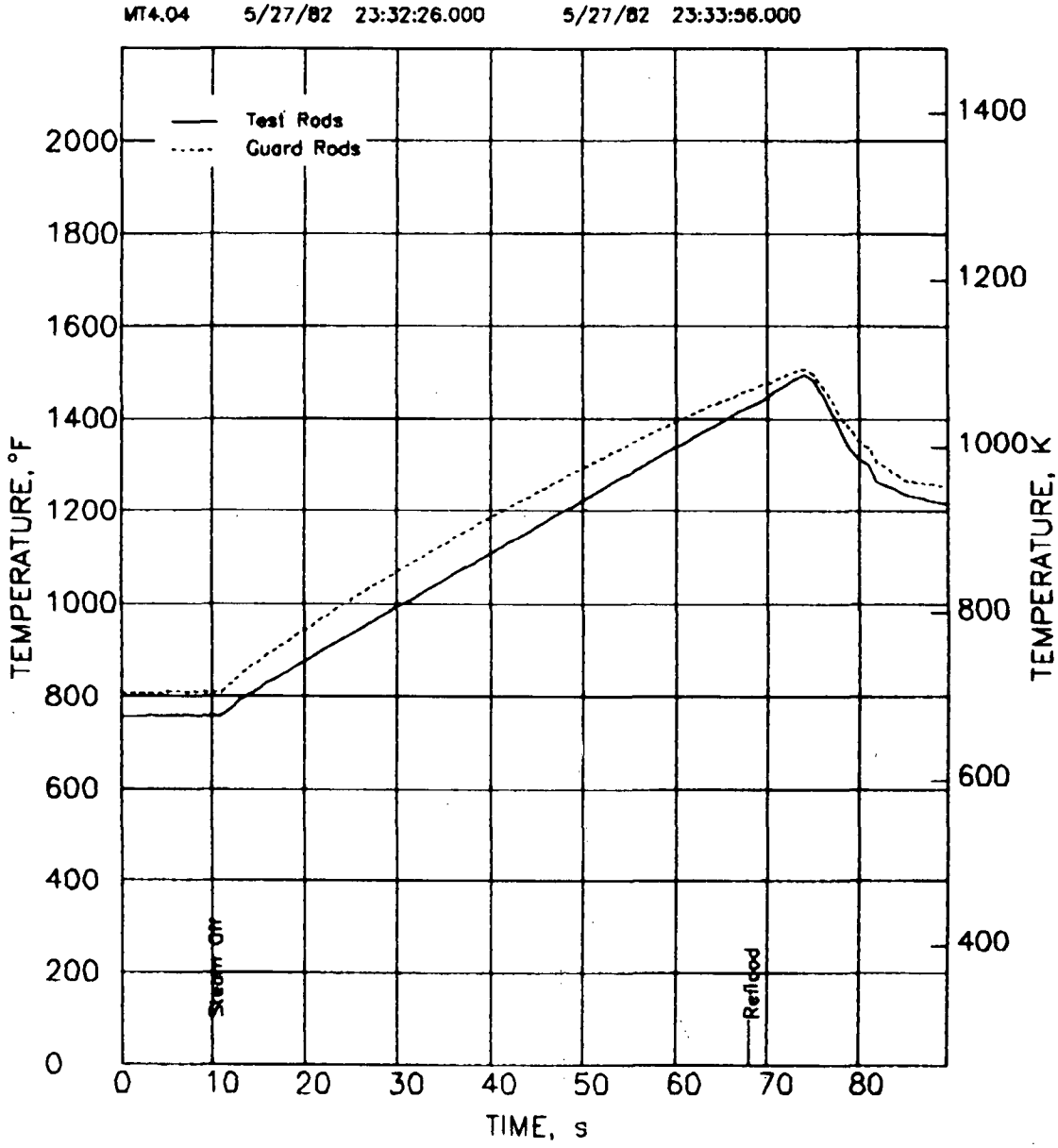

FIGURE C.21. Average Guard and Test Rod Interior Cladding Temperatures at Level 118.9 for First 90 s of MT-4.04

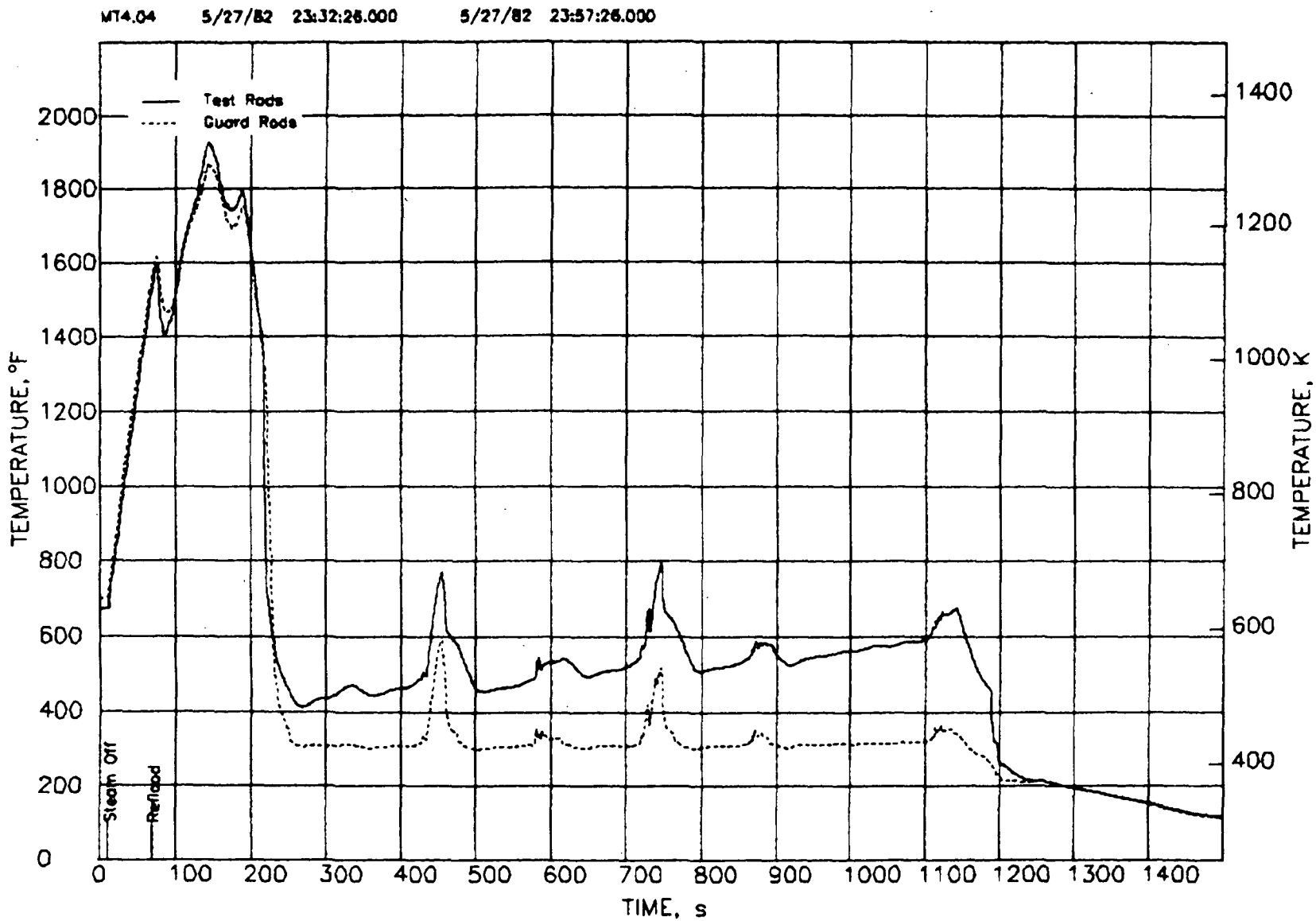

FIGURE C.22. Average Guard and Test Rod Interior Cladding Temperatures at Level 76.9 for 1500 s of MT-4.04

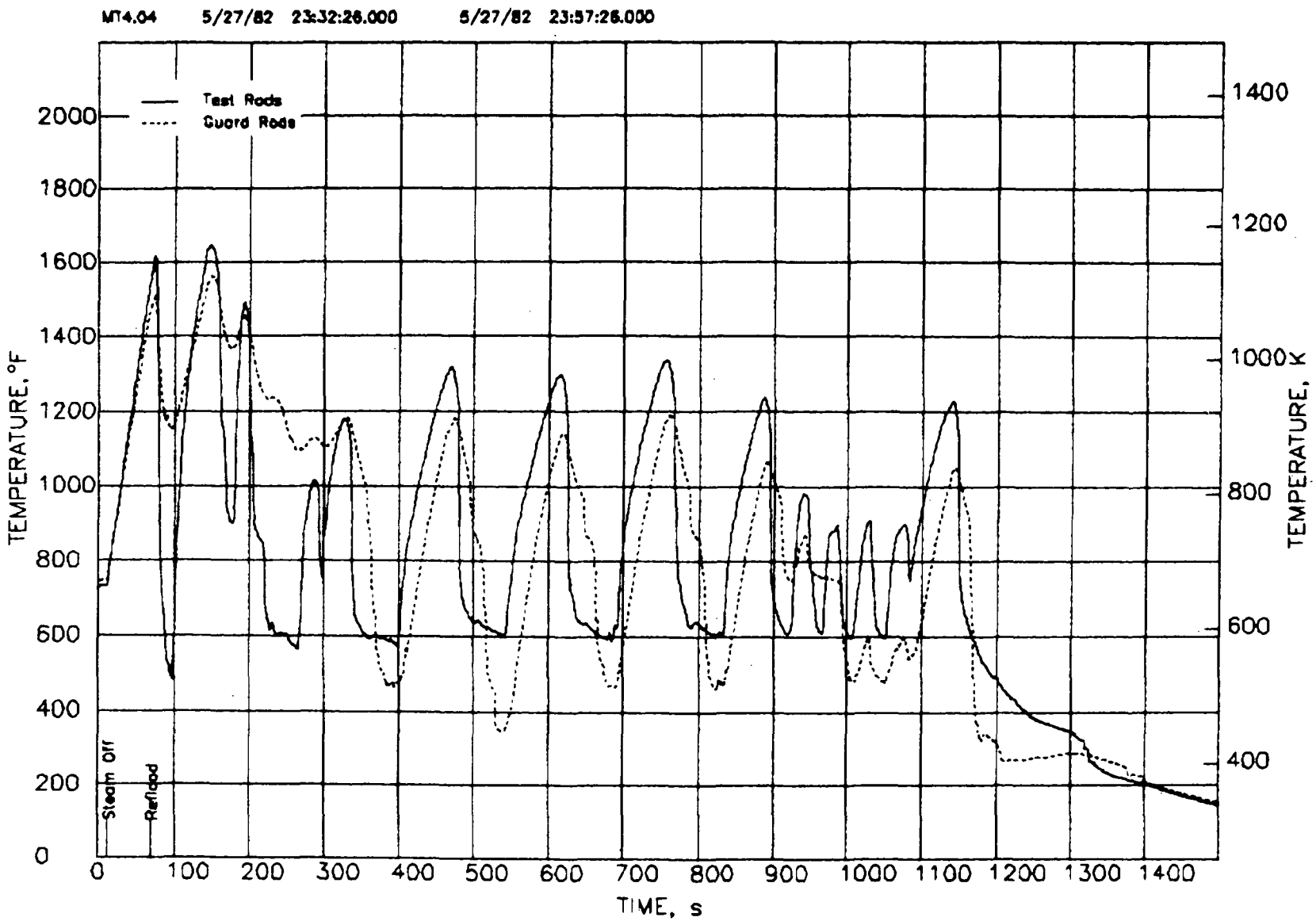

FIGURE C.23. Average Guard and Test Rod Interior Cladding Temperatures at Level 97.9 for 1500 s of MT-4.04

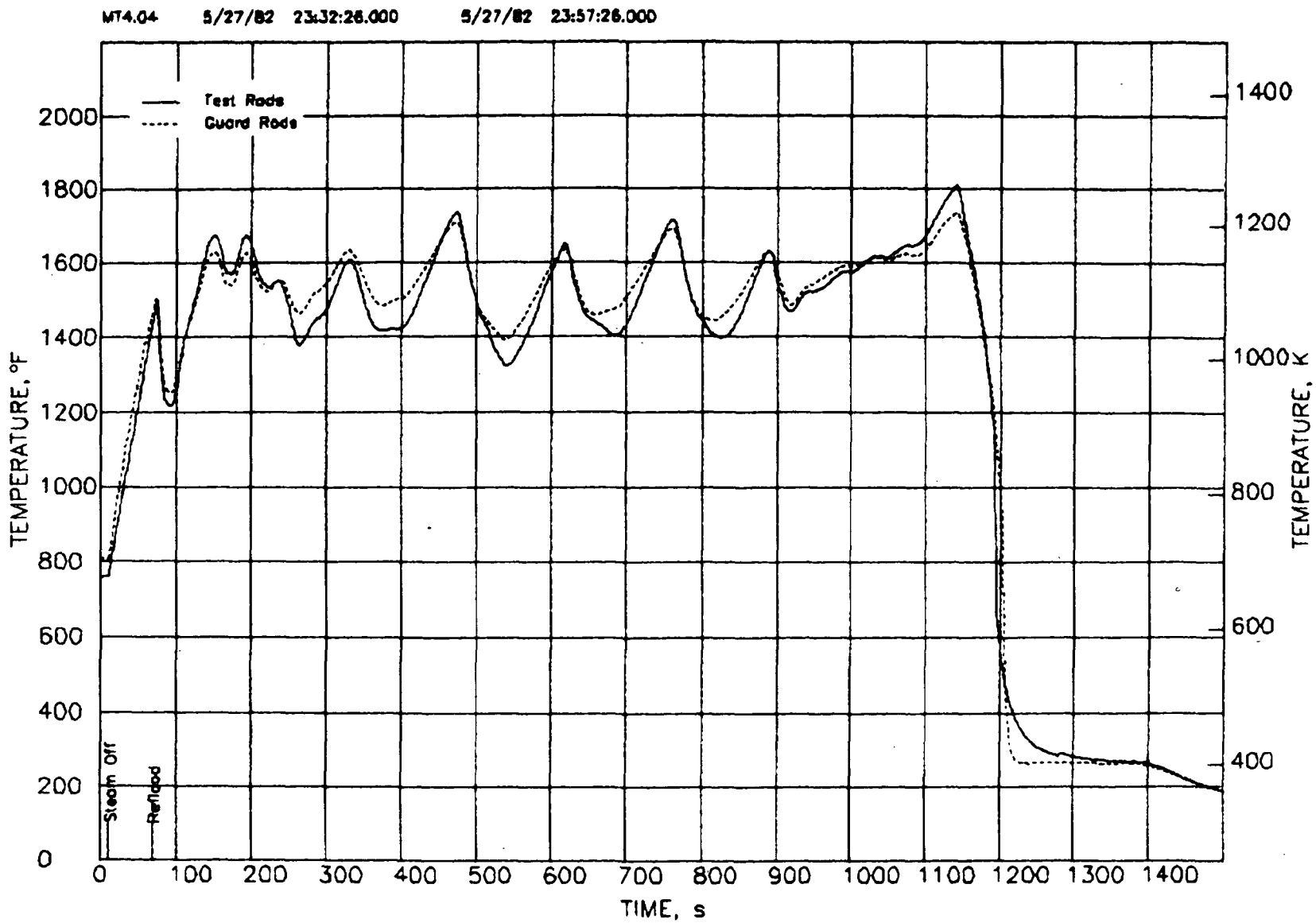

FIGURE C.24. Average Guard and Test Rod Interior Cladding Temperatures at Level 118.9 for 1500 s of MT-4.04

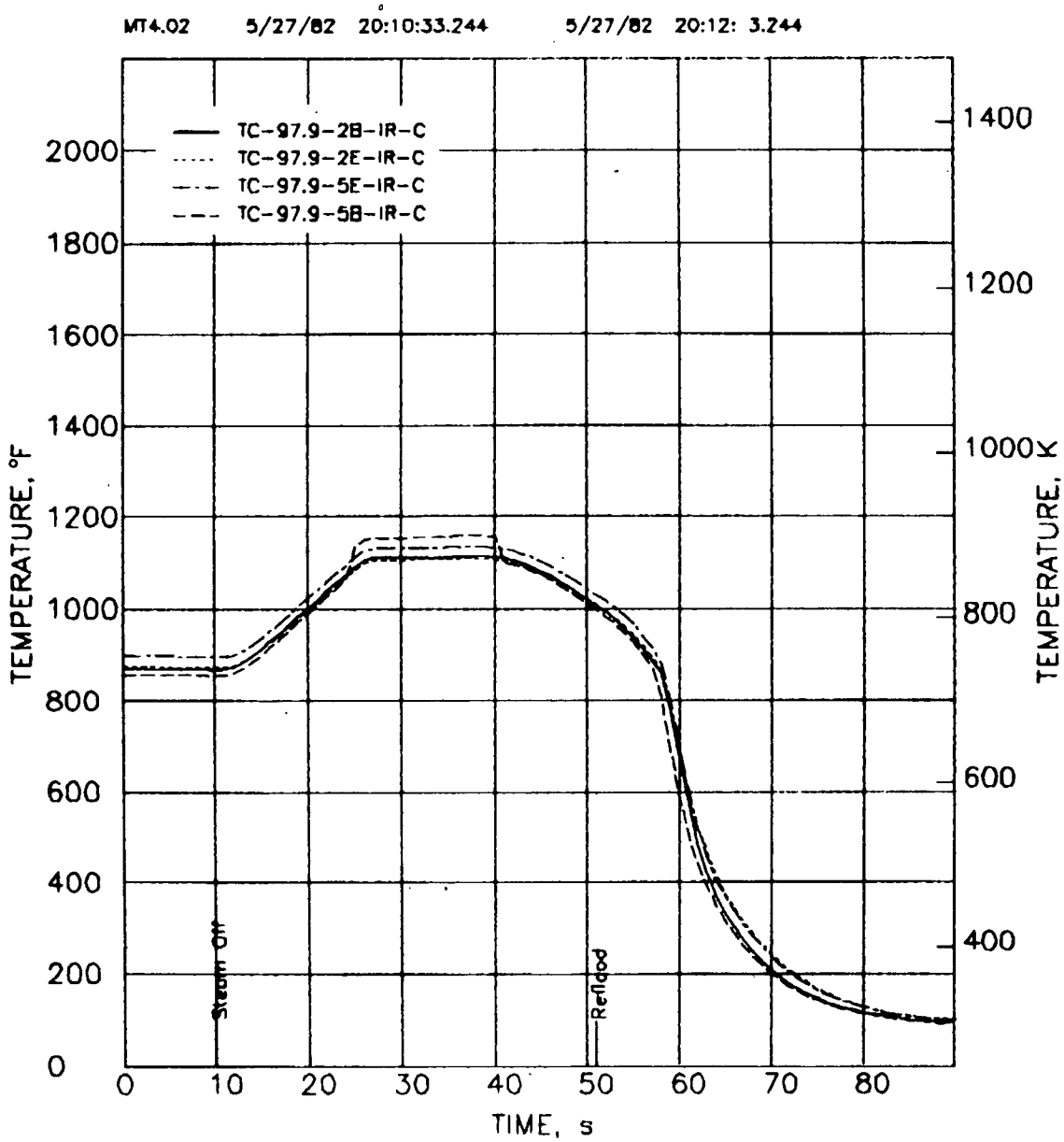

FIGURE C.25. Fuel Centerline Temperatures at Level 97.9 for Adiabatic Test MT-4.02

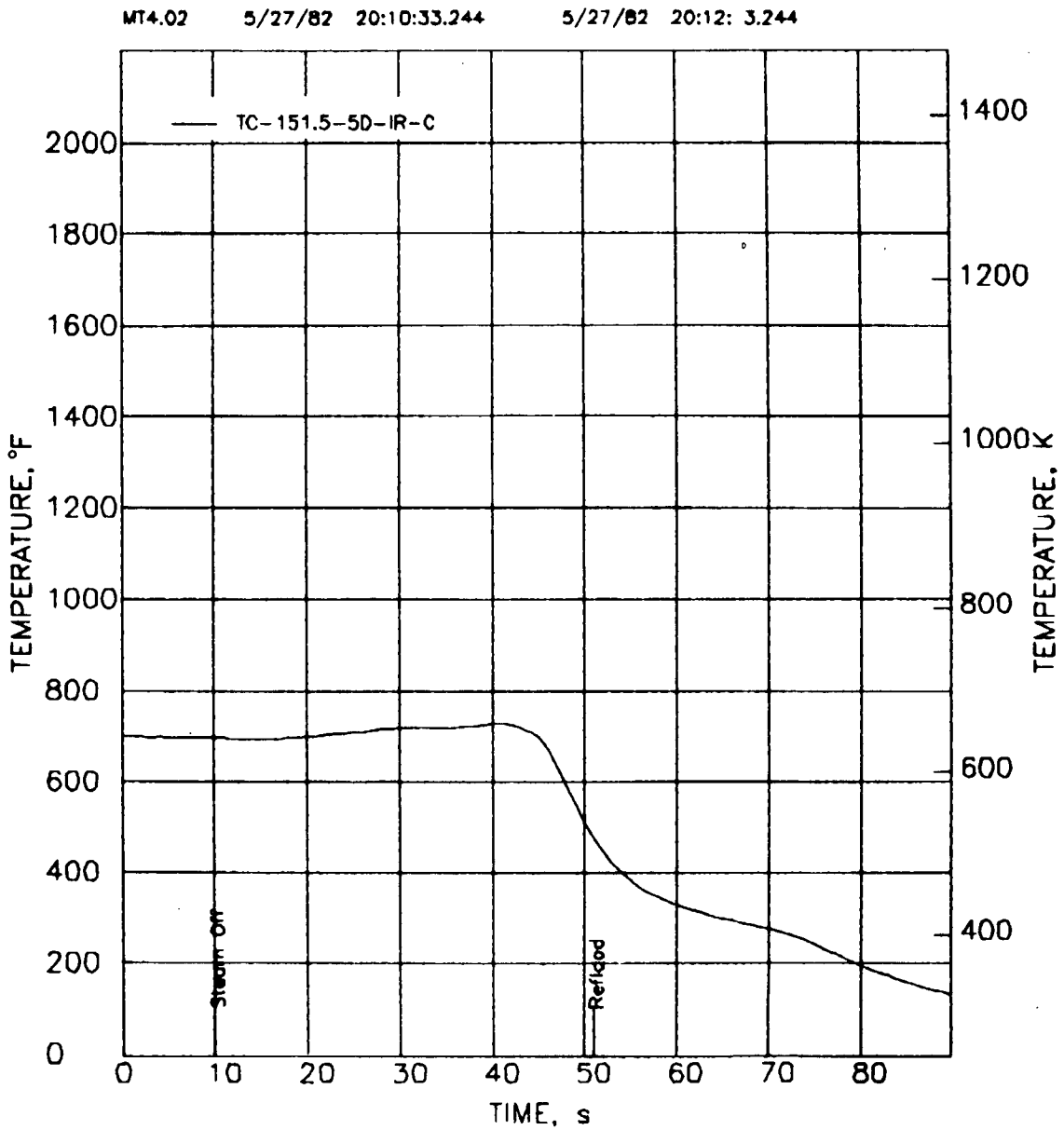

FIGURE C.26. Fuel Plenum Temperatures at Level 151.5 for Adiabatic Test MT-4.02

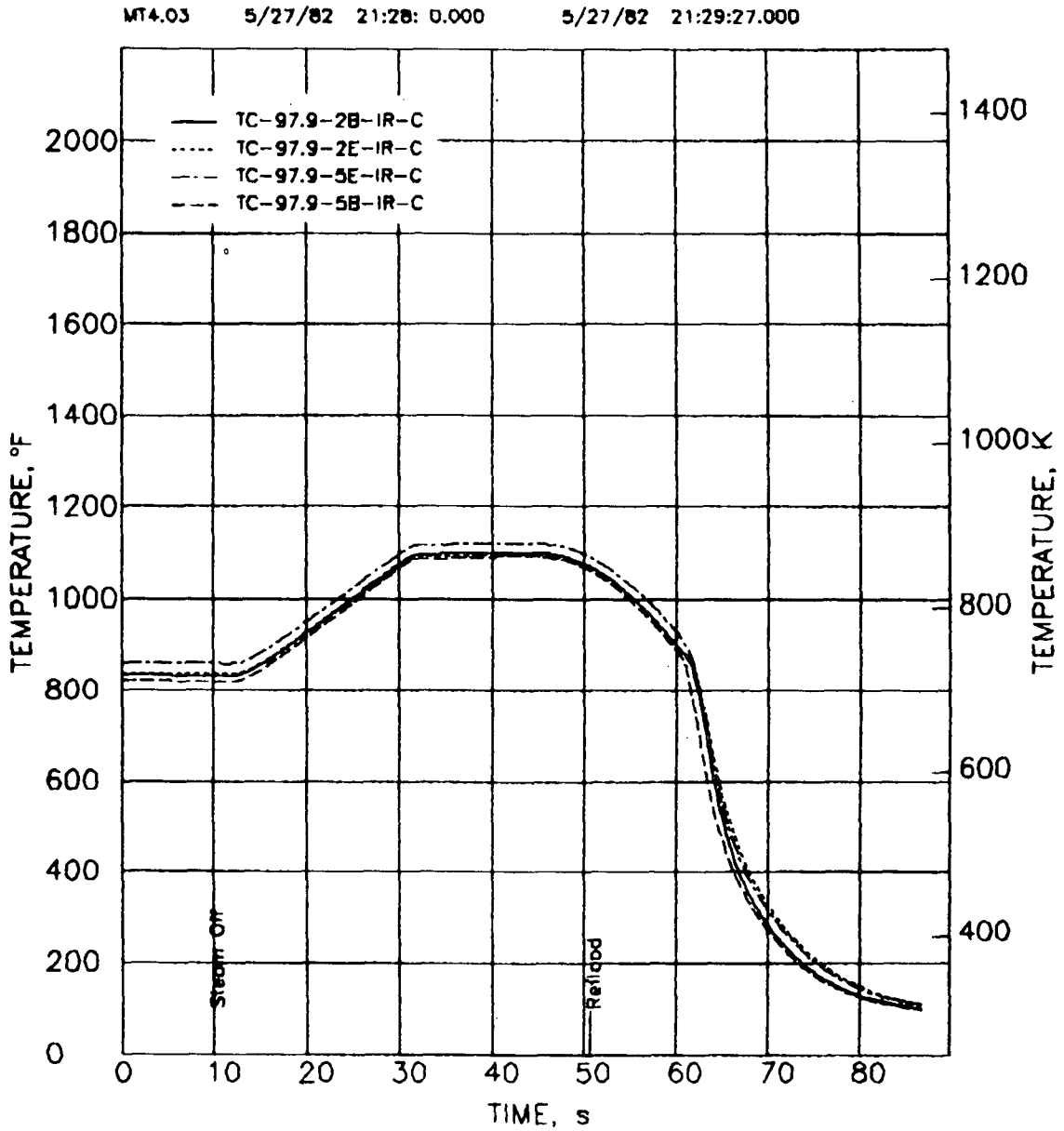

FIGURE C.27. Fuel Centerline Temperatures at Level 97.9 for Adiabatic Test MT-4.03

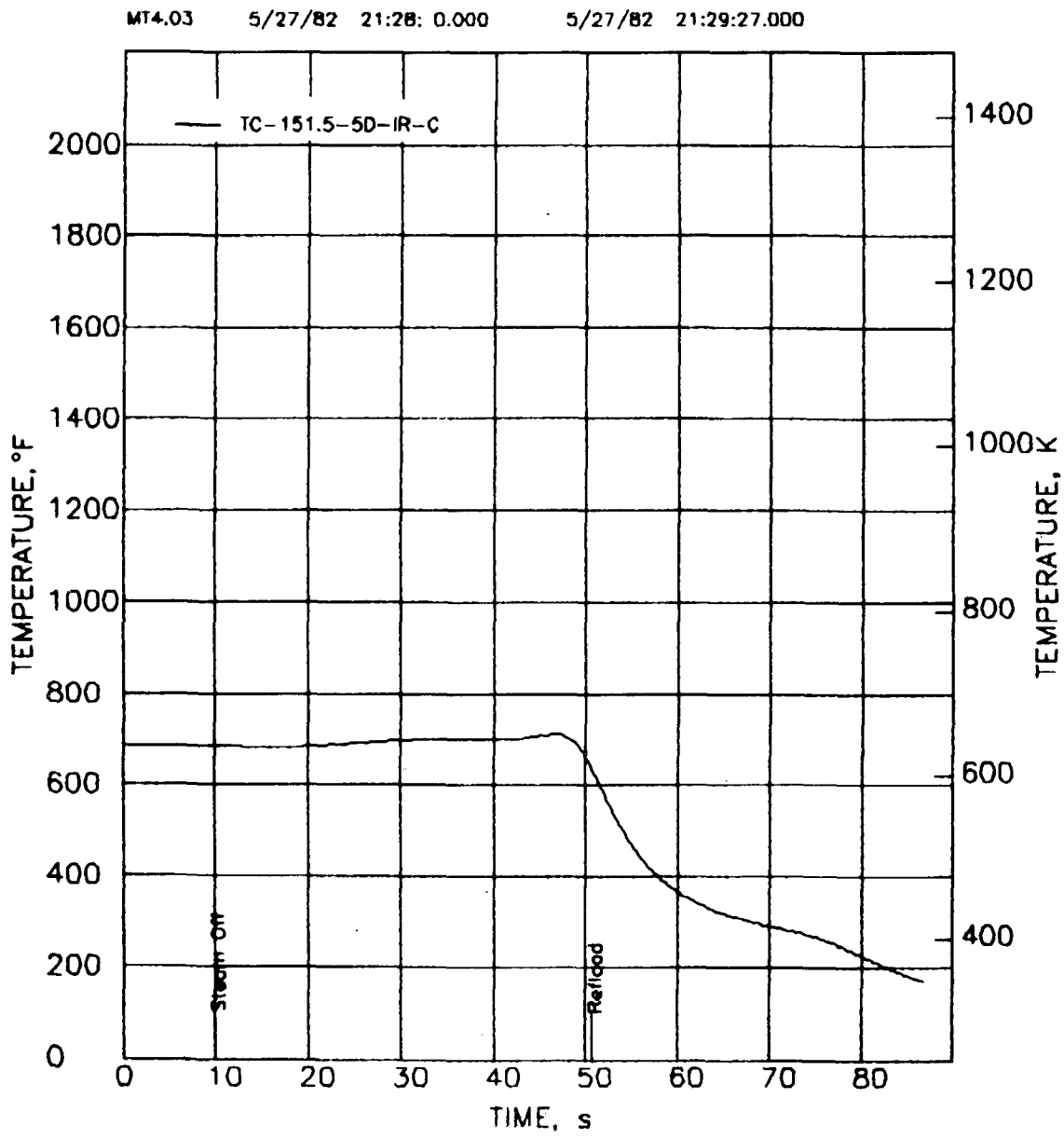

FIGURE C.28. Fuel Plenum Temperatures at Level 151.5 for Adiabatic Test MT-4.03

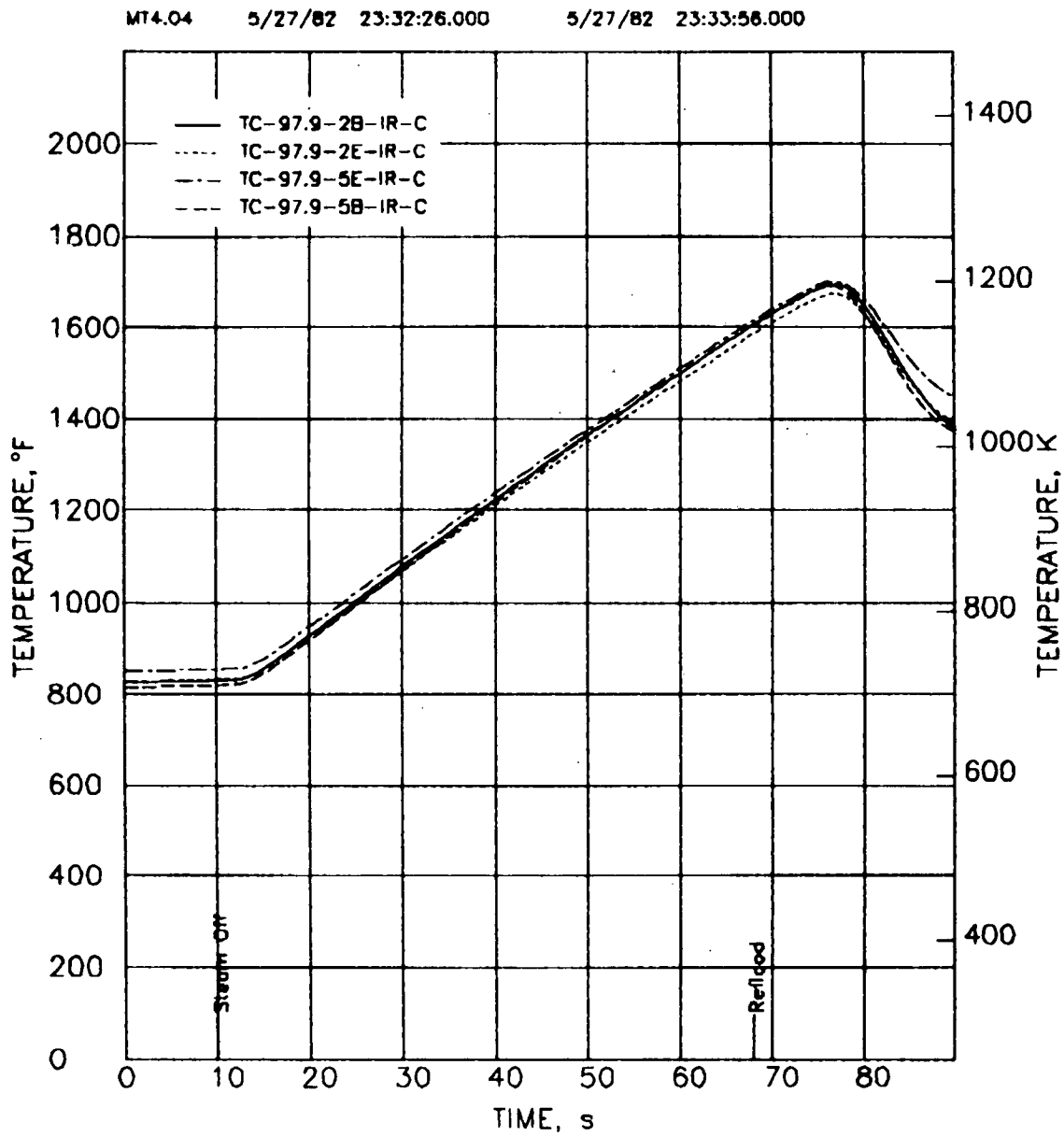

FIGURE C.29. Fuel Centerline Temperatures at Level 97.9 During First 90 s of MT-4.04

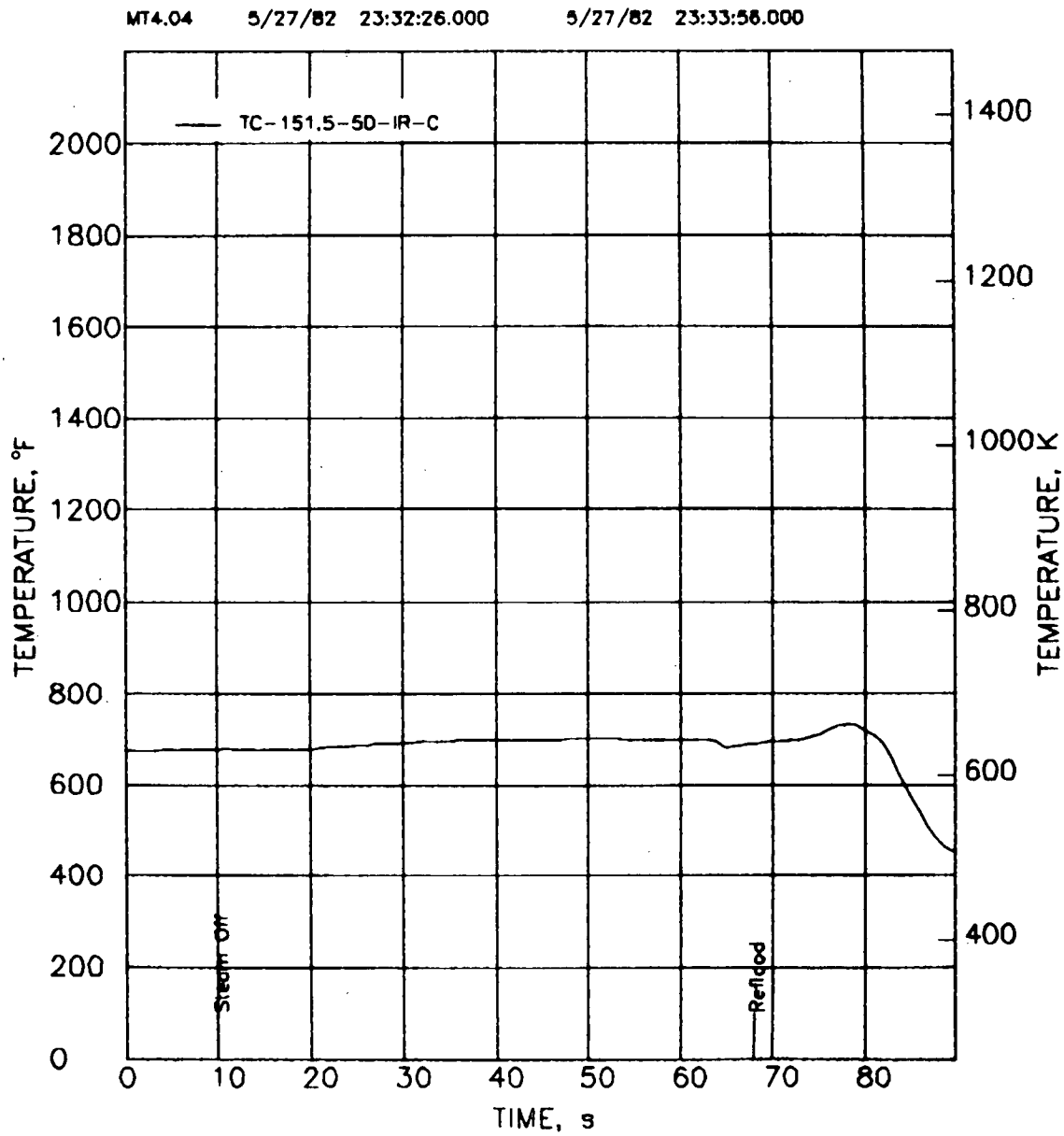

FIGURE C.30. Fuel Plenum Temperatures at Level 151.5 During First 90 s of MT-4.04

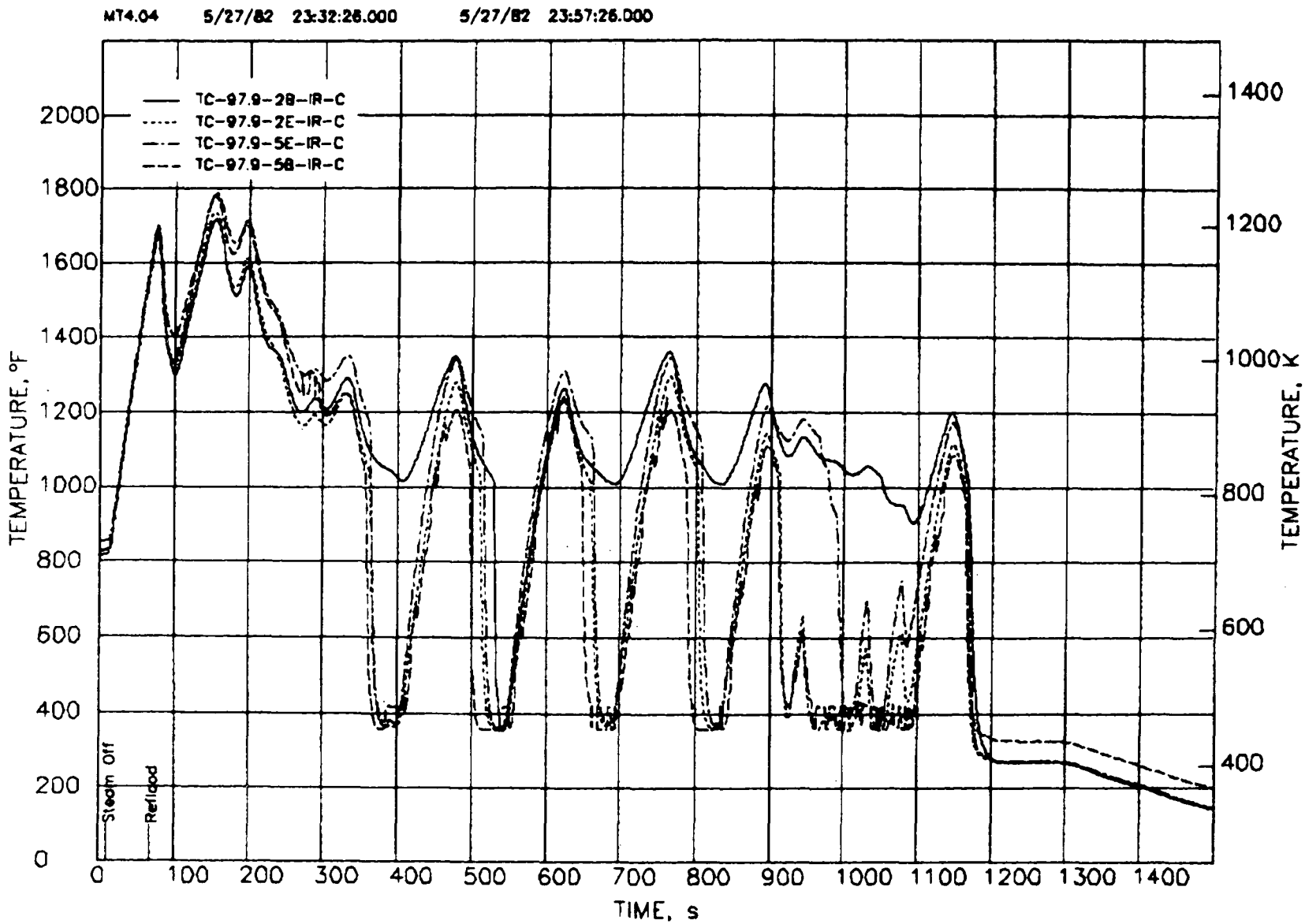

FIGURE C.31. Fuel Centerline Temperatures at Level 97.9 During 1500 s of MT-4.04

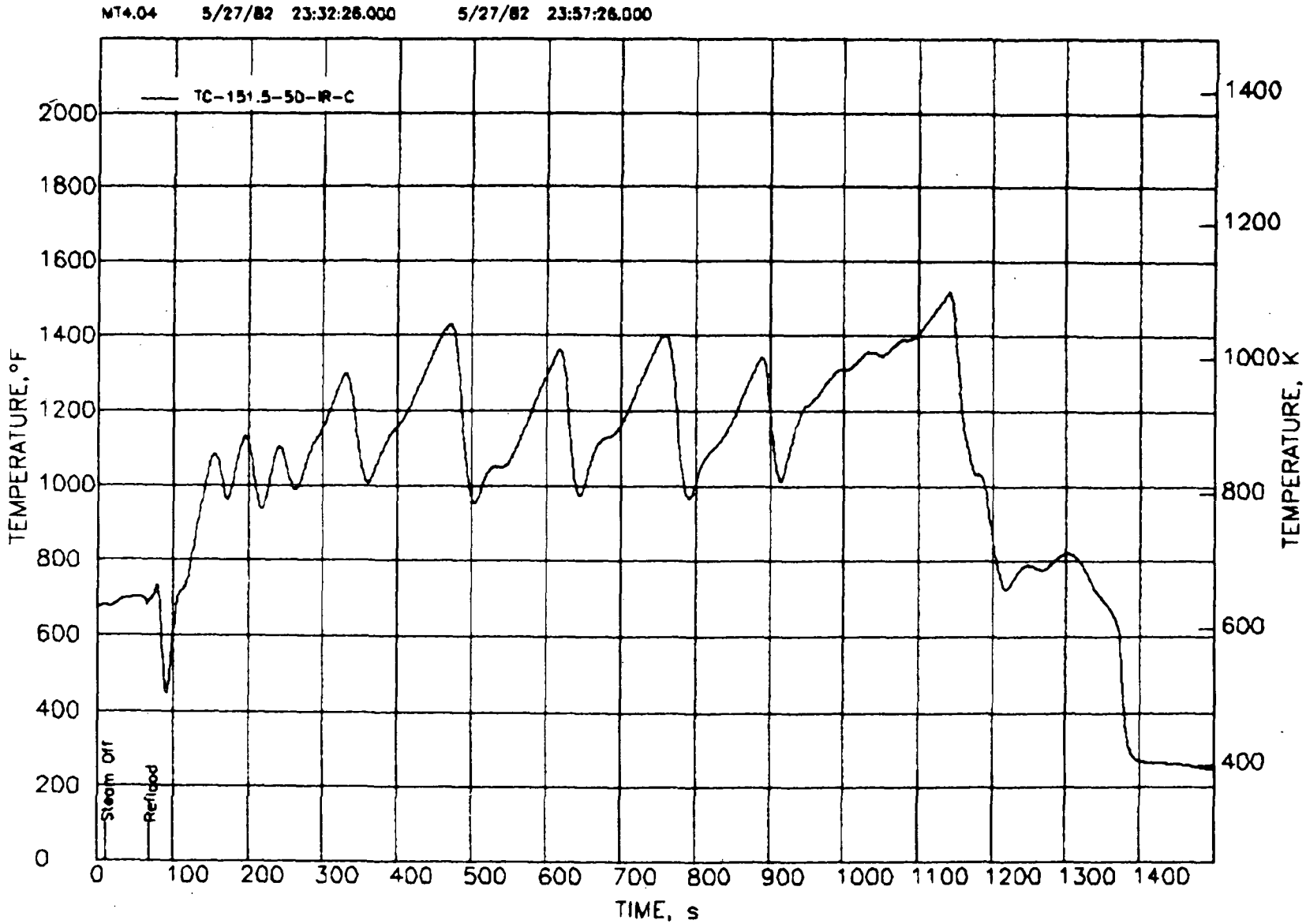

FIGURE C.32. Fuel Plenum Temperatures at Level 151.5 During 1500 s of MT-4.04

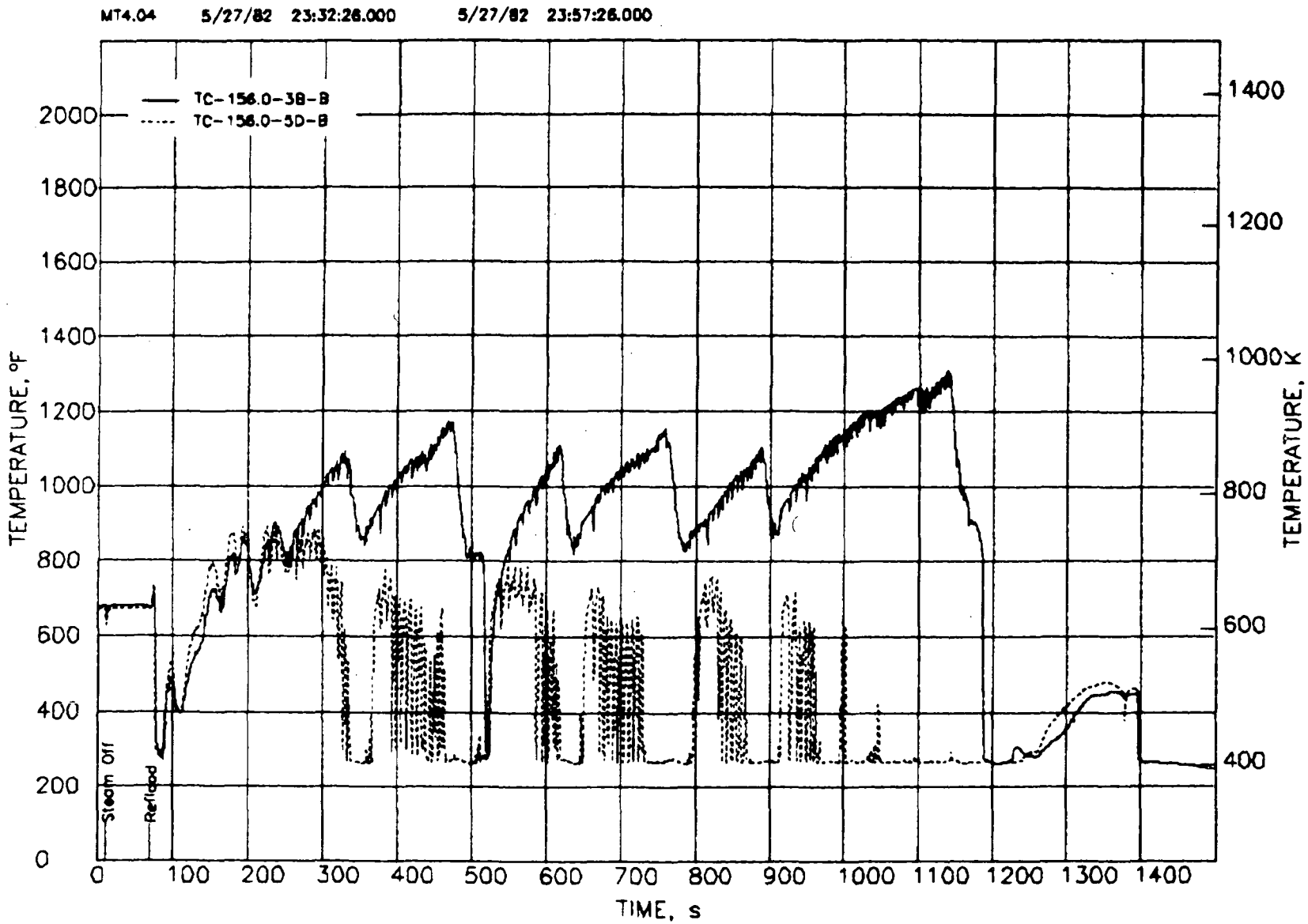

FIGURE C.33. Fuel Rod Upper End Cap Braze Temperatures at Level 156.0 for MT-4.04

APPENDIX D

TEST COOLANT AND SHROUD TEMPERATURES

APPENDIX D

TEST COOLANT AND SHROUD TEMPERATURES

It was difficult to measure the temperature of the coolant once reflooding occurred because much of the time the coolant was in two phases. Thermocouple (TC) coolant temperature data are thus a rough indication of the steam and water temperature with the additional effects of the instrument response time and in situ environment. Test assembly inlet, outlet, and steam probe TCs at Levels 69.0, 90.0, and 111.0 are shown in Figures D.1 through D.8 for MT-4.04.

Shroud temperatures at Levels 55.9, 76.9, 97.9, 118.9, and 139.9 for MT-4.02, MT-4.03, and MT-4.04 are shown in Figures D.9 through D.12. It was important to know the shroud temperature to insure that the shroud did not get too hot. If it did, it could have warped and delayed removal of the test assembly from the test site. Shroud temperatures tended to be lower than coolant temperatures, which indicates that heat was transferred radially outward, allowing the shroud TCs to quench before the coolant TCs. There was a tendency for upper level shroud and coolant TCs to be hotter, which might be caused by less quenching by entrained liquid at the higher levels.

The remainder of this appendix consists of the following graphical data:

FIGURE D.1. Steam Probe Temperatures for Rod 2B and Inlet and Outlet Coolant Temperatures During First 90 s of MT-4.04

FIGURE D.2. Steam Probe Temperatures for Rod 2E and Inlet and Outlet Coolant Temperatures During First 90 s of MT-4.04

FIGURE D.3. Steam Probe Temperatures for Rod 5B and Inlet and Outlet Coolant Temperatures During First 90 s of MT-4.04

FIGURE D.4. Steam Probe Temperatures for Rod 5E and Inlet and Outlet Coolant Temperatures During First 90 s of MT-4.04

FIGURE D.5. Steam Probe Temperatures for Rod 2B and Inlet and Outlet Coolant Temperatures During 1500 s of MT-4.04

FIGURE D.6. Steam Probe Temperatures for Rod 2E and Inlet and Outlet Coolant Temperatures During 1500 s of MT-4.04

FIGURE D.7. Steam Probe Temperatures for Rod 5B and Inlet and Outlet Coolant Temperatures During 1500 s of MT-4.04

FIGURE D.8. Steam Probe Temperatures for Rod 5E and Inlet and Outlet Coolant Temperatures During 1500 s of MT-4.04

FIGURE D.9. Average Shroud Temperatures at Levels 55.9, 76.9, 97.9, 118.9, and 139.9 During MT-4.02

FIGURE D.10. Average Shroud Temperatures at Levels 55.9, 76.9, 97.9, 118.9, and 139.9 During MT-4.03

FIGURE D.11. Average Shroud Temperatures at Levels 55.9, 76.9, 97.9, 118.9, and 139.9 During First 90 s of MT-4.04

FIGURE D.12. Average Shroud Temperatures at Levels 55.9, 76.9, 97.9, 118.9, and 139.9 During 1500 s of MT-4.04

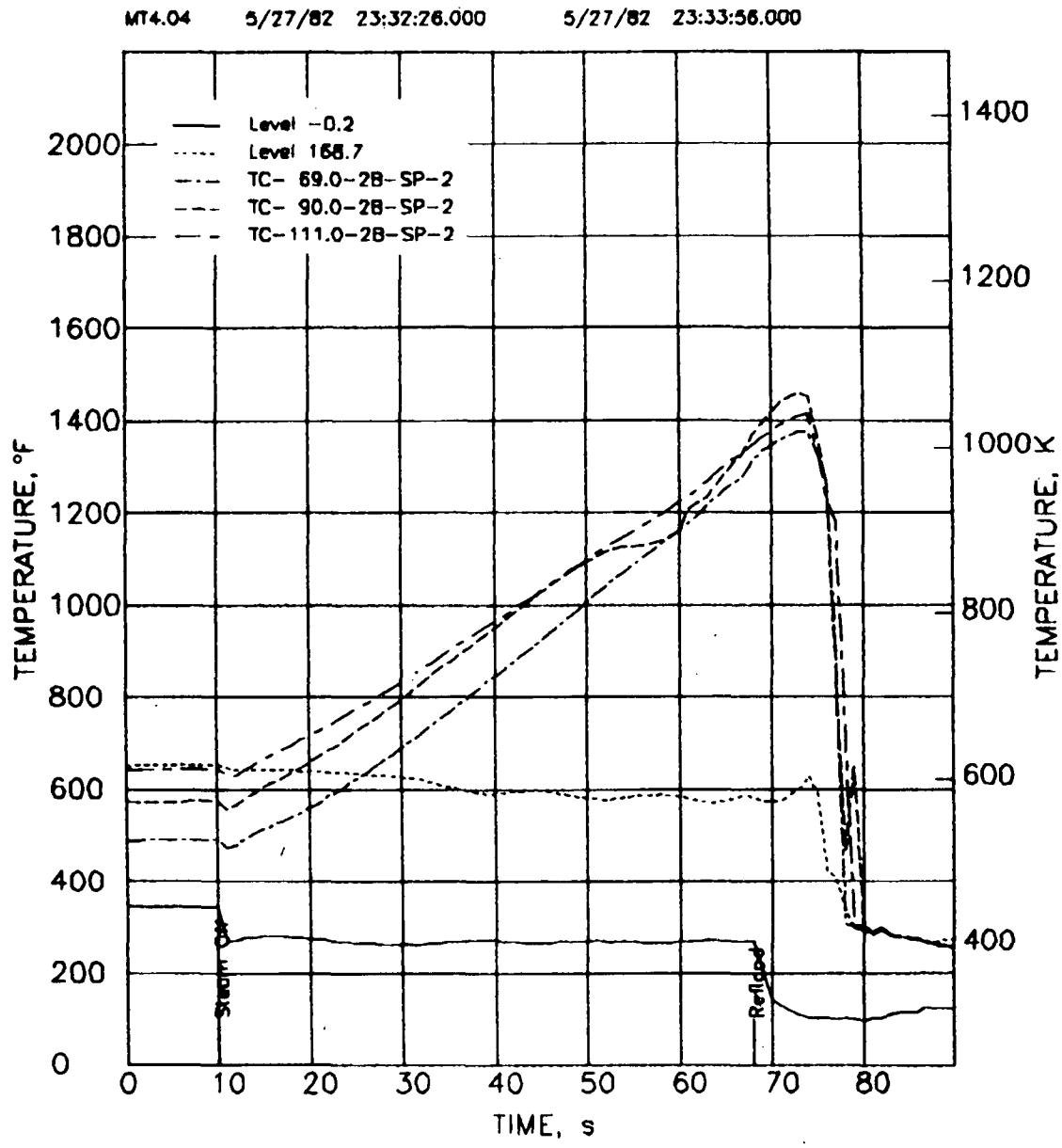

FIGURE D.1. Steam Probe Temperatures for Rod 2B and Inlet and Outlet Temperatures During First 90 s of MT-4.04

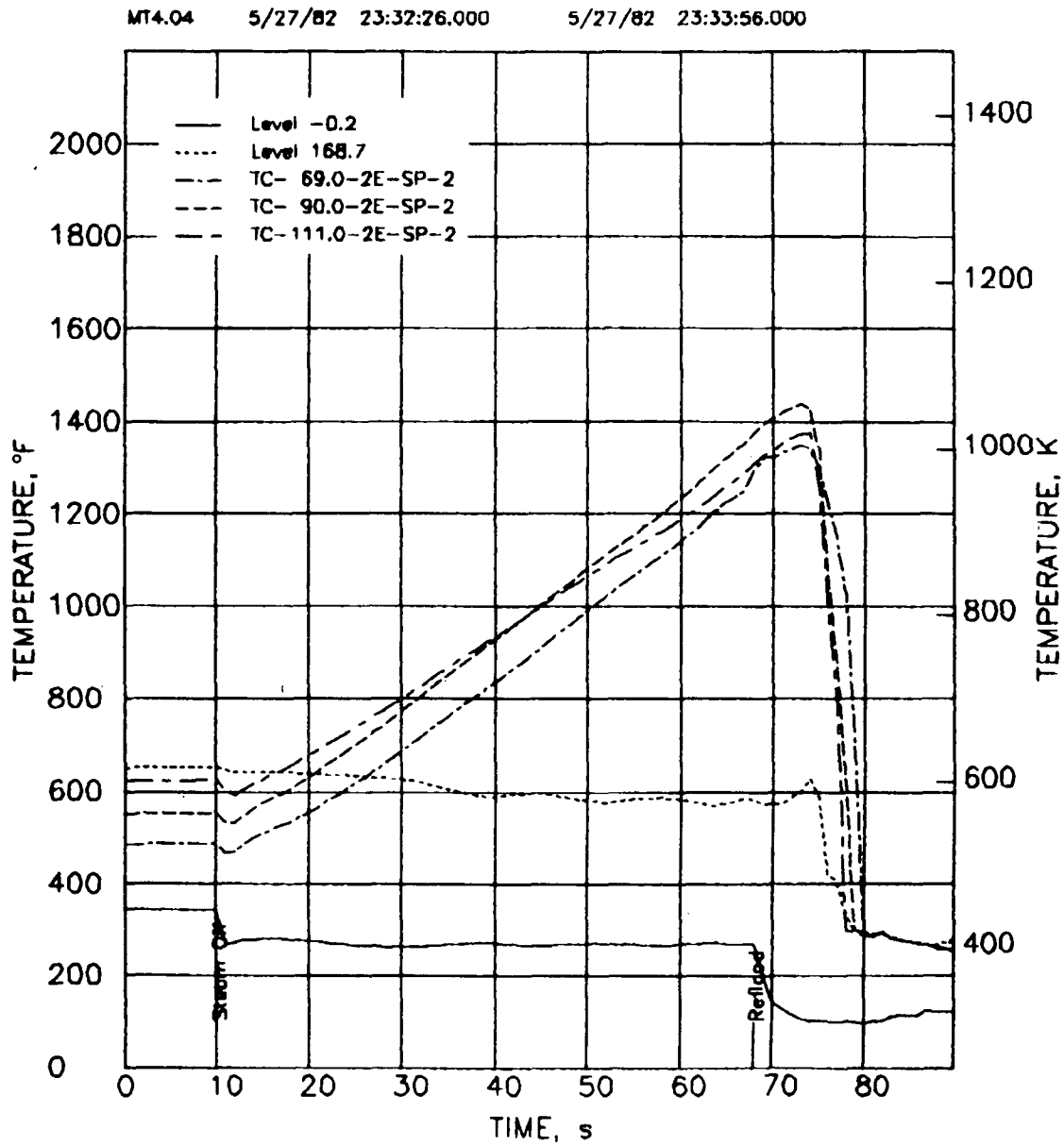

FIGURE D.2. Steam Probe Temperatures for Rod 2E and Inlet and Outlet Coolant Temperatures During First 90 s of MT-4.04

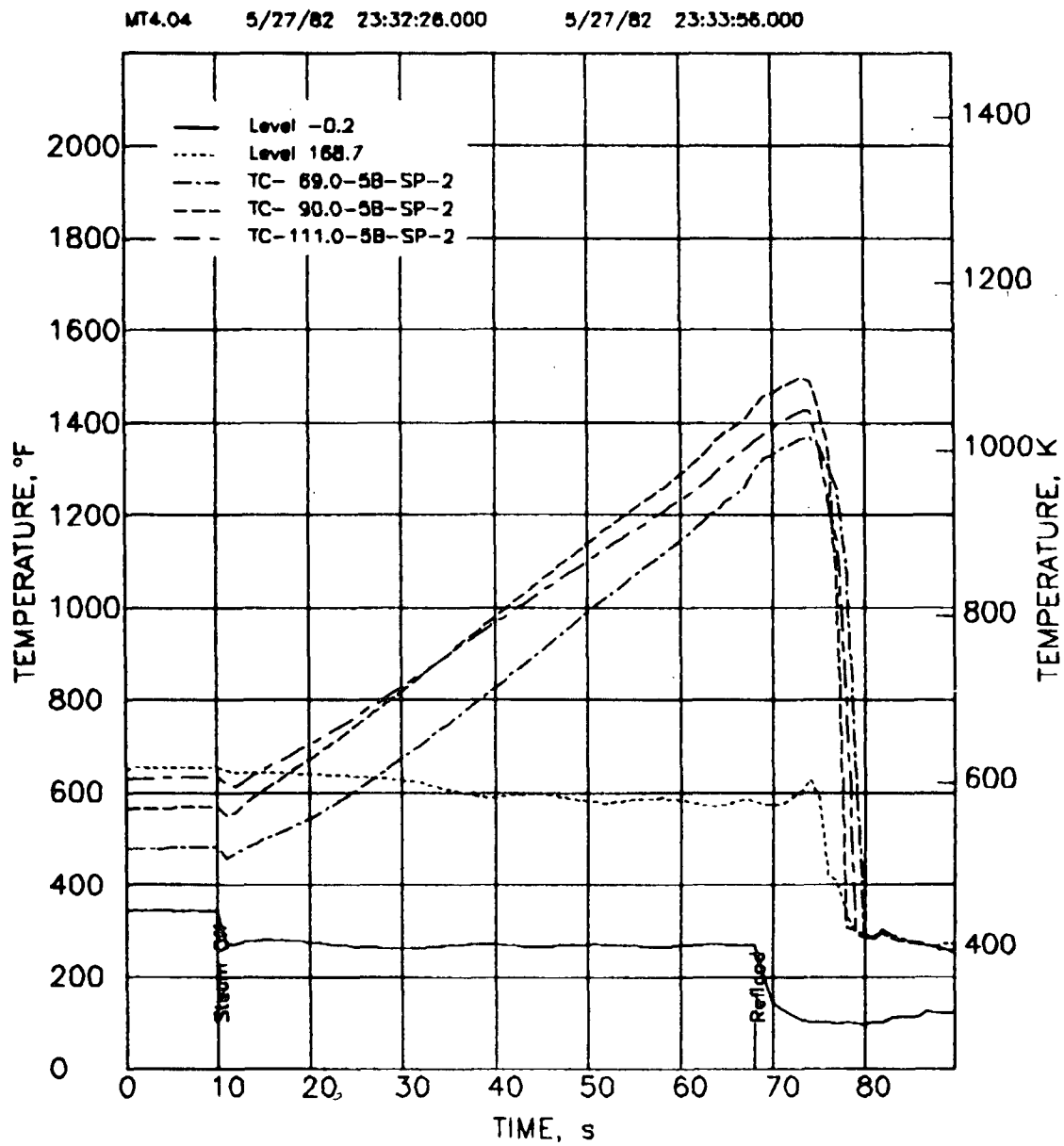

FIGURE D.3. Steam Probe Temperatures for Rod 5B and Inlet and Outlet Coolant Temperatures During First 90 s of MT-4.04

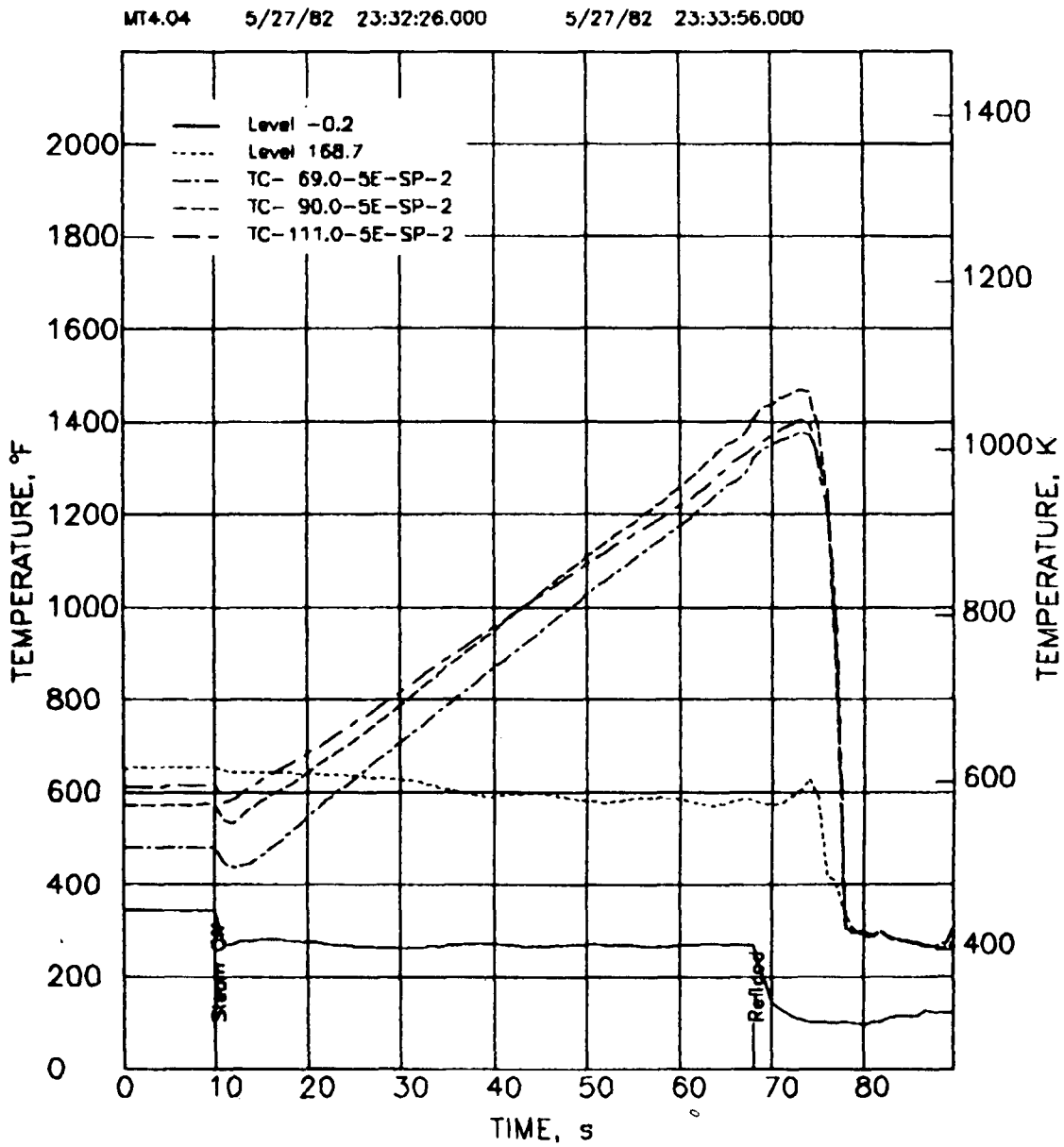

FIGURE D.4. Steam Probe Temperatures for Rod 5E and Inlet and Outlet Coolant Temperatures During First 90 s of MT-4.04

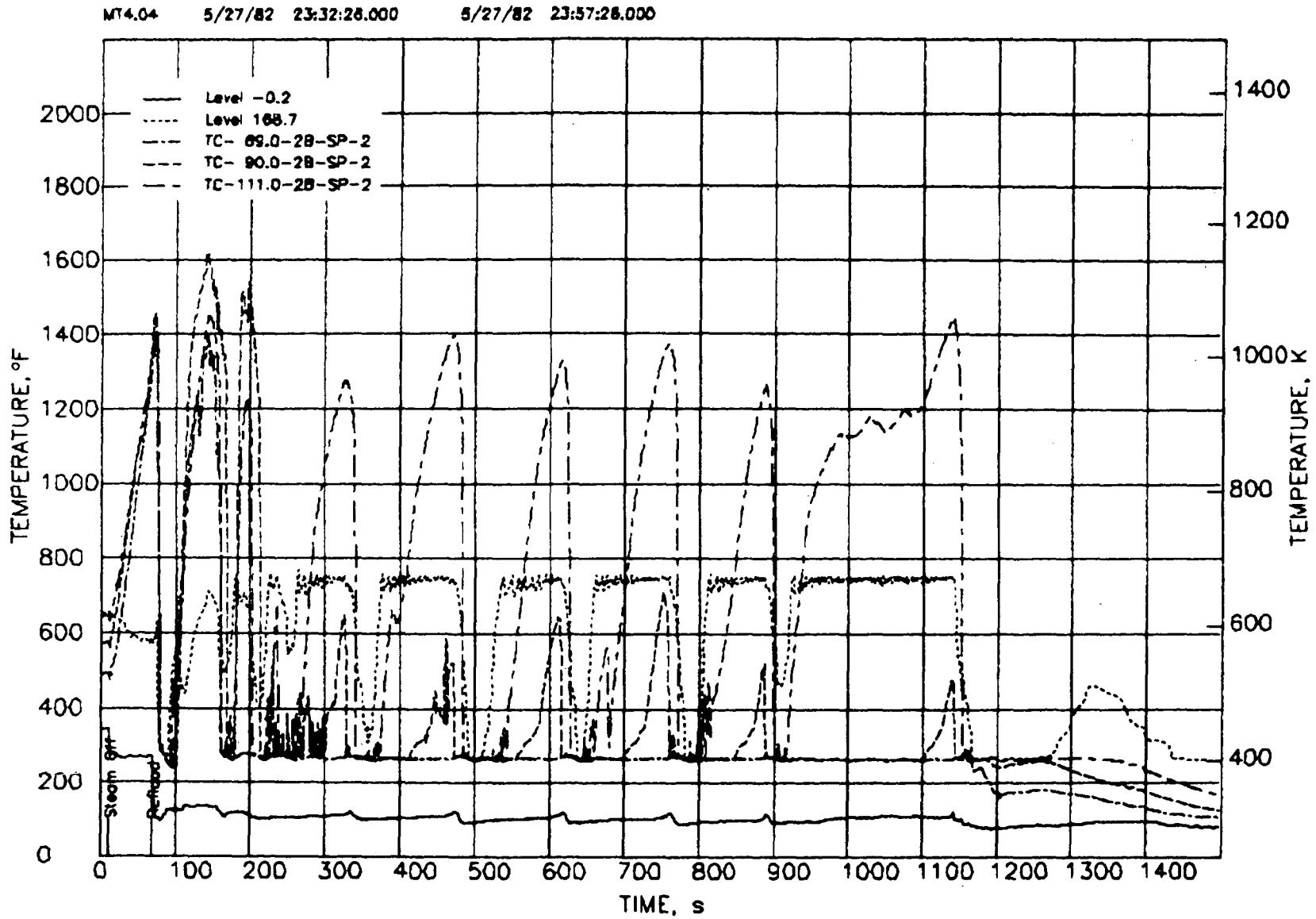

FIGURE D.5. Steam Probe Temperatures for Rod 2B and Inlet and Outlet Coolant Temperatures During 1500 s of MT-4.04

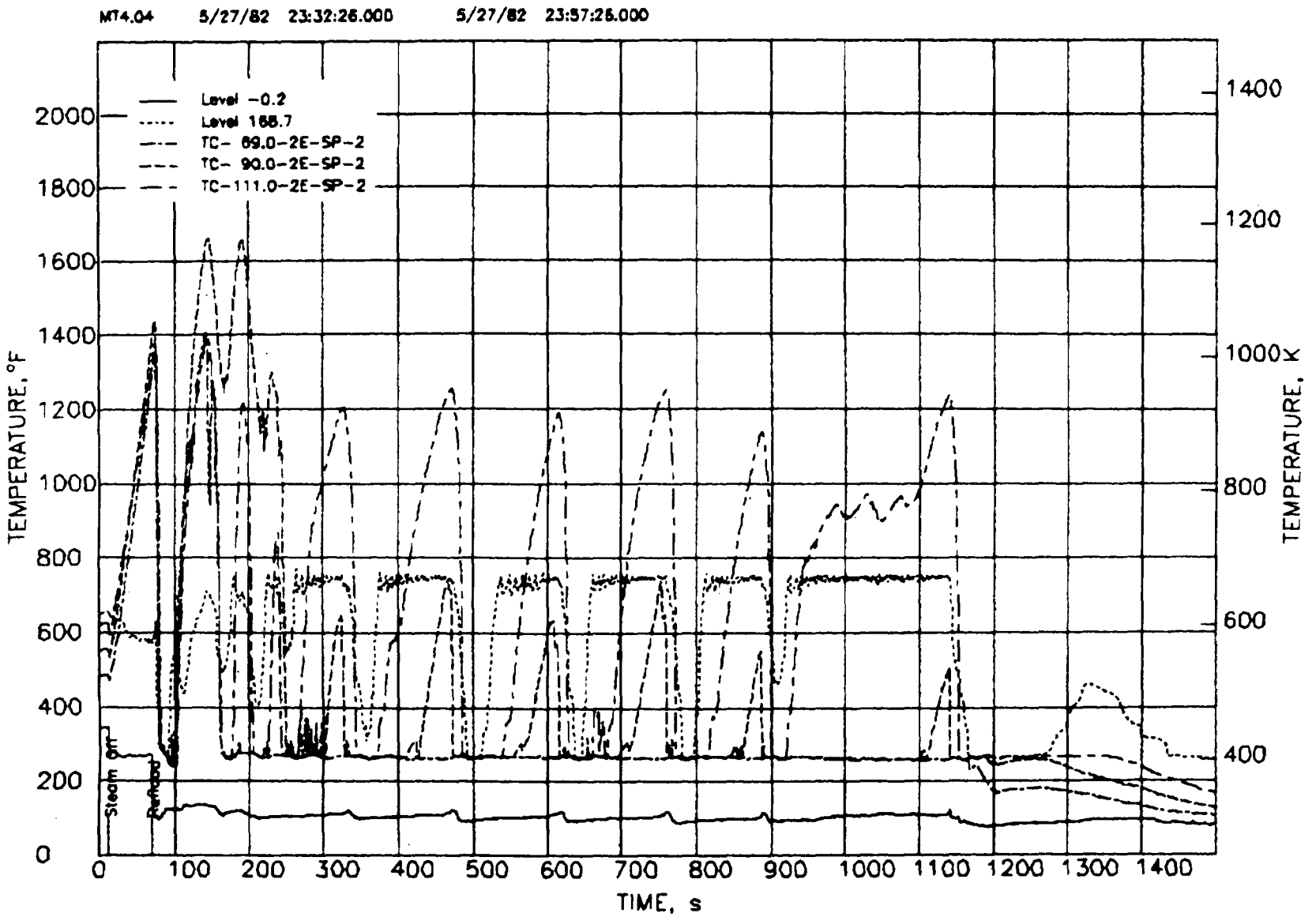

FIGURE D.6. Steam Probe Temperatures for Rod 2E and Inlet and Outlet Coolant Temperatures During 1500 s of MT-4.04

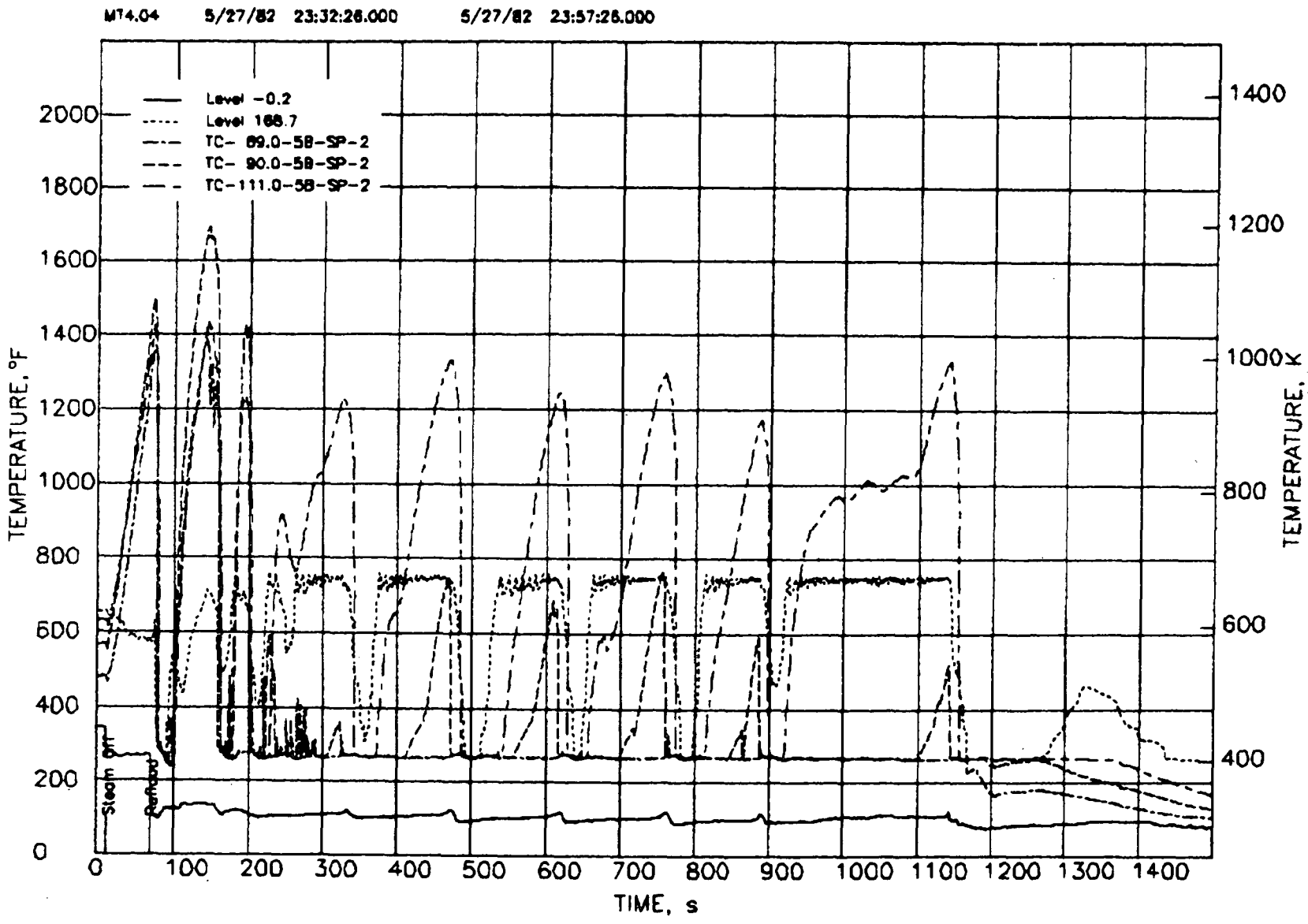

FIGURE D.7. Steam Probe Temperatures for Rod 5B and Inlet and Outlet Coolant Temperatures During 1500 s of MT-4.04

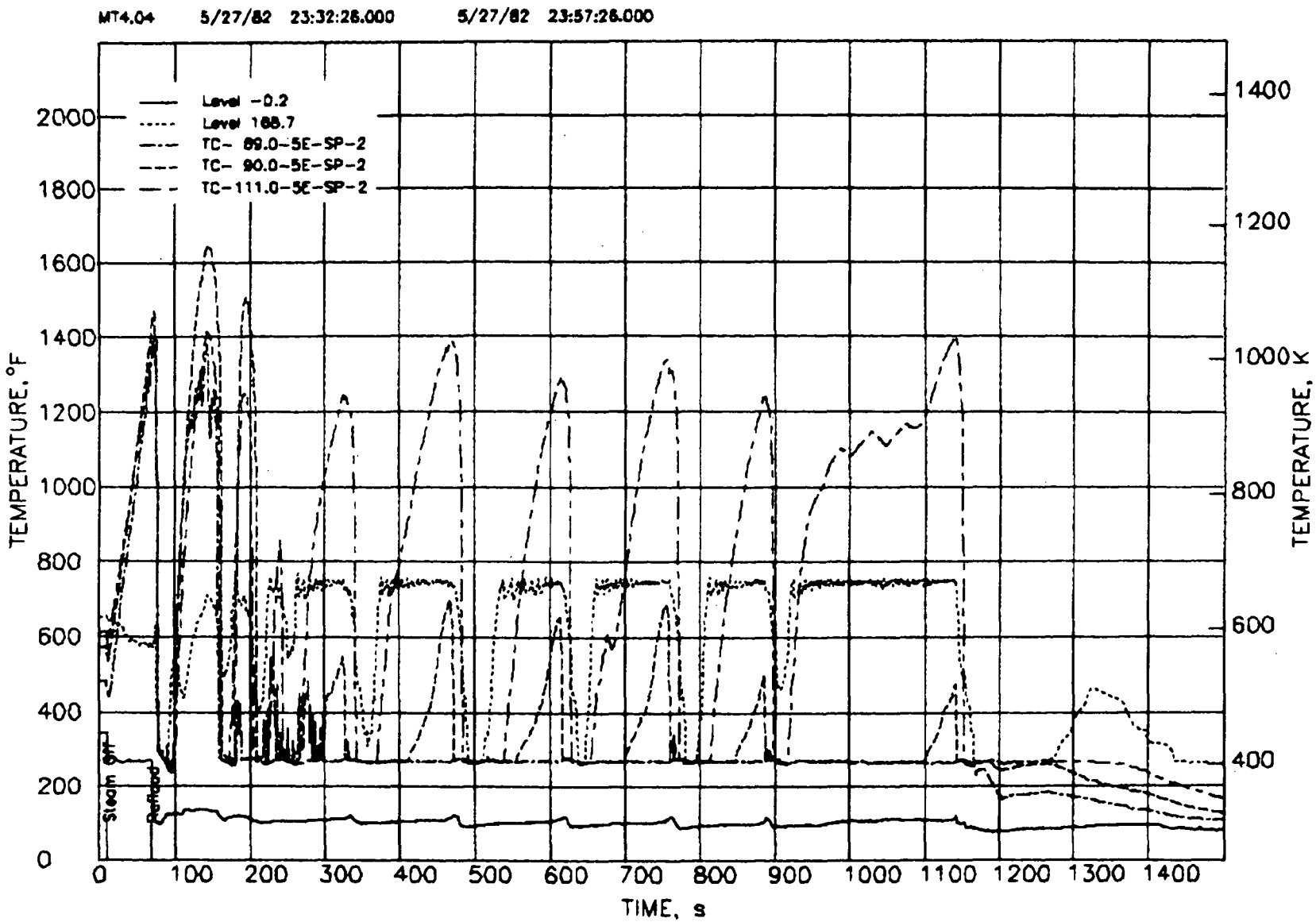

FIGURE D.8. Steam Probe Temperatures for Rod 5E and Inlet and Outlet Coolant Temperatures During 1500 s of MT-4.04

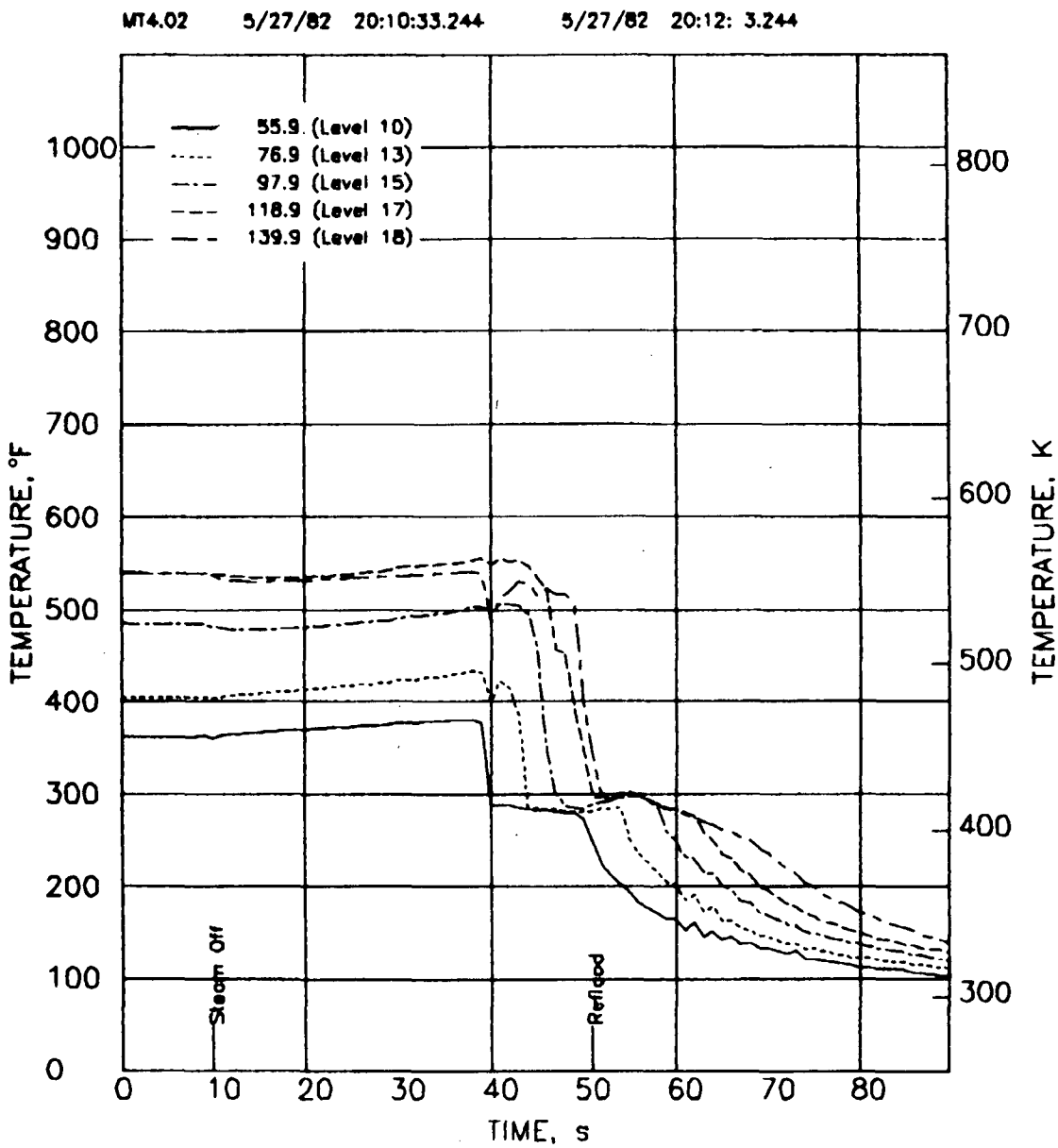

FIGURE D.9. Average Shroud Temperatures at Levels 55.9, 76.9, 97.9, 118.9, and 139.9 During MT-4.02

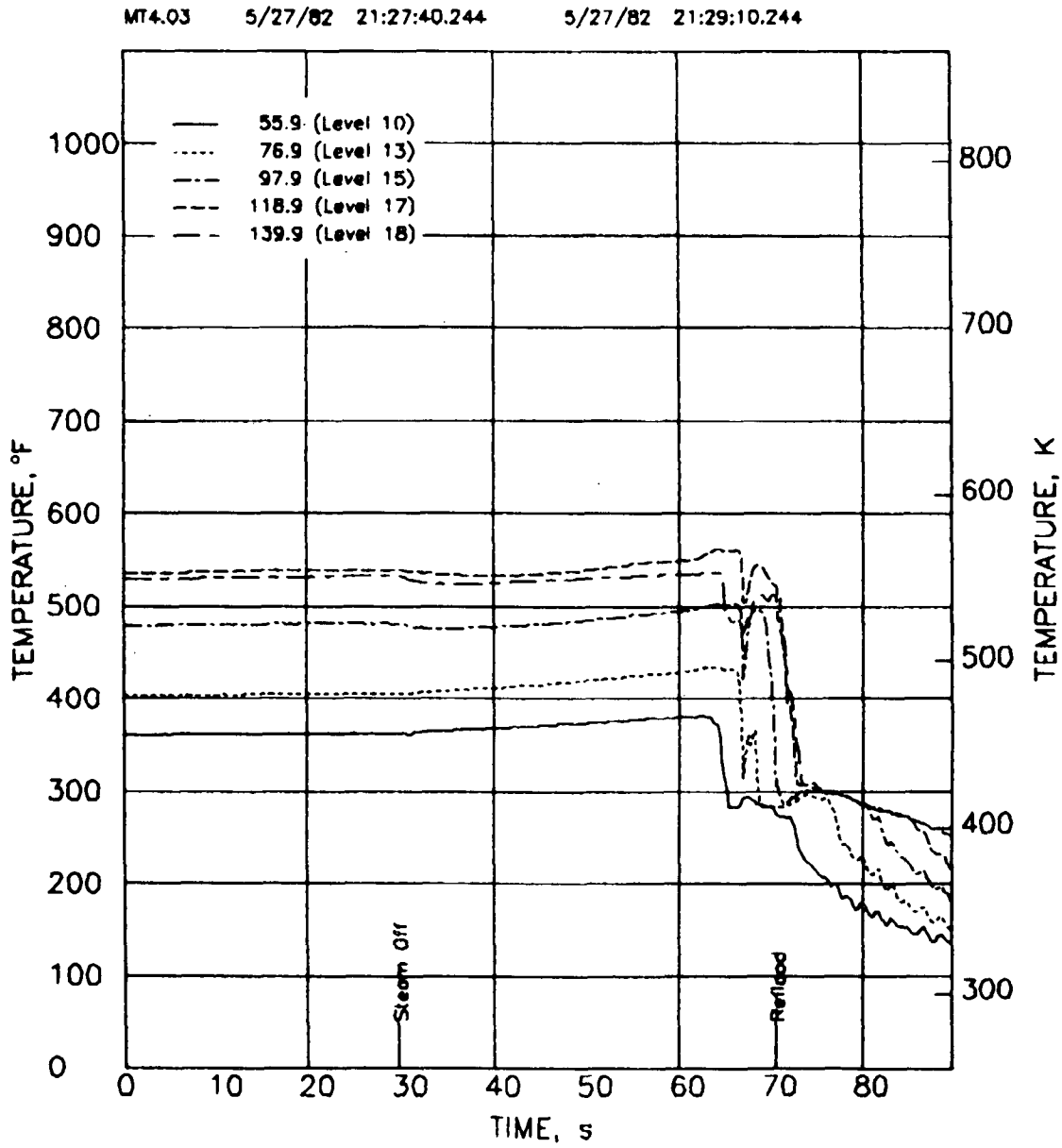

FIGURE D.10. Average Shroud Temperatures at Levels 55.9, 76.9, 97.9, 118.9, and 139.9 During MT-4.03

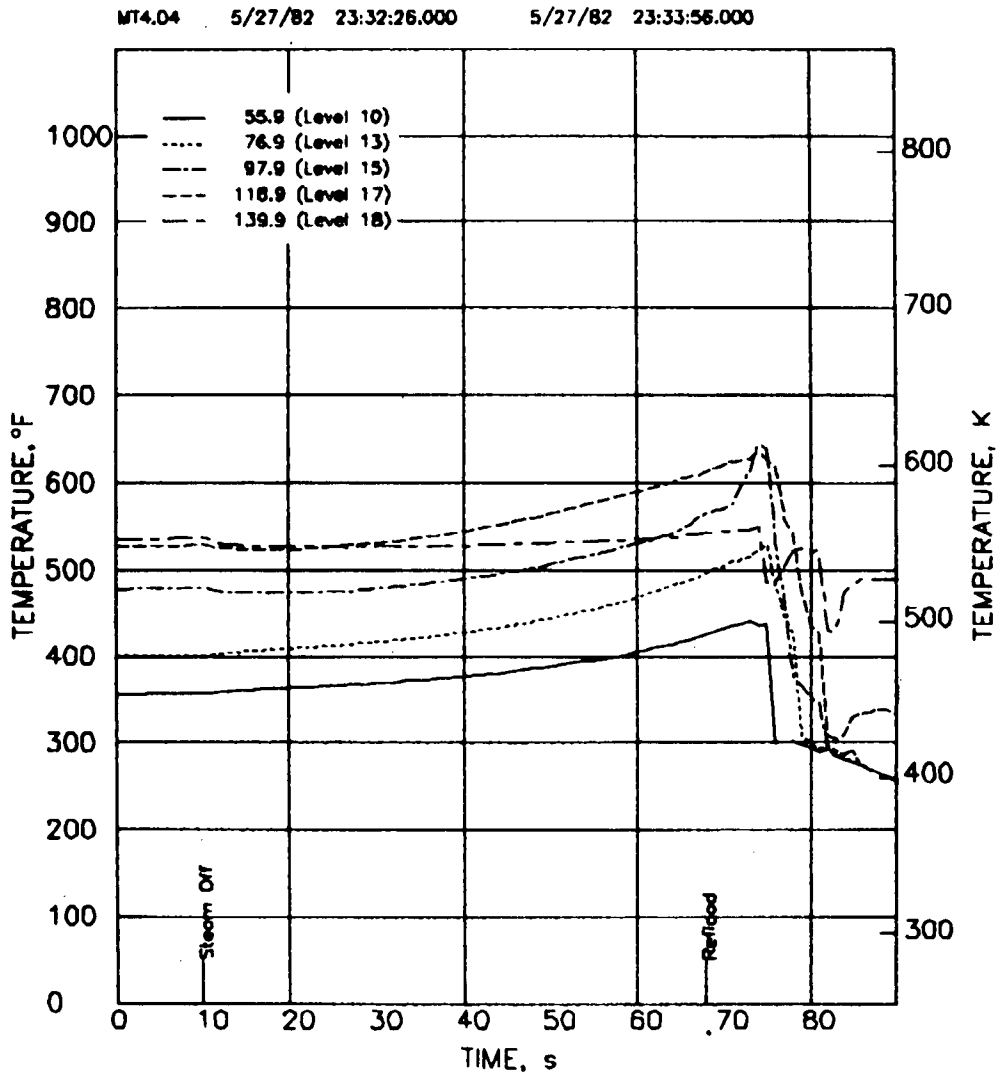

FIGURE D.11. Average Shroud Temperatures at Levels 55.9, 76.9, 97.9, 118.9, and 139.9 During First 90 s of MT-4.04

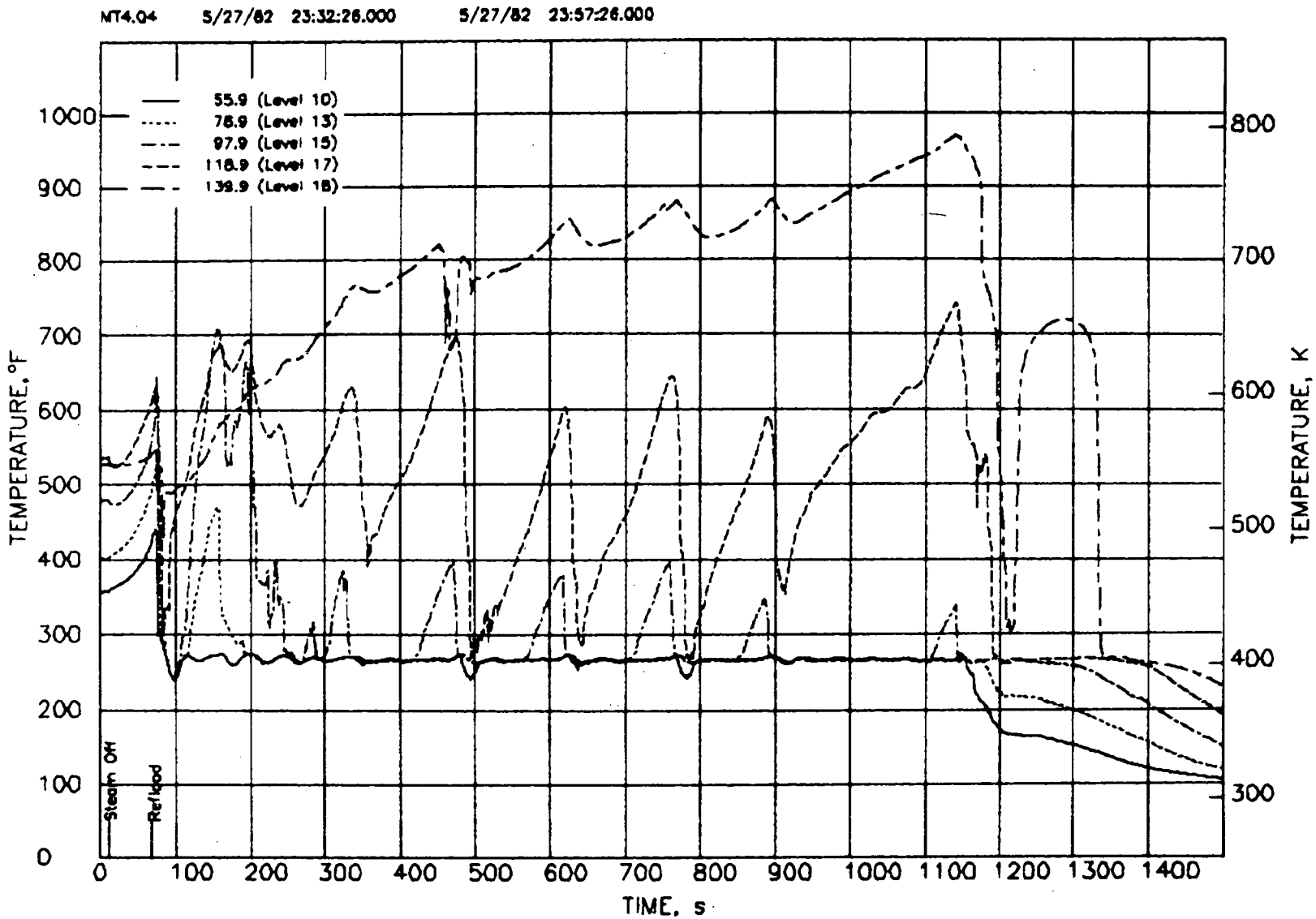

FIGURE D.12. Average Shroud Temperatures at Levels 55.9, 76.9, 97.9, 118.9, and 139.9 During 1500 s of MT-4.04

APPENDIX E

NEUTRON FLUX DATA

APPENDIX E

NEUTRON FLUX DATA

Neutron flux data were collected by self-powered neutron detectors (SPNDs), a traveling (vertical) fission chamber,[a] and four 0.127-cm (0.050-in.) diameter copper wires located within the test assembly next to the shroud. SPNDs were located at spacer grid elevations, thus limiting their effect on cladding ballooning. The SPNDs were made from a 15.2-cm (6-in.) long by 0.381-cm (0.150-in.) diameter shell containing a 10.2-cm (4-in.) long emitter. The longitudinal axes of the SPNDs were parallel to the fuel rods. The SPNDs measured neutron flux throughout the test. Flux wire activation primarily represents neutron fluence accumulated during preconditioning. The traveling fission chamber was only used during preconditioning.

The fission chamber and flux wire axial neutron flux profiles for preconditioning are compared in Figure E.1. The lower curves represent measured copper wire activation or neutron fluence normalized to the peak near the test assembly center. A significant amount of data variation was caused by swaging that produced nonuniform diameter wire.[b] However, a nominal depression in neutron fluence is evident at SPND locations. The flux wires were terminated just below the SPNDs at Level 109.5. The wires were 269 to 274 cm (106 to 108 in.) long, which allowed them to fit into the instrument lead carrier.

The upper curve on Figure E.1 represents the total neutron flux measured during preconditioning at full power. During full-power operation, the NRU reactor operated at ~110 MW; the MT-4 test assembly produced ~2.1 MW. The traveling fission chamber was used in site J-22, and the MT-4 test assembly was in the L-24 site. The fission chamber and the test assembly were separated by two lattice sites; consequently, the fission chamber did not detect the neutron flux depression caused by the SPNDs.

Neutron flux histories from SPNDs at Levels 25.5 through 151.5 are provided in Figures E.2 through E.10. Both reliable and failed sensor data are

---

(a) Allan, C. J., et al. November 1980. "The Development and Use of a Traveling Flux Detector System for CANDU Reactors." In Proceedings of the IEEE.

(b) Okazaki, A., and D. A. Kettner. July 1982. Activity Distribution in Copper Wires from Battelle MT-4 LOCA Simulation Test in NRU. APRP-RP-101, AECL, Chalk River Nuclear Laboratories, Chalk River, Ontario.

presented. Some failed sensor signals drifted, some were off-scale, and others were inexplicably uncalibrated. Axial temperature data have shown that resultant axial fuel powers were relatively smooth.

During the simulated loss-of-coolant accident (LOCA) transient, light water was used to reflood the test assembly. In the heavy-water moderated National Research Universal (NRU) reactor, this introduction of a neutron-absorbing material resulted in relocation of the dynamic control rod. Up until the time of the reactor trip, the control rod relocation did not have much effect on neutron flux in the test assembly. The neutron noise evident in the figures was primarily caused by water boiling, entrainment, and carryover (or ejection) from the test assembly.

One previous concern about SPND operation was the effect of temperature on instrument leads that conduct signals to the data-recording system. Previous tests have shown the temperature effects on dielectric property changes (and signal shunting) in the SPND leads. This was not a problem in the MT-3 or MT-4 experiments because all SPND leads were mounted on the shroud walls, which remained relatively cool during experiment.

This appendix consists of the following graphical data:

FIGURE E.1. Normalized Axial Neutron Fluence and Neutron Flux Measured During Preconditioning

FIGURE E.2. Neutron Flux at SPND Level 25.5

FIGURE E.3. Neutron Flux at SPND Level 45.5

FIGURE E.4. Neutron Flux at SPND Level 67.5

FIGURE E.5. Neutron Flux at SPND Level 69.0

FIGURE E.6. Neutron Flux at SPND Level 88.5

FIGURE E.7. Neutron Flux at SPND Level 109.5

FIGURE E.8. Neutron Flux at SPND Level 111.0

FIGURE E.9. Neutron Flux at SPND Level 130.5

FIGURE E.10. Neutron Flux at SPND Level 151.5

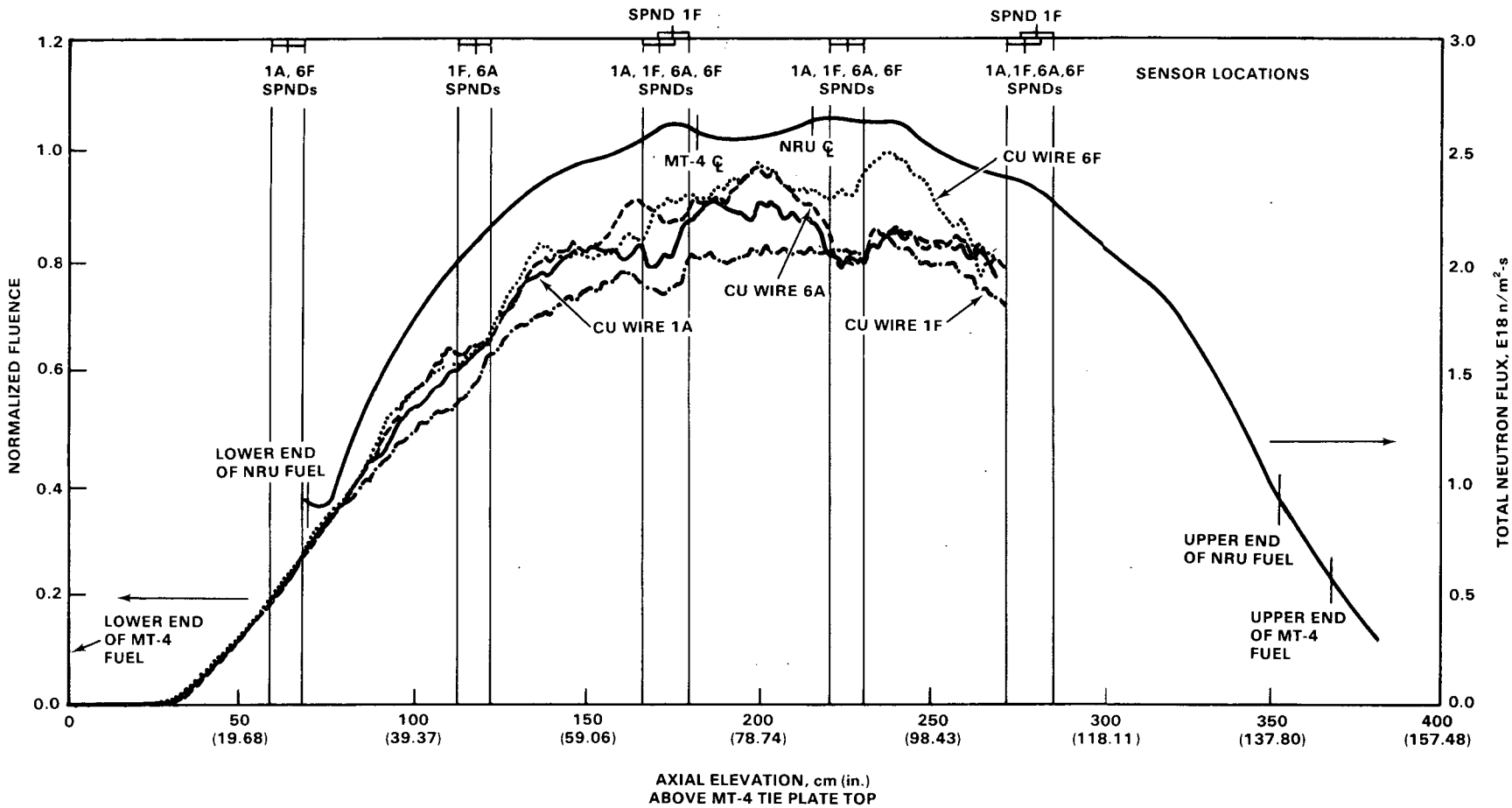

FIGURE E.1. Normalized Axial Neutron Fluence and Neutron Flux Measured During Preconditioning

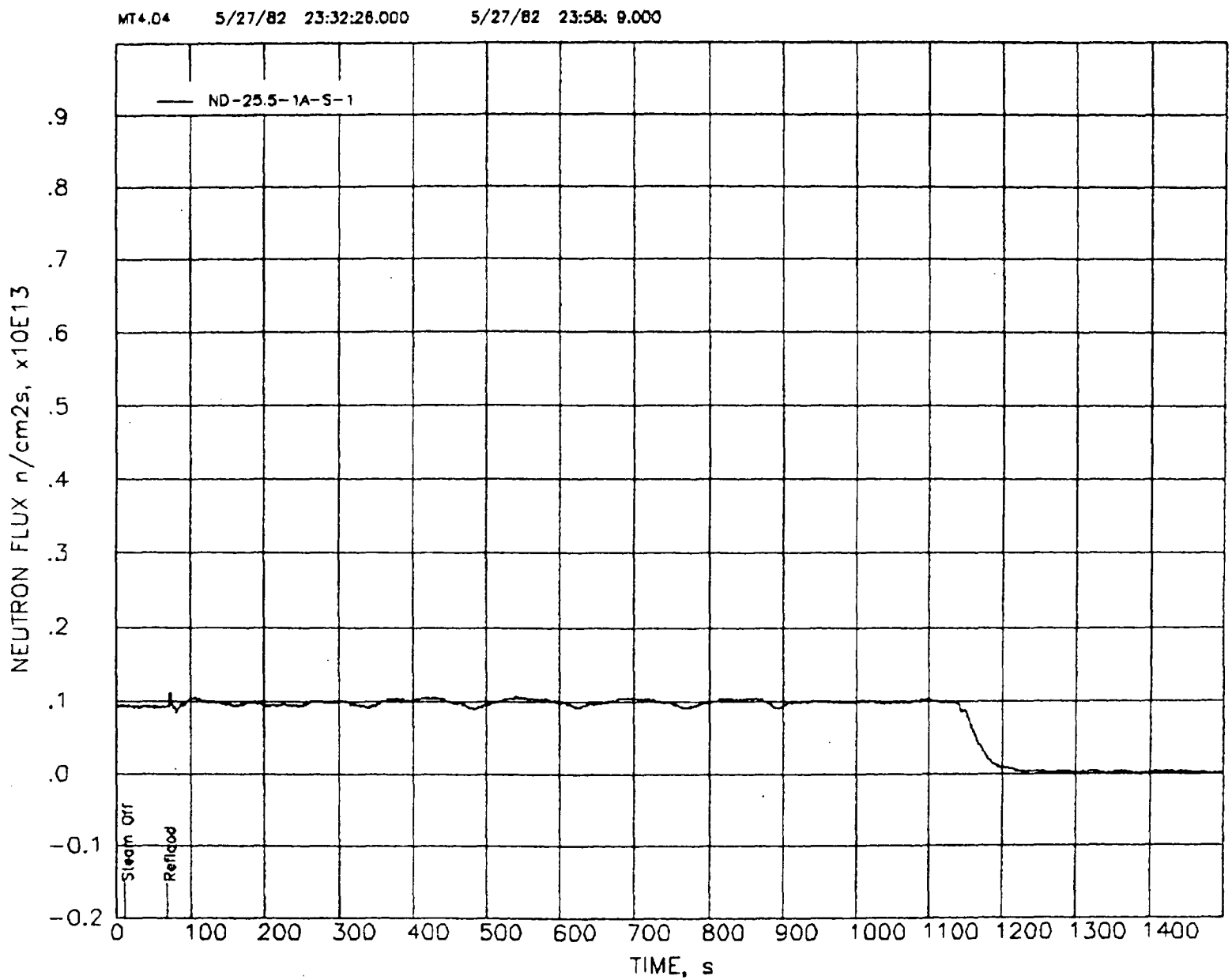

FIGURE E.2. Neutron Flux at SPND Level 25.5

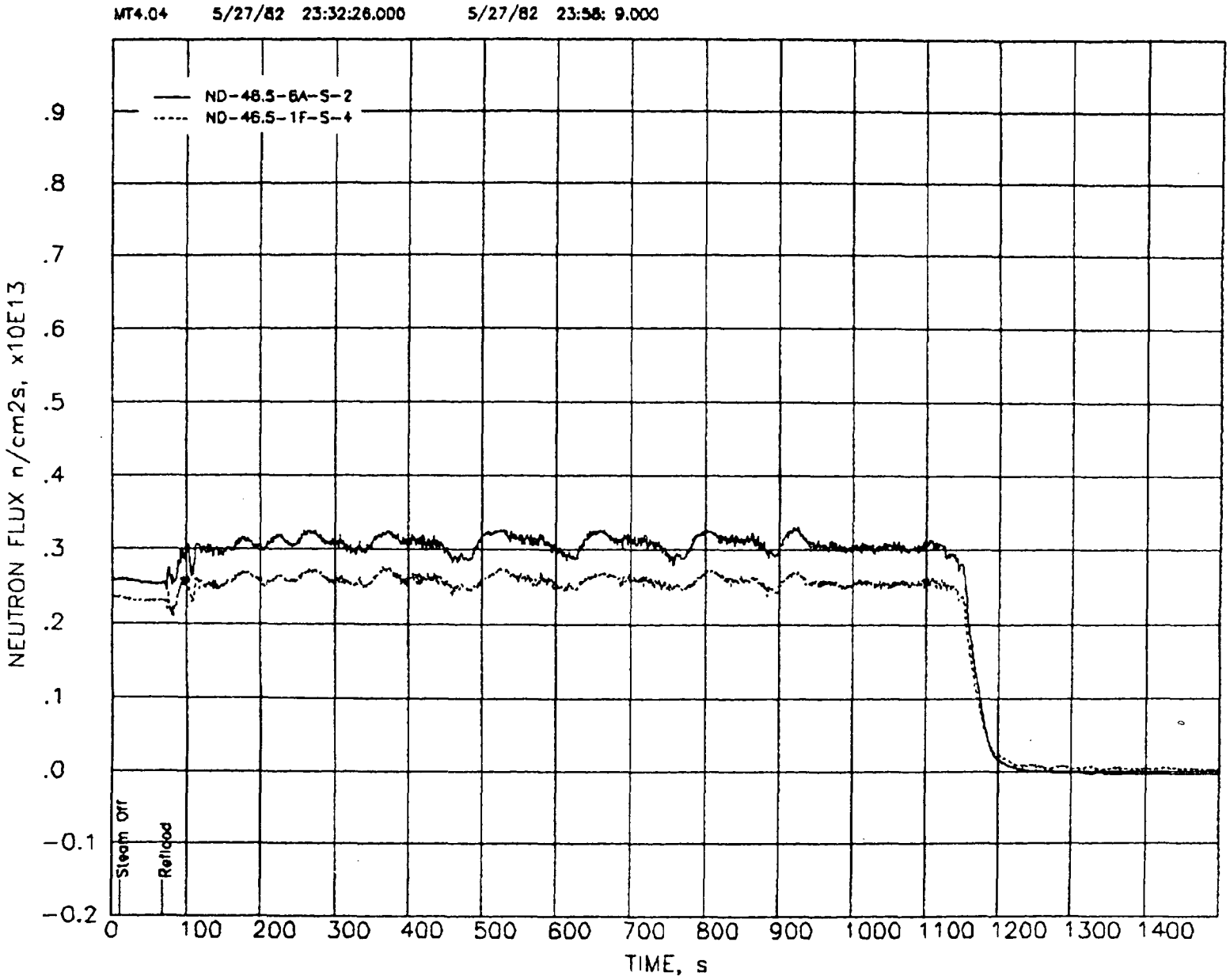

FIGURE E.3. Neutron Flux at SPND Level 45.5

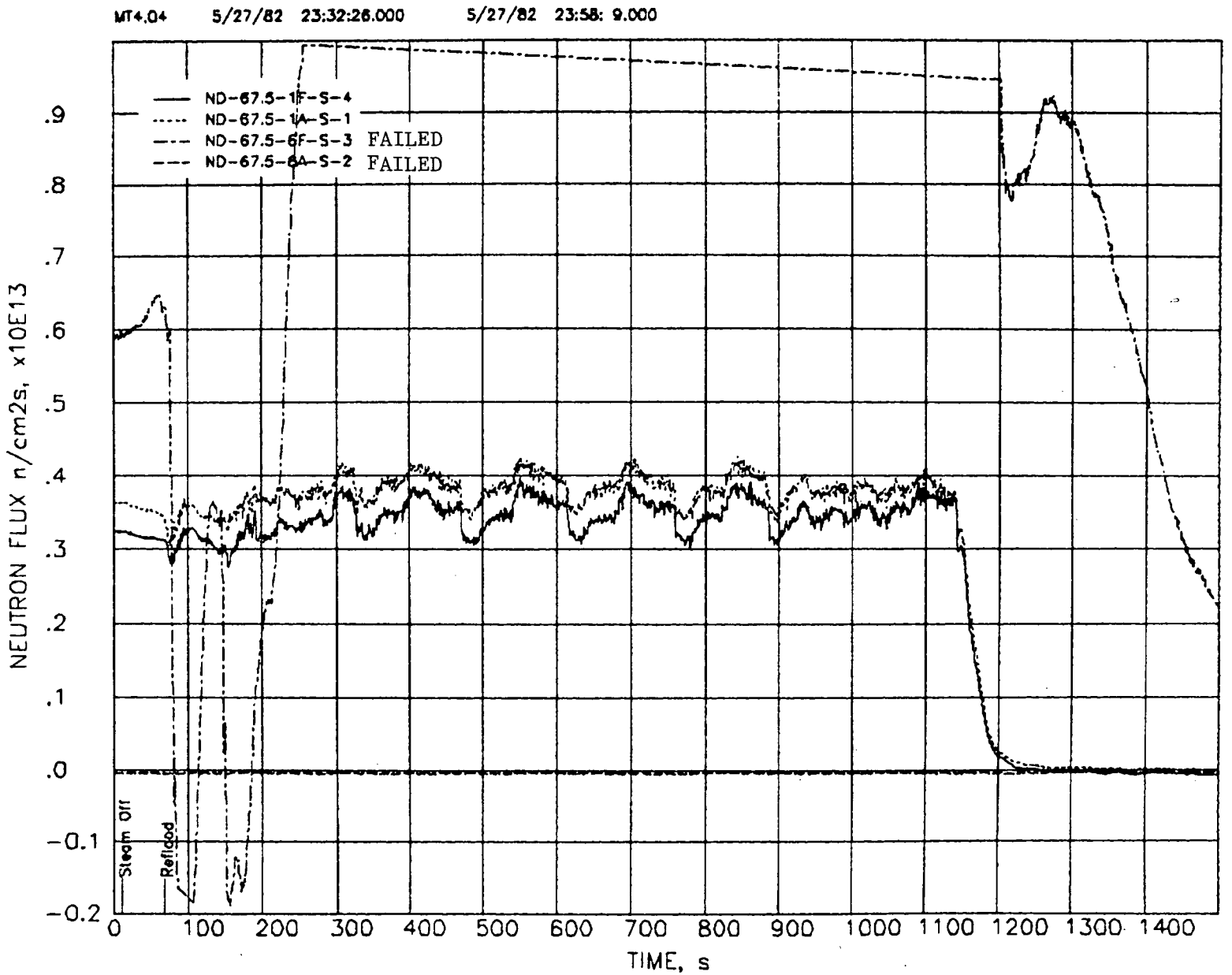

FIGURE E.4. Neutron Flux at SPND Level 67.5

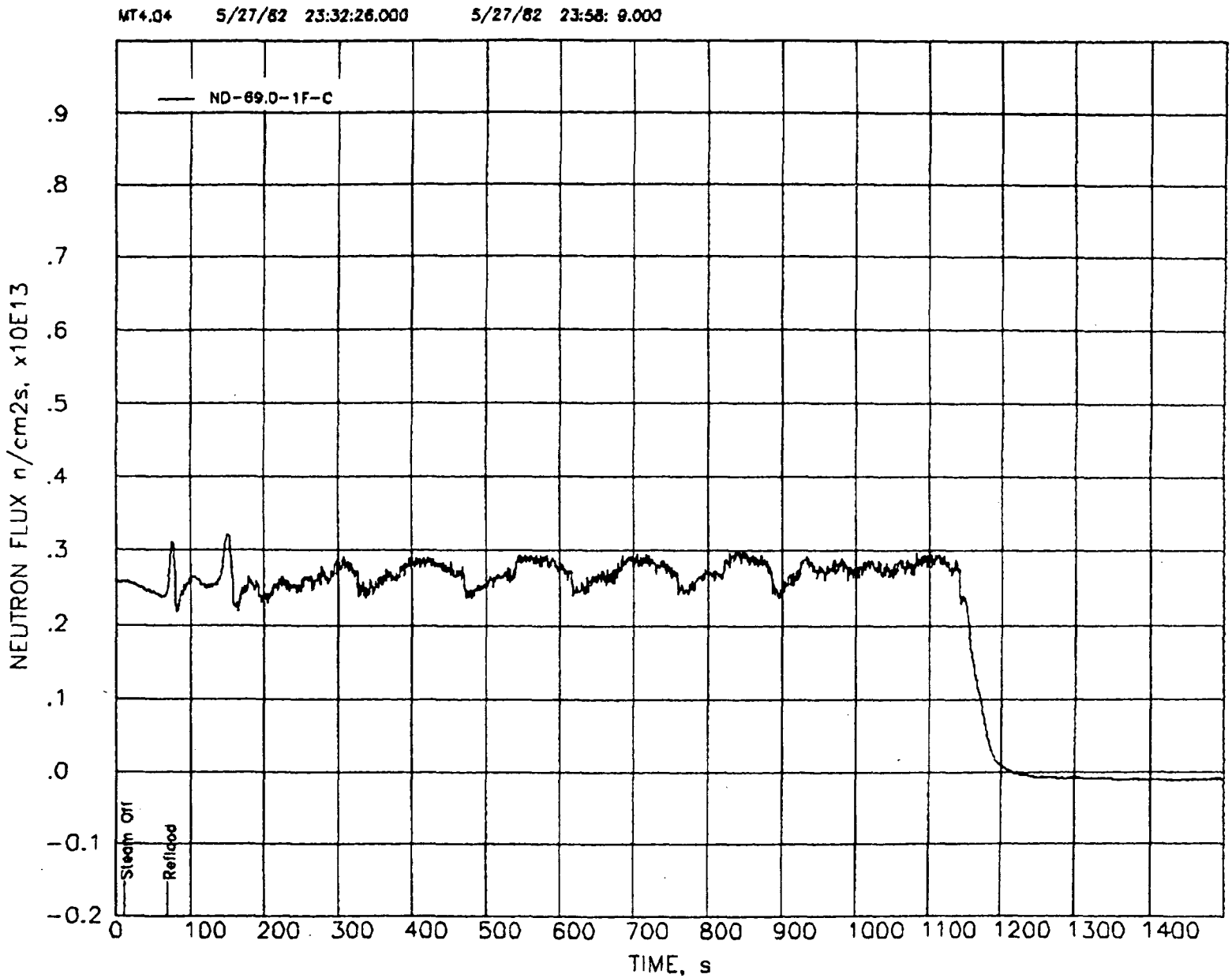

FIGURE E.5. Neutron Flux at SPND Level 69.0

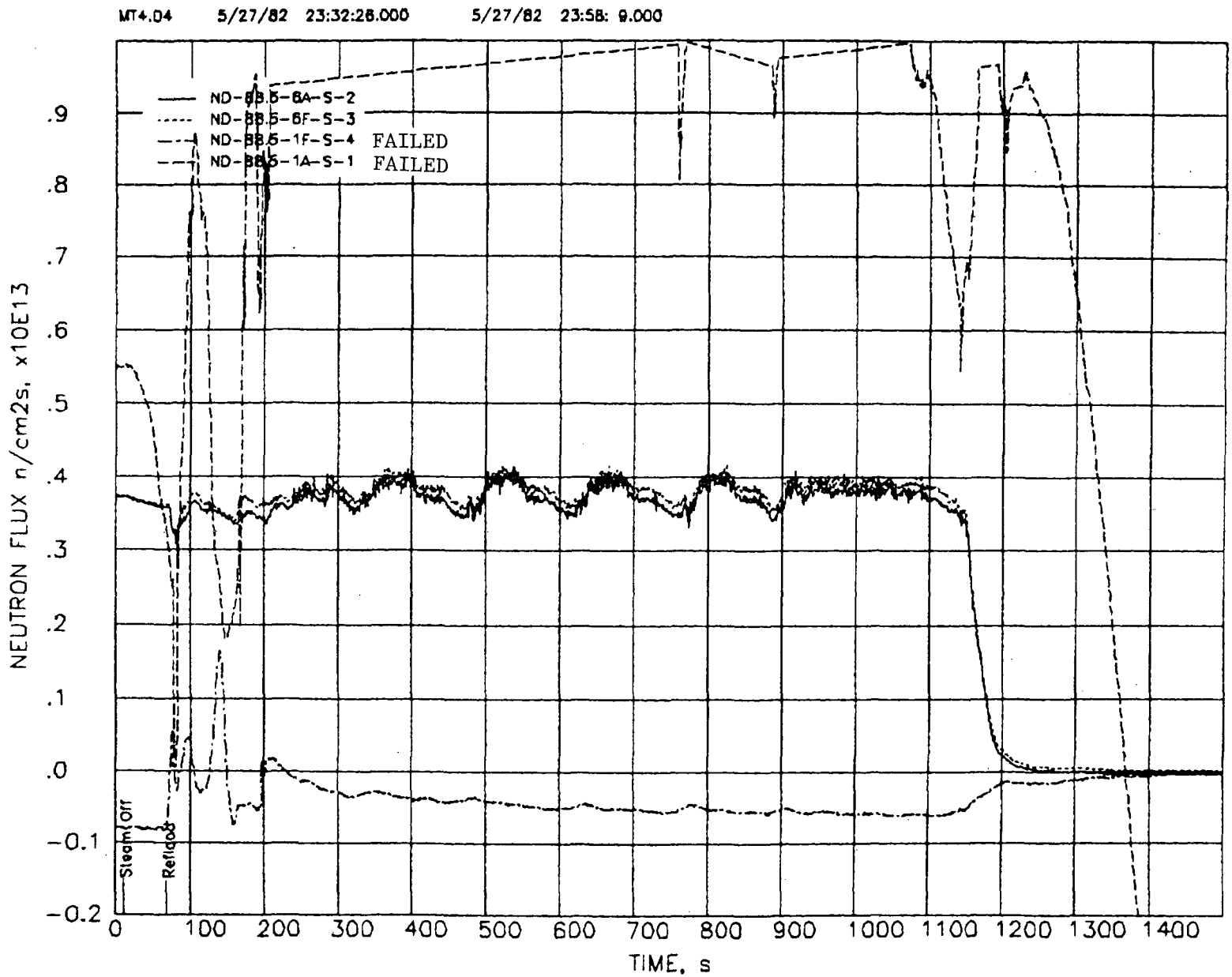

FIGURE E.6. Neutron Flux at SPND Level 88.5

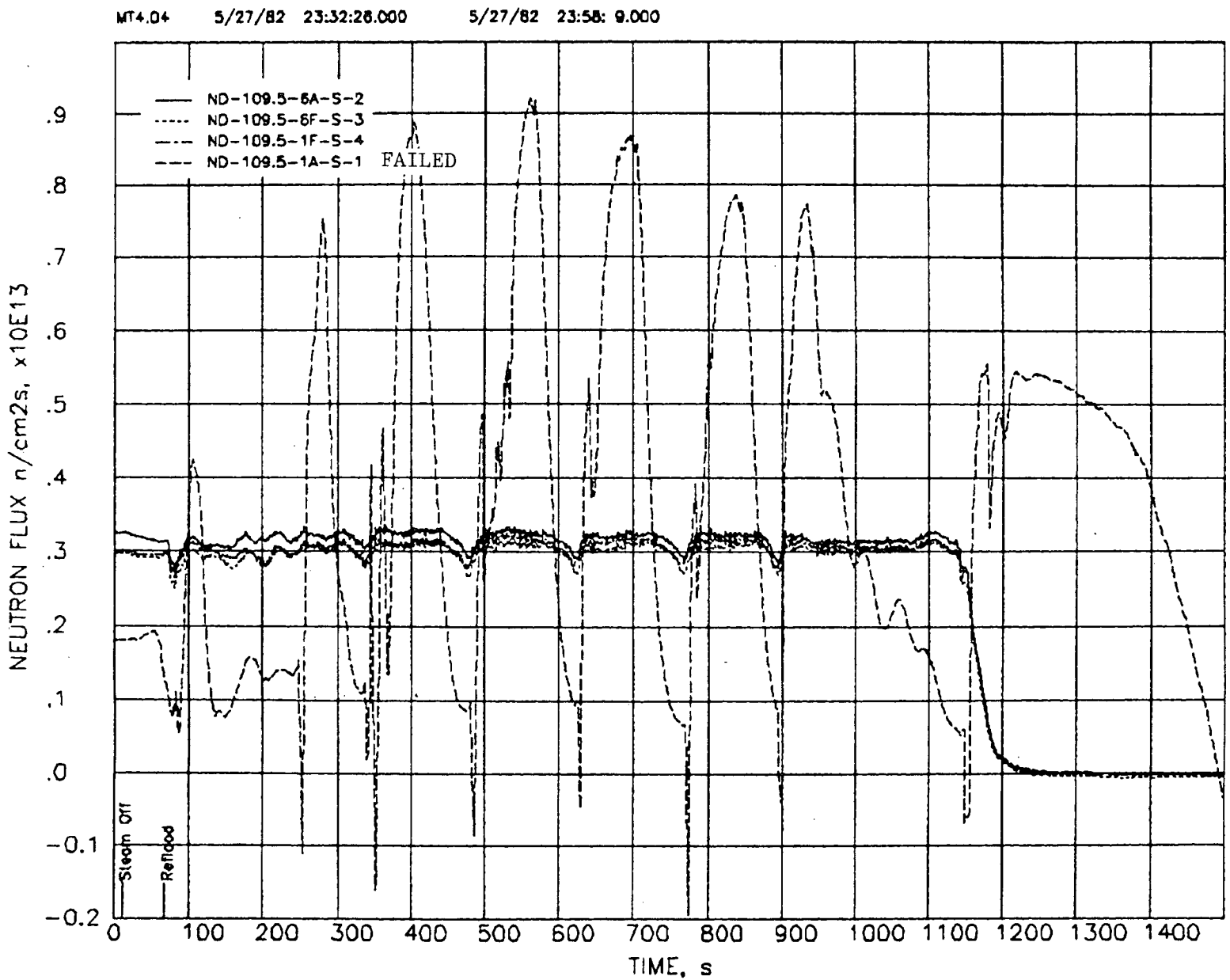

FIGURE E.7. Neutron Flux at SPND Level 109.5

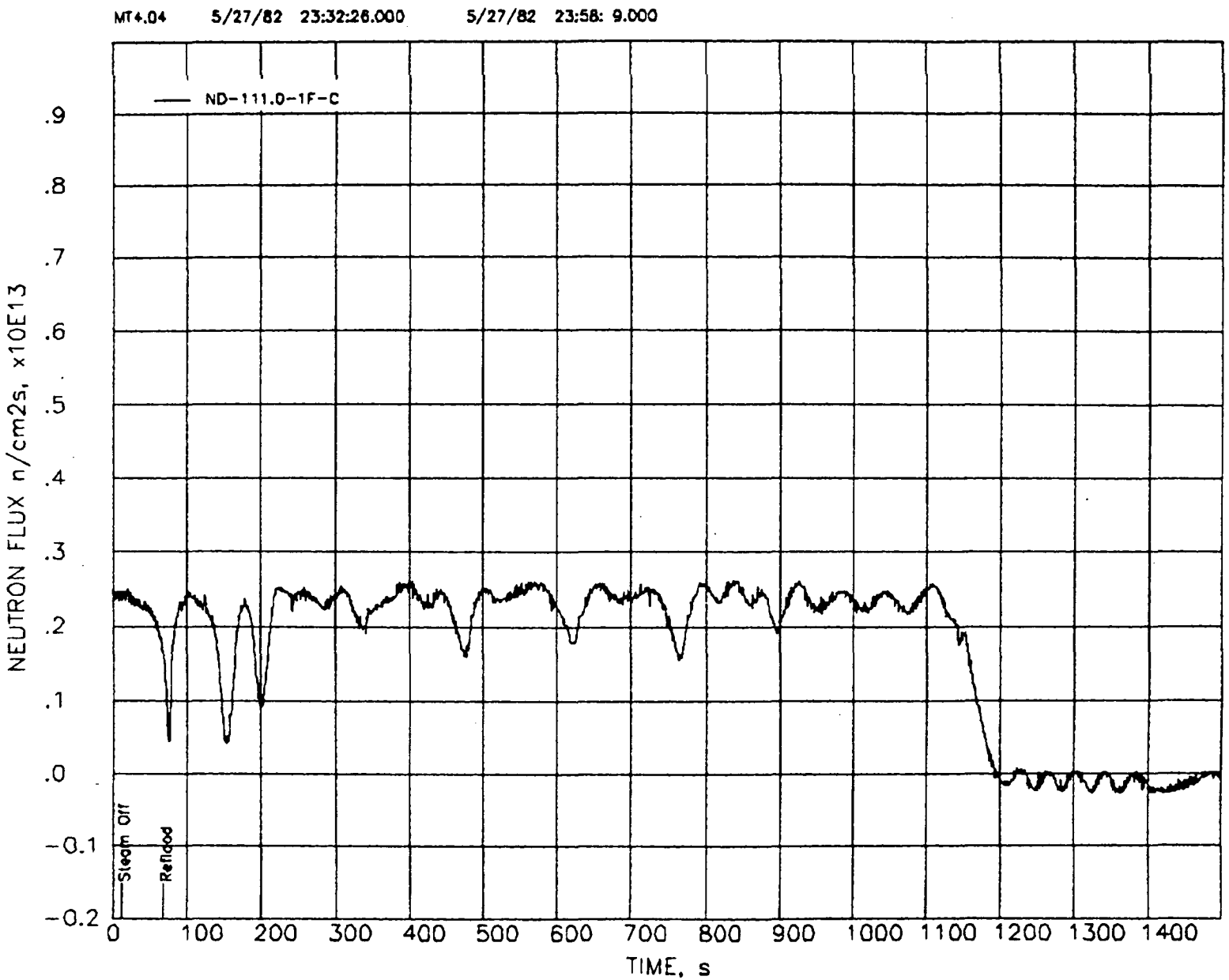

FIGURE E.8. Neutron Flux at SPND Level 111.0

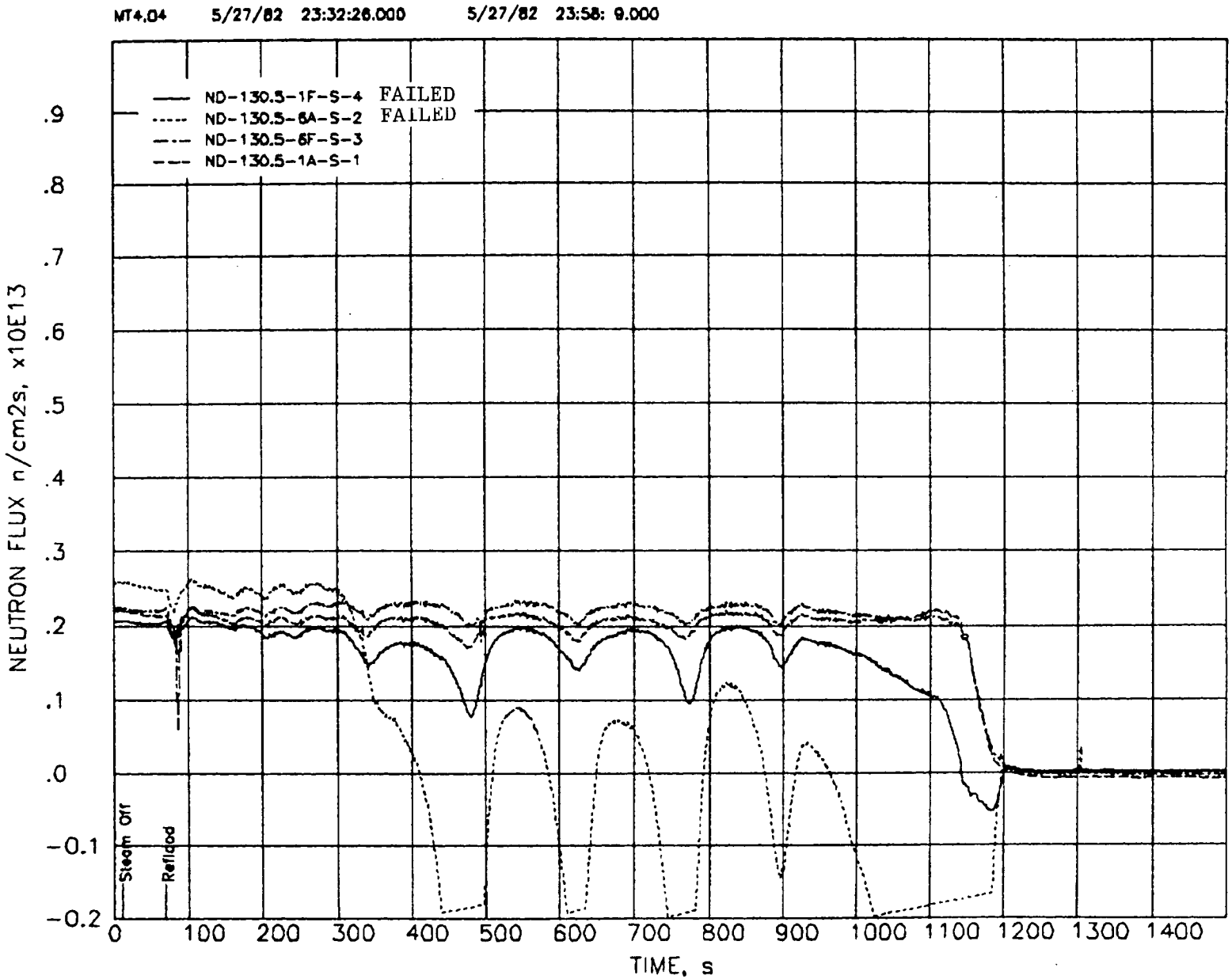

FIGURE E.9. Neutron Flux at SPND Level 130.5

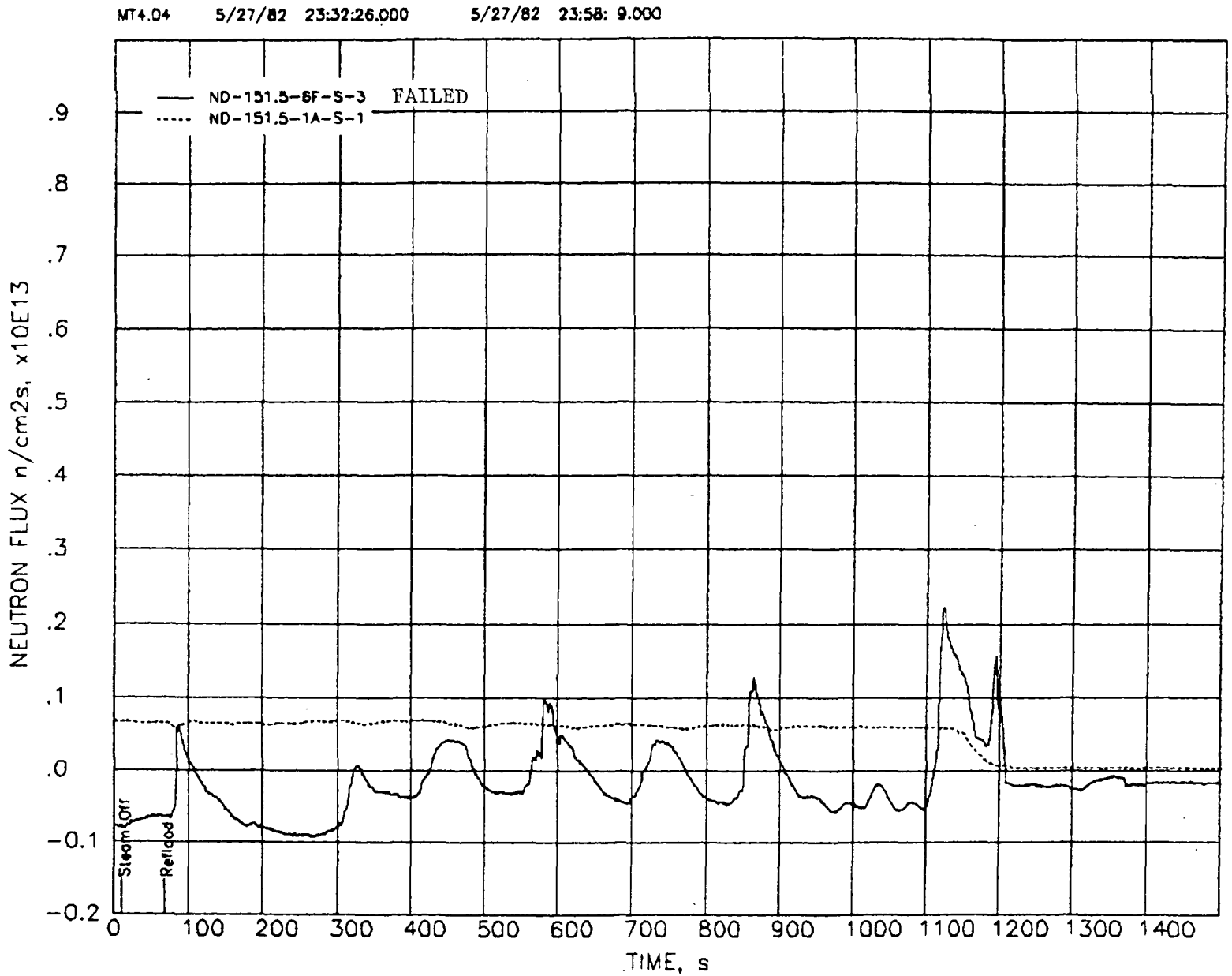

FIGURE E.10. Neutron Flux at SPND Level 151.5

APPENDIX F

REFLOOD FLOW MEASUREMENTS

APPENDIX F

REFLOOD FLOW MEASUREMENTS

The reflood flow system included a Fisher-Porter turbine flowmeter in the high flow rate line and series-connected Barton and Fisher-Porter turbine flowmeters in a parallel flow rate line. A parallel standby reflood line was also provided to supply emergency reflood coolant but was not used during the MT-4 experiment. The reflood control system was calibrated prior to the first transient using steam probe data to determine the water/steam interface during reflood operation. Three reflood calibration tests were performed at ~0.051 m/s (2 in./s), 0.089 m/s (3.5 in./s), and 0.109 m/s (4.3 in./s).

Reflood flow was determined by turbine flowmeters that measured the total flow rate into the assembly, by a time domain reflectometry instrument, and by thermocouples (TCs) at various levels that revealed the reflood level inside the shroud. Prior to calibration, steam flowed through the test assembly. For a calibration test, the steam was shut off and the reflood water was turned on. As the water level increased in the assembly and passed a given level, the TCs at that level showed a marked decrease in temperature. Reflood flow data for the three calibration tests are shown in Figures F.1 through F.9.

Transient test starting times and reflood delay times depended on the flow conditions at the bottom of the active fuel. These flow conditions are related to the temperature response of TCs located at Level -0.2, which is 0.023 m (0.9 in.) below the active fuel. The transients began when the steam coolant was shut off as determined from a quick drop in temperature at Level -0.2. The reflood initiation times occurred when the reflood water quenched TCs at Level -0.2 as indicated by a second quick drop in temperature.

The initial three tests--MT-4.01, MT-4.02, and MT-4.03--were adiabatic tests and did not use reflood water to control temperature. For the final test--MT-4.04--a combination of the loop control system (LCS) and the data acquisition and control system (DACS) was used. Once 11 of the 12 test rods ruptured, the LCS controlled reflood rates at 0.203 m/s (8 in./s) for 6 s, 0.102 m/s (4 in./s) for 6 s, and then 0.0254 m/s (1 in./s) for 3 s. For the lower reflood rates, the LCS controlled reflood using the low-flow control value instead of the high-flow control value. Finally, 15 s after the LCS-initiated reflood, the DACS took over temperature control using variable reflood rates. The DACS used hot spot sensors (TCs) at Levels 97.9 and 118.9 for temperature feedback control. The resultant reflood rates for MT-4.04 are shown in Figures F.10 through F.13.

The remainder of this appendix consists of the following graphical data:

FIGURE F.1. Total Reflood Flow Rate for Reflood Calibration Test 1

FIGURE F.2. Time Domain Reflectometry Response for Reflood Calibration Test 1

FIGURE F.3. Temperatures at Levels -0.2 Through 168.7 for Reflood Calibration Test 1

FIGURE F.4. Total Reflood Flow Rate for Reflood Calibration Test 2

FIGURE F.5. Time Domain Reflectometry Response for Reflood Calibration Test 2

FIGURE F.6. Temperatures at Levels -0.2 Through 168.7 for Reflood Calibration Test 2

FIGURE F.7. Reflood Flow Rate for Reflood Calibration Test 3

FIGURE F.8. Time Domain Reflectometry Response for Reflood Calibration Test 3

FIGURE F.9. Temperatures at Levels -0.2 Through 168.7 for Reflood Calibration Test 3

FIGURE F.10. Total Reflood Flow Rate for First 90 s of MT-4.04

FIGURE F.11. Time Domain Reflectometry Response for First 90 s of MT-4.04

FIGURE F.12. Total Reflood Flow Rate for 1500 s of MT-4.04

FIGURE F.13. Time Domain Reflectometry Response for 1500 s of MT-4.04

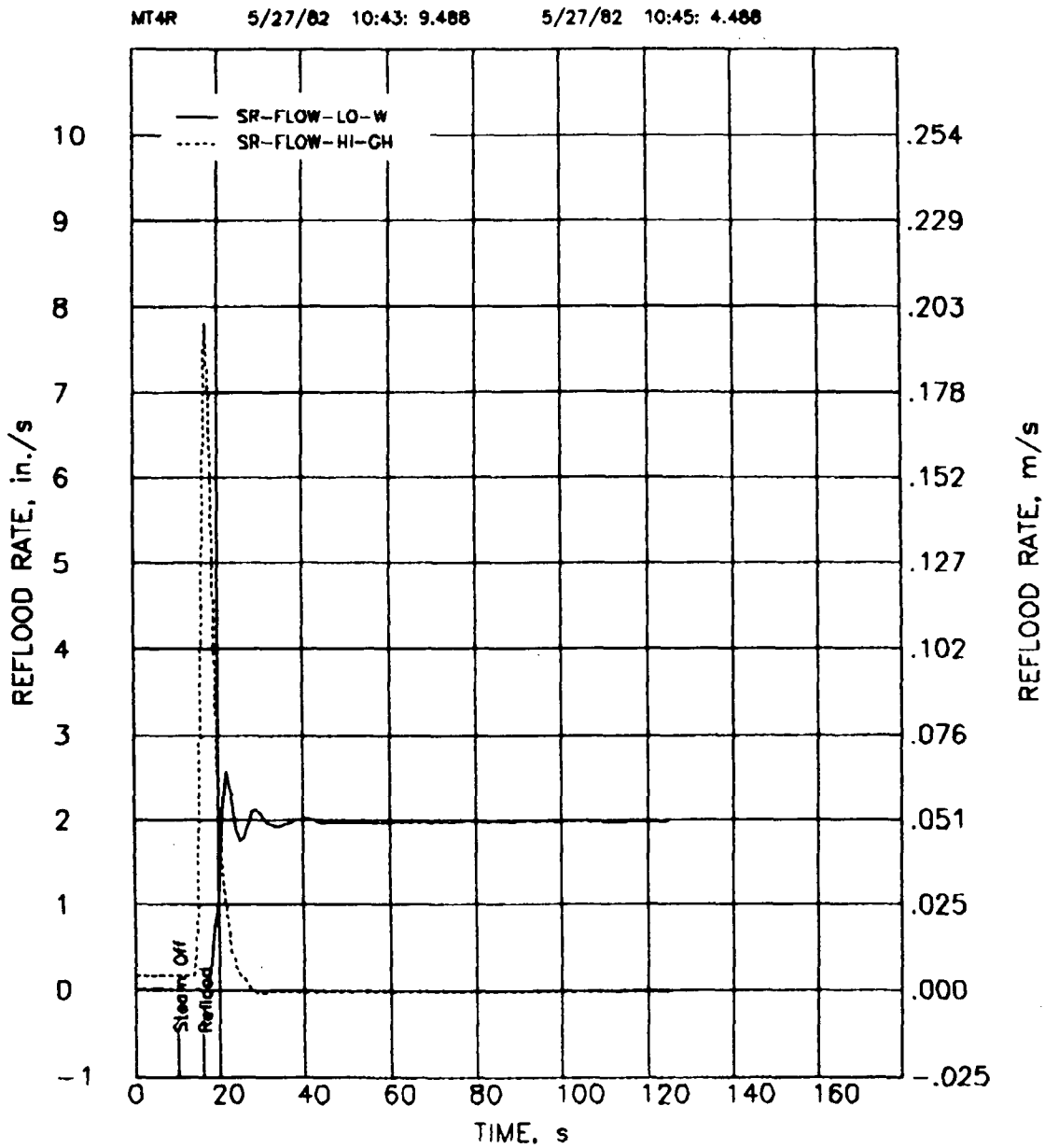

FIGURE F.1. Total Reflood Flow Rate for Reflood Calibration Test 1

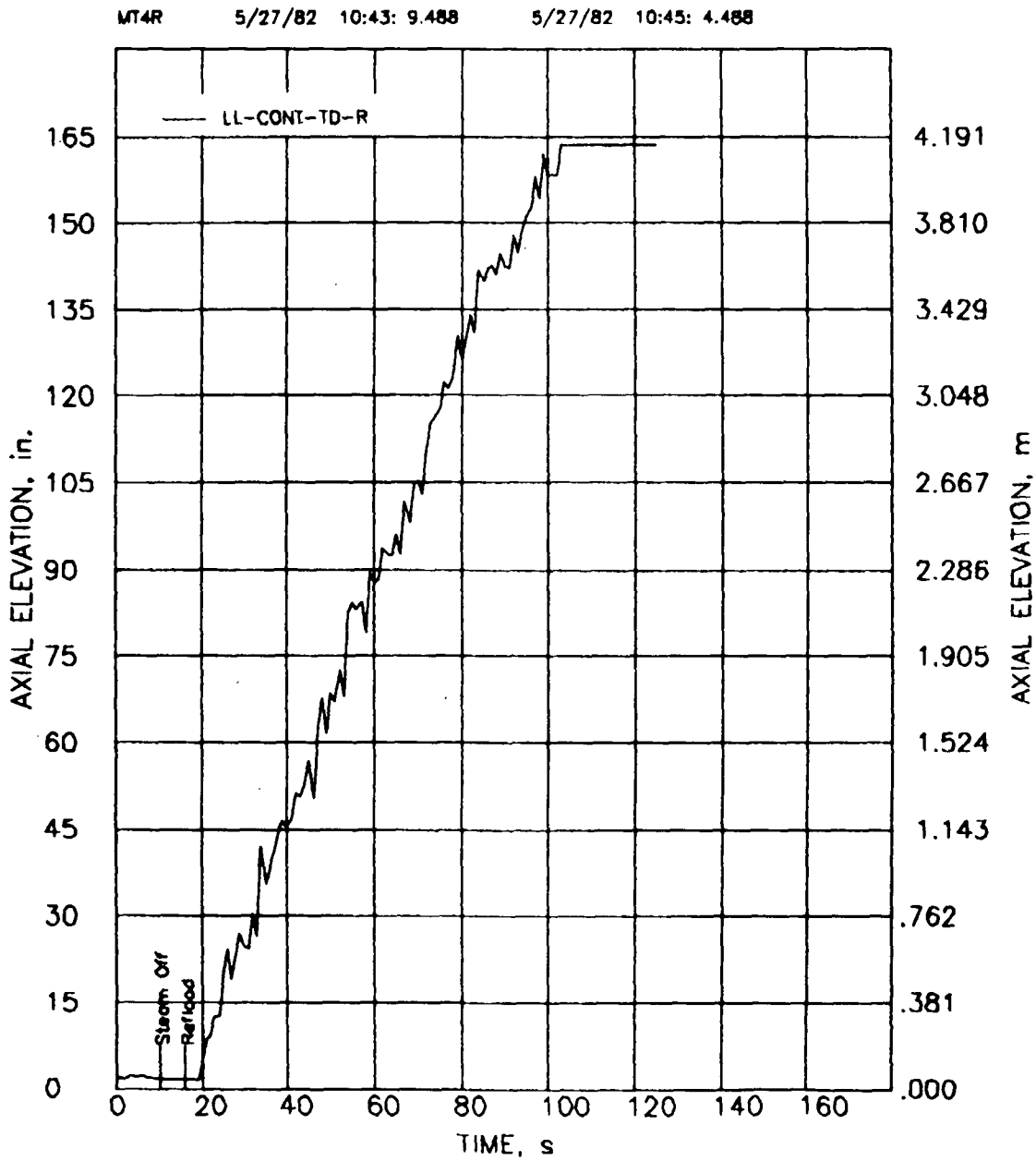

FIGURE F.2. Time Domain Reflectometry Response for Reflood Calibration Test 1

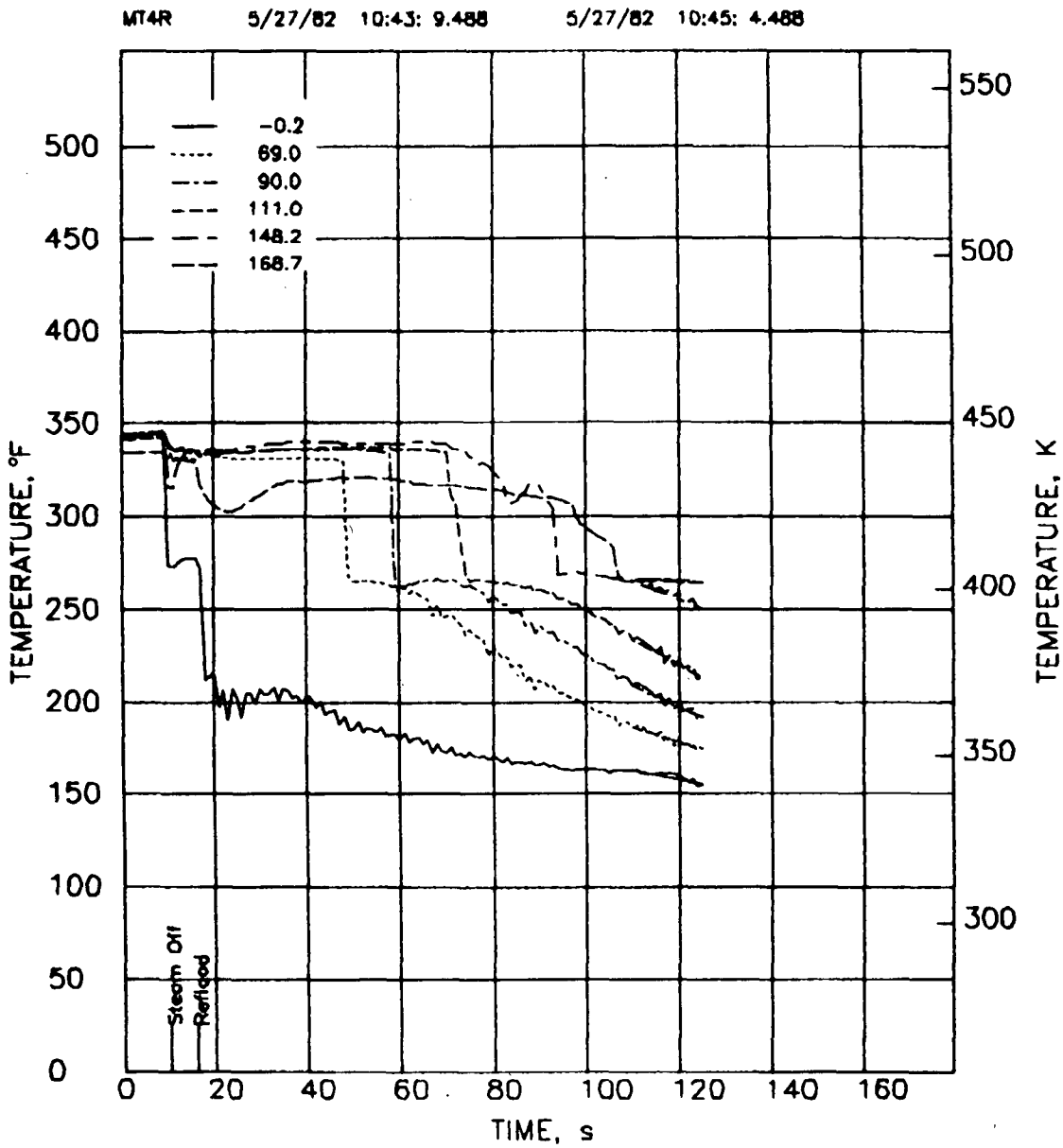

FIGURE F.3. Temperatures at Levels -0.2 Through 168.7 for Reflood Calibration Test 1

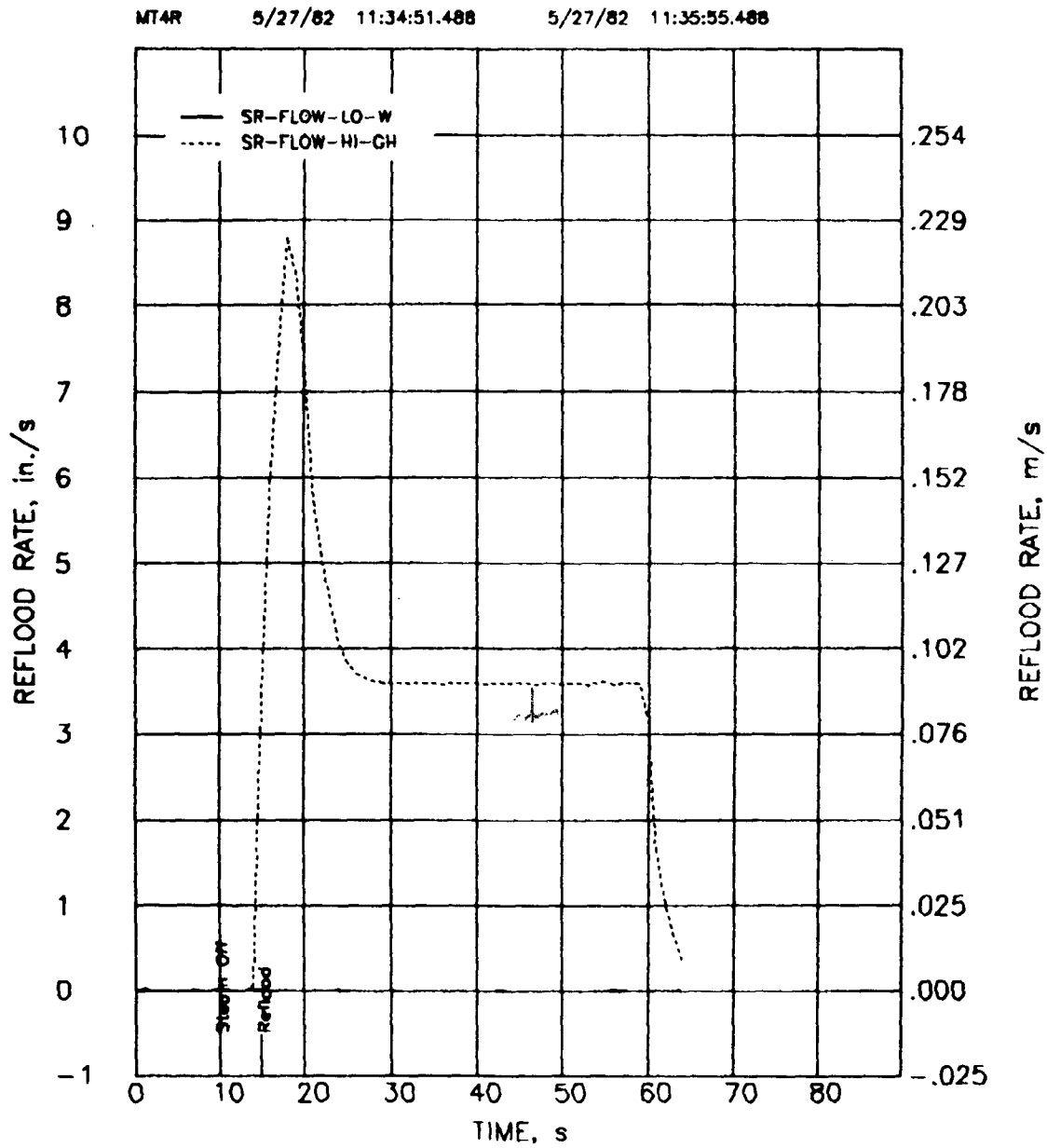

FIGURE F.4. Total Reflood Flow Rate for Reflood Calibration Test 2

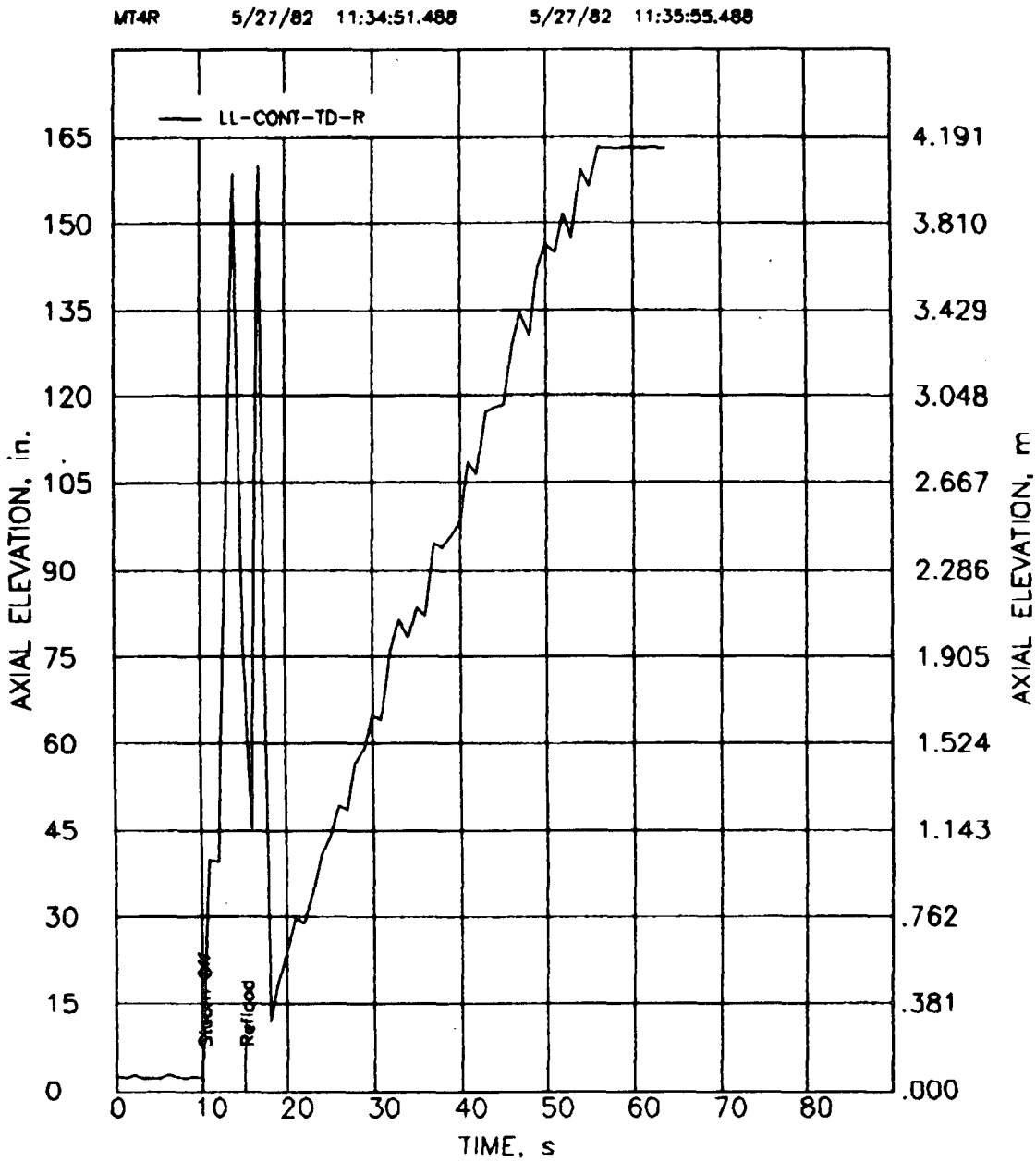

FIGURE F.5. Time Domain Reflectometry Response for Reflood Calibration Test 2

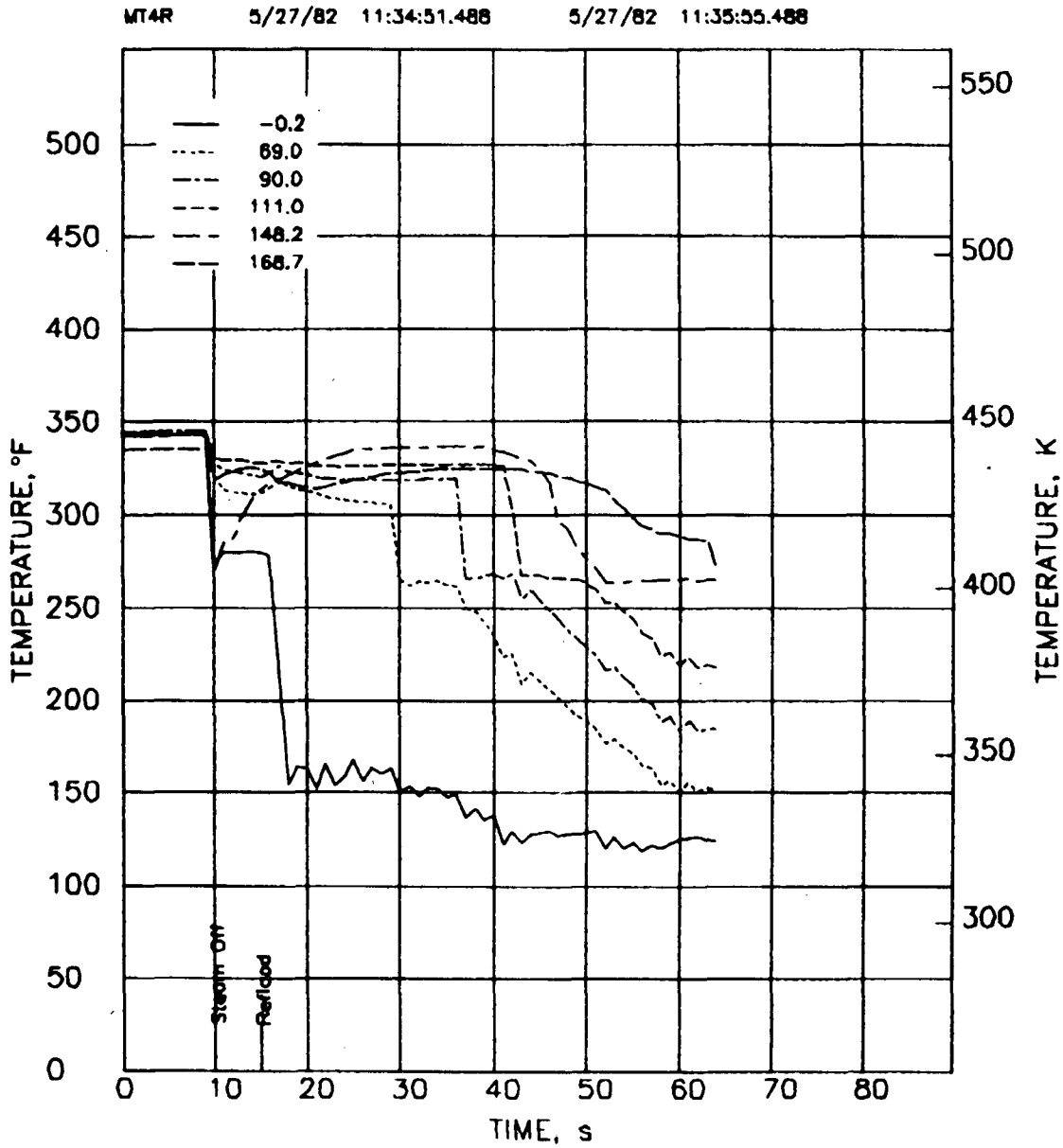

FIGURE F.6. Temperatures at Levels -0.2 Through 168.7 for Reflood Calibration Test 2

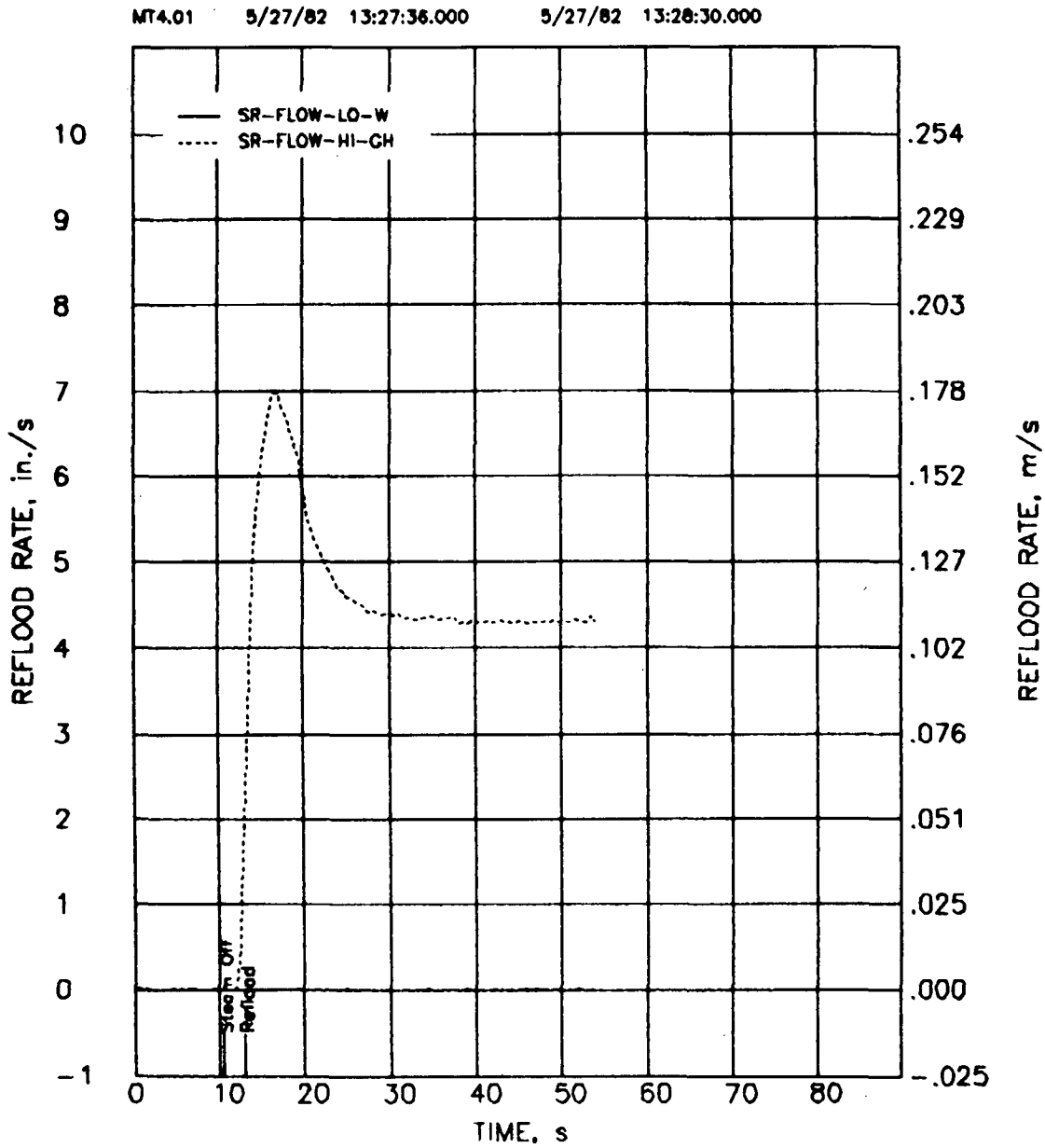

FIGURE F.7. Reflood Flow Rate for Reflood Calibration Test 3

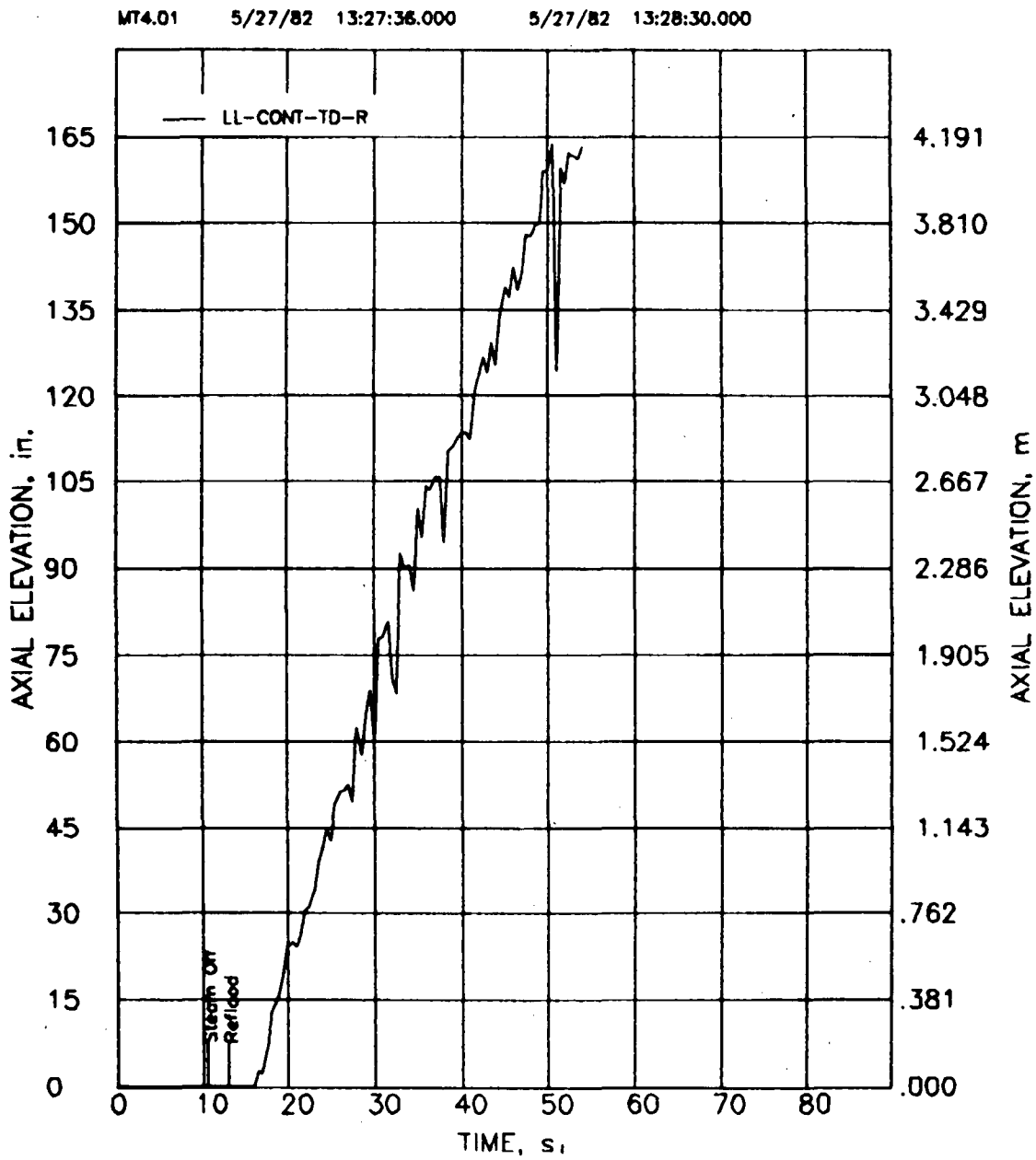

FIGURE F.8. Time Domain Reflectometry Response for Reflood Calibration Test 3

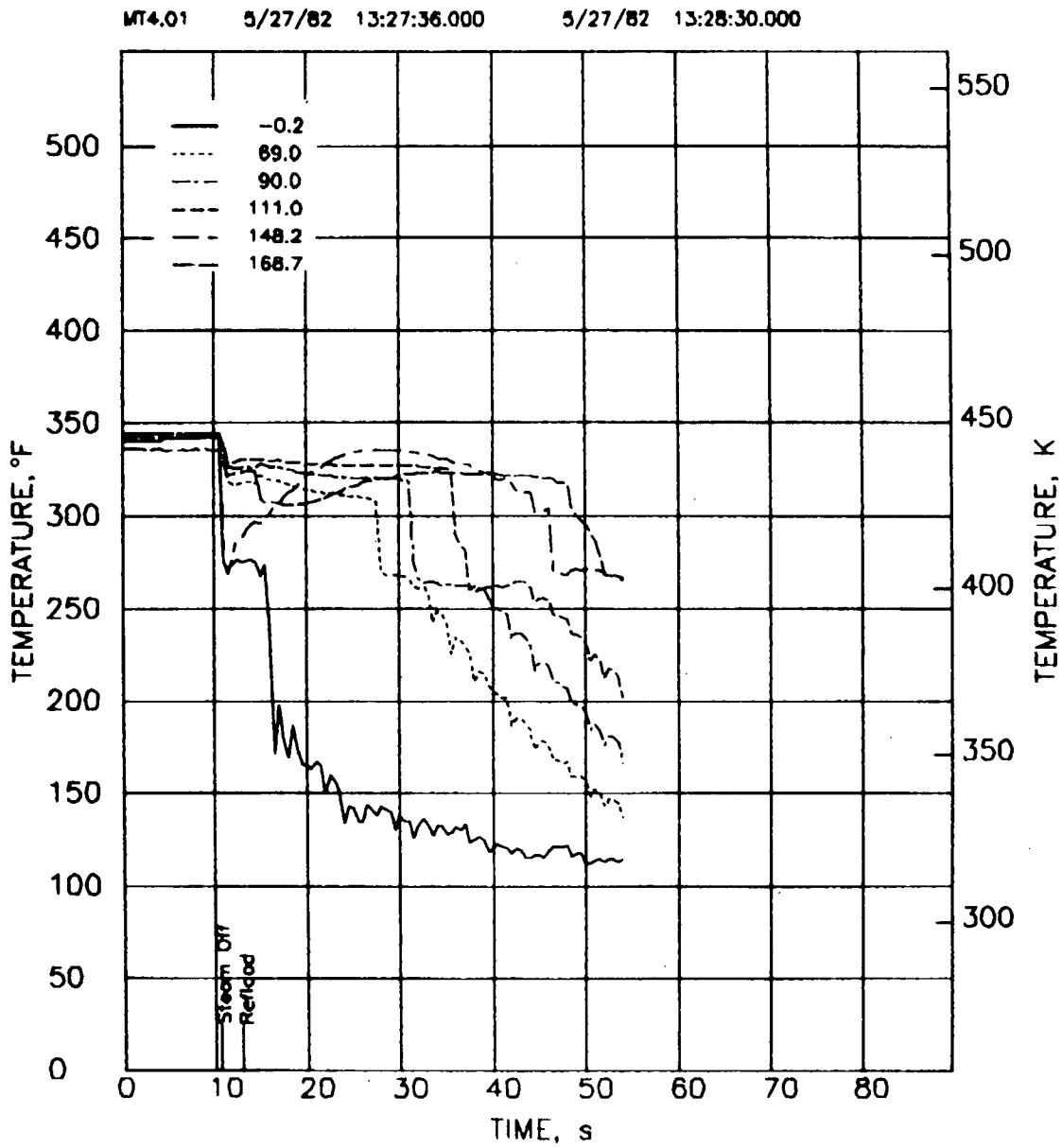

FIGURE F.9. Temperatures at Levels -0.2 Through 168.7 for Reflood Calibration Test 3

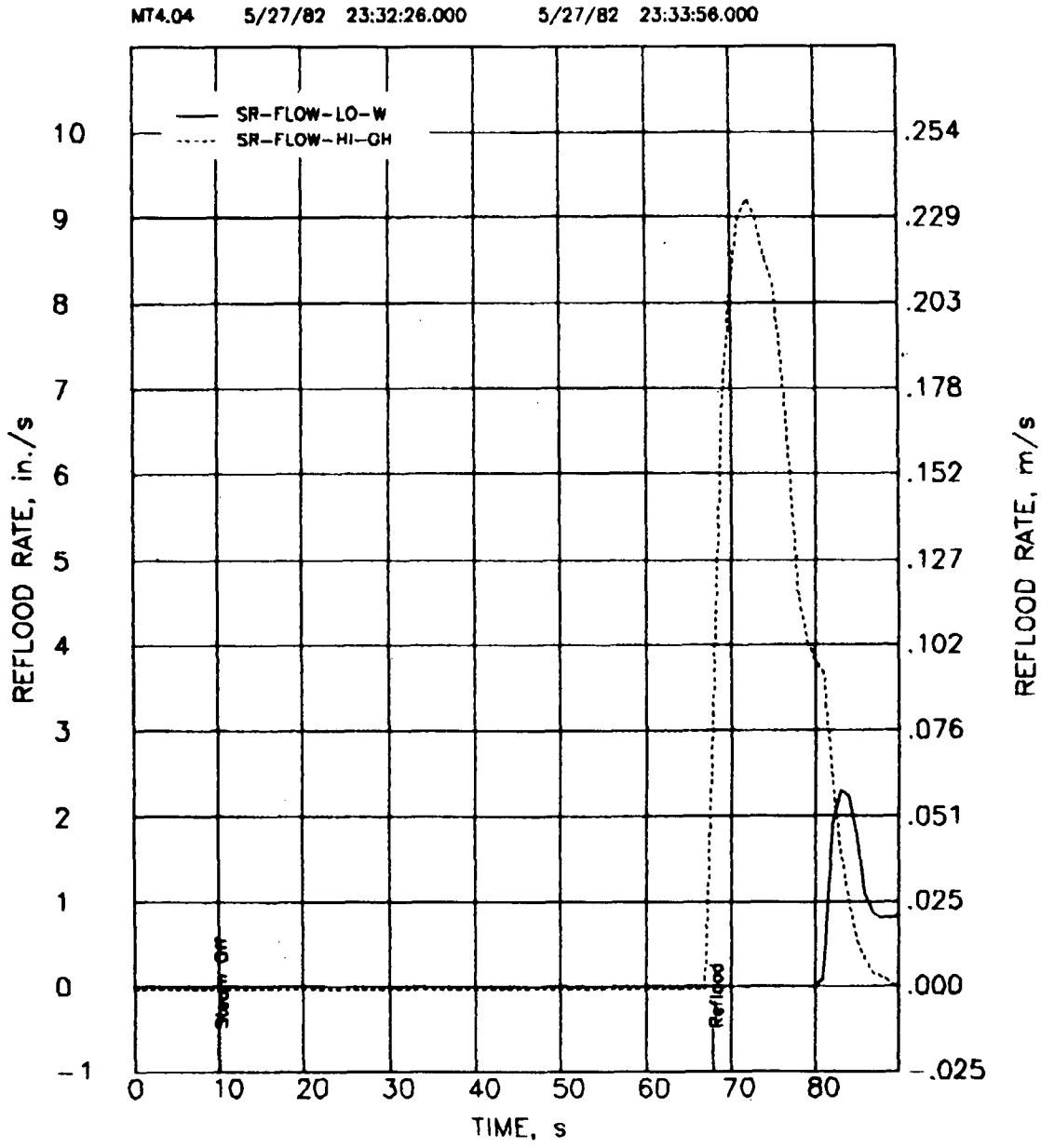

FIGURE F.10. Total Reflood Flow Rate for First 90 s of MT-4.04

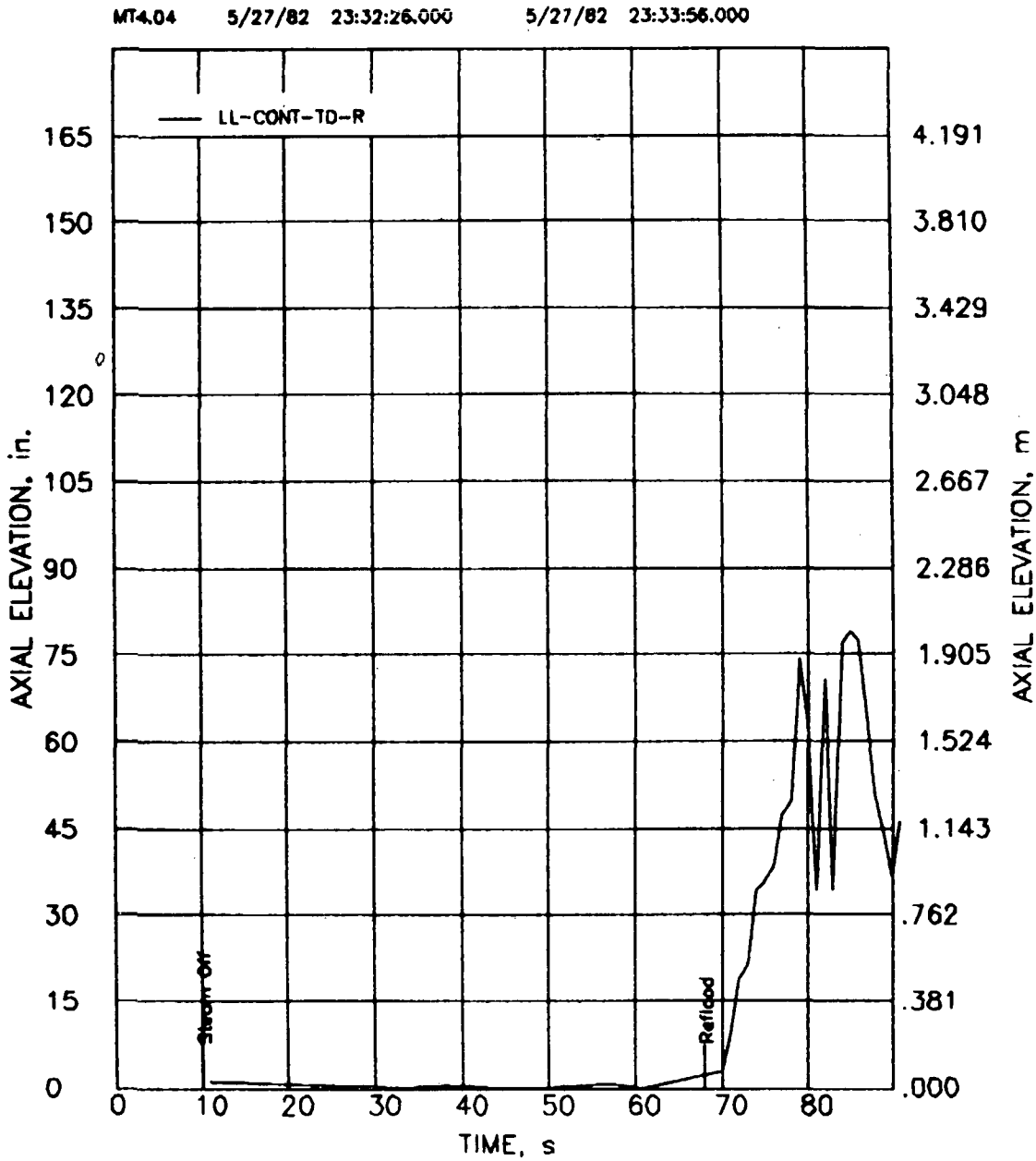

FIGURE F.11. Time Domain Reflectometry Response for First 90 s of MT-4.04

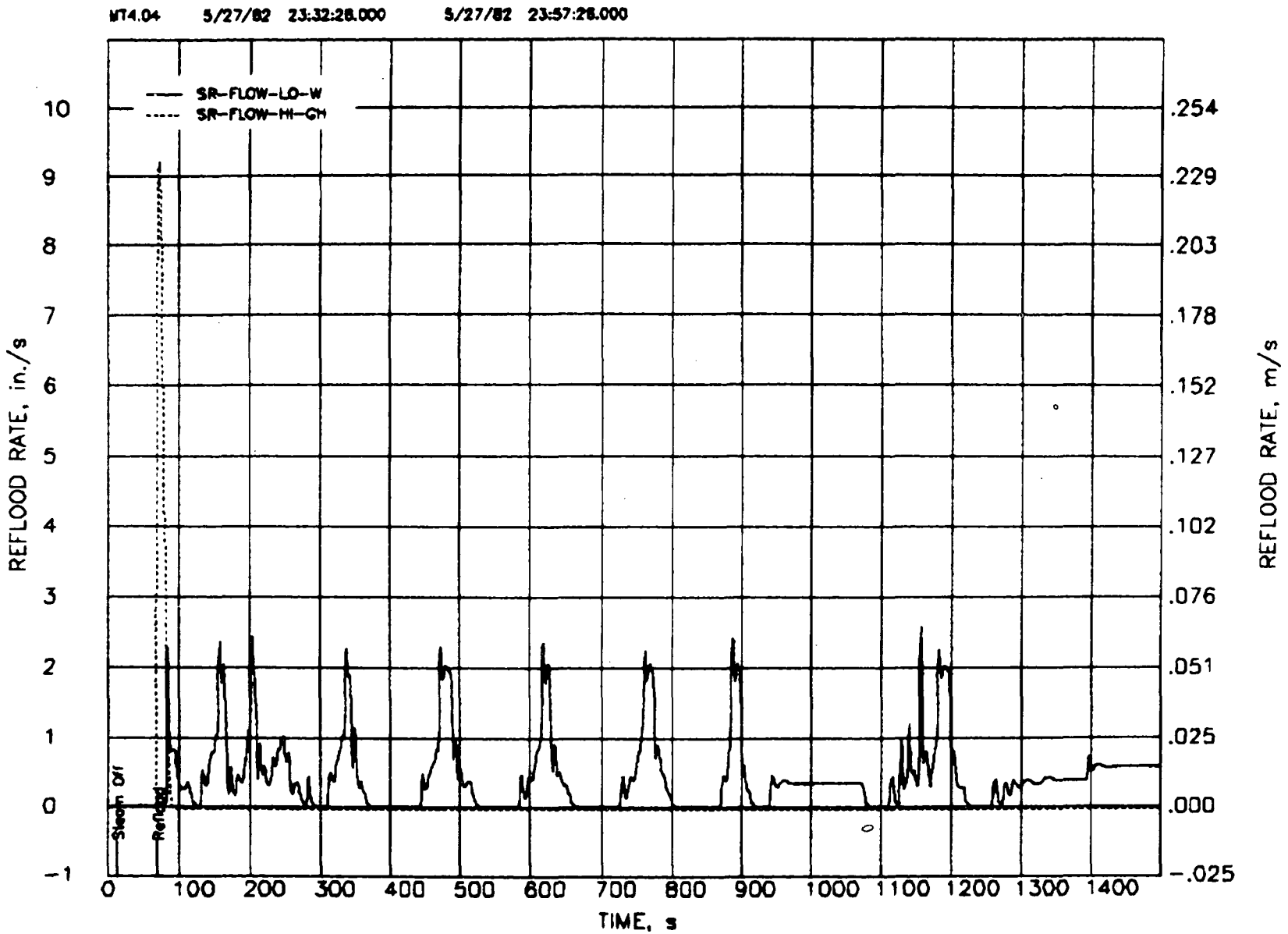

FIGURE F.12. Total Reflood Flow Rate for 1500 s of MT-4.04

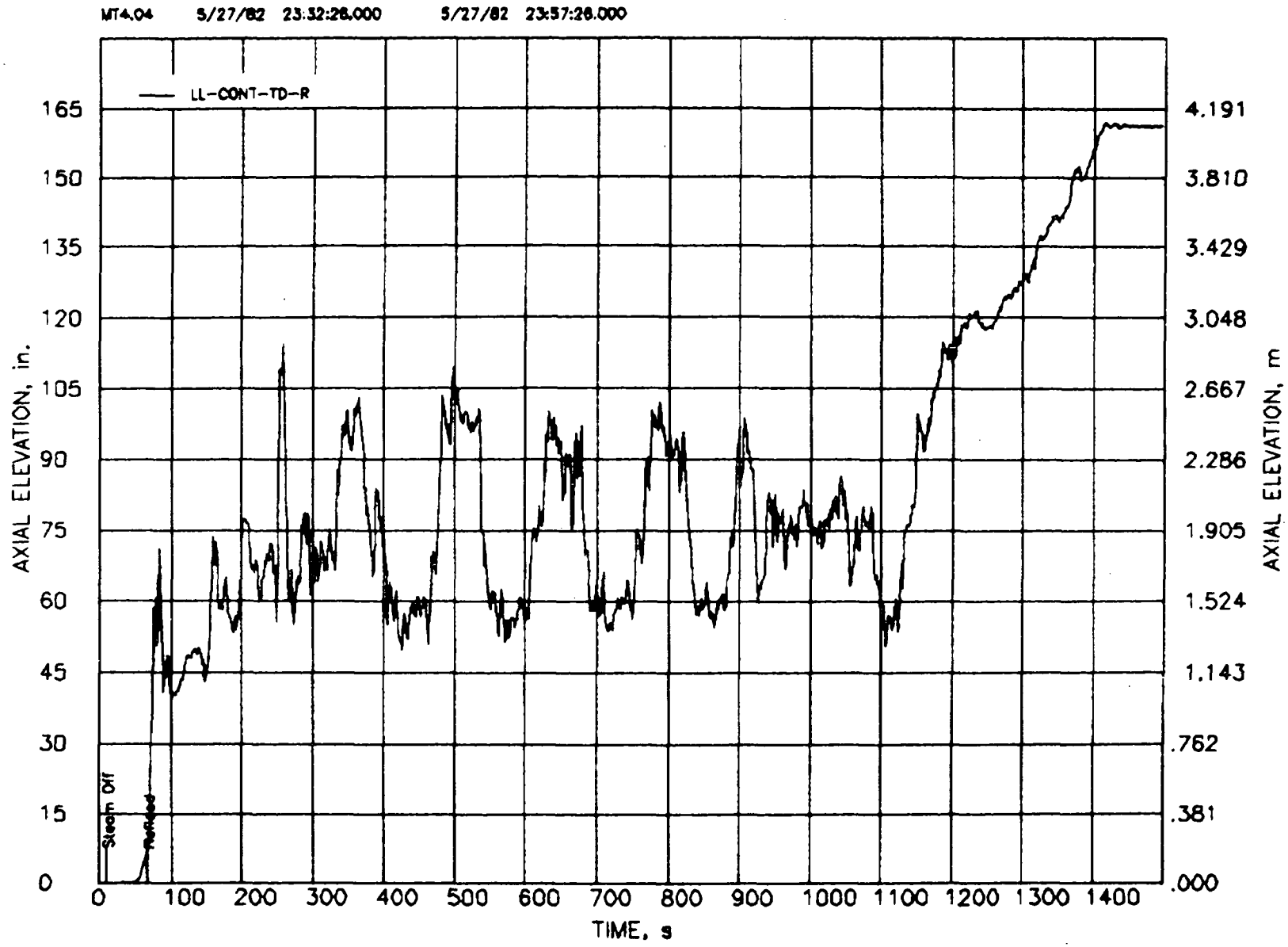

FIGURE F.13. Time Domain Reflectometry Response for 1500 s of MT-4.04

APPENDIX G

FUEL ROD DEFORMATION DATA

APPENDIX G

FUEL ROD DEFORMATION DATA

The MT-4 test assembly and fuel rod data were measured and computer-stored using the disassembly, examination, and reassembly machine (DERM). The computer-controlled DERM is designed to remotely perform these functions on radioactive test assembly components when they are available for postirradiation examination.

The test assembly was placed on the DERM for visual examination under 1.83 m (72 in.) of water in the Chalk River Nuclear Laboratories (CRNL) fuel rod bay. This appendix provides details of fuel rod deformation data. Single rod cross sections before and after deformation are shown in Figures G.1 through G.12. The axial distribution of average fuel rod diameter measurements for the bundle are shown in Figure G.13. The corresponding reduced flow area is shown in Figure G.14, and the corresponding average diametral strain is shown in Figure G.15. Diametral measurements along the length of the fuel rods are shown in Figures G.16 through G.27.

The remainder of this appendix consists of the following graphical data:

FIGURE G.1. Deformation Cross Sections of Test Rod 2C at Various Elevations

FIGURE G.2. Deformation Cross Sections of Test Rod 2D at Various Elevations

FIGURE G.3. Deformation Cross Sections of Test Rod 3B at Various Elevations

FIGURE G.4. Deformation Cross Sections of Test Rod 3C at Various Elevations

FIGURE G.5. Deformation Cross Sections of Test Rod 3D at Various Elevations

FIGURE G.6. Deformation Cross Sections of Test Rod 3E at Various Elevations

FIGURE G.7. Deformation Cross Sections of Test Rod 4B at Various Elevations

FIGURE G.8. Deformation Cross Sections of Test Rod 4C at Various Elevations

FIGURE G.9. Deformation Cross Sections of Test Rod 4D at Various Elevations

FIGURE G.10. Deformation Cross Sections of Test Rod 4E at Various Elevations

FIGURE G.11. Deformation Cross Sections of Test Rod 5C at Various Elevations

FIGURE G.12. Deformation Cross Sections of Test Rod 5D at Various Elevations

FIGURE G.13. Axial Distribution of Average Diametral Measurements for MT-4 Test Bundle

FIGURE G.14. Axial Distribution of Reduced Flow Area for MT-4 Test Bundle

FIGURE G.15. Axial Distribution of Average Diametral Strain Measurements for the MT-4 Test Bundle

FIGURE G.16. Axial Distribution of Diametral Measurements for Test Rod 2C

FIGURE G.17. Axial Distribution of Diametral Measurements for Test Rod 2D

FIGURE G.18. Axial Distribution of Diametral Measurements for Test Rod 3B

FIGURE G.19. Axial Distribution of Diametral Measurements for Test Rod 3C

FIGURE G.20. Axial Distribution of Diametral Measurements for Test Rod 3D

FIGURE G.21. Axial Distribution of Diametral Measurements for Test Rod 3E

FIGURE G.22. Axial Distribution of Diametral Measurements for Test Rod 4B

FIGURE G.23. Axial Distribution of Diametral Measurements for Test Rod 4C

FIGURE G.24. Axial Distribution of Diametral Measurements for Test Rod 4D

FIGURE G.25. Axial Distribution of Diametral Measurements for Test Rod 4E

FIGURE G.26. Axial Distribution of Diametral Measurements for Test Rod 5C

FIGURE G.27. Axial Distribution of Diametral Measurements for Test Rod 5D

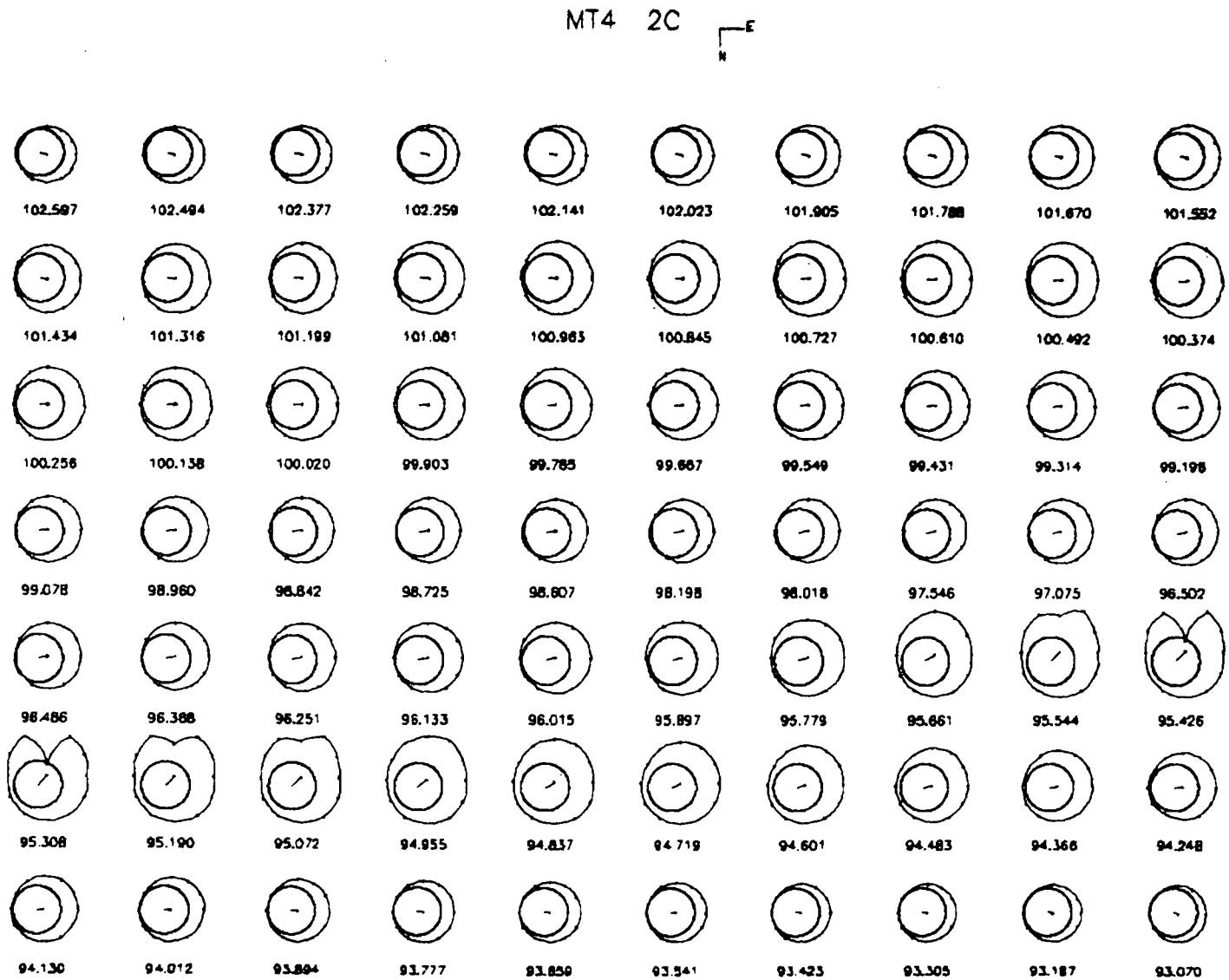

FIGURE G.1. Deformation Cross Sections of Test Rod 2C at Various Elevations

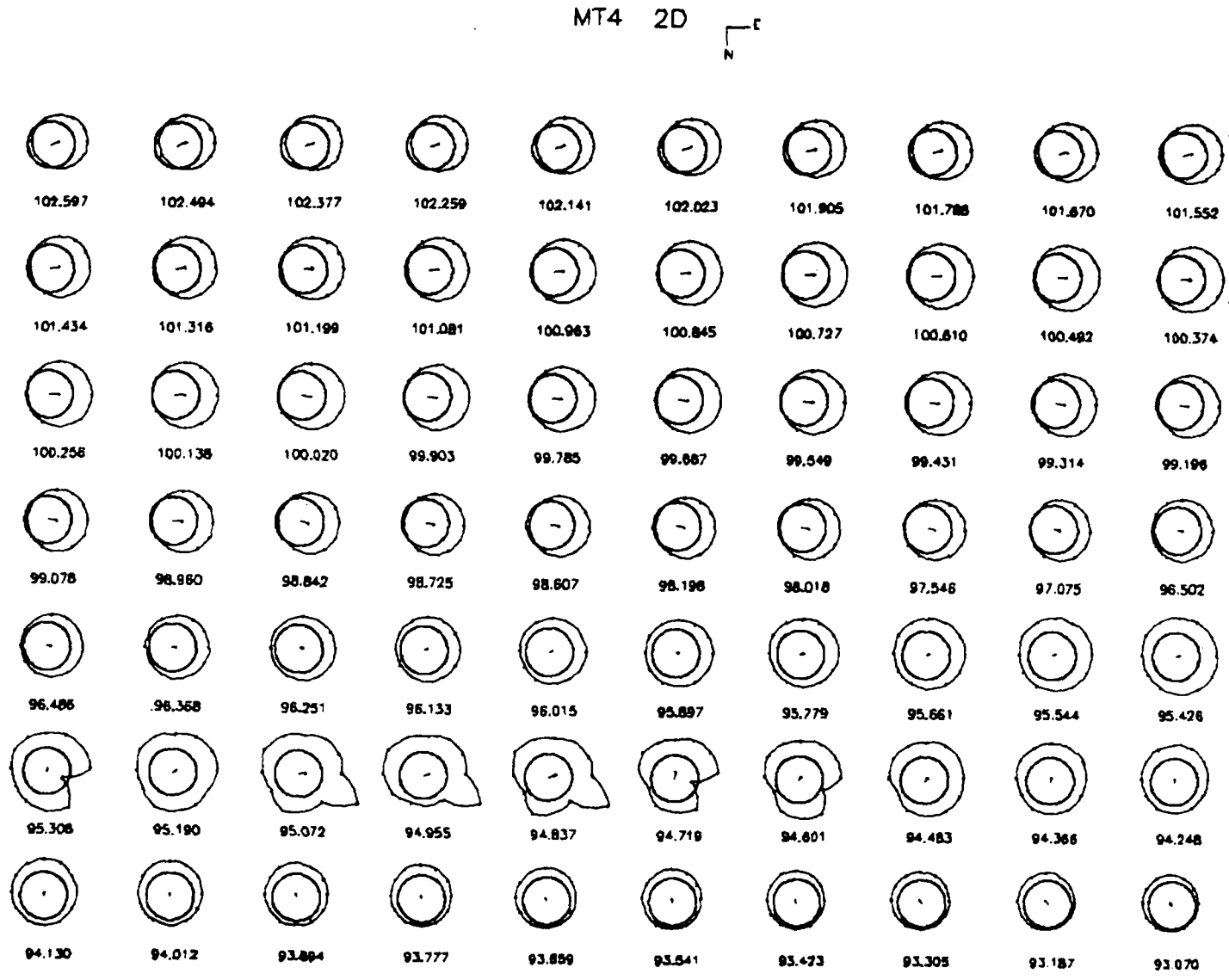

FIGURE G.2. Deformation Cross Sections of Test Rod 2D at Various Elevations

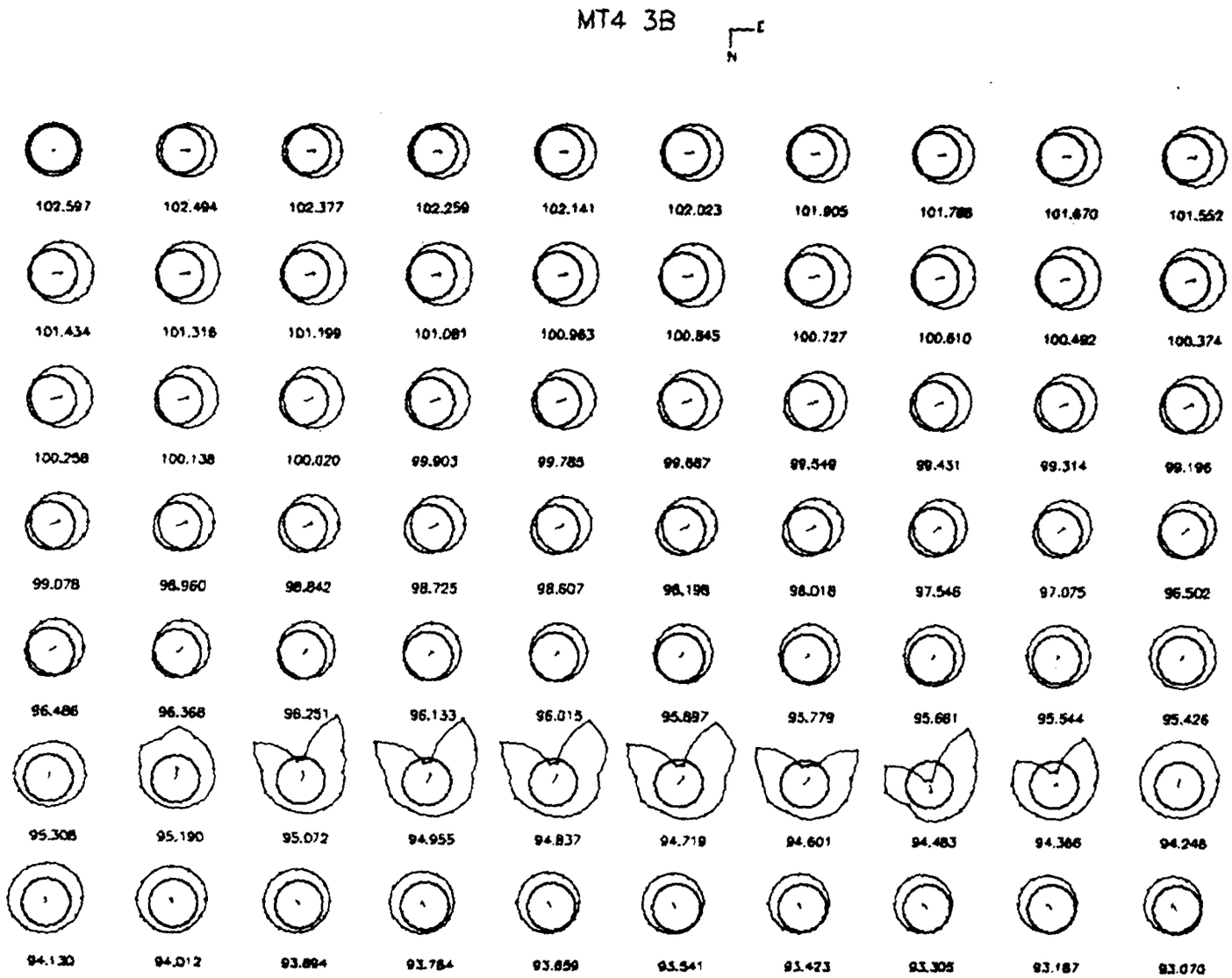

FIGURE G.3. Deformation Cross Sections of Test Rod 3B at Various Elevations

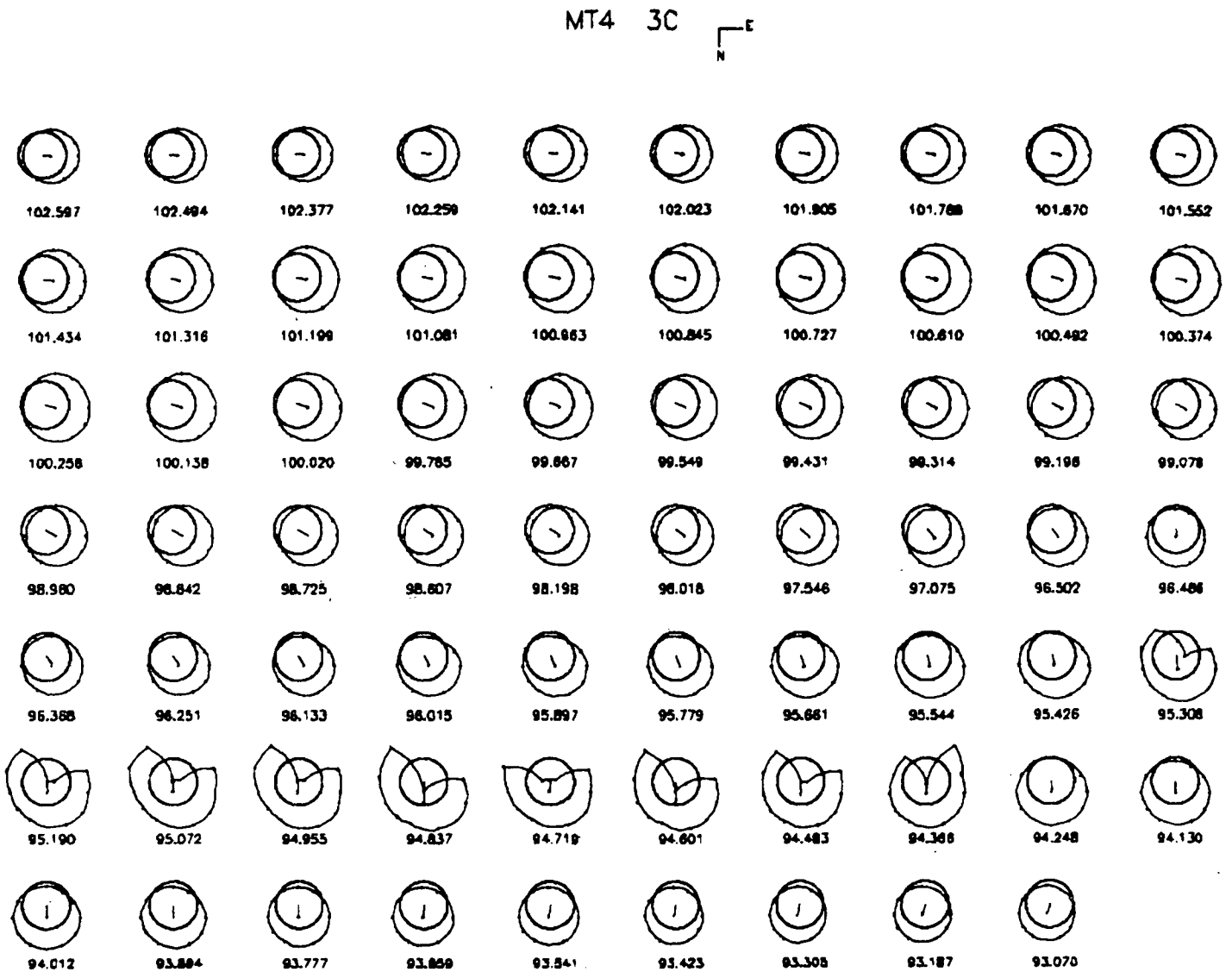

FIGURE G.4. Deformation Cross Sections of Test Rod 3C at Various Elevations

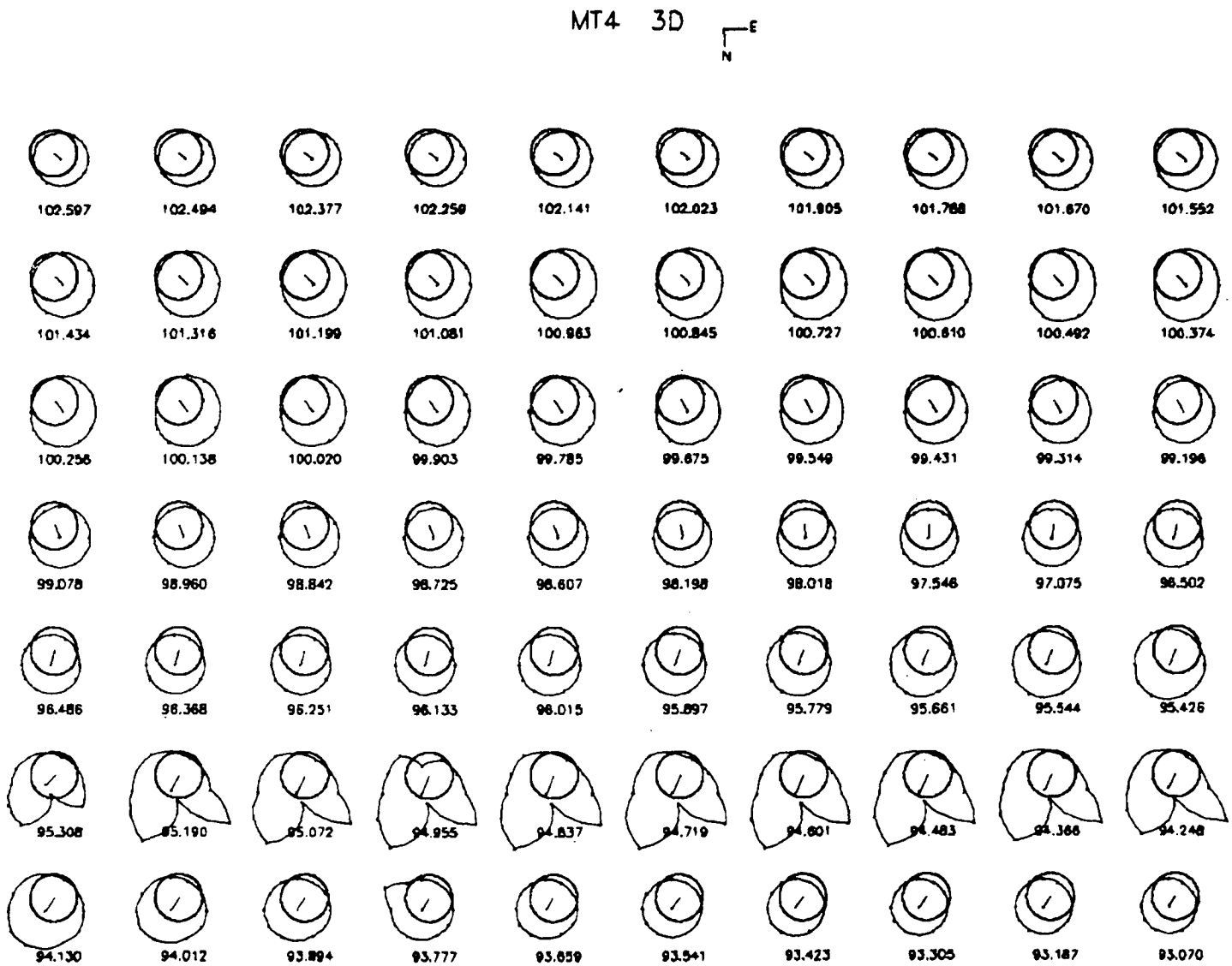

FIGURE G.5. Deformation Cross Sections of Test Rod 3D at Various Elevations

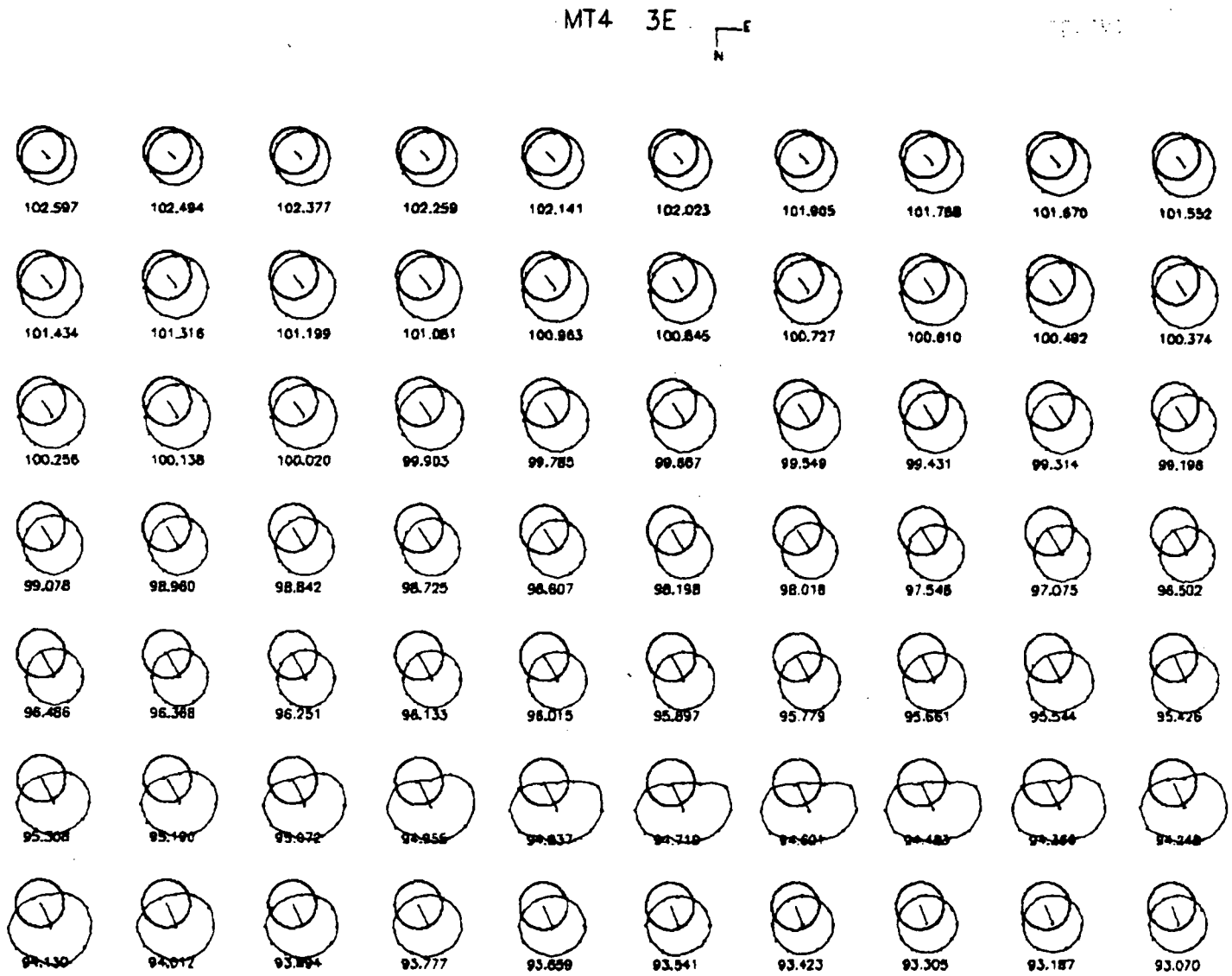

FIGURE G.6. Deformation Cross Sections of Test Rod 3E at Various Elevations

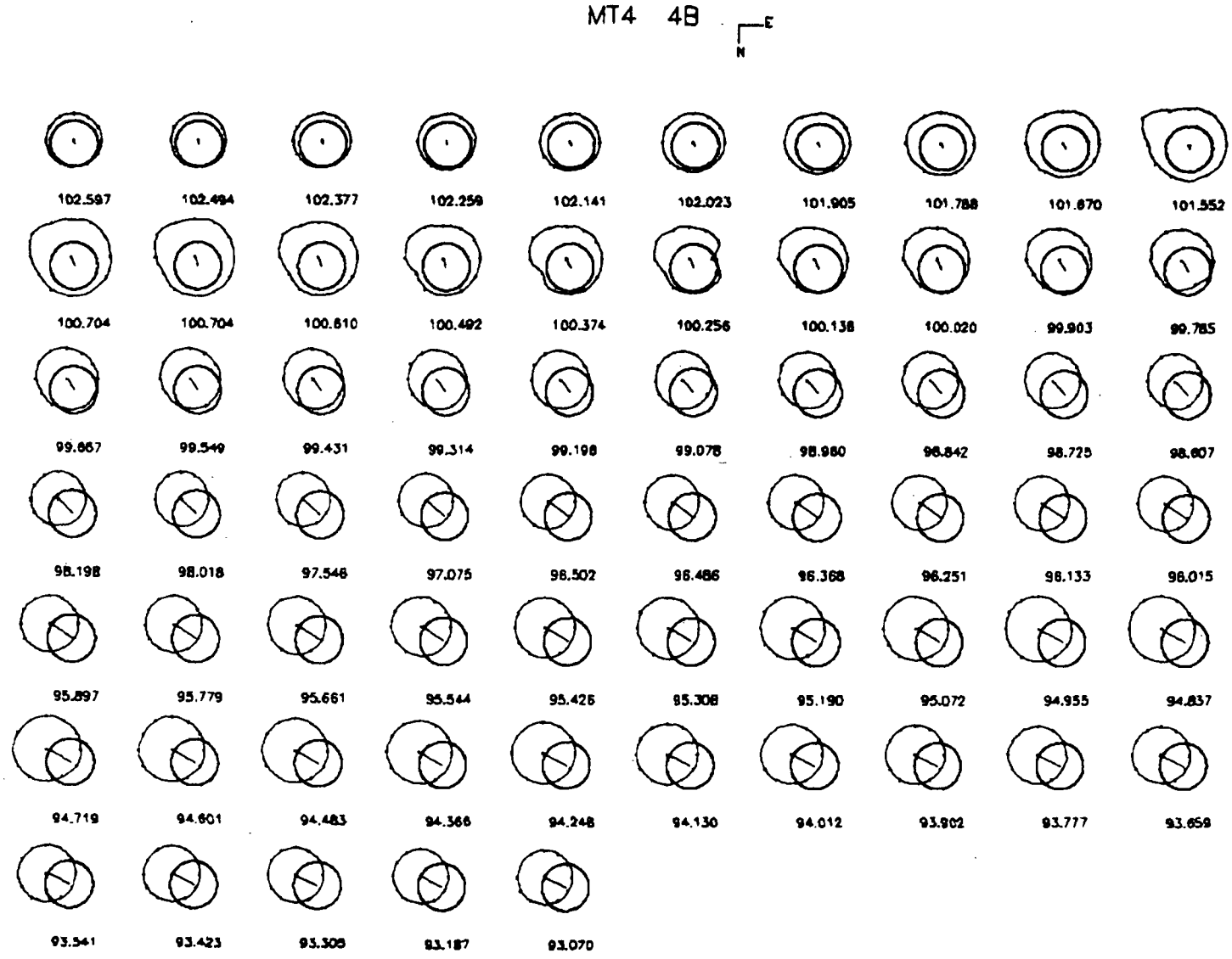

FIGURE G.7. Deformation Cross Sections of Test Rod 4B at Various Elevations

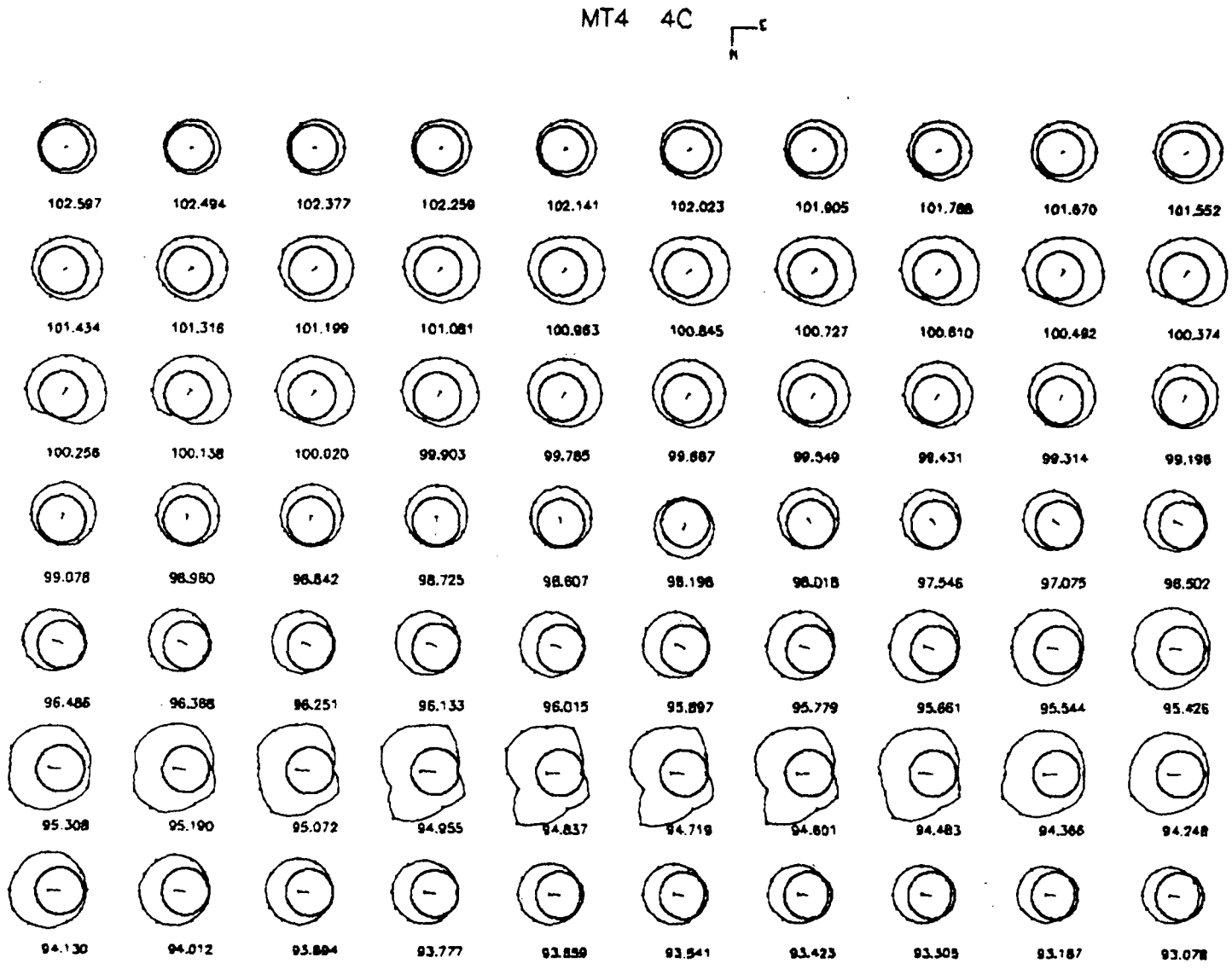

FIGURE G.8. Deformation Cross Sections of Test Rod 4C at Various Elevations

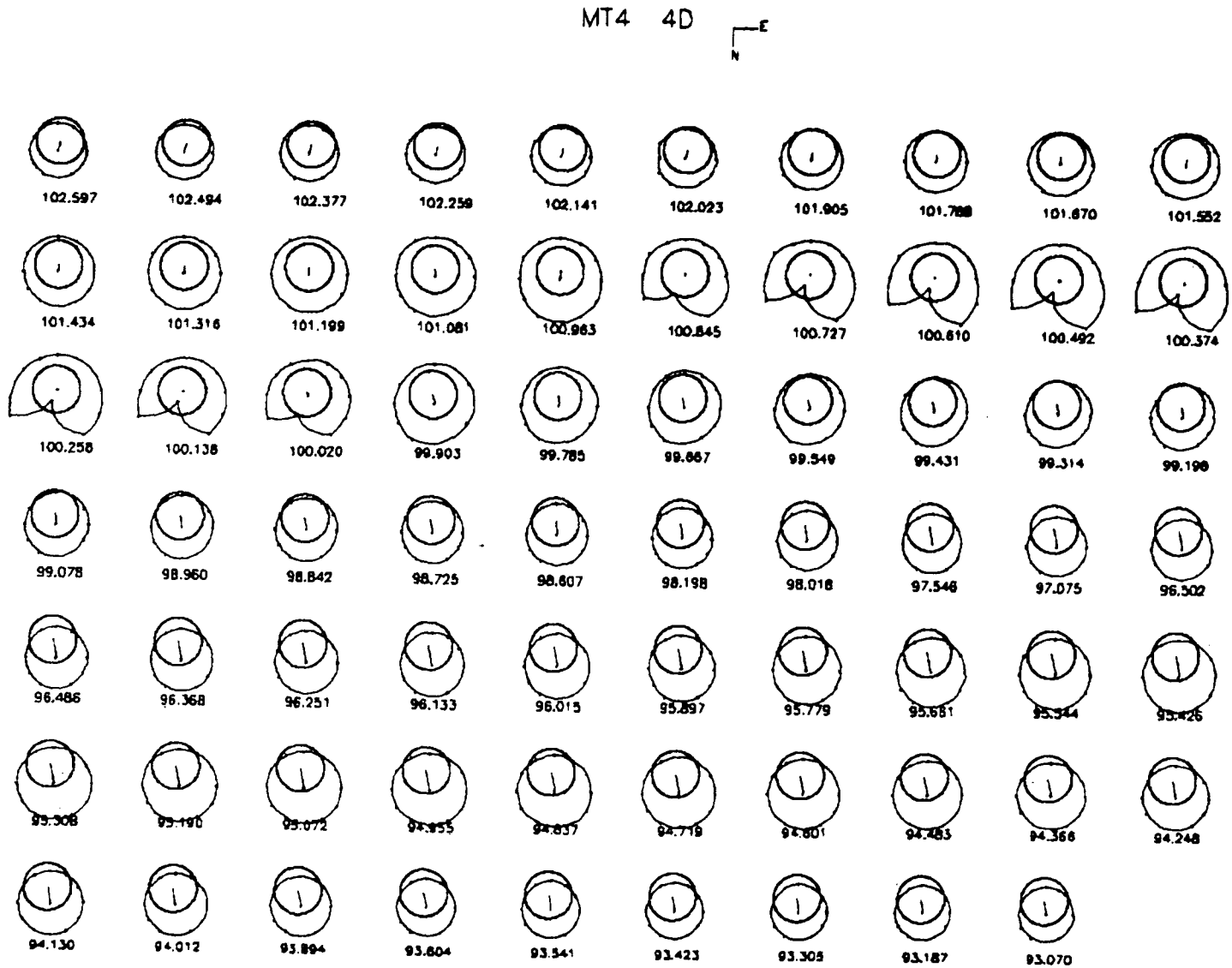

FIGURE G.9. Deformation Cross Sections of Test Rod 4D at Various Elevations

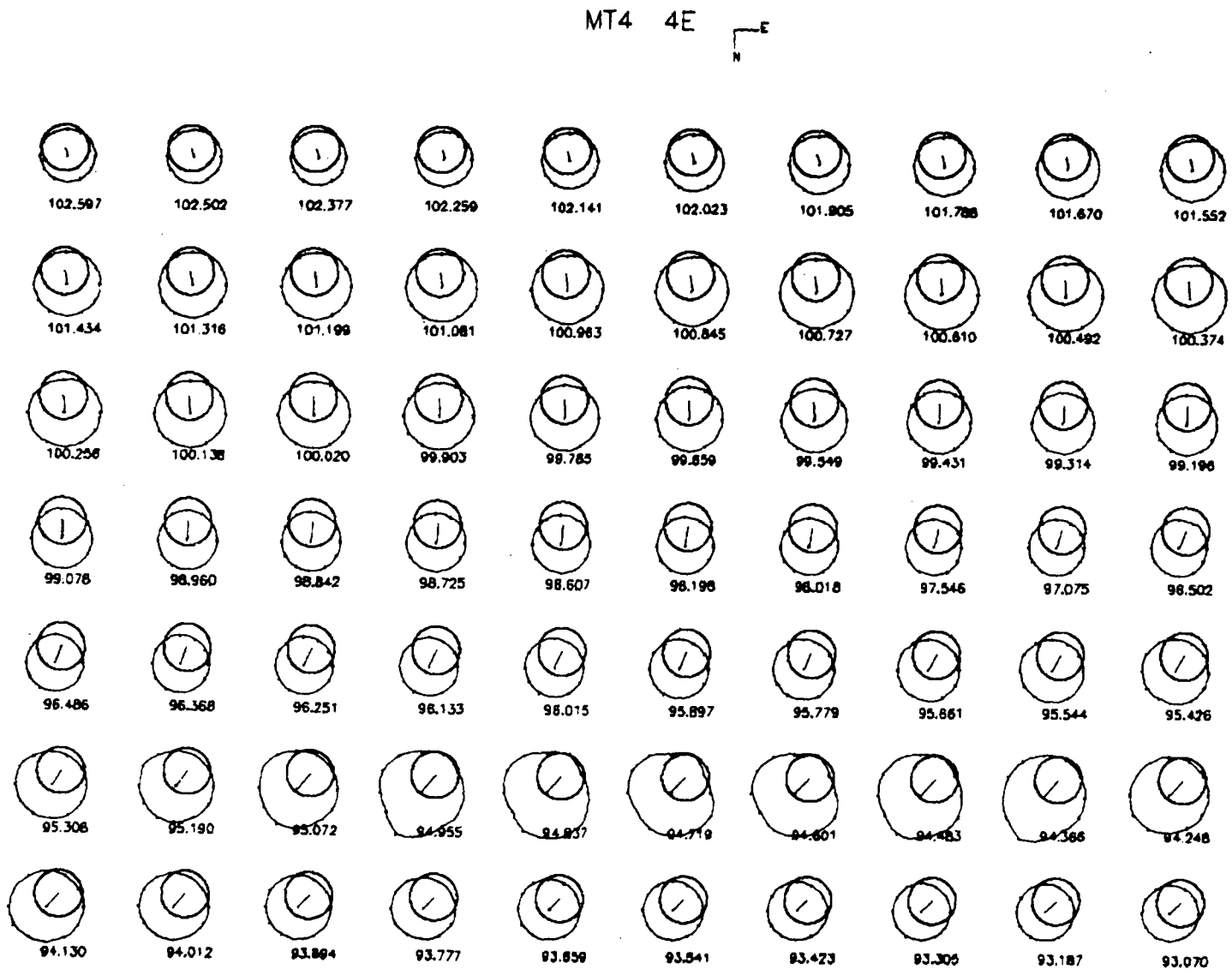

FIGURE G.10. Deformation Cross Sections of Test Rod 4E at Various Elevations

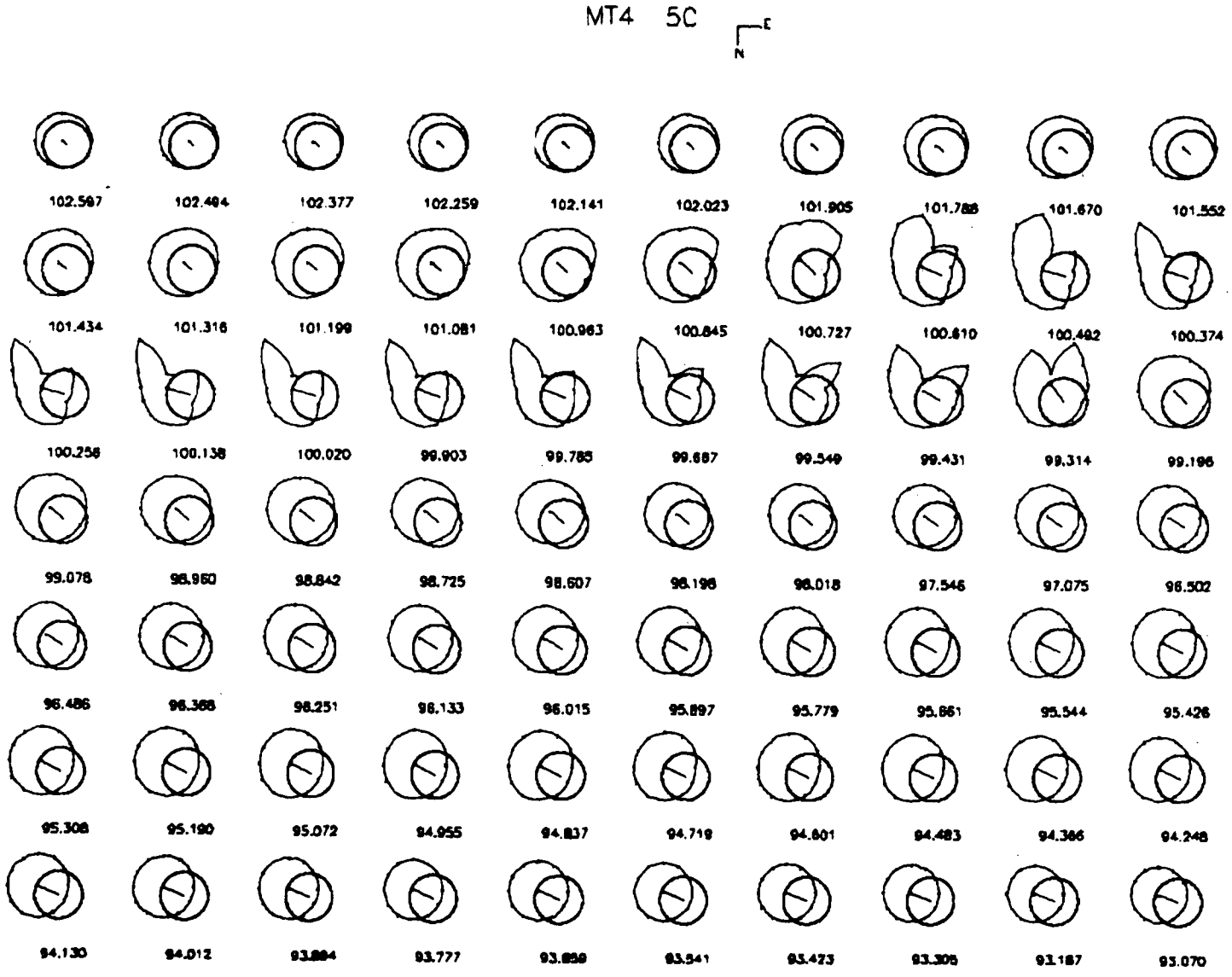

FIGURE G.11. Deformation Cross Sections of Test Rod 5C at Various Elevations

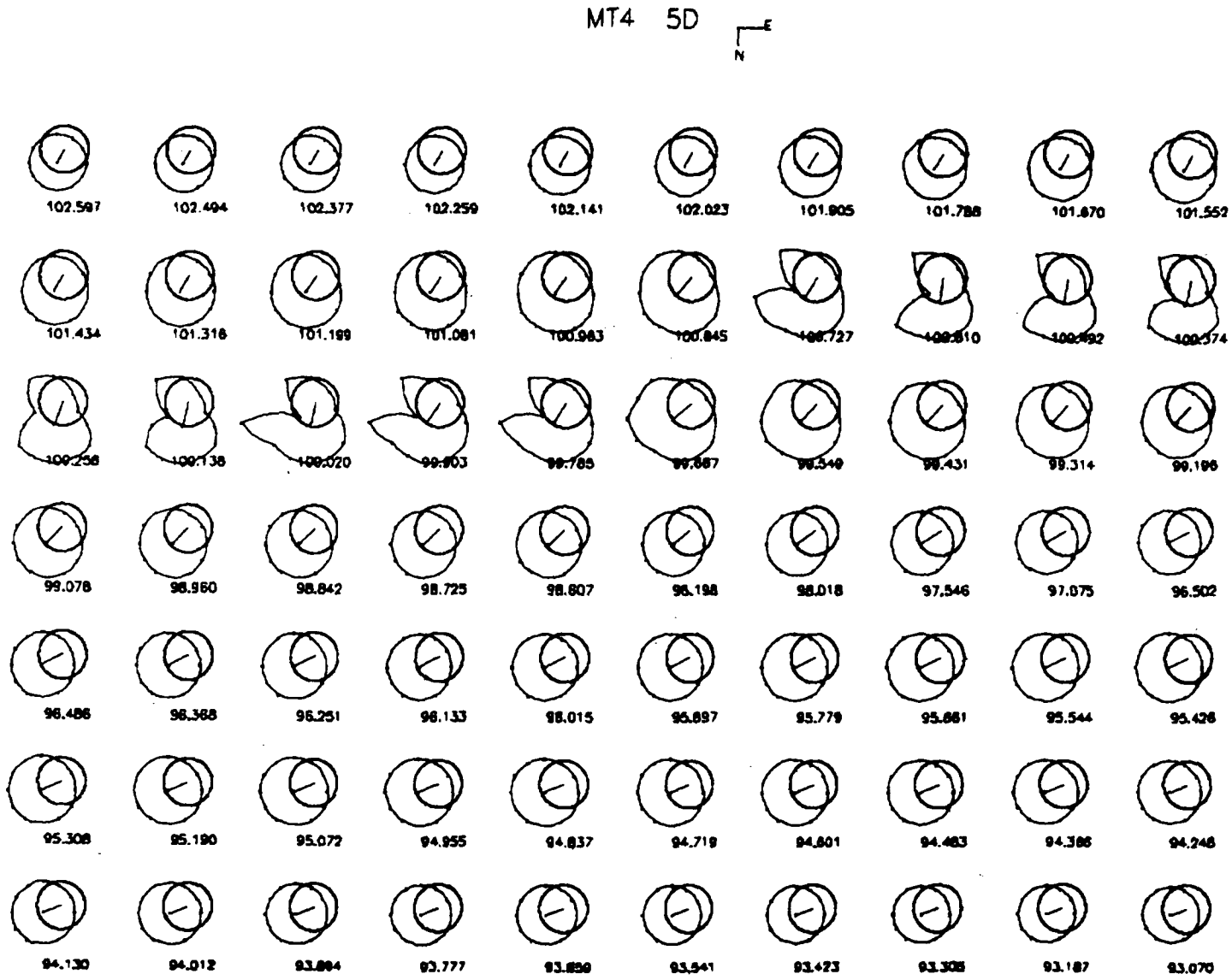

FIGURE G.12. Deformation Cross Sections of Test Rod 5D at Various Elevations

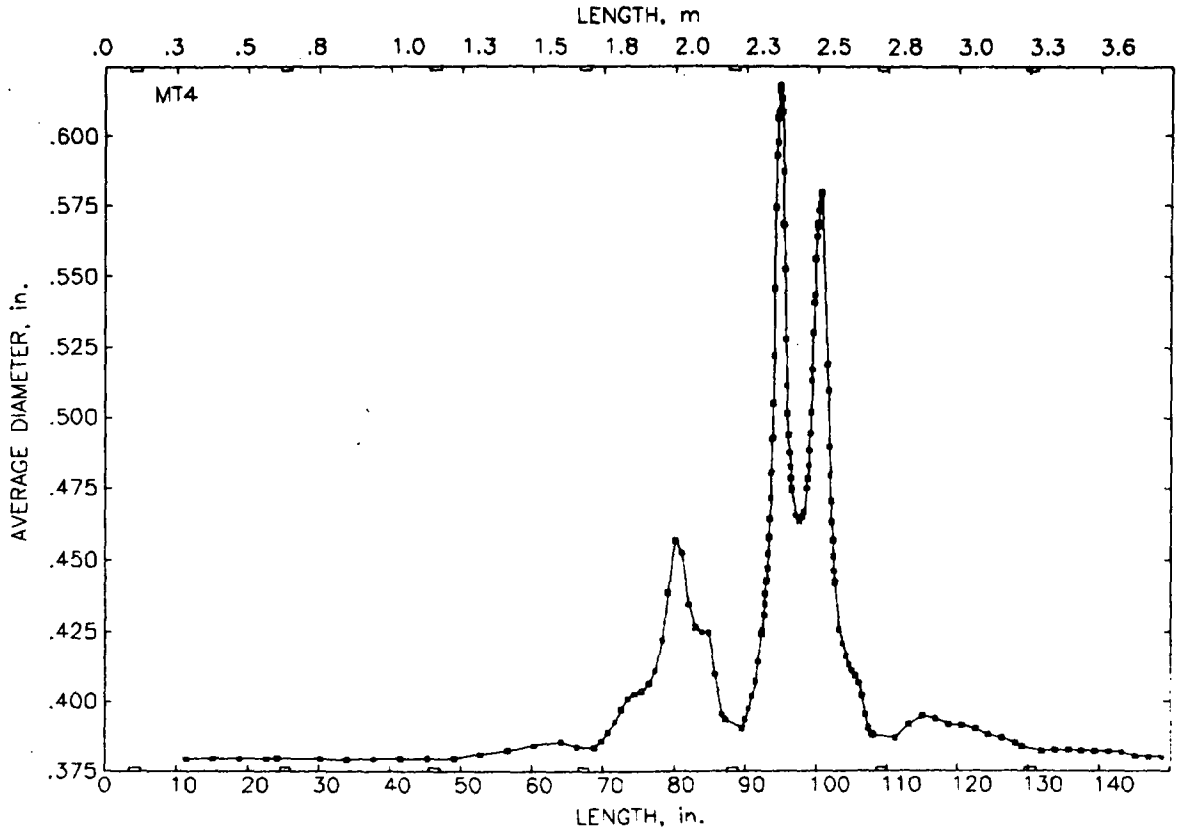

FIGURE G.13. Axial Distribution of Average Diametral Measurements for MT-4 Test Bundle

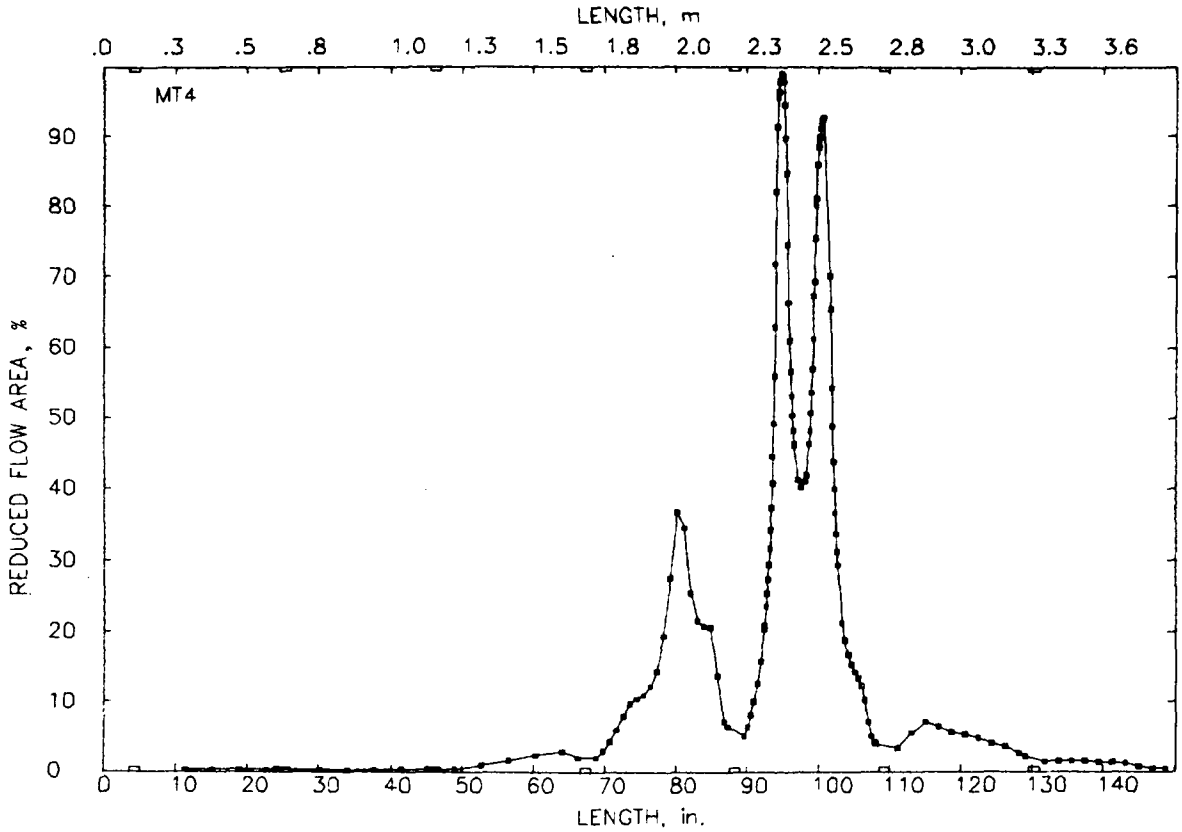

FIGURE G.14. Axial Distribution of Reduced Area for MT-4 Test Bundle (based on test rod flow area)

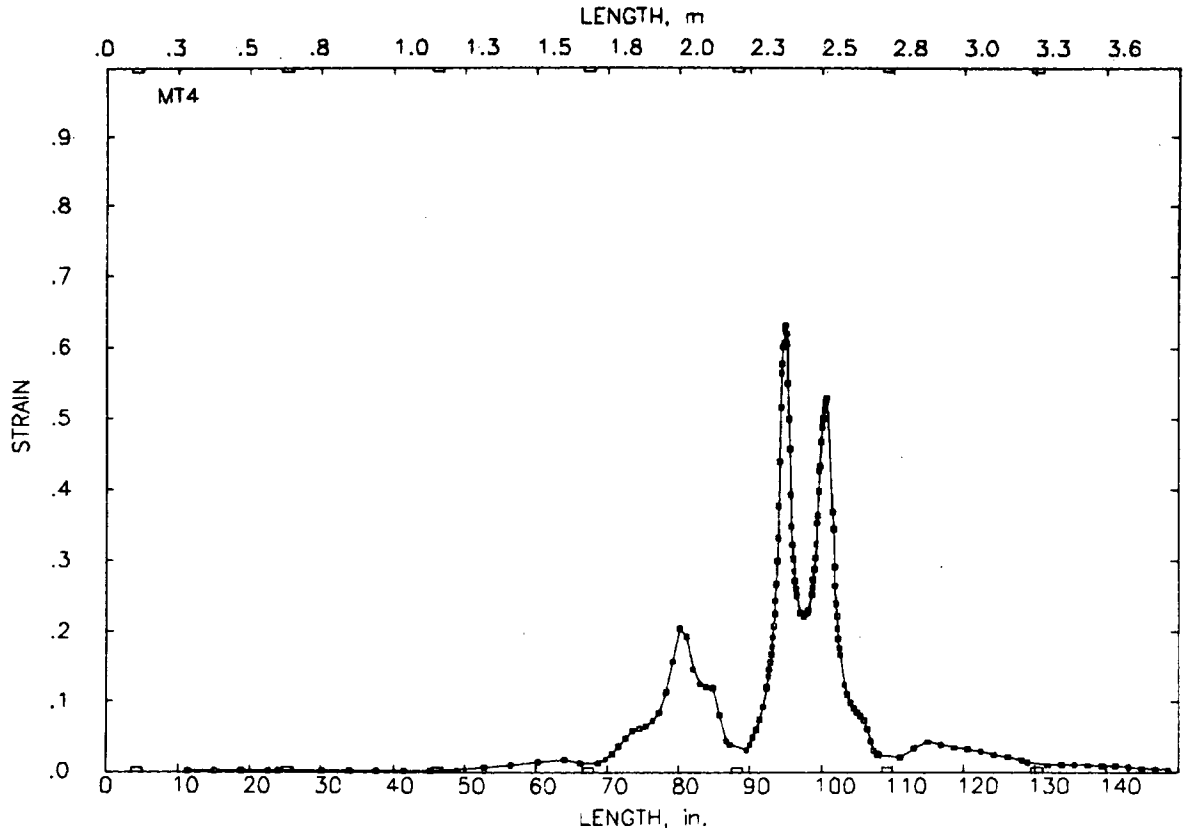

FIGURE G.15. Axial Distribution of Average Diametral Strain Measurements for the MT-4 Test Bundle

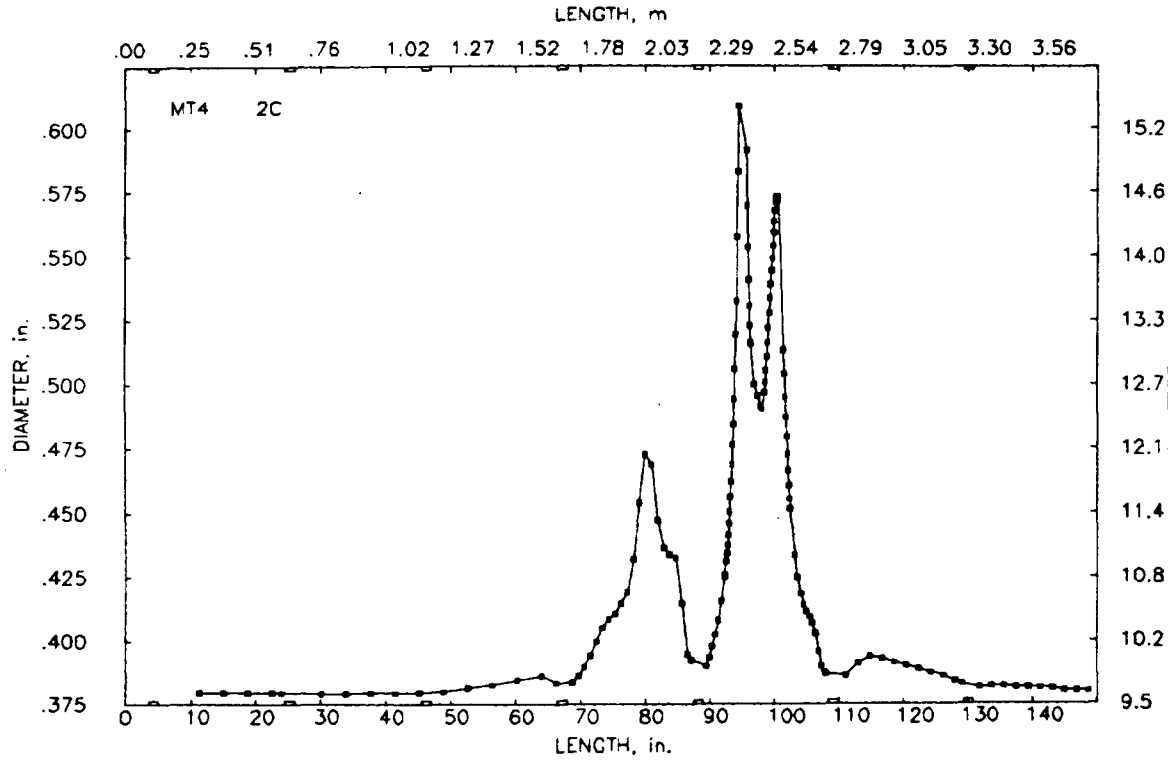

FIGURE G.16. Axial Distribution of Diametral Measurements for Test Rod 2C

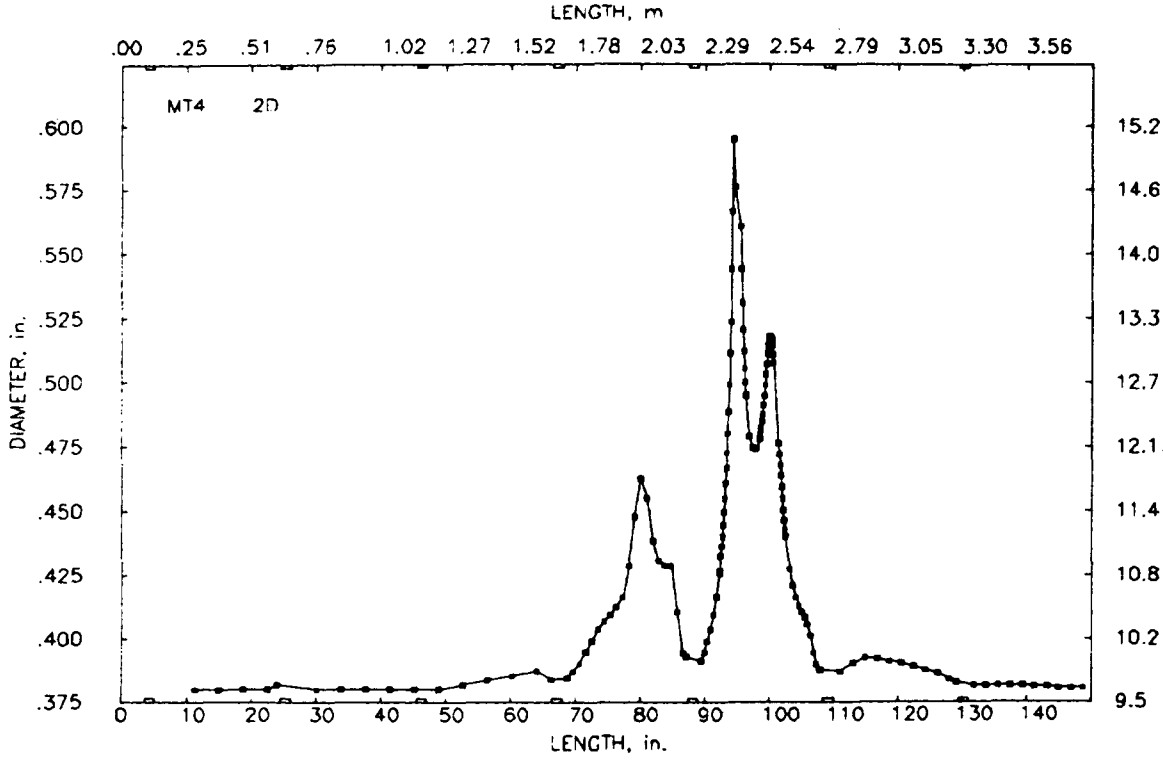

FIGURE G.17. Axial Distribution of Diametral Measurements for Test Rod 2D

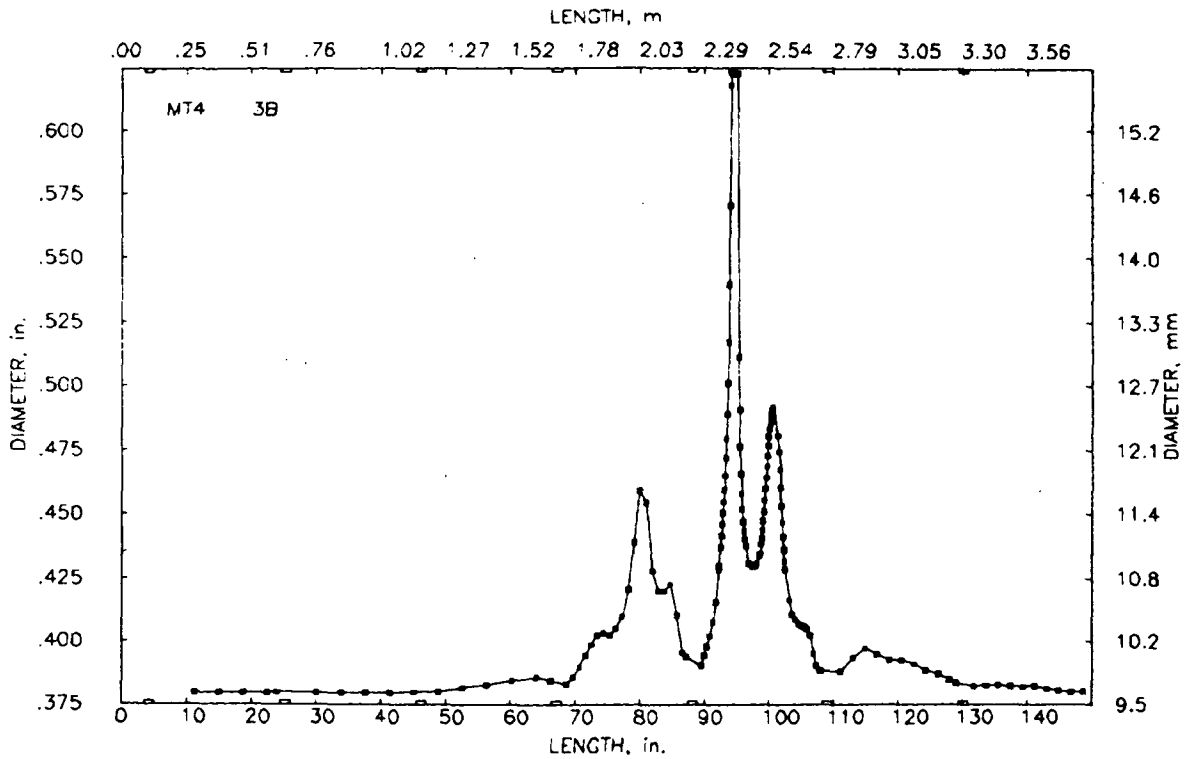

FIGURE G.18. Axial Distribution of Diametral Measurements for Test Rod 3B

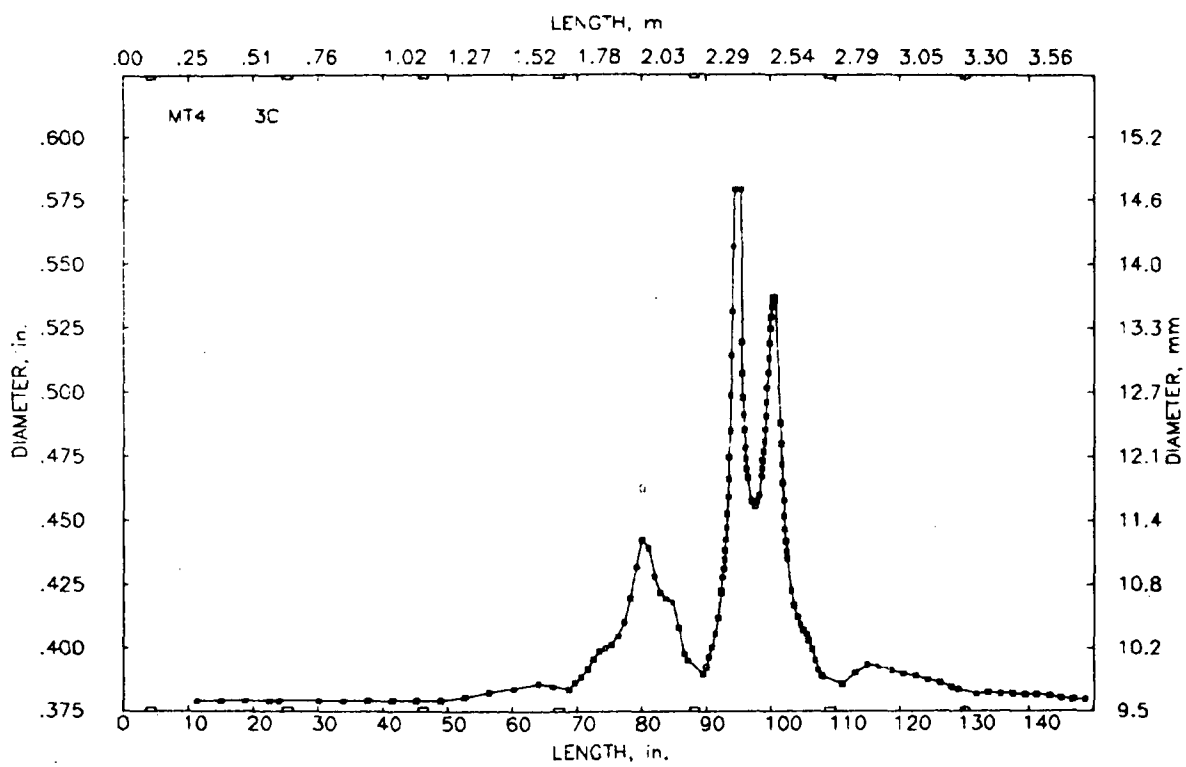

FIGURE G.19. Axial Distribution of Diametral Measurements for Test Rod 3C

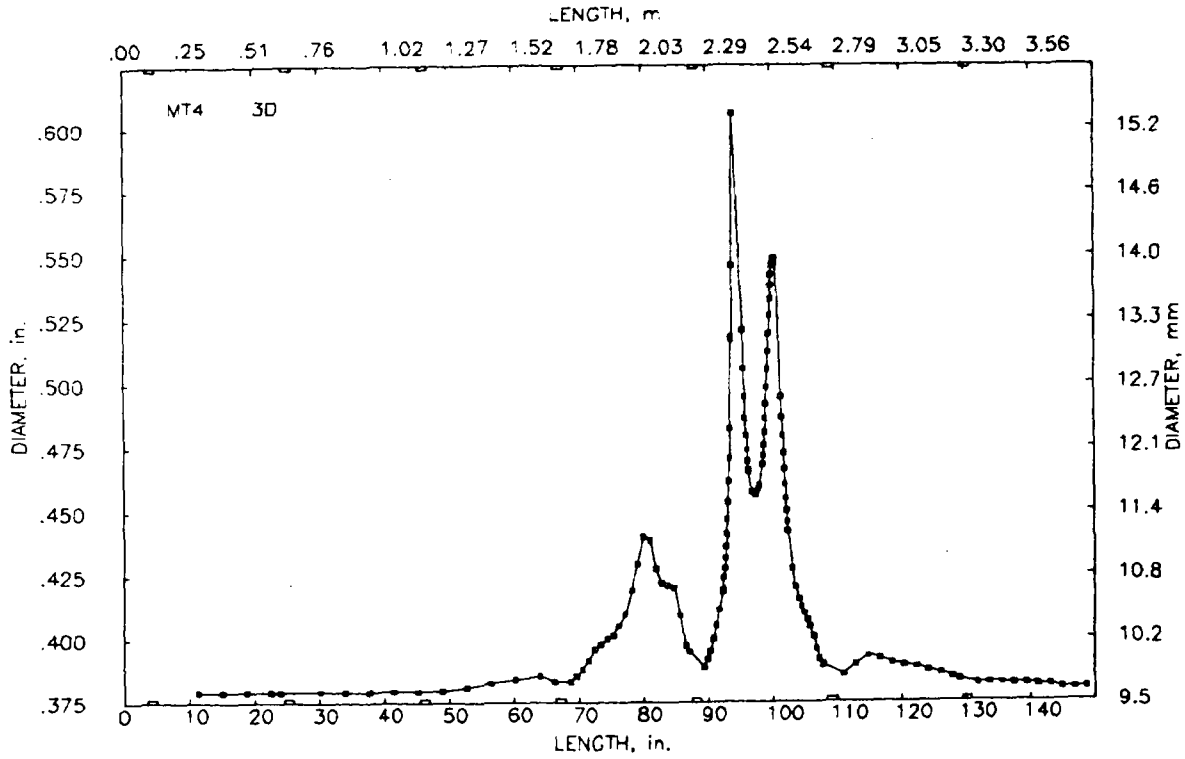

FIGURE G.20. Axial Distribution of Diametral Measurements for Test Rod 3D

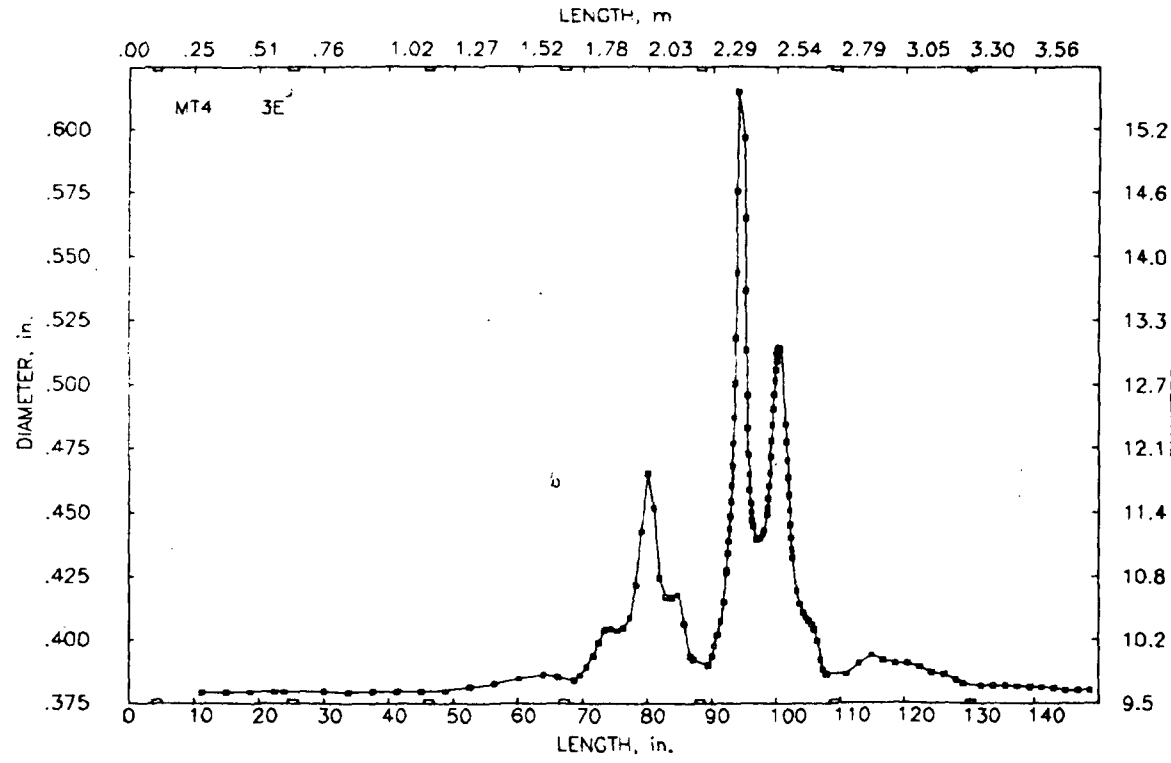

FIGURE G.21. Axial Distribution of Diametral Measurements for Test Rod 3E

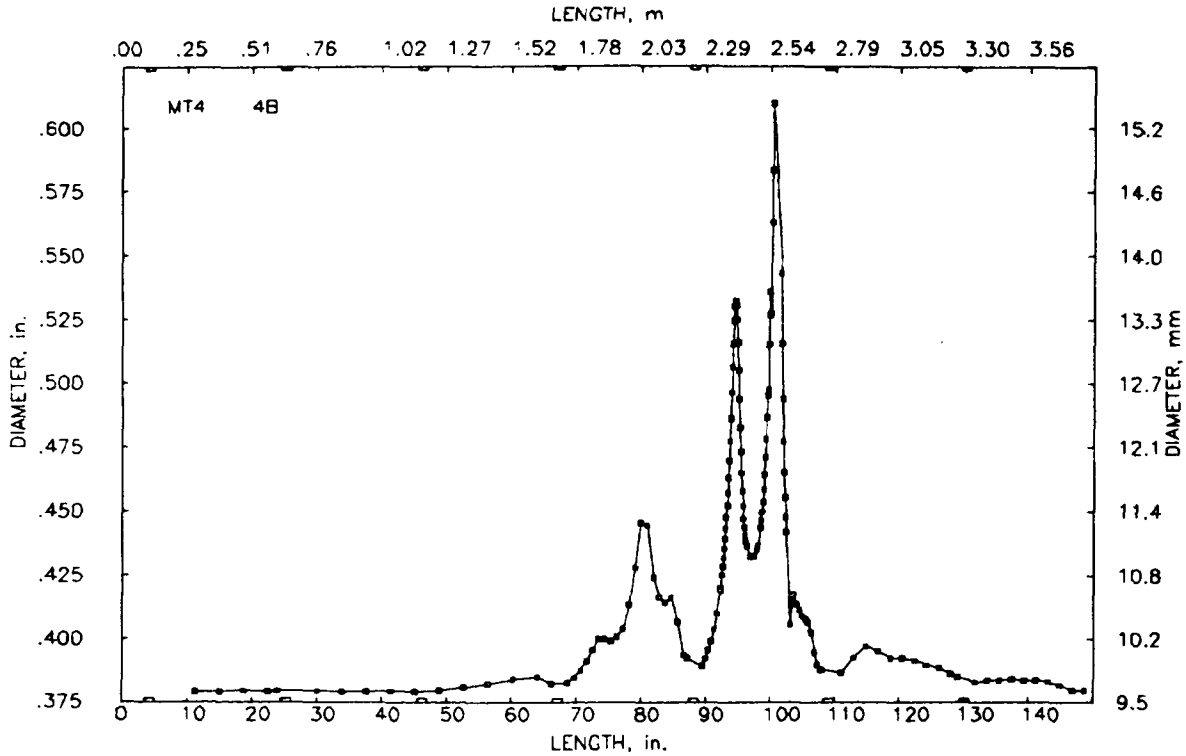

FIGURE G.22. Axial Distribution of Diametral Measurements for Test Rod 4B

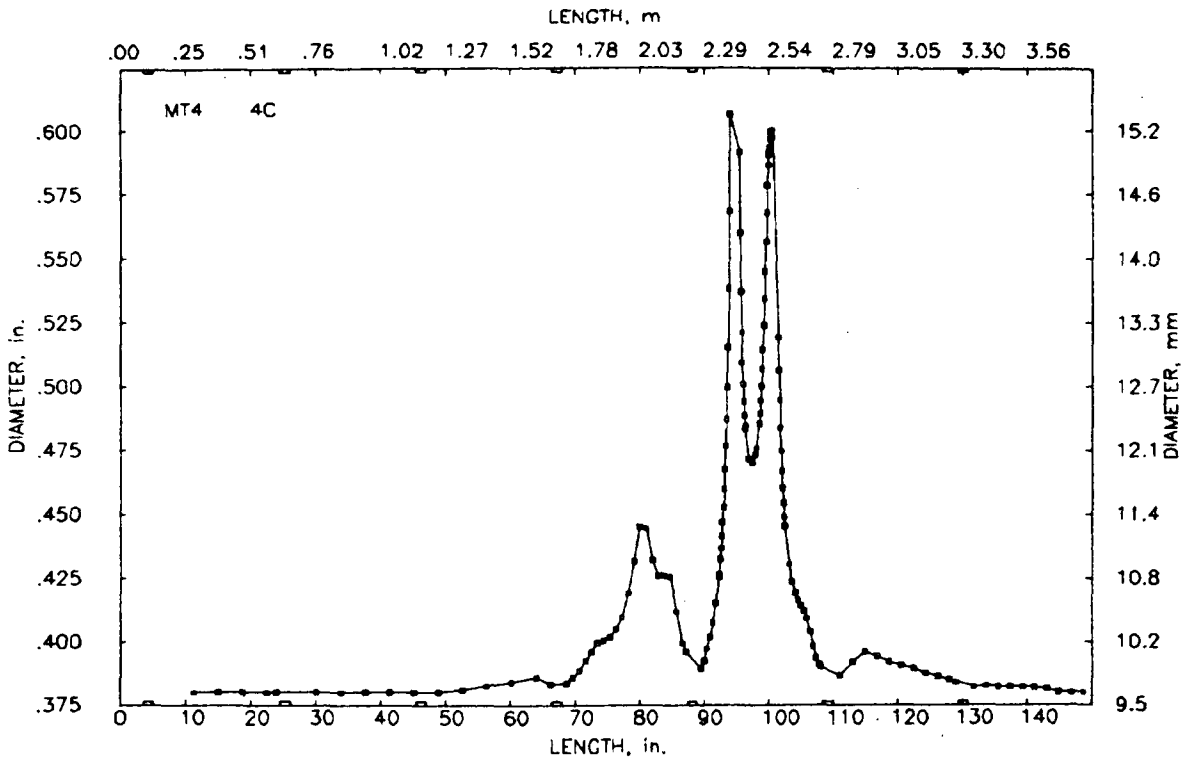

FIGURE G.23. Axial Distribution of Diametral Measurements for Test Rod 4C

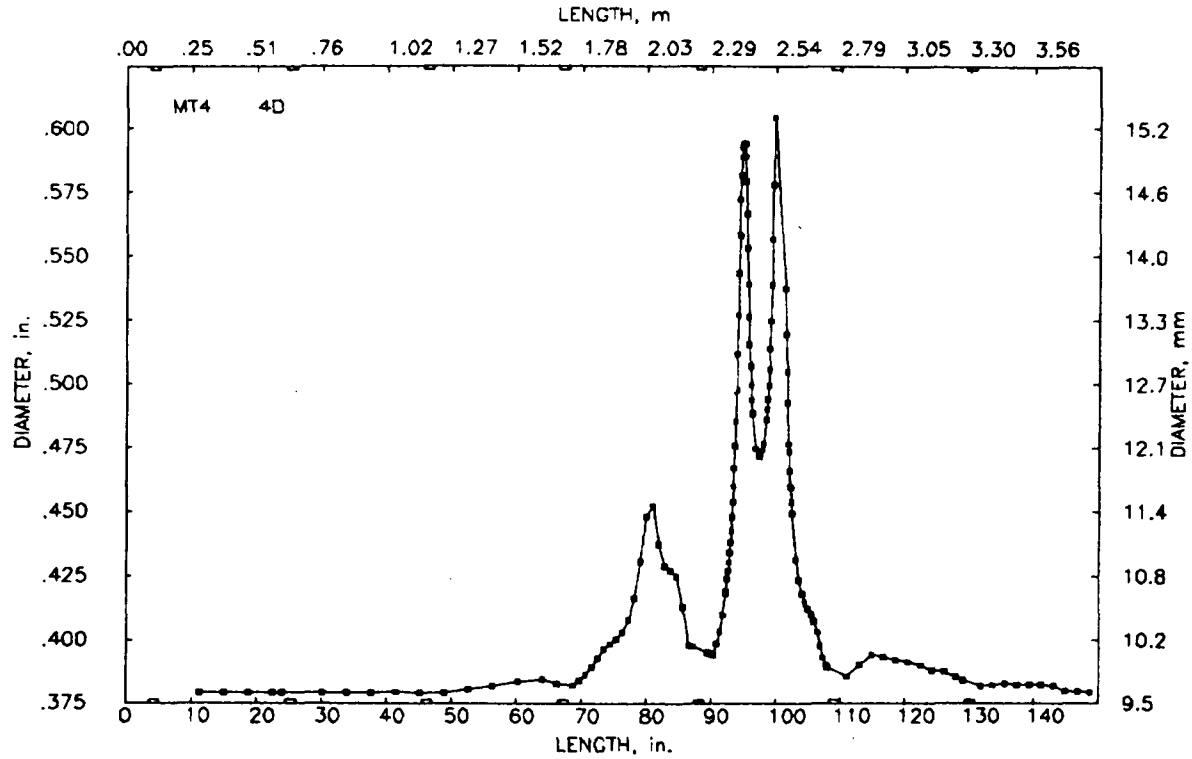

FIGURE G.24. Axial Distribution of Diametral Measurements for Test Rod 4D

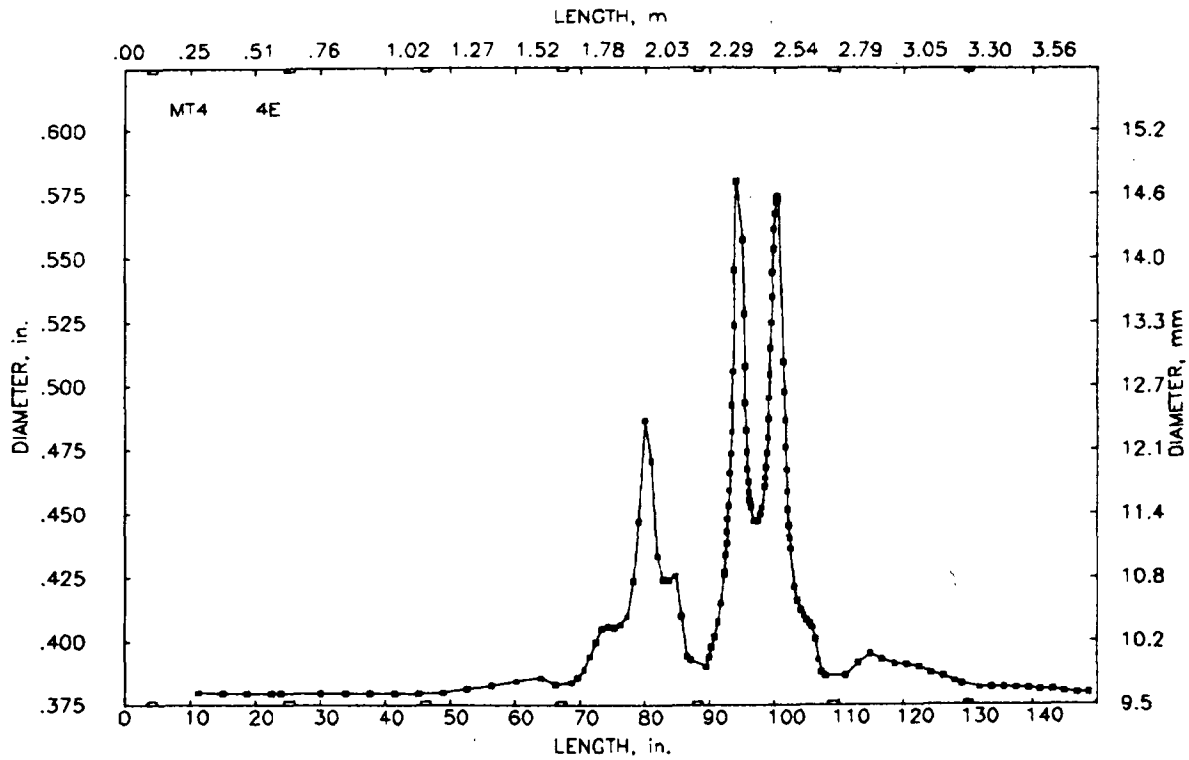

FIGURE G.25. Axial Distribution of Diametral Measurements for Test Rod 4E

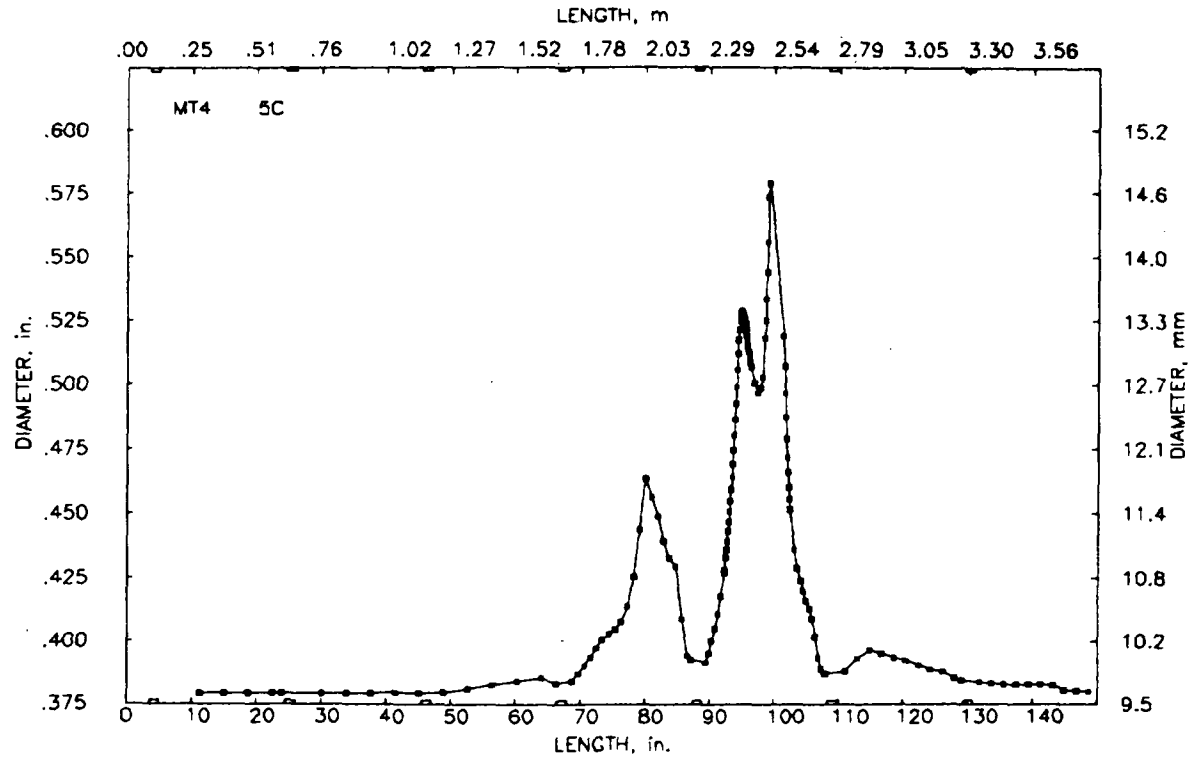

FIGURE G.26. Axial Distribution of Diametral Measurements for Test Rod 5C

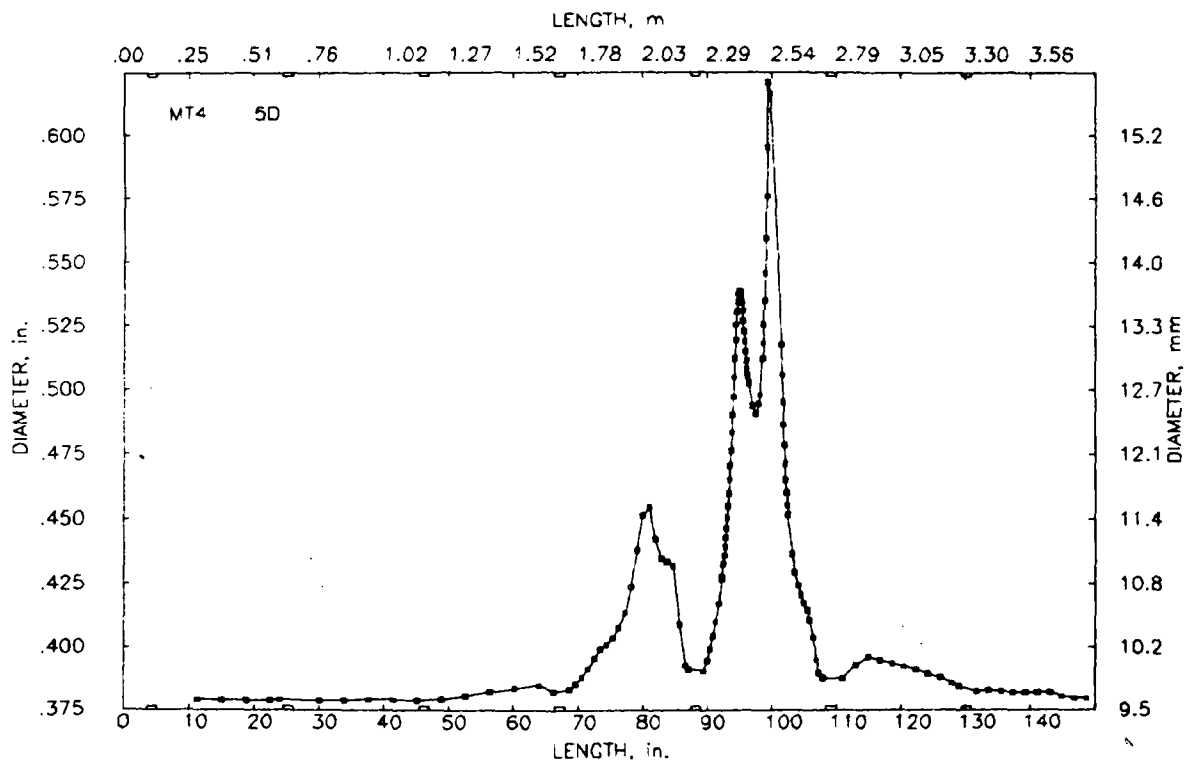

FIGURE G.27. Axial Distribution of Diametral Measurements for Test Rod 5D

DISTRIBUTION

No. of Copies

OFFSITE

U.S. Nuclear Regulatory Commission
Division of Technical Information and Document Control
7920 Norfolk Avenue
Bethesda, MD 20014

O. E. Bassett
U.S. Nuclear Regulatory Commission
M/S P-1102
Washington, DC 20555

W. Hodges
U.S. Nuclear Regulatory Commission
M/S P-1132
Washington, DC 20555

A. Hon
U.S. Nuclear Regulatory Commission
M/S 1130-SS
Washington, DC 20555

Y. Hsu
U.S. Nuclear Regulatory Commission
M/S 1130-SS
Washington, DC 20555

W. Johnston
U.S. Nuclear Regulatory Commission
M/S P-1114
Washington, DC 20555

No. of Copies

N. Lauben
U.S. Nuclear Regulatory Commission
M/S P-1132
Washington, DC 20555

G. Marino
U.S. Nuclear Regulatory Commission
M/S 1130-SS
Washington, DC 20555

G. McPherson
U.S. Nuclear Regulatory Commission
M/S 1130-SS
Washington, DC 20555

R. Meyer
U.S. Nuclear Regulatory Commission
M/S P-1114
Washington, DC 20555

J. Norberg
U.S. Nuclear Regulatory Commission
M/S NL-5650
Washington, DC 20555

L. Phillips
U.S. Nuclear Regulatory Commission
M/S P-1114
Washington, DC 20555

D. Power
U.S. Nuclear Regulatory Commission
M/S P-1114
Washington, DC 20555

No. of Copies	
	D. F. Ross U.S. Nuclear Regulatory Commission M/S 1130-SS Washington, DC 20555
	L. Shotkin U.S. Nuclear Regulatory Commission M/S 1130-SS Washington, DC 20555
	L. Tong U.S. Nuclear Regulatory Commission M/S 1130-SS Washington, DC 20555
3	R. Van Houten U.S. Nuclear Regulatory Commission M/S 1130-SS Washington, DC 20555
	Z. Zuber U.S. Nuclear Regulatory Commission M/S 1130-SS Washington, DC 20555
	P. Boehnert U.S. Nuclear Regulatory Commission Advisory Committee on Reactor Safeguards M/S H-1016 Washington, DC 20555
	D. Okrent U.S. Nuclear Regulatory Commission Advisory Committee on Reactor Safeguards M/S H-1016 Washington, DC 20555

No. of Copies	
	P. Shewmon U.S. Nuclear Regulatory Commission Advisory Committee on Reactor Safeguards M/S H-1016 Washington, DC 20555
	B. Bingham Babcock and Wilcox Co. P.O. Box 1200 Lynchburg, VA 24505
	C. Morgan Babcock and Wilcox Co. P.O. Box 1200 Lynchburg, VA 24505
2	R. Duncan Combustion Engineering 1000 Prospect Hill Road P.O. Box 500 Windsor, CT 06095
	S. Ritterbush Combustion Engineering 1000 Prospect Hill Road P.O. Box 500 Windsor, CT 06095
	L. P. Leach EG&G Idaho, Inc. P.O. Box 1625 Idaho Falls, ID 83401
	P. E. McDonald EG&G Idaho, Inc. P.O. Box 1625 Idaho Falls, ID 83401
	D. Ogden EG&G Idaho, Inc. P.O. Box 1625 Idaho Falls, ID 83401

No. of
Copies

P. Davis (ITI)
Electric Power Research
Institute
3412 Hillview Avenue
Palo Alto, CA 94022

R. Duffey
Electric Power Research
Institute
3412 Hillview Avenue
Palo Alto, CA 94022

M. Merilo
Electric Power Research
Institute
3412 Hillview Avenue
Palo Alto, CA 94022

R. Oehlberg
Electric Power Research
Institute
3412 Hillview Avenue
Palo Alto, CA 94022

W. Sun
Electric Power Research
Institute
3412 Hillview Avenue
Palo Alto, CA 94022

2 G. Thomas
Electric Power Research
Institute
3412 Hillview Avenue
Palo Alto, CA 94022

L. Thompson
Electric Power Research
Institute
3412 Hillview Avenue
Palo Alto, CA 94022

S. Armijo
General Electric Company
175 Curtner Avenue
San Jose, CA 95114

No. of
Copies

L. Noble
General Electric Company
175 Curtner Avenue
San Jose, CA 95114

N. Shirley
General Electric Company
175 Curtner Avenue
San Jose, CA 95114

G. Sozzi
General Electric Company
175 Curtner Avenue
San Jose, CA 95114

R. Williams
General Electric Company
175 Curtner Avenue
San Jose, CA 95114

W. Kirchner
Los Alamos Scientific Laboratory
P.O. Box 1663
Los Alamos, NM 87544

D. M. Chapin
MPR Associates, Inc.
1140 Connecticut Avenue, NW
Washington, DC 20036

P. Griffith
Massachusetts Institute of
Technology
Department of Nuclear
Engineering
Cambridge, MA 02139

J. Davis
Nuclear Engineering Department
Potomac Electric Avenue, NW
Washington, DC 20068

2 R. Chapman
Oak Ridge National Laboratory
P.O. Box X
Oak Ridge, TN 37830

No. of
Copies

F. Mynatt
Oak Ridge National Laboratory
P.O. Box X
Oak Ridge, TN 37830

2 D. Burman
Westinghouse Electric
Corporation
P.O. Box 355
Pittsburgh, PA 15230

2 L. D. Hochreiter
Westinghouse Electric
Corporation
P.O. Box 355
Pittsburgh, PA 15230

R. Rosal
Westinghouse Electric
Corporation
P.O. Box 355
Pittsburgh, PA 15230

FOREIGN

D. J. Axford
Chalk River Nuclear Laboratories
Atomic Energy of Canada, Ltd.
Chalk River, Ontario, Canada
K0J 1J0

C. A. Herriot
Chalk River Nuclear Laboratories
Atomic Energy of Canada, Ltd.
Chalk River, Ontario, Canada
K0J 1J0

J. W. Logie
Chalk River Nuclear Laboratories
Atomic Energy of Canada, Ltd.
Chalk River, Ontario, Canada
K0J 1J0

No. of
Copies

M. D. Atfield
Chalk River Nuclear Laboratories
Atomic Energy of Canada, Ltd.
Chalk River, Ontario, Canada
K0J 1J0

D. Hall
Chalk River Nuclear Laboratories
Atomic Energy of Canada, Ltd.
Chalk River, Ontario, Canada
K0J 1J0

I. C. Martin
Chalk River Nuclear Laboratories
Atomic Energy of Canada, Ltd.
Chalk River, Ontario, Canada
K0J 1J0

6 D. T. Nishimura
Chalk River Nuclear Laboratories
Atomic Energy of Canada, Ltd.
Chalk River, Ontario, Canada
K0J 1J0

M.J.F. Notley
Chalk River Nuclear Laboratories
Atomic Energy of Canada, Ltd.
Chalk River, Ontario, Canada
K0J 1J0

A. Okazaki
Chalk River Nuclear Laboratories
Atomic Energy of Canada, Ltd.
Chalk River, Ontario, Canada
K0J 1J0

D. Thompson
Chalk River Nuclear Laboratories
Atomic Energy of Canada, Ltd.
Chalk River, Ontario, Canada
K0J 1J0

A. Smith
Chalk River Nuclear Laboratories
Atomic Energy of Canada, Ltd.
Chalk River, Ontario, Canada
K0J 1J0

No. of Copies

4 T. Healey
Central Electricity Generating Board
Berkeley Nuclear Laboratories
Berkeley, Gloucestershire GL13 9PB
England

4 M. Ishikawa, Chief
Reactivity Accident Laboratory
Japan Atomic Energy Research Institute
Tokai Research Establishment
Tokai-Mura, Naka-Gun
Ibaraki-Ken
Japan

S. Kawasaki
Fuel Reliability Lab III
Division of Reactor Safety
Japan Atomic Energy Research Institute
Tokai Research Establishment
Tokai-Mura, Naka-Gun
Ibaraki-Ken
Japan

T. Doyle
JRC-ISPRA, EURATOM
CCR ESSOR Division
21020 Cento Euratom Di Ispra (Varese)
Italy

H. Holtbecker
JRC-ISPRA, EURATOM
CCR ESSOR Division
21020 Cento Euratom Di Ispra (Varese)
Italy

J. Randles
JRC-ISPRA, EURATOM
CCR ESSOR Division
21020 Cento Euratom Di Ispra (Varese)
Italy

No. of Copies

O. Simoni
JRC-ISPRA, EURATOM
CCR ESSOR Division
21020 Cento Euratom Di Ispra (Varese)
Italy

F. Erbacher
Kernforschungzentrum Karlsruhe
Weberstrasse 5
75 Karlsruhe 1
Federal Republic of Germany

A. Fiege
Kernforschungzentrum Karlsruhe
Weberstrasse 5
75 Karlsruhe 1
Federal Republic of Germany

2 H. Rininslandd
Kernforschungzentrum Karlsruhe
Weberstrasse 5
75 Karlsruhe 1
Federal Republic of Germany

2 J. H. Gittus
United Kingdom Atomic Energy Authority
Atomic Energy Tech. Branch
Harwell, DIDCOT
Oxfordshire OX11 ORA
England

C. A. Mann
Springfields Nuclear Power Development Laboratory
United Kingdom Atomic Energy Authority
Springfields, Salwick
Preston PR 4 ORR
England

3 I. H. Gibson
Atomic Energy Establishment Winfrith
Dorchester, Dorset DT2-8DH
England

No. of
Copies

ONSITE

4 Exxon Nuclear Company, Inc.

T. Doyle
W. Kayser
J. Morgan
W. Nechodom

50 Pacific Northwest Laboratory

W. J. Bailey
J. O. Barner
S. K. Edler
M. D. Freshley (5)
R. L. Goodman
C. R. Hann
G. M. Hesson (2)

No. of
Copies

U. P. Jenquin
L. L. King
R. R. Lewis (2)
R. K. Marshall
P. N. McDuffie
F. E. Panisko
L. J. Parchen (2)
J. P. Pilger
W. N. Rausch
G. E. Russcher (5)
J. W. Upton
B. J. Webb
N. J. Wildung
C. L. Wilson (10)
M. C. Wismer
N. A. Wogman
Publishing Coordination YO(2)
Technical Information (5)

NRC FORM 335 (11-81)

U.S. NUCLEAR REGULATORY COMMISSION

BIBLIOGRAPHIC DATA SHEET

1. REPORT NUMBER (Assigned by DDC)
NUREG/CR-3272
PNL-4669

4. TITLE AND SUBTITLE (Add Volume No., if appropriate)
LOCA SIMULATION IN NRU PROGRAM
Data Report for the Fourth Materials Experiment (MT-4)

2. (Leave blank)

3. RECIPIENT'S ACCESSION NO.

7. AUTHOR(S)
C.L. Wilson, C.L. Mohr, G.M. Hesson, N.J. Wildung, G.E. Russcher, B.J. Webb, M.D. Freshley

5. DATE REPORT COMPLETED
MONTH: May YEAR: 1983

9. PERFORMING ORGANIZATION NAME AND MAILING ADDRESS (Include Zip Code)
Pacific Northwest Laboratory
P.O. Box 999
Richland, WA 99352

DATE REPORT ISSUED
MONTH: July YEAR: 1983

6. (Leave blank)

8. (Leave blank)

12. SPONSORING ORGANIZATION NAME AND MAILING ADDRESS (Include Zip Code)
Division of Accident Evaluation
Office of Nuclear Regulatory Research
U.S. Nuclear Regulatory Commission
Washington, DC 20555

10. PROJECT/TASK/WORK UNIT NO.

11. FIN NO.
B2277

13. TYPE OF REPORT
Topical

PERIOD COVERED (Inclusive dates)

15. SUPPLEMENTARY NOTES

14. (Leave blank)

16. ABSTRACT (200 words or less)

A series of in-reactor experiments were conducted using full-length 32-rod pressurized water reactor (PWR) fuel bundles as part of the Loss-of-Coolant Accident (LOCA) Simulation Program by Pacific Northwest Laboratory (PNL). The fourth materials experiment (MT-4) was the seventh experiment in the series of thermal-hydraulic and materials deformation/rupture experiments conducted in the National Research Universal (NRU) reactor, Chalk River, Ontario, Canada. This experiment was funded by the U.S. Nuclear Regulatory Commission (NRC) to evaluate ballooning and rupture during adiabatic heatup in the temperature range of 1033 to 1200K (1400 to 1700°F). The 12 test rods in the center of the 32-rod bundle were initially pressurized to 4.62 MPa (670 psia) to insure rupture in the correct temperature range. All 12 test rods ruptured with an average strain of 43.7% at the maximum flow blockage elevation of 2.68 m (105.4 in.). Experimental data for the MT-4 transient experiment and post-test measurements and photographs of the fuel are presented in this report.

17. KEY WORDS AND DOCUMENT ANALYSIS

thermal-hydraulics
materials deformation/rupture
heat transfer coefficients
loop control system
data acquisition and control system

17a. DESCRIPTORS

loss-of-coolant accident simulation
National Research Universal (NRU) reactor
pressurized water reactor fuel bundles

17b. IDENTIFIERS/OPEN-ENDED TERMS

18. AVAILABILITY STATEMENT
Unlimited

19. SECURITY CLASS (This report)
Unclassified

20. SECURITY CLASS (This page)
Unclassified

21. NO. OF PAGES
215

22. PRICE
$

NRC FORM 335 (11-81)

UNITED STATES
NUCLEAR REGULATORY COMMISSION
WASHINGTON, D.C. 20555

OFFICIAL BUSINESS
PENALTY FOR PRIVATE USE, $300

FOURTH-CLASS MAIL
POSTAGE & FEES PAID
USNRC
WASH. D. C.
PERMIT No. G-67

PNL-4669
G. Marino
U.S. Nuclear Regulatory
Commission
M/S 1130-SS
~~Washington, DC 20555~~